AC Voltage Control of a Future Large Offshore Wind Farm Network Connected by HVDC

HO, TERRY,CHI,YOUNG

AC Voltage Control of a Future Large Offshore Wind Farm Network Connected by HVDC

Terry Chi Young Ho

A Thesis presented for the degree of
Doctor of Philosophy

School of Engineering and Computer Sciences
Durham University
United Kingdom

September 2015

AC Voltage Control of a Future Large Offshore Wind Farm Network Connected by HVDC

Abstract

The offshore wind resource around the seas of the UK is a very large renewable energy resource. Future offshore wind farm sites leased by the Crown Estate for Round 3 development will need high power capacity grid connection, but their remote location presents a challenge for the electrical connection to the grid. Long distance AC cable transmission is not practical due to the large cable capacitance which leads to reactive power loss. This thesis considers the voltage source converter and high voltage direct current (VSC-HVDC) technology as the future grid connection for the offshore wind farm network, which is more controllable and has better transmission efficiencies for long distance and high power cable transmission applications. The offshore AC network is weak with very little inertia and has limited rating at the HVDC converter substation. The dynamics in key variables in the offshore wind farm AC network and how they affect certain components in the system were studied. Without proper control, the offshore voltage and the frequency will be sensitive to change. The capacitor of the AC filter at the offshore VSC-HVDC station was found to be vulnerable to over-voltage, therefore a closed loop AC voltage controller was proposed here to maintain a constant capacitor voltage and to prevent tripping or over-voltage damage. The tuning of the control gains were optimised with a pole placement design method and small signal analysis for observing the system eigenvalue damping. The control parameters were then tuned for a fast and well damped controller. The AC voltage controller was evaluated and compared to an open loop system. The controller was able to limit the resonance in the LC filter that can be triggered by large and fast disturbances in the current, voltage and frequency. Current saturation could be implemented within the control structure for device protection from over-currents. Insight on how the wind turbine fully rated frequency converters and controllers may interact with the VSC-HVDC converter station is also discussed.

Declaration

This thesis is based on the works carried out by Terry Chi Young Ho, under the Supervision of Prof. Li Ran and Prof. Peter Tavner within the School of Engineering and Computer Sciences at Durham University in the United Kingdom. Parts of Chapter 4 and 5 was also carried out in collaboration with Prof. Aurelio García-Cerrada from Comillas Pontifical University in Madrid. No part of this thesis has been submitted elsewhere for any other degree or qualification and it is all my own work unless referenced to the contrary in the text.

Acknowledgements

I would like to first thank my PhD supervisors, Prof. Li Ran and Prof. Peter Tavner, for giving me the opportunity and guidance in carrying out the research. Prof. Ran has been continually providing his expertise throughout the PhD process, even after his move to the University of Warwick where he continued to offer opportunities and extra funding for collaboration and further experimental work. His fatherly support was far beyond the boundaries of his professional obligations. Although my contact with Prof. Tavner as my second supervisors was short before he retired, his managerial and assertive approach never failed to inspire me.

I am thankful for the extensive support of Prof. Aurelio García-Cerrada (Comillas Pontifical University, Madrid) as a supervisor, a collaborator, and as a friend during his stay in Durham while on Sabbatical leave and beyond. His expertise in state-variable control, modelling the electrical system and small signal analysis has been tremendously valuable.

I would not be able to complete the PhD without the support and funding provided by a UK EPSRC doctoral training award as part of the SUPERGEN Wind Energy Technologies Consortium, EP/H018662/1. I would also like to thank Dr Behzad Kazemtabrizi for joining us at Durham at the time when we desperately needed the extra manpower to complete the deliverables for the Supergen Wind 2 project.

The electrical technician in both Durham and Warwick for their patience, expertise and quality of their work on the experimental test rig.

I am very grateful to have great colleagues and friends, Dr. Peter Wyllie, Dr. Mustafa Elsherif, Tianqu Hao, Dr. Sean Norris, Dr. Song Guo, Dr Paddy McNabb, Mananolis Loukarakis, Dr. Donatella Zappala, Dr. Wenjuan Wang, Dr. Bindi Chen, Dr

Hongbo Shao, Guy Hutchinson, Sarah Sheehy and Dr. Mahmoud Shabazi. Without them, the work place wouldn't be a fun and memorable atmosphere. I would also especially thank Meng Xu, for her encouragement, giving me the motivation and that extra push for the final leg of my PhD journey.

I thank my parents, my family and members of my local church for their love, prayers, understanding, spiritual support and guidance from above, teaching me to be humble, patient, loving and to stay positive during tough times.

"In everything give thanks..." (1 Thessalonian 5:18)

Contents

List of Figures

List of Tables

Nomenclature

A	Area
B	Flux density
C	Capacitance
C_p	Coefficient of performance
dq	Direct-Quadrature
f	Frequency, or Function
i	Current
j	Imaginary unit
P	Real power
Q	Reactive power
R	Resistance
S	Apparent power
t	Time
v	Wind speed
V	Voltage
W	Weibull probability
X	Reactance
Z	Impedance
λ	Tip speed ratio
ρ	Density of air
τ	Time constant
ω	Angular velocity (rotational speed)

List of Abbreviations

AC	Alternating Current
ADC	Analogue to Digital Converter
CB	Circuit Breaker
DFIG	Doubly-fed Induction Generator
DSP	Digital Signal Processor
EMF	Electromotive Force
FACTS	Flexible AC transmission system
GTO	Gate Turn-Off Thyristor
HVDC	High Voltage Direct Current
IGBT	Insulated-Gate Bipolar Transistor
IGCT	Integrated Gate-Commutated Thyristor
LCC	Line Commutated Converter
MIND	Mass Impregnated Non-Draining
MOSFET	Metal-Oxide-Semiconductor Field-Effect Transistor
MPPT	Maximum Power Point Tracking
MVDC	Medium Voltage Direct Current
PCB	Printed Circuit Board
PI	Proportional-Integral
PID	Proportional-Integral-Derivative
PLL	Phase-Locked Loop
PMSG	Permanent Magnet Synchronous Generator
PSCAD®	Power System Computer Aided Design
PWM	Pulse Width Modulation
RMS	Root Mean Square

SCADA	Supervisory Control and Data Acquisition
SCIG	Squirrel Cage Induction Generator
SCR	Short Circuit Ratio
Si	Silicon
SiC	Silicon Carbide
SISO	Single-Input and Single-Output
STATCOM	Static Synchronous Compensator
TF	Transfer Function
UK	United Kingdom
VAR	Volt-Ampere Reactive
VCO	Voltage-Controlled Oscillator
VSC	Voltage Source Converter
WF	Wind Farm
WRIG	Wound Rotor Induction Generator
WRSG	Wound Rotor Synchronous Generator
WT	Wind Turbine
XLPE	Cross-Linked Polyethylene

Chapter 1

Introduction

1.1 Background and Statement of Problem

The world has become highly dependent on fossil fuels to meet its energy needs. Fossil fuels are a finite resource that will eventually deplete. Burning the carbon in this type of fuel, which has been stored in the earth for many thousands of years, will continue to pollute the environment and contribute to global warming through CO_2 emissions.

Over recent years, the UK government has used subsidies to drive the development of wind power generation for both onshore and offshore. Although the energy used to manufacture and commission wind turbines (WT) creates CO_2 emissions, none is emitted during the operational life. The WT life cycle's overall net effect in the environment will be much more favourable than conventional power generation. The carbon payback period for a UK offshore WT, i.e. the time it takes to become carbon neutral, is typically 6 months [1]. The reliability and efficiency of WTs are important for increasing the operational life, offsetting more CO_2 emission from non-renewable sources, as well as to provide more energy and revenue.

As WT move further away from shore, the average speed is higher and the wind is smoother due to low surface friction. More power can be extracted from the offshore wind than from onshore wind. Onshore wind development is saturating due to local opposition citing noise pollution and visual blight to the countryside. The impact of offshore wind farms to local inhabitants is reduced with increasing

distance. However, the challenge of offshore electrical grid connection increases with distance.

Electrical power can be transmitted in direct current (DC) or alternating current (AC) form. During what became known as the "War of the Currents" in the late 19th century, Thomas Edison promoted DC systems against AC power distribution systems that were advocated by George Westinghouse. The same voltage level was used in DC systems for all generation, transmission and load, which meant that thick, heavy and expensive conductors were needed for distribution. In the end, DC lost out in favour of AC power, and it became the standard form of transmission throughout the 20th century. It was more cost effective to step up the AC voltage using transformers and AC generators were simpler and more efficient, therefore AC power was able to be cheaply transmitted over thinner and longer distant lines [2].

It was difficult and expensive to step the DC voltage to the high voltage direct current (HVDC) level, until the advent of efficient power electronic converters in recent times and interest in DC transmission revived. During the 20th century, mercury arc valves were developed, and then silicon based thyristors for early first line commutated converter (LCC) systems for conversion between AC and HVDC. Such systems were initially expensive, bulky and inefficient compared to AC transformers. It was until the development of solid-state power electronic devices in the late 20th century, switching capabilities improved and enabled the use of voltage source converter (VSC) topologies, which offered better controllability over LCCs. They are also progressively becoming smaller, lighter, cheaper and more efficient over time, and their applications are increasing within HVDC connections, flexible AC transmission systems (FACTS) and renewable energy conversion.

HVDC transmission does not exhibit reactive power, proximity effect and skin effect losses that are normally associated with AC transmission. The efficiency of HVDC for long distance and high power will justify the cost and the losses in the converter stations. This is ideal for subsea transmission, where the capacitance in the cable and therefore reactive power is significantly higher. Therefore HVDC application is trending for larger offshore wind farms (WF) further away from shore, where the wind resource is greater.

Harsh offshore conditions and long distances makes accessing the offshore WF site difficult and challenging. There is a lack of field-experience for HVDC connected offshore wind farms, and little knowledge about their reliability and impact on down-time. Access is difficult to deal with any serious failures hazards immediately, and if adverse conditions persist it can significantly delay repairs.

The heavy duty sub-assemblies, such as the gearbox, transformer, generator, etc., are the most difficult to repair because of their size and weight. They will contribute to very high downtimes per failure, however, given the recognition of this issue in the design process, and their simplicity and robustness, the failure rates of these heavy components are actually relatively lower than expected in practice. Wind turbine field-experience revealed that power electronics and the control system were found to have the highest failure rate. These failures often contribute to high overall downtime as therefore loss of power generation. These types of components are often complicated, but also crucial for control, efficiency, stability, and maximum wind power extraction. As the wind farms are going further offshore, access for repair and maintenance will become increasingly more challenging. This thesis will, however, focus more on the components in the electrical system in the offshore WF.

The Borwin1 project was the first HVDC connection in the world built for an offshore wind farm off the coast of Germany. However, it was not entirely successful as it has experienced a number of outages and has been unable to export much power since it was first commissioned. A fire in an electrical component at the offshore platform was cited for an unplanned outage [3]. It was also cited that disturbance in the system lead to automatic shut-down due to overload in the filter capacitor [4]. Little is understood about the control stability, resonance and harmonics in such systems and therefore this problem needs to be addressed.

1.2 Aim of Research

The research is part of the Supergen Wind 2 Plus Project, for which the title was proposed as “Connection Technology for Large Offshore Wind Farms - Achieving Control Performance, Reliability, Maintainability and Cost Effectiveness”. This

proposal complements the Supergen Wind 2 Core Renewal Project, which is built upon the findings of the Supergen Wind 1 Project. While the Core Renewal Project addresses the resource, reliability, scaling and cost of the offshore wind farm unit, the Plus Project addresses the technical barriers in the electrical grid connection of the wind farm. The two projects together aims to improve the future prospect of offshore wind power generation.

The focus of the research in this thesis is within the topic of the grid connection and electrical system of the offshore wind farm. The steady-state and dynamic characteristics of the offshore wind farm connection system are studied using tools such as MATLAB/Simulink® and PSCAD/EMTDC®, and small signal analyses and time domain simulations were carried out. The control interactions between power electronic WT frequency converters and HVDC transmission system were also observed. It is important that the overall system is design to be robust and well damped.

The suitability of selected concept network topologies proposed for offshore wind farm application is examined. Topologies that centralise components in the electrical system that traditionally have high failure rates, such as the power electronics and control system, can also improve the access, repair rate and maintainability of these components. In turn, this can reduce the post-failure downtime and minimise the component shut-down period during maintenance. However, other problems will arise from this, such as in the voltage level and cable arrangement. As increased complexity and the number of components in the system tend to reduce the system reliability, simplification and component reductions in the system topologies are also considered with the aim of improving system robustness and reliability.

An offshore AC network is considered to be a weak network due to the limited rating of HVDC connection and the large impedance in the long transmission cables and the collection network. The voltage in the network will be prone to fluctuations. This research aims to study how an offshore AC voltage terminal can be controlled and decoupled to minimise voltage fluctuation and prevent over-voltages such as those that appeared at the Borwin1 offshore HVDC connection and caused its shunt filter capacitors to trip. An insight will also be provided to show how an over-voltage

here may arise in the first place.

1.3 Scope of Thesis

This thesis begins with a literature review in Chapter 2, where the motivation, technology and reliability for a large scale future offshore wind farm are discussed in detail. The motivation for going offshore to harness wind energy is first addressed. The electronic frequency converter, HVDC systems, and wind turbine technologies and their characteristics are explained in further detail. Learning that the power electronics have a relatively high failure rates and require regular maintenance to keep the devices fully operational, Chapter 3 then aims to address the accessibility of power electronics in the wind farm system for repair and maintenance. Different types of offshore wind farm network topologies, including traditional and conceptual, are examined and reviewed.

The AC voltage control strategy for an AC collection type network connected by HVDC is proposed, tuned and discussed in Chapter 4. The offshore network model was simplified, and small signal analysis is used to characterise the dynamics of the system and control. The network voltage is controlled by the offshore HVDC converter substation. Further insight into the pole-zero characteristics of controller are also discussed and compared with the small signal analysis results.

In Chapter 5, the control system is evaluated and compared to an "open loop" method, where the closed loop feedback is not used and a fixed voltage reference signal is simply applied at the converter output instead. A step input current disturbance in the open loop systems would trigger under-damped resonance at the filter, which can lead to over voltages up to 50% above the nominal level. The voltage controller was able to limit this resonance and keep the system well damped at the filter capacitor, while minimising the need for passive resistive damping and therefore losses in the filter. It works by forcing the capacitor to be a fixed voltage source, which is also at the point of common coupling where the network and the WT devices are connected. The chapter also investigates the use of current saturation for device protection inside the voltage controller, and explored how over-voltage in

the filter capacitor can occur in this case. It is important for the offshore network voltage to have as little disturbance as possible for the WT converters to follow using their phase locked loops, and so that it does not interfere with the torque of the generator even if no frequency converter is used at the WT.

1.4 Original Contributions

The main contribution lies in Chapters 4 and 5 of this thesis. A speculative insight is provided as to how the filter capacitor in the Borwin1 HVDC station would overload and trip. One of the causes for this is the resonance, which is triggered by disturbance in the current input into the filter. A case scenario has been simulated to demonstrate how this can happen. An AC voltage control strategy has been proposed and evaluated. It can regulate the voltage at the filter capacitor to prevent over-voltage. The application of this voltage controller for the offshore wind farm network using the VSC-HVDC converter is new. The controller needs to be fast in order to react to fast current disturbances. The controller and a simplified offshore network system was modelled in MATLAB/Simulink®. The small signal analysis was used as a tool to study the state variable eigenvalues in the system and is used as an indicator of the dynamic characteristics of the system, and to see how the system dynamics. The tool was used to observe how the system dynamics are affected by different control parameters. This also helped to find an optimum voltage control gain parameter that have both fast control action and sufficient system damping. The method is fast and can be reiterated in a script, for example with an optimisation algorithm for further improving the control design and for study of similar control systems with different parametric constraints. The minimum system eigenvalue damping results from small signal analyses are also compared with the poles and zeros for simplified frequency domain model of the controller to further explain the results.

Interactions between the HVDC converter under voltage control and an aggregated WT converter under current or power control were also studied. It was then found that a fast inner loop for power control and proper voltage dynamic compen-

sation was beneficial to the system damping. A current saturation technique within the structure of the voltage controller was also tested in simulation, and an insight has been provided about how this works and how this will interact with a power controller model for the WT. How the current saturation lead to an over-voltage was also demonstrated and a solution with power control was discussed to over come the issue.

Practical challenges and considerations for implementing the AC voltage controller experimentally are discussed in Chapter 6. The issue with the delay in a timer-based PWM output of the controller interface was addressed, and how it affected the control performance is also presented.

Two conference papers were published in the course of the PhD at the PEDG 2012 conference [5] and the ICRERA 2013 conference [6]. Contributions were also made in in the output of the Supergen Wind 2 Deliverables D3.1.1a.

Chapter 2

Components in a Future Large Offshore Wind Farms

The United Kingdom is an island country surrounded by sea with a vast area of offshore energy resource available to exploit. Government subsidy and support have been a huge incentive to push for offshore wind energy development, which will help meet envisaged legally-binding decarbonisation and renewable energy generation targets. Up to 32 GW of estimated installed capacity in 2010 [7], will be leased to developers for offshore wind development within the Crown Estate Round 3 offshore sites shown in Figure 2.1. In 2013, there were 3.32 GW operating wind farms and 36.6 GW of wind farms in development [8].

The sea is an open area with low surface friction therefore offshore wind speeds are higher than on land. In theory, the mechanical power from wind is proportional to the cube of the wind speed, so a 10% increase in average wind speed could results in about 30% increase in wind power production [9]. The depth of the waters around the UK, from seabed to surface, are relatively shallow compared to most other coastal countries around the world, which is ideal for fixed foundation structures for the offshore wind turbines (WT). The cost of offshore installations will be considerably higher, however, it has the biggest potential for growth for installed capacity and power.

The current technology for onshore WTs has matured and is cost-effective, but onshore sites for wind energy development are saturating. In years 2013/14, 73%

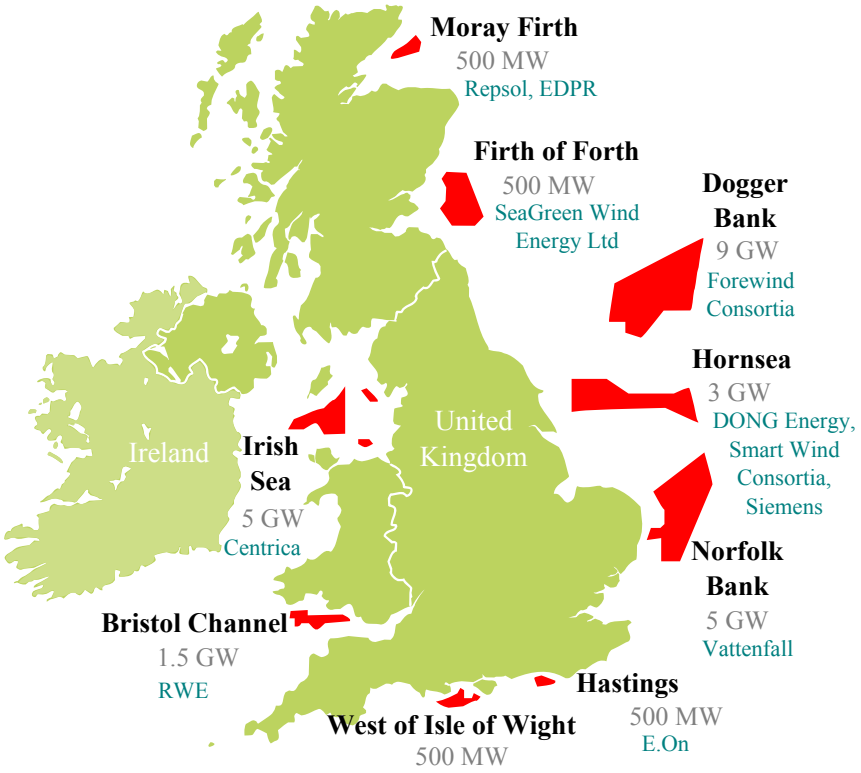

Figure 2.1: Site locations of the Crown Estate Round 3 wind farm sites for lease adapted from [10] with major players and 2013 estimated capacity data from RenewableUK [8].

of new wind energy capacity approved for deployment in the UK was for offshore projects [11]. The "not in my backyard" public perception toward the WTs regarding the impact of the visual and noise pollution they have on the local environment has been a challenge for planning consent for onshore development. Large wind farm (WF) projects have moved further offshore so they are less noticeable by the public eye compared to onshore WTs. Although they will not be completely invisible, due to noticeable blade movement and night navigation lighting, which is then magnified with increased WT numbers in the WF, their impact will be greatly reduced with distance [12].

This chapter is a literature review on future large offshore WTs, their grid connection and electrical system. Their characteristics, reliability and impact on the downtime are also discussed.

2.1 The Grid Connection and Power Electronics

Traditionally the transformer is used to step up the wind turbine AC voltage output for high voltage alternating current (HVAC) transmission. This increases the power delivery capacity by reducing the current to a level that is more efficient. However, unlike overhead lines, long distance cables are disadvantaged with relatively large inherent shunt capacitance in the cable, which makes it unsuitable for long distance subsea HVAC transmission. The reactive power produced by the shunt capacitance is proportional to the square of the voltage across it, see equation (2.1):

$$Q = j\omega CV^2 \tag{2.1}$$

The reactive power and hence current take up the ampacity of the cable copper conductor, leaving less available for real power transmission. The I^2R transmission losses are higher because the current per unit of real power is higher. In order to reduce this, reactive power compensators are needed at certain stages along the cable, but each station to house these will further step up the cost of an AC transmission scheme. During low loads, the reactive power can lead to undesired voltage rise at the cable terminal opposite to the energised side, where the phenomenon is also known as the Ferranti effect [13].

At present, near-shore wind farms are close enough to shore to be connected by AC cables. However, future wind farms will move further away and generate more power than the current near-shore WTs. High voltage AC cable transmission has a limit on the length and the voltage before losses become too significant.

2.1.1 High Voltage DC Transmission

High Voltage Direct Current (HVDC) is the ideal choice for high power, long distance and efficient subsea power transmission for future large offshore wind farms [14, 15]. The key advantages for HVDC transmission are:

- Better efficiency over AC, with no eddy current and skin effect losses.
- DC is always unity power factor, with no losses associated with reactive power.

- Low cost cables can be used.
- Asynchronous AC systems can be connected together.

The cable insulation is usually rated to the peak of the voltage. The DC voltage can theoretically be $\sqrt{2}$ higher than the r.m.s AC voltage. For any given constant power and cable insulation thickness, the DC current in a cable core can be $\sqrt{2}$ times less than the AC r.m.s phase current. Given this in addition to the absence of skin effect and eddy losses, less copper can be used for DC power transmission. The thinner cables will be more flexible, cheaper and easier to manufacture, transport and deploy. The only significant losses in the DC cable are the I^2R copper losses.

The main drawbacks of HVDC are the losses in the converter stations and the high initial capital investment for the stations. However, HVDC cables are cheaper and more efficient, therefore the cost of HVDC investment will break-even and become more cost-effective than AC as the distance increases, as shown in Figure 2.2. The typical break-even distance is about 50 km for underground or sub-sea cable transmission, and about 500–800 km for overhead lines [2, 16].

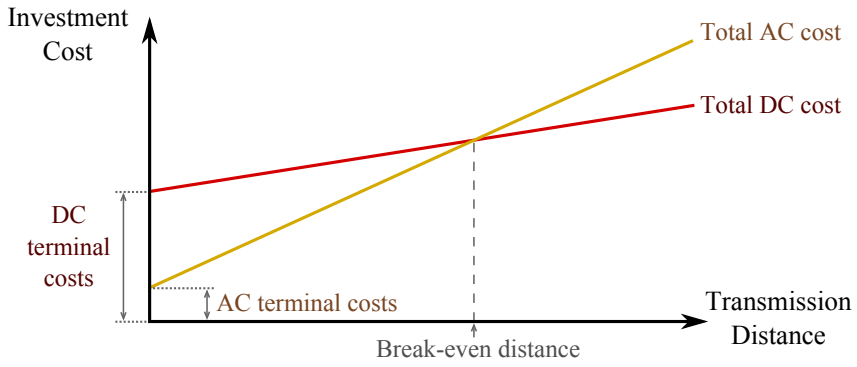

Figure 2.2: The investment cost of AC and HVDC subsea transmission with distance.

The two main types of AC-to-HVDC converters are:

- Line commutated converters (LCC) and
- Voltage source converters (VSC).

2.1.2 Strength of an HVDC-connected AC Offshore Network

The strength of the AC system can be represented by the short circuit ratio (SCR) as shown in equation (2.2), where the system consists of a Thévenin impedance (Z) and V is the voltage at the point of common connection [17]. The SCR is the ratio of the short circuit capacity to the rated power of the HVDC link (P_{rated}) [18]. The AC system strength is considered weak if the SCR is less than three [19]. The HVDC converters are very expensive and its limited power rating contributes to the weakness of the offshore wind farm network as well as the AC voltage and impedance.

$$SCR = \frac{V^2}{Z.P_{\text{rated}}} \tag{2.2}$$

2.1.3 Current Source Line Commutated Converters

Line commutated converters (LCC) for HVDC previously used large mercury arc valves from the 1930s until the advent of solid-state semiconductor thyristor valve technology in the 1970s. Thyristors are cost-effective and robust devices that can be easily stacked for high voltage and high power applications. Their conduction losses are low and they are able to withstand short-circuit currents, whereas most VSC devices are more sensitive and would require much faster protection. The LCC system for HVDC is also referred to as traditional, classic HVDC or LCC-HVDC.

Thyristors are not fully controllable; a gate signal switches on a positively biased valve device, but the device will stay latched on until the anode current falls below the holding current and is unable to switch off at will. The time from when the voltage across a thyristor valve becomes positive to the time when the gate is activated is known as the firing angle, and it is used to regulate the HVDC voltages on both ends of a point-to-point link to control the power. The nature of such delayed switching, means that the AC side current is always lagging the corresponding phase voltage and the LCC is always absorbing reactive power [20]. In order to balance the reactive power for voltage stability, VAR compensation is usually required, which is provided by passive capacitors and flexible AC transmission system (FACTS) devices such as static synchronous compensators (STATCOM) and may

further contribute to a larger overall system size.

A high level of harmonic distortion is produced by the discontinuous nature of the thyristor LCC bridge switching every half cycle of the AC fundamental, which requires large filters to eliminate them. Vast space is usually required to accommodate the filters as well as the converter, transformers, switch-yard, the valve hall and the extra clearance space for high voltage isolation. Traditionally LCC-HVDC systems were used for grid interconnections where converter stations were based on land, therefore size was not an issue. An offshore structure to support an LCC-HVDC station with such a large footprint is far too impractical and costly to install. Approximately 75% of the total cost of energy cost for WTs is already associated with the upfront cost of the infrastructure [21].

The LCC is a current source converter that requires a grid with a strong voltage source on both AC sides of the link to operate. The offshore network is weak and its voltage and frequency may need to be established and regulated by a separate generator powered with a stored fuel source or a VSC with electrical energy storage.

It has been suggested in literature that the LCC-HVDC converter stations can be strategically placed on a geographic island, which can also accommodate a small generator to support the AC voltage [22]. However, suitable uninhabited islands for this purpose do not exist within large Crown Estate Round 3 sites. The clear open sea is preferred, a land mass in contrast is usually regarded as an obstacle, which increases surface friction to air flow and thus reduces wind speed and quality.

2.1.4 Voltage Source Converters

Commutation does not fail in voltage source converters (VSC) as it would in an LCC during an AC grid disturbance. VSCs can allow forced commutation because they use semiconductor power electronic switches that are fully controllable for both turning on and off [23], such as gate turn-off thyristors (GTO), integrated gate-commutated thyristors (IGCT), insulated-gate bipolar transistors (IGBT) and metal-oxide-semiconductor field-effect transistors (MOSFET).

VSC technologies are more advanced but more expensive and induce higher switching and conduction losses than LCC. They have a wide range of industrial

applications, such as traction motors, drives and solar energy conversion, apart from applications in the wind turbine frequency converter and HVDC conversion. As popularity and demand increases they will improve and become cheaper, more reliable and more efficient.

VSCs are capable of independent active and reactive power control to allow four-quadrant operation. Reactive power control can be both leading and lagging, which can be used to control the voltage level without the need of VAR compensators and help improve the stability of the network.

Unlike an LCC, a VSC has black start capability and is able to provide a strong voltage source for the weak offshore WF network because its switching devices can turn both on and off, and force commutation.

Two-level VSC

The two-level converter, as shown in Figure 2.3, is the simplest VSC topology to design and control. The switching devices will selectively turn 'on' or 'off' to connect the AC side to either the positive or negative DC busbar. Therefore, the AC side voltage output from one leg of the converter has two states, which is either the plus or minus the DC voltage. When two converter phase legs are in the same state, the corresponding line to line voltage potential is zero, therefore the line to line measurements will appear to have three levels.

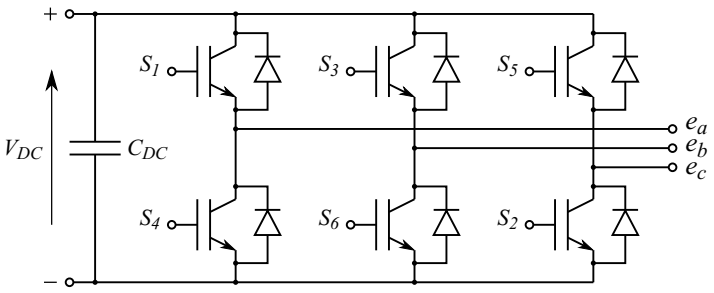

Figure 2.3: A two-level three-phase voltage source converter topology.

The wind converter industry often choose IGBT devices rated between 1 kV to 1.7 kV because of their availability and cost-effectiveness. The operating AC voltage rating is often limited to the low AC voltage level of 690 V, which is then stepped up to distribution voltage level by a transformer for the local collection network. The

price data of twenty-three IGBT devices in [24] is converted to Pound Stirling and the price per unit power rating (£/MVA) is calculated. The cheapest £/MW (in 2011) for each voltage level rating is then shown in Figure 2.4, which also demonstrates the cost-effectiveness of devices rated at 1.7 kV. The highest blocking voltage for an IGBT switch is currently 6.5kV [25]. Devices with higher blocking voltages including those based on Silicon Carbide (SiC) are at the moment much more expensive.

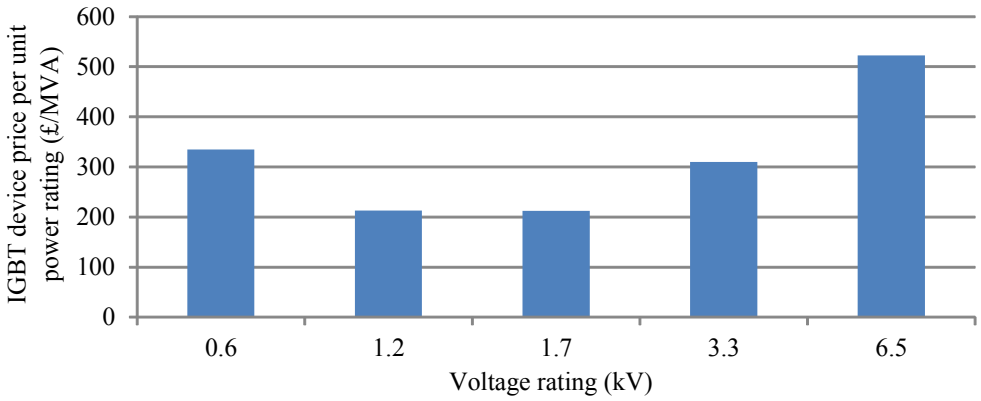

Figure 2.4: The cheapest IGBT device price per unit MVA rated power for each voltage level ratings between 0.6 and 6.5 kV, out of 23 devices in 2011.

VSC devices cannot be simply stacked for high voltage rating like how thyristors can. Each IGBT in series does not switch exactly at the same time, which leads to uneven voltage sharing between them during fast switching. This problem is magnified with higher switching frequencies and more devices in series. Therefore, devices with higher blocking voltages are preferred over stacking them in series to increase the overall voltage rating and reduce the on-state voltage drop per kV voltage rating. However, such devices are more expensive, so an active voltage sharing strategy or a multilevel converter topology may be used, although this will complicate the system and will require more devices.

HVDC Light® is the ABB Ltd trademark for VSC-HVDC because they are more lightweight compared to the traditional LCC-HVDC. The size of the VSC converter including the filter is more compact than an LCC of the same rating, which is ideal for offshore applications where space is a premium. More recent development by Siemens and Alstom has resulted in modular multilevel converter topologies which have demonstrated advantages in terms of implementation of a VSC. But from the

voltage control point of view, their response bandwidth is similar to a two-level PWM VSC. Therefore the difference in VSC topologies will not be very important in the control aspect part of this thesis.

The AC filter can be smaller and does not need to be very large to smooth the output voltage and eliminate the harmonic distortion that are at the higher end of the frequency spectrum. The higher the cut-off frequency, the smaller the size and the cost of the passive components in the AC filter. Offshore VSC technology is trending towards higher switching frequencies for this reason. The switching frequency of a GTO device is typically up to 1 kHz and for an IGBT around 2 kHz.

For each switching cycle, the switching loss per switching cycle is the product of the slight overlap of the falling voltage across the switching device with the rising current as it switches on and vice versa for switch-off. So for higher switching frequencies, however, this will add up to increased switching losses per second. This is in addition to the $V_{\text{on}}I + I^2R_{\text{on}}$ conduction losses and the total loss for a VSC can be much higher than an LCC. These losses then become a challenge to keep the device from overheating.

Pulse Width Modulation

In a two-level converter topology, pulse width modulation (PWM) is used for the switching sequence to modulate a sine wave for the AC side voltage. The simplest method to produce this, is to use a comparator with an input reference sine wave (V_{ref}) and a triangular carrier wave (V_{carrier}), as shown in Figure 2.5 and equation (2.3). The output PWM signal is then used to drive a switching device to turn 'on' or 'off'. A VSC is able to modulate any voltage between the + and − DC voltage, and its response can be as fast as the switching frequency.

$$\text{PWM signal} = \begin{cases} 1, & \text{if } V_{\text{ref}} > V_{\text{carrier}} \\ 0, & \text{if } V_{\text{ref}} < V_{\text{carrier}} \end{cases} \tag{2.3}$$

Scaling VSC for High Voltage and Power

To accommodate for a larger power capacity in VSCs, the number of switching devices needs to increase, which will increase the system complexity and cost. These

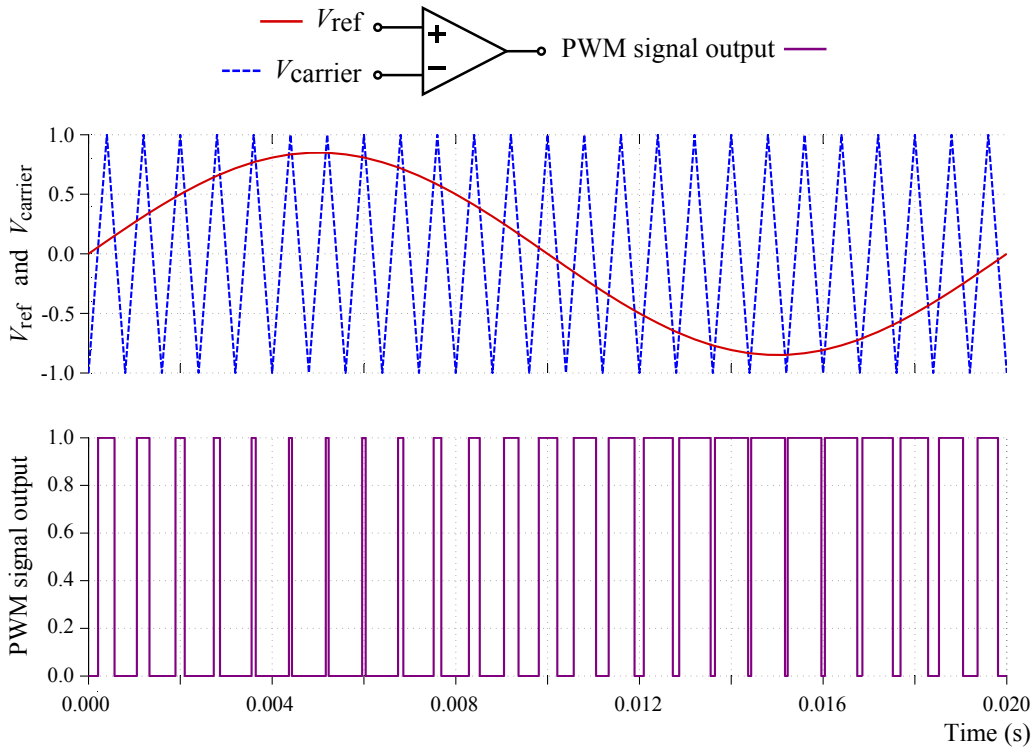

Figure 2.5: Using the comparator to generate the PWM signal from the sine wave reference and the triangular carrier wave.

can be connected in parallel to increase the current carrying capacity. However, for limited voltage level, currents will be much higher for higher power, which is not ideal if more conducting cross sectional area is needed to reduce losses. Connecting IGBT devices in series can increase the overall voltage level, but voltage sharing between devices during fast switching is an issue which requires active sharing voltage control [26]. Multilevel topologies do not inherit such issues, however the complexity of gate control and the number of devices is significantly increased.

Multilevel VSC

Using multilevel voltage source converter topologies is an effective way to overcome the limited voltage rating of single devices. Multilevel topologies can have three or more voltage levels in the converter phase voltage output. Three-level converters are typically rated between 3.3 kV and 6.6 kV AC. Increasing the number of levels will increase the voltage rating of the overall multilevel converter system.

Neutral point clamped and flying capacitor topologies are well known multilevel converters, but mainly popular with three levels. For higher number of levels, modular multilevel converter (MMC) topologies can be adopted [24]. Each MMC module will consist of either a half bridge of a full H-bridge arrangement, as shown in Figure 2.6. A half-bridge sub-module has two states, where it either connects the terminals to the capacitor voltage U_{sm} or it bypasses it. This will either add or drop a voltage level from the AC voltage output.

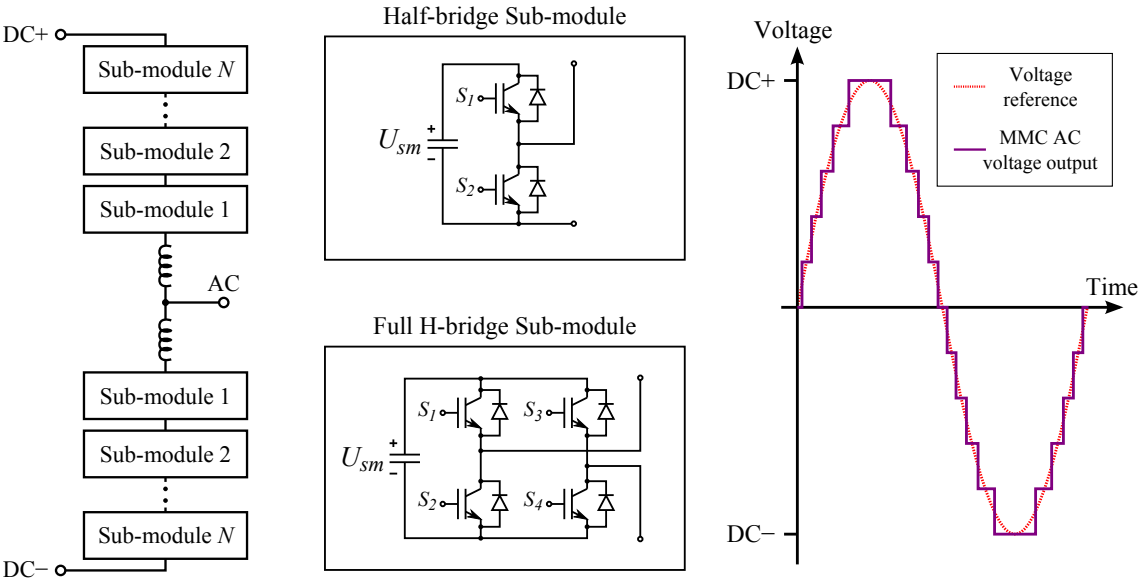

Figure 2.6: A phase leg structure of a modular multilevel converter, where each sub-module can be a half-bridge or a full H-bridge arrangement. An example of the AC voltage waveform output is also shown.

Although multilevel converters require more devices, they have lower levels of harmonic distortion in the converter voltage output compared to the two-level converter. Therefore electrical filters can be smaller or even eliminated. This will balance the weight and cost so the overall system can remain compact. The more levels there are, the more it can synthesise closely to the voltage reference waveform. Each IGBT will also experience low switching frequencies, therefore the switching losses are reduced.

Multilevel topologies require more IGBTs and their control is generally more complex so they are generally more expensive. Three to five level multilevel converters are becoming more readily available in industry, and the technology is advancing

towards maturity.

2.1.5 Switching Devices

The power rating verses the operational switching frequency for a selection of power semiconductor devices is shown Figure 2.7, which has been adapted from [27]. Higher switching frequency is a desirable characteristic for converter devices because it can drive down the size of the converter and filter system for offshore use and increase the control bandwidth. However, devices with increased frequency switching is usually associated with higher loss, expense and lower reliability, which often limits the power ratings too. Likewise, high power devices, such as thyristors and GTOs, tend to be limited to lower frequencies. The IGBT is at the middle ground for both power and high operational switching frequency, therefore is a popular choice for wind power conversion and VSC-HVDC.

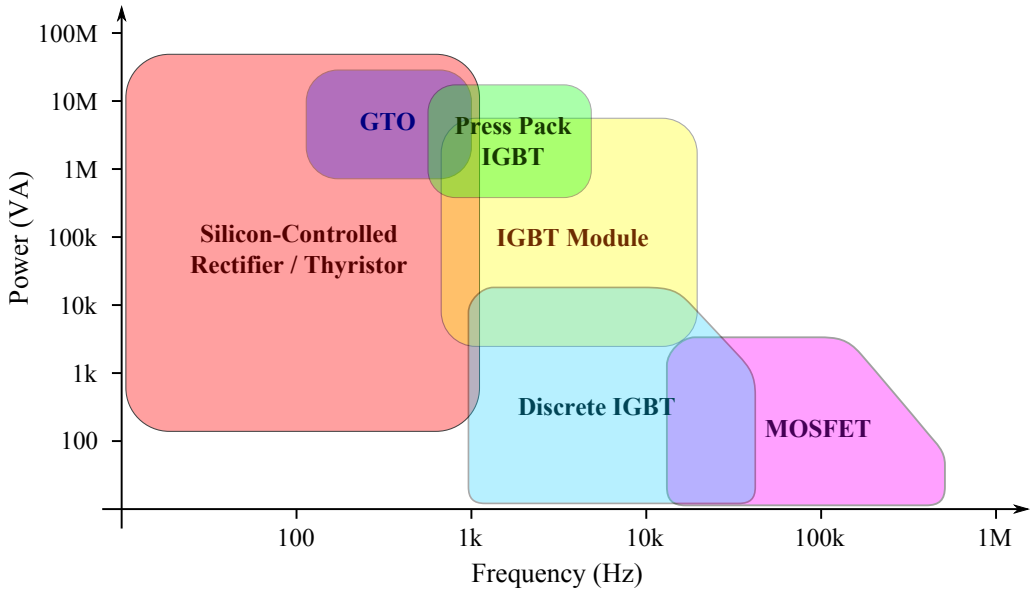

Figure 2.7: General ratings for power and operational switching frequency of power semiconductor devices.

This section further discusses in detail and compares other types of power electronic semiconductor devices and their potential for the future, such as those made from silicon carbide (SiC).

VSC Silicon Devices

A GTO device is a type of solid-state thyristor that is fully controllable because of the additional ability to turn off, where normal thyristors were unable to. Thus this enabled its application in high power VSCs. Its maximum dI/dt rating and the long switch-off time limits the switching frequency to about 1 kHz. An IGCT is similar to the GTO but with lower conduction losses and smaller cell size, however operating frequency is typically up to 500 Hz because the gate currents and switching losses are high, even though their switch-off times are much faster [20].

The IGBT is another gate controlled switching device, which has the combined advantages of a GTO in terms of high power switching capability with those of a transistor regarding low driving power and fast efficient voltages and current control in both the On and Off states. This results in a robust converter design and contributes to high reliability of the overall transmission scheme [28].

MOSFET devices have low switching losses and are able to switch at higher frequencies, which is ideal for compact applications. However they are not very attractive for high voltage and high power applications, because the on-resistance increases sharply with the breakdown voltage and therefore the conduction losses are higher.

Thermal management is important to keep the device cool, ideally operating under 125 °C junction temperature. As temperatures increase, so do the resistance and the losses. IGBTs and MOSTFETs are sensitive to over-voltage and over-currents as well as short circuits. A thin wafer IGBT has a very small heat capacity and therefore a short-circuit currents will lead to thermal runaway and failure after several hundred milliseconds. Silicon (Si) devices cannot withstand more than 150 °C [29].

Silicon Carbide Devices

The silicon carbide (SiC) semiconductor material has a wide band-gap and higher critical electric field meaning that higher voltages can be blocked with thinner and more conductive layers [30]. Although the current ratings of SiC devices are limited, the maximum achievable power level is compensated by the higher voltage rating.

One of the first commercially manufactured SiC devices available was the junction gate field-effect transistor (JFET), however these devices were not ideal for full-bridge VSCs because a high signal is used to switch off, and a failure in the gating signal will risk short circuiting the DC link.

The SiC MOSFET is a promising technology that has recently become commercially available, which can switch at high frequencies, handle higher voltages up to 10 kV and maximise energy delivery with higher efficiencies. The devices have very low switching losses allowing them to deliver switching frequencies in the tens and hundreds of kilo-hertz range. As a result, the switching harmonics become much easier to filter and the size of the passive components can be smaller, which can be an advantage for offshore applications [31].

The SiC MOSFET devices have smaller on-state resistance rate of change with temperature compared to silicon IGBT. The SiC is more tolerant to higher temperatures and is able to cope with thermal losses and therefore deliver more power. The cooling requirement may also be reduced, therefore the cooling system can be more passive, simplified, smaller, more robust and reliable [32].

In [32], Zhang also demonstrated that increasing the switching frequency of a SiC-based WT converter to 6 kHz; its efficiency is the same as the efficiency of a silicon-based IGBT converter switching at only 3 kHz, whilst the size, loss, and cost of the filter are reduced for the SiC-based converter because of the switching frequency is two times higher.

Chinthavali demonstrated that switching losses in SiC GTO are 12 times less than silicon GTO [33]. For the same blocking voltage, the SiC blocking layer is thinner, resulting in lower charge stored in the drift region and thus faster switching and lower conduction losses. For the same thickness, the breakdown voltage is five times higher than silicon, making the devices ideal for high voltage applications as well as high frequency.

Si-based devices are currently more established and mature than SiC-based that are still in their infancy with relatively high premature failure rates [34]. High temperature operation comes with challenges in the packaging of the device. Wind power is not constant and the device may experience extreme deep thermal cycling,

particularly the device in the machine side converter. This leads to high mechanical stresses and fatigue failure, particularly at the bond wire and solder pads [34]. The thermal characteristics of SiC are different from the traditional silicon and it must be packaged and bonded to new suitable materials that are also tolerant to high temperatures up to excess of 400 °C and possess similar coefficients of thermal expansion [35, 36]. At present, commercial SiC devices are all based on packaging technologies for silicon devices. Therefore the high temperature capability of SiC material is yet to be exploited in the future. Ringing oscillation from high frequency fast switching is a reliability concern as it stresses the devices and causes additional switching losses [37].

SiC IGBT devices rated up to 15 kV are currently under development but are not yet fully commercially available. Such high blocking voltage capability presents opportunities for transformer-less grid connections, and simpler topology design with reduced numbers of DC levels and semiconductor switches [38].

2.1.6 LCC and VSC Hybrid HVDC

The main drive for hybridising the LCC with VSC is the lower cost of LCC power conversion and the control benefits of the VSC. Already LCC-HVDC systems have been proposed with VSC-STATCOMs for supporting the voltages at the terminals [39, 40]. The VSC can also establish voltage frequency in the weak decoupled offshore WF network, where LCC cannot provide a voltage source by nature. The VSC can be connected to the same DC voltage source as the LCC instead of a standalone capacitor or battery as found in a STATCOM. The bulk of the power conversion is through the LCC because of its lower losses. There is also potential to use the VSC to provide active filtering, reducing the passive filter requirement which is already large for the LCC.

The voltage polarity of the LCC HVDC link is reversed in order to change the direction of the power flow, as the current can only flow in one direction in the LCC. This is different for VSC, which cannot accept a change of voltage polarity because its anti-parallel free-wheeling diodes would conduct and short circuit the HVDC connection. This is a conflict in the state of operation. An MMC with full H-bridge

modules, which is also shown in Figure 2.6, can operate at reversed polarity, where the half-bridge arrangement could not. This presents opportunities to hybridise the full H-bridge MMC with LCC-HVDC [39]. However, H-bridge MMCs require two times more IGBT devices compared to the half-bridge MMC arrangement. They also have higher power losses because the current is also flowing through twice as many cascaded devices. A WF network is usually only generating so the net power is unidirectional most of the time, if an LCC system is used, its polarity does not need to be reversed most of the time. The VSC can provide power flow in the opposite direction to support standby power consumption and for black start-up of the remote network.

In [40], the VSC and LCC was proposed to take turns in operation for power transmission and connection to the HVDC cable. Only the VSC is connected during low and reverse power operation, because the minimum power of LCC is 5% to 10% of the rated power. Operation with both the LCC and VSC connected to the same HVDC cable is only temporary in the transition phase. During high wind speed and power operation, only the LCC will be connected to HVDC cable because the maximum power can be transmitted at an optimum power factor and at a higher HVDC voltage level, which is usually too high or expensive for a VSC system. The VSC is disconnected from the HVDC and operates as a STATCOM instead and provide reactive power for the LCC and stabilise the voltage level.

The VSC and LCC does not have to share the same HVDC poles, and separate cable in-feed poles may be used. In [41, 42], the LCC and VSC HVDC stations have dual cable in-feeds to a remote network. The LCC converter was shown to be immune to commutation failure and the increased overall rating of the conversion system also improves the short circuit ratio, and therefore strength of the AC network.

2.1.7 Multi-terminal HVDC

A multi-terminal HVDC system has more than one HVDC link and at least three converter station terminals. A flexible number of HVDC cable interlinks between converter station can be established. As cables have the longest post-failure down-

times, which will be also explained in Section 2.3.6, such a system can provide better cable redundancy and system availability [43]. If an HVDC converter station or an interlink is down, the rest of the system can maintain operation.

However, the main challenges for multi-terminal HVDC is protection. Semiconductor devices in VSC-HVDC converters are more sensitive to fault currents than devices for LCC-HVDC due to fast thermal runaway, therefore protection needs to be very fast acting. At the moment, circuit breakers for HVDC are expensive or not fast enough for protection [44]. Normally, a two-terminal HVDC link is isolated by the AC side circuit breakers. If the same method is used for a multi-terminal HVDC system without HVDC circuit breakers, the entire HVDC network has to shut down in order to isolate a single fault inside it and then reconnect it back to the AC system again. This is not ideal as the main intention of multi-terminal is to increase the redundancy and the availability of the connection.

Sudden disconnection of an entire WF can also be detrimental for grid stability. Therefore, energy storage on both sides of the network would be ideal to maintain smooth power flow. Until HVDC circuit breaking technology improves, multiple two-terminal networks seems like a more reliable option. High energy storage capacity is expensive for ensure continuous power flow, therefore the shut-down, isolation and reconnection processes must be very fast in order to minimise the duration of the disturbance and the energy storage capacity needed. The capacitance in the DC network may need to be low to allow the DC voltage to quickly drop for shut-down and rise back up quickly when restarting the system again.

2.1.8 DC Circuit Breakers

When a circuit breaker opens while under load, an arc is often formed between the separated contacts. The arc is still electrically conductive so the circuit is not broken until this arc is extinguished. Normally, circuit breaking with AC is simple as the current waveform has enough zero-crossings to interrupt the arc. It is usually more difficult and expensive to break a DC fault circuit quickly because there are no zero-crossings in the fault current and a DC fault current would rise more quickly [45].

DC circuit breakers are being actively developed and DC networks are getting

"closer to reality" [46]. However, DC breakers that will be commercially available will be considerably more expensive, have limited voltage ratings and slower breaking speeds than AC circuit breaker.

2.1.9 The Cable

The cable is the most necessary component for electrical connection of the wind farm, whether the power is transmitted as AC or HVDC. The main conductor material of choice is usually aluminium or copper. Copper has 70% higher conductivity than aluminium, but 3.5 times more expensive (based on May 2015 metal prices). The material and thickness of the conductor will determine the ampacity of the cable.

Cable Insulation Material

The material and thickness of the cable insulation will determine the voltage rating of the cable. The most popular cables for underground and sub-sea applications are mass impregnated non-draining (MIND) cables and cross-linked polyethylene (XLPE).

MIND cables have very high voltage and power ratings, up to at least ±500 kV DC and 2000 MW for bipolar operation. They are traditionally used in LCC-based HVDC because the system needs to be large scale and high power to be economic viable.

The XLPE material for insulation is the popular cable insulation material of choice for VSC-based HVDC systems because it is cheaper, lighter, more flexible and easier to manufacture. Despite a limited maximum voltage level of up to ±320 kV the XLPE can withstand and about 1000 MW power rating, it is therefore ideal for VSC-based HVDC systems which are of similar ratings. Their converter stations are already very expensive with limited power rating, therefore it is difficult to justify using expensive MIND cables. Furthermore, VSC does not reverse in polarity as LCC does when reversing the power flow direction. Therefore this reduces the influence of polarity reversal on the space charge accumulation that decreases the insulation performance of polyethylene [47].

Moisture ingression into the XLPE insulation material will increase the formations of ions and therefore increase the conductivity of the material [48]. Impurities, cavities and defects in the insulation also increases the conductivity and shortens the life of the cable. It becomes inclined to water tree breakdown, which is a failure mechanisms in XLPE cables as the breakdown voltage is significantly reduced [49]. Overall, the voltage rating of XLPE is lower than MIND cable insulation for a given thickness.

Other Layers in the Cable

A semi-conducting screening layer between the conductors and the XLPE insulation layer is often necessary to distribute the electrical stress. This helps to prevent electrical discharge that can damage the insulation at certain points of the cable. An armour protection layer is usually needed for sub-sea applications to minimise mechanical damage caused by the likes of fishing trawlers and ship's anchors.

Circulating currents and eddy current can be induced into the metal sheath layer and armour outside the insulation layer of the conductor, contributing to further losses in the AC cable power transmission, which can be 30% of the total, but sometimes this is required as the metal sheath layer prevents moisture ingression and acts as an electrostatic shield and a current return path [50].

Cable Cross-sectional Formation

A three-phase cable in trefoil formation has reduced magnetic field around the conductor because the fields from each phase cancel each other out. Therefore its net cable inductance and sheath armour losses are smaller. This is also why the armour of a three-core cable can be made of steel-wire while it should be non-magnetic for a single-core cable. However, high voltage XLPE cables above 275 kV are not available in the three-core trefoil format because thicker insulation material is required, which can then affects the overall size.

Single-core cables are more flexible, has minimal mutual heating and improved cooling with the wide core separation. As a result, this increases the current rating of the core conductor as shown in Figure 2.8. However, it may not be efficient

overall because the armour losses are higher. The current induced into the armour can be as high as the currents in the conductor [51]. However, the core conductor and insulation material layer can be made thicker per single-core cable, for higher current and voltage ratings and therefore higher power capacity.

DC cables on the other hand, do not have the additional losses associated with the AC frequency, therefore the current carrying capacity of a DC pair with close spacing is comparable to a set of AC cables with wide spacing.

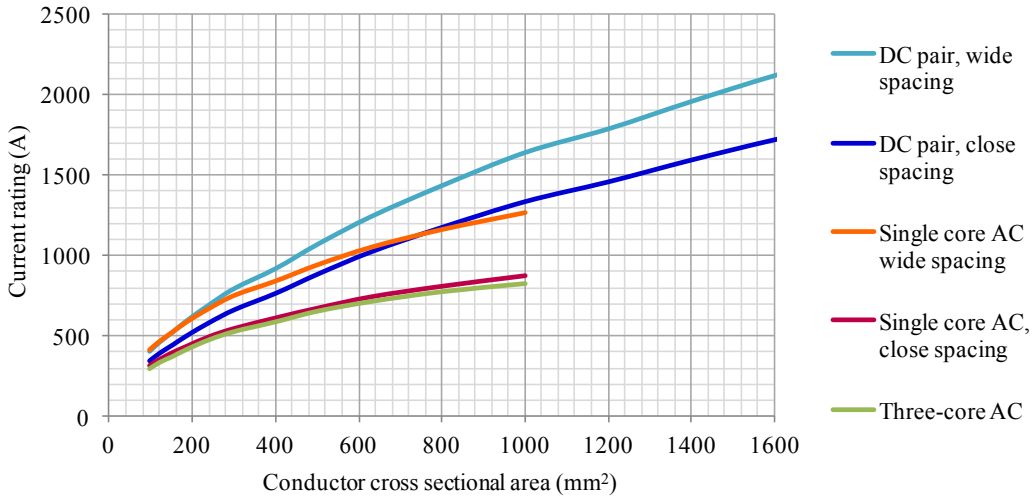

Figure 2.8: The current carrying capacity for various types of copper cables against the conductor cross sectional area, data source: [51].

Capacitance in the Cable

There is significant capacitance in a power cable compared to overhead lines. How much extra capacitance also depends on the separation space between the conductor and outer sheath layer and their surface area. Generally the capacitance decreases with higher voltage ratings because the insulation is thicker, and with smaller current ratings because the conductor diameter is smaller and therefore the circumference surface area is smaller.

2.2 The Offshore Wind Turbine

This section will focus on the basics of the wind turbine (WT) structure, theory, operation and market trends. The characteristics of the WTs is reviewed in order to design and adapted the network topology and electrical system effectively around them.

2.2.1 Wind Turbine Structure and Sub-assemblies

Figure 2.9 shows a typical structure and sub-assembly of an offshore horizontal-axis WT. The foundation, tower, nacelle, hub and the turbine blades are the structural assemblies of some of the most bulky parts to install. The offshore foundation secures the WT in place, either as a structure fixed on the sea bed or as a floating structure for expansion into deeper waters.

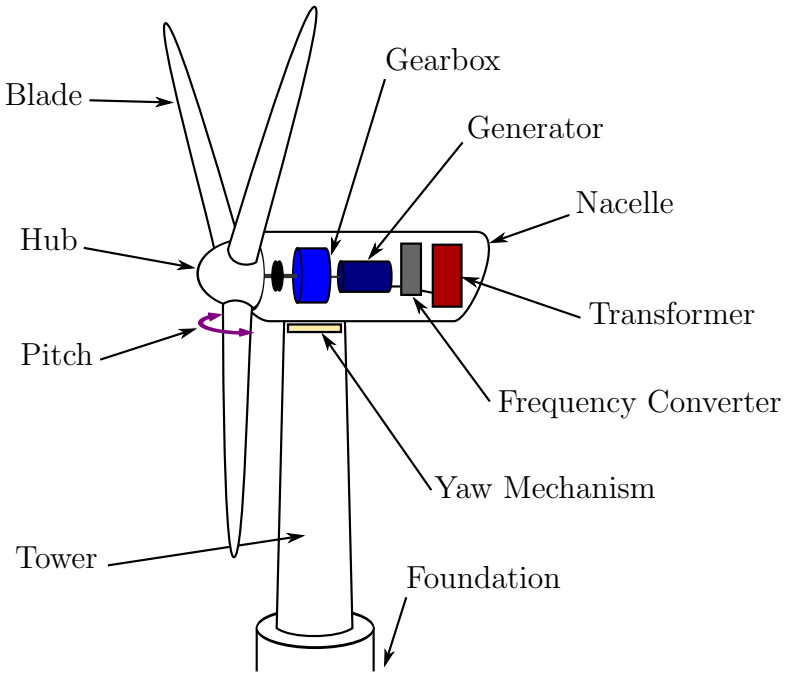

Figure 2.9: The wind turbine structure and major sub-assemblies

The nacelle of a WT will usually house the mechanical-electrical sub-assemblies. Depending on the turbine type and size, the nacelle will typically house the drive train, gear-box, generator, frequency converter, transformer and controllers. WTs that use pitch control will have the actuators inside the hub that will adjust the

rotor blade pitch angle.

Most large WTs will track the direction of the wind and an active yaw mechanism will yaw the turbine so that it directly faces upwind. Due to the nature of the yaw mechanism, flexible loop cables are used for the electrical connection between the tower and the nacelle. This is allowed to be fully twisted about four times in either direction before it is required to rotate back to the starting position.

2.2.2 Wind Power

The power the WT can extract from wind is shown in equation (2.4):

$$P = \frac{1}{2}\rho A v^3 C_p \tag{2.4}$$

where ρ is the density of air, A is the wind turbine blade swept area, v is the wind velocity and C_p is the power coefficient.

The wind speed v and the density of air ρ cannot be controlled as they depend on the weather conditions. However, the swept area A can be made larger by increasing the blade diameter in order to maximise energy capture. The power coefficient C_p is the ratio of the power extracted to the total power in the wind, which primarily depends on the efficiency of aerodynamic blade design, tip speed ratio and MPPT capability of the WT. In theory, a wind turbine cannot extract more than 16/27 (59.3%) of the kinetic energy in wind, as defined by Betz's law [52].

The tip speed ratio λ is the ratio of the tip speed of the WT blade to the speed of the wind (u). This is defined in equation (2.5), where ω is the rotational speed of the rotor in rad.s^{-1} and r is the rotor diameter. A typical relationship between the power coefficient and the tip speed ratio for a typical horizontal axis WT is shown in Figure 2.10, where the curve data for this graph is from [53].

$$\lambda = \frac{\omega r}{v} \tag{2.5}$$

2.2.3 Scale and Size

The cost of offshore structures and foundation costs are very high. WTs are becoming larger, wider in diameter and more powerful in order to maximise revenue from

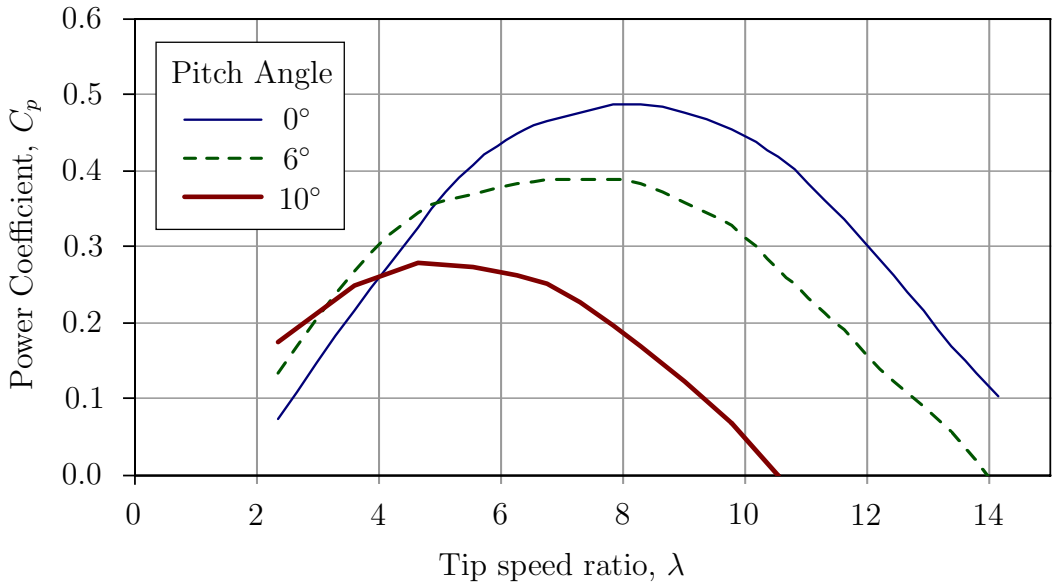

Figure 2.10: The power coefficient against the tip speed ratio curve C_p–λ curve for different blade pitch angles.

power production and returns for the large investments being made [54]. Already they are some of the world's largest rotating machines and are projected to continue to grow in the future. Figure 2.11 shows the growth in WT size over the years since early small scale onshore WT [21]. Scaling up the technology is not simple. As the wind turbines become larger, there is a general trend that they become less reliable because the complexity is high and field-experience is less [55].

2.2.4 From Fixed Speed to Variable Speed WTs

Historically, electrical wind turbines connected to the grid operate at a constant rotor speed that is proportional to the grid frequency. The ultimate speed ratio depends on the gear-box ratio and the number of poles in the generator.

Fixed speed wind turbines are not aerodynamically efficient for capturing the power from the wind over a wide range of wind speeds. If the rotor speed is constant, the tip speed ratio λ is then inversely proportional to the wind speed (equation 2.5). As the tip speed ratio varies with wind speed, then the power coefficient C_p will not always be optimal and will vary as shown in Figure 2.10. When the wind is too far above the rated wind speed, the fixed speed WT passively stalls and the power coefficient inherently reduces, so the power is limited and maintained around the

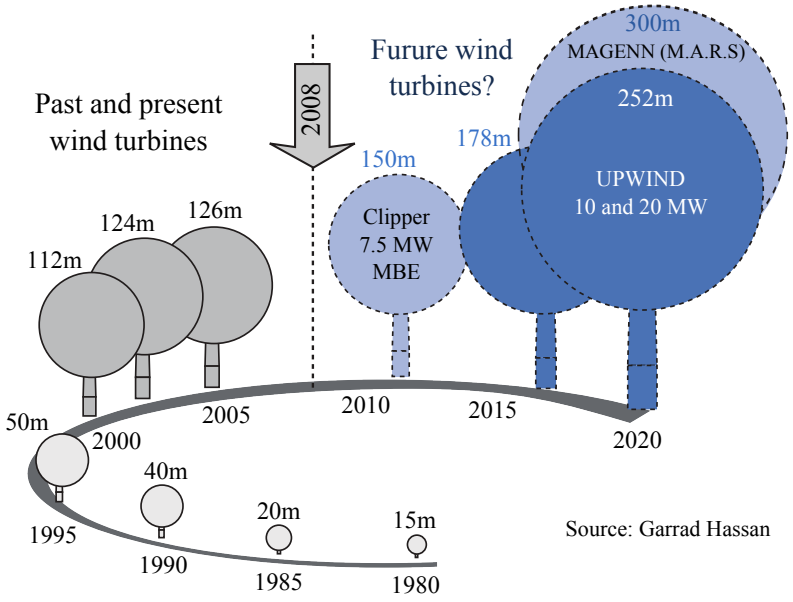

Figure 2.11: Growth in size of commercial wind turbine designs [21].

system rating. Fixed speed machines need to be able to tolerate high mechanical stress and torque fluctuations that can lead to fatigue, which is more undesirable in larger turbines.

In comparison, a variable speed WT is more efficient at capturing the energy across a wide range of wind speeds [54]. More power is captured using variable speed than fixed speed operation for the same turbine blade swept area size, and therefore the structural and mechanical investment is fully utilised. A maximum power point tracking (MPPT) control technique will make sure the rotor speed varies with the wind speed. The tip speed ratio λ is kept constant where the power coefficient C_p is at its maximum, which is typically when $\lambda = 8$ as in the case shown in Figure 2.10.

Active stall control or pitch control will be necessary to limit the power above rated wind speed. Active stall control slows down the rotor speed so that λ and C_p decreases. Pitch control will adjust the rotor blade pitch angle of attack, which alters the C_p–λ characteristic for reduced power coefficient as also shown in Figure 2.10.

2.2.5 Wind Turbine Generator Types

As shown in Figure 2.12, there are four key types of WT generator configurations: fixed speed turbine (Type A), limit variable speed turbine with variable wound rotor resistance (Type B), variable speed with partially rated converter (Type C) and variable speed with fully rated converter (Type D) [9, 56]. The dotted lines around the gearbox for Type D indicates that it may be direct drive without a gearbox. Offshore wind turbines are predominantly variable speed turbines.

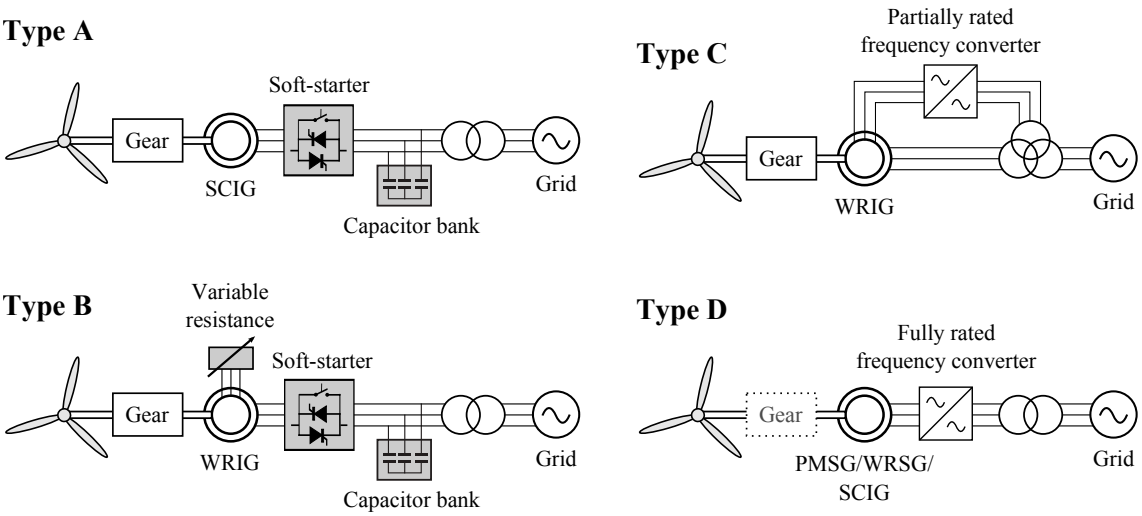

Figure 2.12: Typical wind turbine generator configuration types.

Induction Machines

There are two kinds of induction generator builds: the squirrel cage induction generator (SCIG) and the wound rotor induction generator (WRIG). The SCIG have been used in fixed speed wind turbines, although technically the generator is an asynchronous machine, the slip speed is usually very small with insignificant impact on the tip speed ratio. The SCIG is very robust because no electrical connections or high maintenance slip rings are required to the rotor circuit as the rotor magnetic field is induced by the stator. The speed of the magnetic field in the stator is defined in equation (2.6), where p is the number of pole pairs.

$$N_s = \frac{60f}{p} \tag{2.6}$$

The rotor speed of the induction machine is usually asynchronous to the synchronous N_s. The slip speed is the difference between the asynchronous speed N_a and synchronous speed. The slip in percentage for generation is defined in equation (2.7), where N_a is the asynchronous speed of the rotor.

$$\text{Slip}(\%) = \frac{N_a - N_s}{N_s} \times 100\% \tag{2.7}$$

The WRIG is similar to the SCIG except the construction of the rotor has sets of windings that can be connected externally through slip rings. A Type B wind turbine has rotor windings that can be connected to a set of variable resistors, which controls the current and flux in the rotor to vary the slip speed. If the winding resistance is zero and short-circuited, it will then operate and perform like a Type A SCIG. Although power is lost through the resistors when in use, it offers a limited degree of variable speed, up to 10% above the synchronous speed, for better wind energy extraction [56]. The slip is typically around 2% at rated torque with a short circuit rotor without resistors. Figure 2.13 shows the torque-speed characteristics for a range of rotor resistances, and shows how the slip speed can be varied for the same given torque. If the torque reaches the maximum point, the machine then becomes unstable and over-speeds.

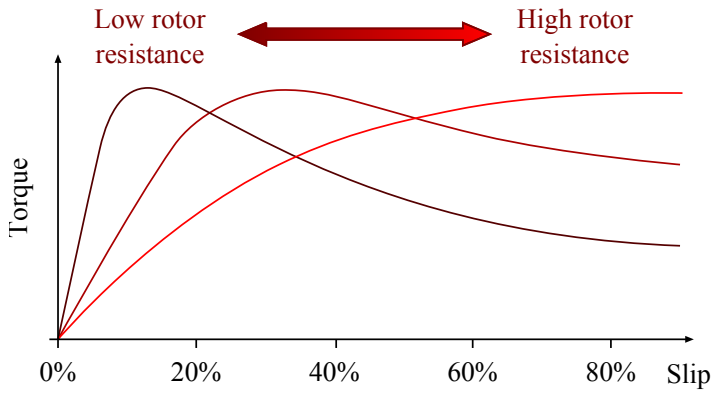

Figure 2.13: The torque-slip characteristic of an induction machine for a range of rotor winding resistances

The OptiSlip® system by Vestas is a Type B wind turbine, but the resistors that are controlled by a set of switches are inside the rotor of the machine, and the resistance is controlled through optical communication link. This eliminates the

need for slip rings for external connections to the windings and therefore improves the mechanical efficiency [57, 58].

The magnetic field of rotor is induced from the stator and always lags behind. Regardless of whether it is generating or motoring, the induction machine always consumes reactive power, even at no-load, which then increases with torque. As the size and power of this WT type is scaled up, so will the reactive power consumption, which will lead to voltage stability issues in the grid. Shunt capacitors are usually required to provide the reactive power and compensate for this. Both Type A and B wind turbine generators will usually require a soft-starter to limit the in-rush currents during start-up magnetisation [59].

The WRIG could then operate as a doubly fed induction generator (DFIG) if the rotor windings are three-phase and connected to a power electronic converter. A DFIG machine can operate at a greater rotor speed range compared to WRIG with variable slip. The converters can be smaller and partially rated compared to the overall WT rating because they only feed the rotor to provide speed control while most of the power is fed through the stator directly to the grid. The partially rated converter for the DFIG can also independently control and contribute to reactive power for the benefit of grid voltage balance.

Permanent Magnet and Wound Rotor Synchronous Machines

A synchronous machine will have a rotor speed equal to the synchronous speed N_s, which is proportional and synchronous to the electrical frequency f to according to equation (2.6). A wound rotor synchronous generator (WRSG) is usually more expensive and larger than other generators types of the same rating. The rotor magnetic field of the WRSG is usually electrically excited by a DC source from a rectifier or converter, connected externally through slip rings. By varying the rotor excitation field with the rotor current, the reactive power can be controlled to absorb or supply, unlike the induction generators where reactive power is always consumed and cannot be controlled.

A permanent magnet synchronous generator (PMSG) is a type of synchronous generator except that the excitation is self-provided by powerful permanent magnets

instead of field windings inside the rotor. The DC supply and slip rings for the field excitation are no longer required, therefore the design is simpler, mechanically more efficient and maintenance free. However, the rotor magnetic field is always constant so the reactive power cannot be controlled, and the permanent magnets are very expensive and in limited supply [54].

Brush-less Generators

The PMSG and the SCIG are inherently brush-less generators, but for the WRSG, its slip rings and brushes can also be eliminated. This can be achieved if the rotor DC currents are supplied through a brush-less exciter, which effectively acts as another small generator on the same shaft that feeds a converter inside the rotor and shaft [60]. This will be mechanically more efficient, but the build will be much larger in size and more expensive. Furthermore, from a maintenance point-of-view, access to external converters are simpler than converters inside the rotor and shaft. Power electronics devices need to have easy access for repair and maintenance, because they have a high failure rate which will be shown in Section 2.3.

The brush-less WRSG is a commonly used for large conventional fixed speed power plants. However, fully rated converters are needed to decouple the stator voltage and frequency from the grid in order to operate as a variable speed WT. The fully rated converter together with the converter for the rotor field variable DC voltage supply leads to a high total number of power electronic devices in the overall system.

A brush-less DFIG is similar to a brush-less WRSG, except the brush-less exciter and a converter from inside the shaft will supply as set of three-phase rotor windings. The field be rotating relative to the rotor frame instead of a DC field as with the WRSG. The stator can be connected directly to the grid as with a normal DFIG, no slip rings and brushes are need for the connection to the partially rated converter inside the rotor shaft, less maintenance is required and will be mechanically more efficient as a result [61]. However, difficult access of the power electronic components inside the rotor is still an issue.

Fully Rated Converters at the WT

Type D wind turbine generators are fed through fully rated converters. They can operate with most generators, typically with the PMSG or SCIG that are inherently brush-less, mechanically efficient and low-maintenance. The system can be gear-less as a direct direct drive concept with low speed multi-pole PMSG machines.

SCIG machine are mechanical efficient and low-maintenance as they do not require slip rings because the rotor current is induced by the stator at the slip frequency. The SCIG on its own is used as a "fixed" speed WT or as the Type A "Danish concept" WT. PMSGs are also mechanically efficient, but as synchronous generators, their speed is inherently fixed and proportional to the grid frequency. For full variable speed control, the stators of these generators are connected to a fully rated back-to-back AC-DC-AC voltage source frequency converter.

The converter decouples the machine speed from the grid frequency. The losses can be significant since all the power is fed through the fully rated converter. However, the converter offers more controllability, such as with providing reactive power, and the grid-fault ride-through capability is less complicated than the DFIG [59].

Passive capacitor banks for reactive power compensation of SCIGs are eliminated. The active inverter on the machine-side should establish the stator voltage for the SCIG. It should be able to supply the reactive power for the lagging magnetising currents so the rotor field can be induced.

On the other hand, the rotor field in a PMSG is provided by permanent magnets and not electrically excited, therefore the EMF can be self-induced onto the stator. This means that generation can be black-started without power from the grid connection or energy storage. The induced AC can then be converted to DC using lower cost passive diode rectifier. The speed of the PMSG will depend the DC-side voltage level, which is controlled by the grid-side converter or boost converter. They produce harmonics and torque ripples that affect the life of the turbine [62]. Therefore a controlled active inverter will be preferred with minimum harmonics in the voltage and torque which will have a lesser impact on larger scale systems.

Trends in Market Penetration

Type A and B fixed speed WTs are gradually fading from the market, while Type C and D that are both variable speed WTs are gaining popularity. Veriable speed WTs have a higher overall power coefficient and are therefore able to extract more power from the wind and hence maximize return gains for the revenue and power.

The DFIG WT (Type C) has been the most popular among small to medium scale wind turbines, where in 2010 this technology type composed of 55% of the market share of wind turbines in Europe [63]. The converter for Type C is usually smaller and partially rated compared to the fully fed and fully rated converter for Type D. When the converter devices were more expensive, the converter size difference was enough to favour the cost-benefit of Type C and its small converter size.

However, as power electronic converters are becoming cheaper and more efficient, the market penetration of Type D WTs has been gradually increasing over the years and it is expected to continue to increase due to their superior grid fault ride-through control performance and mechanical efficiency [56]. As wind turbines increase in size and move offshore, the cost of the structural and mechanical installation are much higher, and the cost of additional power electronics becomes relatively less significant.

2.2.6 Maximum Power Point Tracking

As each turbine in a wind farm will experience a slightly different wind speed due to the wake effect, the maximum power point tracking (MPPT) becomes very important because it maximises the aerodynamics efficiency so the most power is exacted for a given wide range of wind speeds.

The aim of MPPT is to keep a constant tip speed ratio λ where the power coefficient C_p is at the maximum, which is typically around $\lambda = 8$ for a zero pitch angle as shown in Figure 2.10. MPPT is typically used while under the rated wind speed until the maximum power rating is reached, pitch control is then used to limit power so it does not go beyond the WT ratings. MPPT control requires the wind

speed and the rotor speed feedback.

Only full variable speed wind turbines can provides the best MPPT, using Type C DFIGs or the fully rated frequency converters in Type D. In recent years there has been an increasing market penetration for these types of wind turbine technology [64]. Although they can capture more energy to increase the capacity factor, they are more complex and require power electronics that are currently less reliable compared to other more matured wind turbine components.

2.2.7 The Wind Power Curve

The graph in Figure 2.14 shows the wind power characteristic curve against the wind speed, along with the Weibull probability distribution of the wind speed for two different average wind speeds. A constant tip speed ratio and power coefficient for a variable speed wind turbine with MPPT is assumed [9].

The wind power curve assumes the cut-in wind speed is 3 m/s, rated wind speed is 13 m/s, and the cut-out speed is 25 m/s. Below the cut-in wind speed, it is usually not worth operating because the power generated after losses is insignificant.

For a large proportion of the operation time, the wind power is generated between the cut-in and the rated wind speed. Here the wind power is proportional to the cube of the wind speed, according to equation (2.4), assuming the maximum power coefficient C_p is constant for a WT under MPPT control mode.

Between the rated and the cut-out wind speed, the WT is at the maximum constant power control mode. This is usually carried out under pitch control mode, where the pitch angle of the rotor blades is adjusted to limit the aerodynamic power to protect the WT so that it does not exceed its mechanical and electrical rating.

2.2.8 Weibull Wind Speed Distribution

The continuous Weibull probability distribution against wind speed for average wind speed of 8.5 m/s and 9.8 m/s is shown in Figure 2.14. These continuous approximations are based on North Sea offshore wind data, respectively from the MPN and K13 observation stations [65]. Weibull probability $W(v)$ is a function of the wind

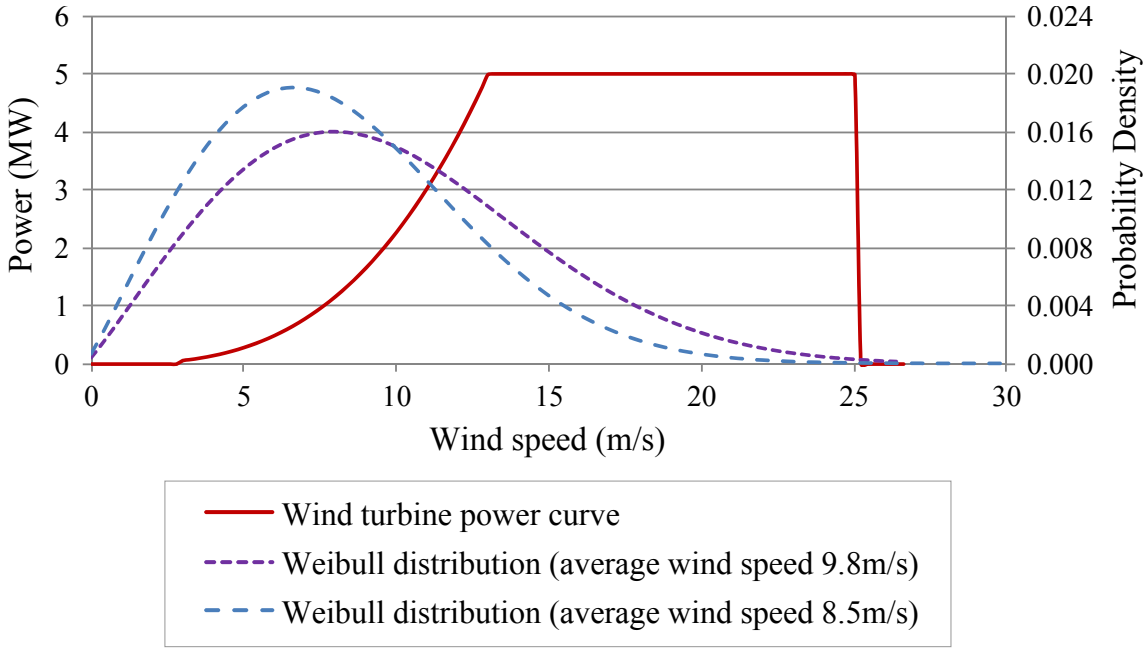

Figure 2.14: The wind turbine power curve against the wind speed and the Weibull wind speed distribution curves.

speed v, which is calculated using equation (2.8):

$$W(v) = \frac{k}{v}\left(\frac{v}{a}\right)^k \exp\left(-\left(\frac{v}{a}\right)^k\right) \tag{2.8}$$

Parameters for the MPN station are $k = 2.1$ and $a = 9.3$m/s, and from the K13 station, they are $k = 2.1$ and $a = 11.1$m/s. Where k is the shape factor and a is the scale factor. Discretisation of the distribution should factor in the size of the discrete intervals to maintain the sum to unity, ie. $\sum_{v=0}^{\infty} W(v) = 1$.

The K13 station has the fastest average wind speed because it is the furthest away from the shore, about 100 km, and the most central in the North Sea between Norfolk and North Holland. The MPN station is located nearer to the shore off the coast of the Netherlands. The measuring height above mean sea level is 74.8m for K13 and 27.6m for the MPN station. The difference in these heights may also be a factor for the the difference in the average wind speeds. In comparison, a large WT rated at least 5 MW would typically have a hub height about 80m or higher. The two sets of data will be considered as a best case and worst case scenario in this thesis.

2.2.9 Spacing Between Wind Turbine due to Wake Effects

The wake effect is when the rotating blades of the wind turbine produce turbulent air wakes that will reduce the wind speed for another wind turbine downstream, which will extract less power compared to if it was exposed to direct free air [66]. They will also experience fluctuating loads due to the turbulence, which eventually leads to fatigue damage, particularly on the yaw bearings [67]. It is important that wind turbines need to be spaced out, typically around 8 times the diameter of the rotor, so the wakes can expand and return to free-stream condition and the impact of turbulence is minimised. According to [68], 5MW sized wind turbines should have at least 700m distance between them, therefore a wind farm of a hundred turbines will occupy an area of at least 7km by 7km.

As offshore wind turbines are expected to be more powerful and bigger, as discussed in section 2.2.3, then the spacing between the WTs is expected to increase in order to mitigate the wake effects. This will have an impact on the cost of cabling because the cable ratings and lengths need to increase in order to respectively cater for the increased power and distances.

2.3 Reliability and Downtime

This section will introduce and discuss how the WF reliability and accessibility from onshore to offshore has an impact on its downtime and availability. The section is mainly focused around the sub-assemblies and components in the electrical and control system.

2.3.1 Onshore WT Reliability

Emphasis has been traditionally placed on the reliability of mechanical parts, such as the turbine blade, rotor, gear box and the drive train. These are often bulkier and heavier than electrical components, therefore repairs and replacements are expected to be more difficult, costly and with longer downtimes [69]. As a result, as shown in Figure 2.15, onshore wind farms tend to have lower failure rates in these components [70].

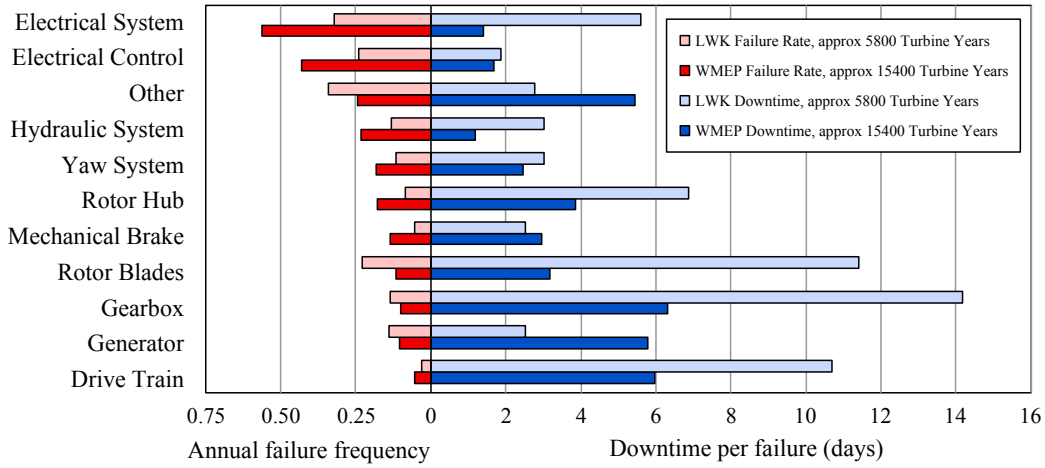

Figure 2.15: European onshore wind turbine reliability and downtime data from two surveys over 13 years [70] (data used with permission).

In the electrical system, however, further onshore reliability data as shown in Figure 2.16 suggest that the power module has a very high failure rate, particularly with the the frequency converter. Complex converter sub-assemblies, which are made up of many components with relatively short thermal time constants, are generally more likely to develop partial if not full failures due to thermal fatigue. Components that are critical to the operation of the WT system have the greatest impact on its availability [71].

Access to onshore WT by road is simple, and components in the electrical part of the system tend to be smaller and therefore problems and failures are relatively easier and quicker to resolve. Therefore the downtime length per failure in the electrical system is generally shorter as shown in Figure 2.15. However, when the failure occurrence is high, the overall downtime of these components shown in Figure 2.17, can be as significant as the failure rates shown in Figure 2.16, even if the downtime per failure is short.

2.3.2 Reflecting Onshore Experience to Offshore

Offshore horizontal-axis WTs were originally directly derived from onshore ones, and therefore share similar components. Extra measures to hermetically seal components are taken for protection from moisture and the harsh salty offshore environment. Corrosion was the main root cause of WT sub-assembly failures [72]. This ultimately

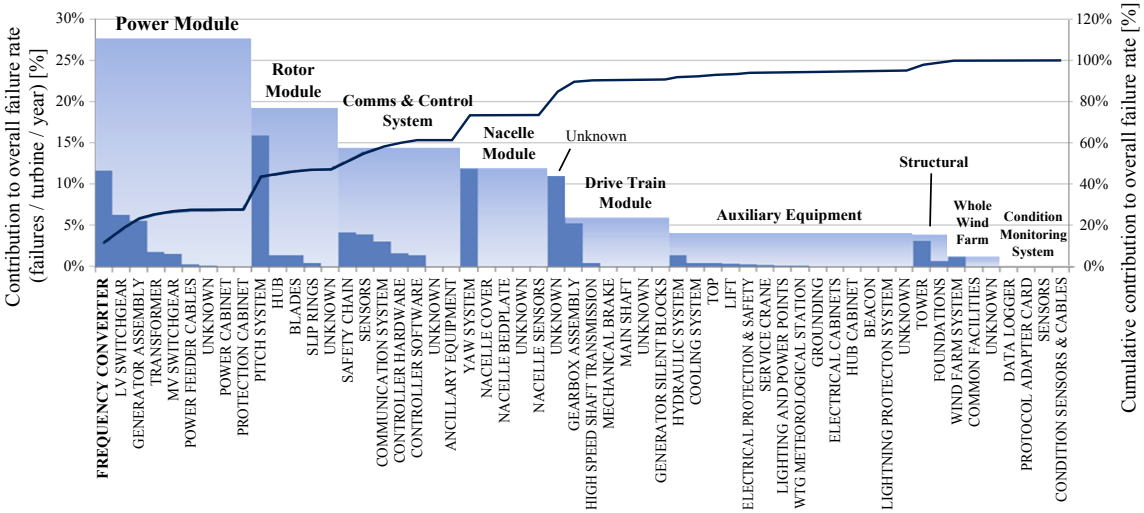

Figure 2.16: Normalised overall failure rates of sub-systems and assemblies of wind turbines of multiple manufacturers [69] (data used with permission).

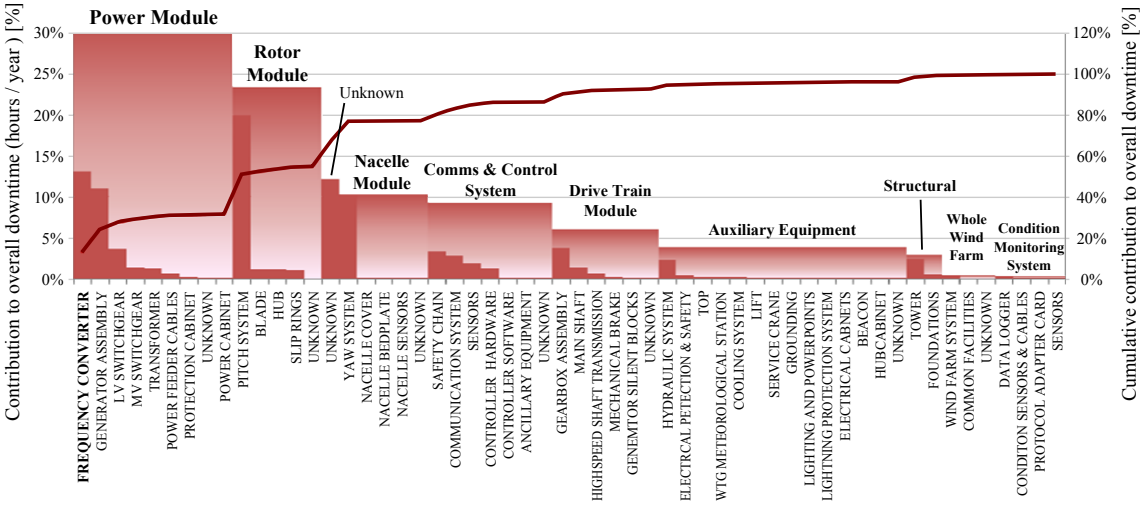

Figure 2.17: Normalised contribution to overall downtimes of sub-systems and assemblies of wind turbines of multiple manufacturers [69] (data used with permission).

contributes to higher costs for offshore reliability.

However, should a failure occur in an offshore scenario, the downtime would be much more significant with distance due to access issues, which also depends on the sea conditions and wind speeds [73]. Longer downtimes contribute to loss of power generation and revenue, especially during the windiest period in winter. The limited access further prolongs downtime, and the WT will be unable to capture wind power during the most windiest period [74]. The wave height is also another barrier for access by water even when it is not windy. Repair is often delayed until the conditions are calm enough for a time frame that is long enough to carry out the work [75].

2.3.3 Current Offshore Experience

Offshore reliability data are limited and relatively recent compared to onshore data. For the Egmond aan Zee offshore wind farm in Figure 2.18, it is shown that the gearbox and generator have the highest downtime per stop, taking an overwhelming proportion of the total downtime, respectively 55% and 15%. This is one of the main reasons for trending toward gear-less direct drive WT. The control system contributes to 36% of the stops and 9.5% of its total downtime [70]. This offshore wind farm is relatively close to shore between 10 and 18 km from the coast. The distribution of the downtimes will change as future wind farms become more remote and inaccessible.

Converter failure rate is low in this case and contributes to about 2.3% of the total downtime. It is unknown whether this is because the data was gather during the healthy phase of its life before the wear-out stage. It is also worth noting that in Figure 2.18 is not fully representative, because only 180 turbines years were gathered over a period of three years, which is only a fraction compared to the data gathered for Figure 2.15. Operators may also already expect a relatively short life span for converters from historical data so they may have them serviced regularly, maintained or replaced early to avoid failure during operation.

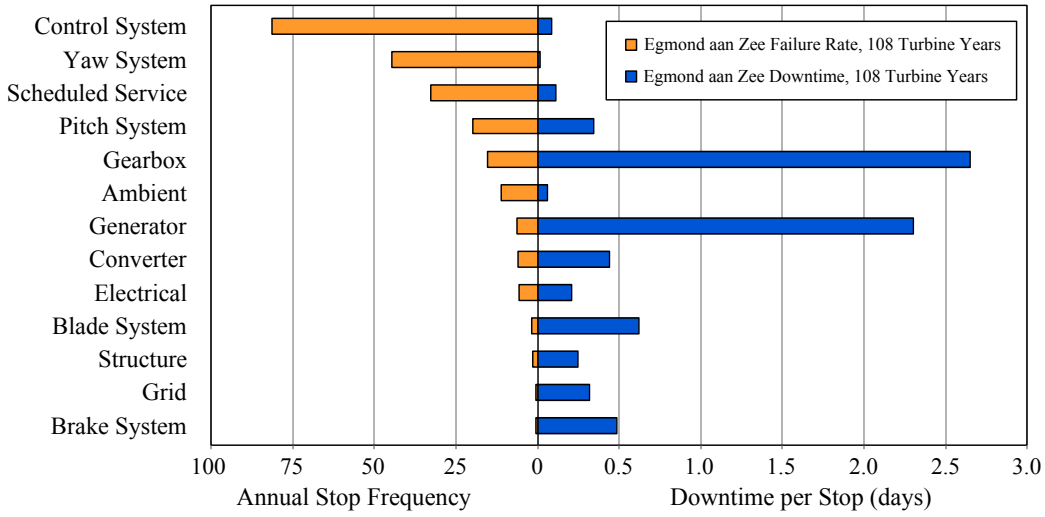

Figure 2.18: Stop rate and downtime data from Egmond aan Zee offshore wind farm in the Netherlands, 108 WT years over 3 years [70] (data used with permission).

2.3.4 Control System and Sensor Reliability

As shown in Figure 2.18, the control system in the Egmond aan Zee offshore WF has the highest annual stop frequency [70]. Some failures, such as in the sensors in the control system, could not be reset automatically or remotely and therefore require manual repairs which will in turn contribute to down time and loss of energy production [76]. Elsewhere, up to 76.5% of supervisory control and data acquisition (SCADA) alarms could not be reset remotely [77].

In [73], sensors are ranked third highest failure rate after the electrical system and control in WTs installed throughout Germany. Swedish data in [78] showed that sensors ranked second after the electrical system, with the highest number of failures. The control system is ranked fifth for failure rate in this case, but it is ranked second for total downtime.

A control system may have many sensors and communication channels for feed-forward and feed-back control within a WT local system. A sensor failure would cause loss of control and undermine the system performance and operation of a WT [79].

2.3.5 BorWin1 Project – HVDC Connected Wind Farm

The BorWin1 project is the first HVDC connection serving an offshore wind farm. The 125 km long submarine and 75 km long underground cables connecting the BARD1 offshore wind farm with mainland Germany, is rated 400 MW and operates at the nominal voltage of ±150 kV [80]. The converter stations are ABB HVDC Light® systems that use IGBT based two-level converters.

Although BorWin1 was commissioned in 2009, it was not without problems operation-wise. The system has suffered from a number of unplanned outages due to AC filter failure, voltage rise overloads and harmonics issues [4]. The root cause is unknown and full technical details were not publicly disclosed.

A system needing repair or maintenance needs to plan a shut-down in order to safely carry out the work. This is usually planned for low wind speed conditions that are favourable for access and the loss of wind power generation is minimised. However the window of opportunity to carry out the work is usually very small. Therefore the amount of maintenance required should be minimised and the speed of the jobs should be maximised. Experience with Borwin1 project found that the shut-down for routine maintenance had to be extended for some months because of difficulty in completing this over the severe winter [81].

2.3.6 Cable Reliability

The subsea cables are the most critical component for offshore wind power availability for the grid. They are normally very robust and reliable, but if a fault occurred anywhere along the cable, locating it for repair is extremely difficult and time consuming and can lead to outages for a significant period [82].

Manufacturing of the XLPE insulation can be improved to reduce the impurities that lead to water-tree breakdown failure. However, faults caused by external damage or force can occur, for example, by ship anchors and fishing trawlers, which are outside the direct control of the system and its operators. This will require liaison with the relevant industries to reduce such risks.

2.3.7 Failure Intensity over Time

The failure intensity curve over time of a system, although mostly valid for mechanical devices, is often characterised as "bathtub" shape as shown in Figure 2.19. The graph starts high during the introduction and infancy of a new system, often because of inexperience, insufficient testing and missed manufacturing faults. As these early faults are detected and fixed, experience accrues and the reliability improves, the failure rate lowers and stabilises for the duration of its useful life, until it increases again due to wear-out towards the end of their service [55]. Borwin1 was the first of its kind, and risked experiencing early problems, commissioning delays and reduced capacity factor but the reliability of such new technologies are expected to improve over time with continued development.

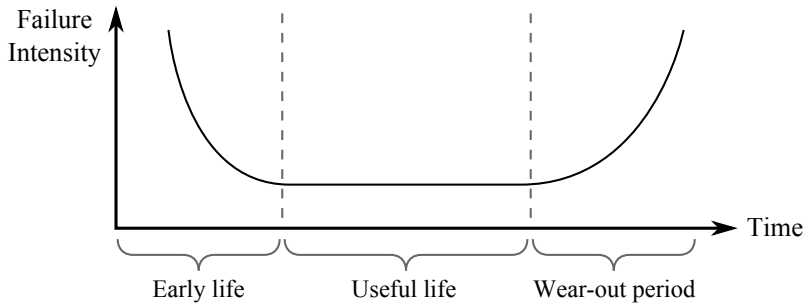

Figure 2.19: Failure intensity over time "bathtub" characteristic curve of a system, typically of mechanical devices.

The Reliawind project, which ended in 2011, had identified that more rigorous pretesting should be performed in order to reduce the early life failure. The use of more reliable components, preventative, reliability centred and condition based maintenance should be adopted to improve the useful life period. Major sub-assembly change-out is recommended to limit failure intensity rise during the wear-out period [69].

2.3.8 Non-constant Wind Power Thermal Cycling

Wind is not constant and therefore the wind farm is not always going to operate at full capacity. However, generators, converters and transformers will have to be rated approximately 15% higher in practice because fluctuating power generation from

non-constant wind speeds cause thermal stress cycling, which then leads to fatigue failure. This is especially for converter devices that have low thermal capacity and the temperature cycle is deeper [83]. The effect of temperature changes in a WT generator leads to micro-cracks or de-lamination between the iron core and stator insulation [84].

2.3.9 Pitch Control vs. Stall Control

Section 2.2.7 discussed that pitch control is used for limiting the power to the rated maximum level, between the rated wind speed and the cut-out wind speed. Pitch control is usually more precise for reducing the aerodynamic power in higher wind speeds, and keeping the rotor speed and torque constant and under the rated power.

However, the sub-assemblies for pitch control mechanisms tend to have high failure rates and downtimes for both onshore and offshore as shown in Figures 2.16, 2.17 and 2.18. A pitch control system is very complex. The change in the pitch angle of the rotor blades are usually driven by a motor with some power electronics or a hydraulic pump system. Power is usually fed into the hub using slip rings, which occasionally require maintenance, and access into the hub is very challenging.

Active-stall control is another method for limiting the wind power, usually by reducing the rotor speed at high wind speeds for a suboptimal tip speed ratio λ, moving the power coefficient value C_p down from the maximum. It may seems to be more reliable to not use pitch control mechanisms that have high failure rates. However, the active-stall method increases the torque by as much as 40% compared to pitch control [85]. It is more expensive to increase the rating of the mechanical sub-assemblies for higher torque demand, which will still need the extra margin in case of sudden gusts.

2.3.10 Maintainability

Condition monitoring and maintenance is important to extended the operation life of components and prevent catastrophic failures. WTs have become advanced, complicated and expensive with more use of power electronics, control circuits, sensors

and actuators. It is expected that the high costs will be compensated by higher returns from more power being extracted from wind per WT generator. However, if the increased complexity generally leads to high failure rates, the impact on the operation and maintenance (O&M) costs will be high, especially for distant offshore wind farm with challenging access. Ideally, the design of the system should ideally be as robust as possible so maintenance can be simple, quick and minimal. On the other hand, a robust design of a system may also be expensive because of the extra materials and redundancies required.

2.4 Grid Frequency Support from the WF with Energy Storage

The United Kingdom has a vast wind resource compared to other renewable resources available. As more wind energy is harnessed, and so will the impact on the grid system increase. Wind power is variable in nature and the timing of its production does not necessarily correlate with the timing of the load demand. As the share of variable wind energy production increases, larger fluctuations and stability problems in the power system may arise as a result when the grid inertia is not sufficient to absorb them [86].

An imbalance in the active and reactive power between the generation and demand will affect the frequency and voltage stability of the grid. The converters in Type C and D WTs are able to control the reactive power injected into the grid, and therefore help with the voltage stability. However, frequency support is challenging without significant energy storage, spinning reserves, flexible loads, smart grid controls, and stronger UK grid interconnections with mainland Europe in the future.

It would be more expensive and inefficient to curtail the power production of large conventional power plants in the power system. Their time constants are very large and will not be fast enough respond to the fast wind power fluctuations. The additional load cycling on the generators also leads to fatigue failure and decreases its lifetime. Financial returns from investments in such assets will be significantly

reduced. Pumped-storage hydroelectricity can provide energy storage and load balancing, but the scale of power is low and there are limited geographical sites with suitable hight and water availability.

It is the wind farms that are producing stochastic power that are contributing to grid problems, therefore the wind farm should ideally contribute to the cost of power balancing and grid support. Instead of fully relying on the grid operators to keep the system stable, the wind farms should, and can, provide partial grid frequency support [87]. However, the incentives for implementing such ancillary services are insufficient and inconsistent at the present [88].

2.4.1 Grid Fault Ride Through

In the past, small WTs can simply disconnect from the grid to protect themselves from over-currents during a low voltage event in the network. However, as wind energy penetration into the grid is increased, a loss of power generation from a disconnection of a large wind farm during a grid fault event will cause the voltage and frequency to drop further. The problem will then cascade to other devices, cause them to disconnect and destabilise the grid. Therefore the grid code requires large WT devices to have grid fault low voltage ride through capability [89]. This capability could be easily implemented in Type D configuration WTs, but is more challenging for Type C (see Section 2.2.5).

During low voltage ride through, either the current output is increased while power is constant, or current is controlled and the output power is reduced. Depending on the control strategy used, it may lead to a temporary over-voltage in the DC link or over-speed of the WT rotor with torque reduction. This can be avoided with the help of an energy storage device at the WT to absorbs any excess power.

2.4.2 Wind Curtailment Reserves vs. Energy Storage

Wind energy can be curtailed when there is too much wind, or this energy can be stored and then released later when needed the most. Either of the two methods can smooth the wind farm power output, so they behave more like conventional

generators with controllable fuel source and power.

Wind power curtailment requires little additional investment to implement. Modern wind turbines already have stall and/or pitch control, which is often used for limiting the mechanical power to the rating of the system as mentioned in Section 2.2. When the grid frequency is too high, pitch controls can be used to reduce the coefficient of performance (C_p) and therefore curtail power generation. However, the grid more often requires support when the frequency is too low, to prevent it collapsing. In this case, some wind power capacity should be reserved during normal operation [90]. Reserving capacity can be achieved by proportionally limiting power below the maximum power point. When the grid requires the extra capacity, the limit can be lifted back to maximum power extraction.

Wind turbines already have a low annual capacity factor that is typically less than 40%. Power curtailment will further reduce this capacity factor. The actual wind power generation does not always coincide with the demand. Therefore the opportunity for operating at the maximum power point and maximum revenue from power production is reduced.

Sufficient energy storage will be able to minimise wind power curtailment and therefore maximise power production and energy security. If energy pricescontinue to increase in the future as non-renewable source diminish, and the wind capacity factor is low, it will be more valuable to capture whatever wind energy is available and store it for later use. However, it is currently difficult to justify very expensive large scale energy storage options. At the moment the electricity market tariffs are subsidised and favouring wind energy, but it will not be sustainable in the future as grid penetration of unpredictable variable wind energy grows and becomes a large source of grid voltage fluctuation and instability. There needs a flexible pricing strategy and market design, where the wholesale price of electrical energy depends on the real-time demand. Although stochastic generation may be penalised or disadvantaged, the strategy can provide reasonable incentives to fund energy storage, reserve capacity and ancillary services that help balance and stabilise the grid [91, 92].

2.4.3 Energy Storage Located Offshore

The wind is not always blowing when there is onshore demand. While the turbines are not producing power, the spare current carrying capacity in the cables is available to export any stored energy to supply any demand onshore. Therefore a large offshore energy storage system will fully utilise the investment of the HVDC connection even when it is not windy. It will support the main grid during times of uncertainties when onshore demand is either too high or too low. The smoothing effect of the power flow provided by storage can also reduce fatigue degradation caused by thermal cycling from non-constant wind power, for example in the packaging of power electronic device modules. Smooth out the operational peak can also help reduce the cost of needing to over-rate such devices.

A DC multi-terminal network that needs to shut down in order to isolate a DC fault using simple circuit breakers as described in Section 2.1.7. For such a case, the grid connection for the WF is temporarily lost. Therefore, if energy storage exists on both sides of network, this will provide continuity of power flow to keep the system stable until the network connection is established again.

Batteries and super-capacitors are compact high capacity energy storage solutions that are ideal for offshore use. Super-capacitors for wind energy applications have been gaining attention in recent days [93]. They are highly regarded for their high power density, efficiency and life cycle compared to their battery counterpart. Batteries generally have a higher energy capacity and lower self-discharge rate. The fundamental drawback of providing such energy storage for the wind farm is the cost. As both development and demand of these technologies increase, they will become more affordable, not just for the power system and wind industry, but for other markets too [94].

Cost is the primary limiting factor for the total storage capacity as energy storage technologies for offshore applications are at their infancy, particularly in regards to their expensive power electronics interface. The total contribution for grid support may not be significant in comparison to a conventional power plant spinning reserve. However, power electronics can act very fast, well within a few hundred milliseconds and will be able to provide early power ramping for a short period of time until larger

capacity spinning reserves respond. Larger capacity energy storage and spinning reserve devices, such as compressed air and high-speed flywheels, can be cost effective for onshore and inland build. However offshore builds for such devices require more expensive offshore structures because they are much larger and heavier.

2.4.4 Energy Storage Concept in the HVDC Cable Capacitance

Electro-static energy in the HVDC-link capacitance can be extracted to provide an inertial response for grid frequency support [95]. The distance of future offshore wind farms to shore are estimated to be between 80 and 300 km. As the distance and number of cables increase in the HVDC network, the total cable capacitance may become significant to store energy. Some energy in the capacitance in the HVDC link can be extracted when the HVDC voltage is dropped. How fast this energy can be released depends on the control speed, the peak instantaneous current rating, and the relative stability of the system. Even if the power level being transmitted is low, there is still energy in the capacitance in the HVDC system while the voltage is high and still fully charged.

Assuming an HVDC subsea cable is 190km with a capacitance of 0.17 uF per kilometre [51], the total cable capacitance can be 32.3 uF. This may seem small, but the stored energy increases quadratically with voltage. Using equation 2.9, it can be estimated that a 15% voltage drop from 330kV would allow the extraction of 488 kJ from the cable capacitance alone. It is equivalent of a small 1MW wind turbine providing full power for half a second, although this is an insignificant small fraction of the total rating of such a system which could be typically rated around 500MW.

$$E_{\text{cap}} = \frac{1}{2}C(V_{high}^2 - V_{low}^2) \tag{2.9}$$

With potentially hundreds of turbines in a farm, collectively the same concept of energy extraction may be applied for the DC link capacitor in the wind turbine system with converters. However, there is a limit to how far the voltage can be dropped. For constant power, current rises as the voltage is dropped, so the current

rating of the system is then a limitation. Furthermore, the HVDC voltage cannot be lower than the peak AC voltage, otherwise the free-wheeling diodes will conduct and recharge the DC side from the grid.

The cable capacitance alone is usually not enough for DC voltage smoothing. Even if extra capacitance in the HVDC system is added for that purpose, the total storage would not be enough to provide meaningful grid support, except for some energy contribution in the initial power ramping. In the case of an HVDC transmission fault, if very large capacitors are connected at the HVDC side, they should be disconnected to prevent the extra energy feeding the fault that would cause further damage. This would require additional expensive HVDC circuit breakers, which adds to the cost of the system.

Using a higher DC voltage than necessary for storing more charge also increases the voltage stresses, which reduces reliability of capacitors and IGBT devices [96]. It would not be cost effective to increase the voltage rating of an already very large expensive system to handle larger voltage range for the purpose for energy storage.

The maximum energy storage capability of capacitors cannot be achieved with a limited voltage range. In order to fully achieve the maximum voltage range for maximum energy storage, they should be interfaced with additional power electronics and controls [97]. This interface should also help isolate these capacitors in case a fault develops inside it.

2.4.5 Energy Stored in the Moment of Inertia

Providing grid support without dedicated energy storage is challenging. The mechanical energy stored in the moment of inertia of a single wind turbine rotor may be small, but in a farm where there will be hundreds, the stored energy combined can be significant. Power can be extracted from the kinetic energy in to rotation of the blades momentarily by suddenly slowing them down [98].

During normal operation speed, the rotor should be already spinning faster than the MPPT speed. It would then slow down towards the maximum power point to extract more mechanical energy from the wind as well as to recover the stored energy in the inertia. The drawback is that it would undermine the investment

of the wind turbine because the speed is not always aerodynamically efficient to extract the maximum power. The turbine rotor and drive train are expensive and bulky assets that are more difficult to repair and maintain. A sudden change in torque may adversely affect the mechanic integrity, but can be avoided if there were additional auxiliary energy storage [99].

Although larger inertia is able to smooth the power output, the energy capture would be less [100]. A lighter variable speed wind turbine with less inertia is also able to track the maximum power point more quickly and a lighter design is usually simpler and cheaper to install. If this is the case, the inertia in the rotor may not be practically enough for energy storage.

2.4.6 Communicating Power Demand using Frequency Droop without Hard-wire Communication to WTs

If energy storage is used and distributed across the many offshore wind turbines, there needs to be an effective means of communicating the onshore demand so the wind farm can contribute to grid support when needed the most. In a conventional power system, the frequency is an indicator for the active power balance between generation and demand. If the frequency droops, generators often have governors to increase the power production to meet the load demand to prevent the frequency from running away or collapsing. A grid support system through generation should react fast enough, which helps minimise the cost of interruption from load shedding.

A droop control method of communicating the onshore demand for offshore wind energy to respond to was proposed in [101]. The concept artificially couples the onshore grid frequency to the offshore AC network. A change in the onshore grid frequency would trigger a change in the HVDC voltage and in turn this is detected to trigger the change in frequency in the offshore network. The decision of how much power the wind turbine should export is based on the frequency of the network it is connected to.

From a reliability and maintenance point of view, this droop control communication method is preferred because it does not depend on an auxiliary long distance subsea hard-wire communication link. Such infrastructure is expensive and any fail-

ure in the cable is difficult to trace and repair. Even wireless data transmission may have drawbacks such as poor reception during bad weather and possible vulnerability to interference and hacking. The droop control method functionality can be included in existing equivalent electrical control systems at no extra cost, as simply programming to the new control strategy is only required. Alternatively, it can be used as the backup communication system for grid support in case the hard-wire communication link fails.

2.5 Chapter Summary

- The cost of offshore wind energy is much higher than onshore, but it is a vast available resource in the UK, able to supply growing energy demands and meet government set renewable and decarbonisation targets.
- The thyristor devices for LCC are efficient, reliable, robust and cost effective for bulk high voltage power conversion. The large harmonic distortion, a consequence of low frequency switching, needs to be attenuated by filters that would be too large to be supported by offshore structures.
- Switching devices technology for VSCs are trending towards higher frequencies for better control bandwidth and smaller filter requirement. IGBT is currently the device of choice for the power electronic applications of today. Their reliability and cost performance has considerably improved in recent years. Silicon carbide is a promising technology, but still at its infancy and therefore very expensive and currently not reliable enough for offshore use due to packaging issues.
- Multilevel converter topologies have higher voltage ratings and smoother phase voltage output. They do not have the same problem as series connected IGBTs, however, the topology demands a higher number of switching devices and a higher level of complexity.
- Regardless which power electronic device and converter topology will be used, the average voltage source output and the overall control dynamics will be

similar. Therefore a simplified voltage source model may be used and dynamics studies. The principal difference is in the harmonics injected to the system and the filter size requirement. The switching frequency may also determine maximum speed of control.

- Literature survey revealed that the electrical system had the highest failure rate for onshore WT systems, which was mainly in the frequency converter and control system. Reliability offshore is extremely important. If a component fails, the downtime will be more severe because offshore access is difficult. Maintainability is also important to maintain high system reliability. Better accessibility of sub-assemblies can improve the repair rate and minimise downtime. In order to maximise the overall wind power production and availability to the grid, both the failure rate and downtimes must be reduced. An improved system topology that is also cost effective is needed to address such issues.

- A calm window of opportunity for access for maintenance and repair is usually very small, due to difficult offshore conditions. The system should be designed to speed up and minimise the amount of these types of work.

- Providing energy storage is expensive but would benefit the stability of the onshore grid frequency. If the energy storage can be situated offshore, protection and stability is also provided for the offshore network and WT in case the grid connection is lost. Smoothing the power flow will minimise the thermal cycling and maximise the reliability of the power electronic converter devices.

Chapter 3

Offshore Wind Farm Collection Network Topologies

The conditions and constraints for future offshore wind farms far away from shore are very different compared to current near-shore offshore wind farms. As discussed in Section 2.3, the power electronics have one of the highest failure rates that contribute to high total downtime, and the cable is usually very reliable but has the longest post-failure downtimes. This chapter will discuss the feasibility of topologies that eliminate certain components in the systems. Components and subsystem, such as the generators and cables, are fundamental and cannot be eliminated. However, the number of converter stages and transformer stages may be reduced from the wind farm electrical system, with the aim to improve robustness and reduce cost. Alternatively, such components may be moved and centralised so that access is better for faster repair and maintenance. However, centralising the fully rated frequency converters for WTs will require a different network topology and more cables, because of individual maximum power point tracking control constraints and therefore opposing desired frequency operation between each WT. Overall, this chapter focuses on the design of network topologies that are generally orientated to improve the overall system reliability, availability, accessibility, repair rate and maintainability. The benefits and challenges that arise from the proposed topologies are evaluated.

3.1 Centralising the Power Electronic Converters

To improve the access for repair and to reduce the downtimes caused by frequent failures of power electronics, a new concept is suggested to relocate and centralise all the power electronics in the offshore substation platform as shown in Figure 3.1. The time and cost for regular maintenance of these components can also be reduced because they are accessed in one centralised location and they are no longer distributed across individual wind turbines, while high above in the nacelle. Centralising the converter system allows common components to be shared, such as the cooling system and the transformers.

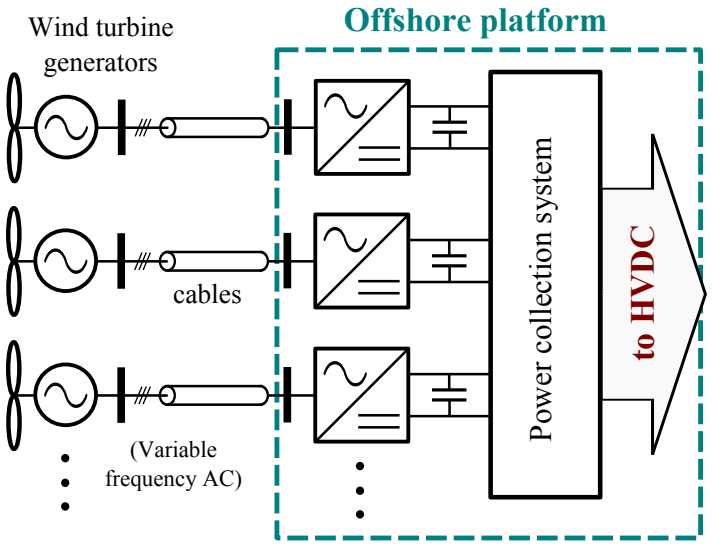

Figure 3.1: Concept with power electronic converters grouped at the offshore platform

Before conversion to HVDC, the power can be collected either on the AC or the DC bus. This is where the interconnection can be made between multiple substations in the wind farm network. The DC voltages from each converter set could even be connected in series as an option to build up the voltage to the HVDC level [102]. Sharing the DC-link using a DC bus in a centralised topology may also simplify the topology in terms of construction. However, the operation of sharing a DC-bus is very similar to a multi-terminal DC network but more compact. They will also share the same disadvantages and challenges with the DC-side fault protection as discussed in Section 2.1.8. Where the option is to use very expensive circuit breakers or to deal with the fault event by temporarily shut-down of the entire system.

3.1.1 Star Network Connection

In the centralised star network topology, each wind turbine is controlled by its own converter for efficient operation with MPPT and torque control. If the converters are at the substation platform, each wind turbine will require their own cable connection arranged radially as a star. More cabling will be required, but benefits include better voltage regulation, the rating of each connection is lower, and a higher security and availability can be achieved. Only one wind turbine will be down per connection fault, unlike in a chain network of interconnected wind turbines, where everything preceding the point of fault in that chain will be disconnected, resulting in higher unavailability [103].

3.1.2 Communication Challenges

MPPT control with variable speed WTs may be challenging if the generator and the converters are remote from each other in the centralised converter and star network topology. Decoupling the dynamics in the parasitic passive components in the cable and compensating the additional impedance of the cable between the machine and the converter may be difficult. Tuning the compensators will be inconsistent for difference cable lengths and impedances.

Since a wind turbine will already need electrical cable for power collection, including an extra communication links in a spacing of the cable in the manufacturing process can be straightforward, and the cost is very small compared to the cables itself. Often extra channels are included as redundancy and future expansion. However, if real-time communication links are needed for every WT to connect to the substation, then the complexity of the control system significantly increases.

A failure in communication would cause loss of control and undermined system performance and operation [104]. A failed offshore communication link is as difficult and expensive to repair as an offshore electrical cable. A system that does not require communication links is recommended. Sensor-less control strategies, should be considered where possible, while maintaining the controllability, operational performance and stability. For example, sensor-less estimation of the wind speeds, shaft

mechanical power and speed, and the rotor position have been used [79].

3.1.3 DC Star Network

Point-to-point two-terminal DC links are a more mature and established technology over multi-terminal DC networks. Each link is set up between the wind turbines and the star network cluster substation platform as shown in Figure 3.2. DC circuit breakers are expensive, and typically a fault can be quickly isolated from the AC side. Shutting down individual links is less disruptive than having to shut down the entire multi-terminal DC network to isolate a single fault.

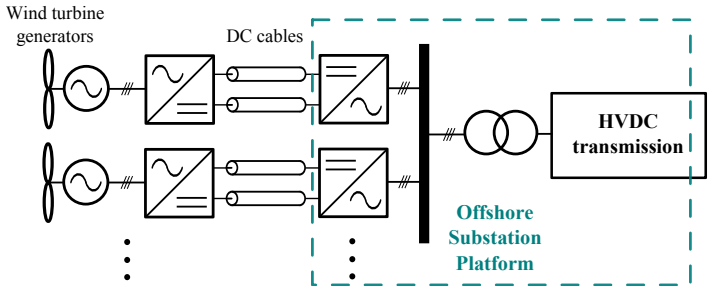

Figure 3.2: A star network with point-to-point DC connections between wind turbines and an offshore platform.

The total number of converter stages required in the Figure 3.2 DC connection topology, is the same as the number required by a WT with fully rated frequency converters for AC networks, and therefore the total converter losses can be assumed the same. The two converters on either side of the AC-DC-AC frequency converters are separated by a DC cable in this case.

The frequency converter is partially centralised for easy access at the cluster substation in this network topology, but only a little benefit is added to this. The machine side converter is exposed to deeper junction thermal cycling, which contributes to fatigue failure of the device, because the fundamental frequency is often lower than the grid side frequency [105]. It is the machine side converters that need the most attention, but is a problem if they are still distributed inside individual wind turbine nacelles, where access is the most difficult.

If compared with the AC star network topology at the beginning of Section 3.1, in the DC star network, the inverter is closer to the WT generator and therefore

is more controllable with direct sensor feedback to the local controller and inverter. The DC cables are cheaper than AC cables, more efficient and only require two conductors. A coaxial cable can be used for each DC connection, which has a single central core and an outer conductive layer. The design is thinner, flexible and cheaper to manufacture compared to three-phase multi-core AC cables and less copper is needed. The DC connection has no eddy current looses, skin effect losses, reactive power losses, and the reactance in the cable has no effect on voltage drop across the length of the cable.

The inductance in the DC cable can be beneficial for smoothing the DC current, rather than a hindrance as found for a low-medium voltage AC connection, which lead to high voltage drops across the connection during high loads [5].

3.1.4 Low-medium Voltage Connection

The ANSI/IEEE 1585-2002 defines the medium voltage level as 1 – 35 kV. Below this range is the low voltage level, and above is the high voltage level. This thesis refers to low-medium voltage level as the lower end of that medium voltage range, around 1 – 6.6 kV.

If each WT in a star network have its own cable connection directly to the offshore substation without any other WT interconnections, then the spare current capacity in the cable can be used to support voltage level operation in the low-medium range. This further presents an opportunity to directly connect devices without transformers. The electrical stresses on the cables for the low-medium voltage level will be much lower and therefore cable insulation can be thinner and cheaper. Alternatively the insulation material can last longer before it breakdowns, but the cost of the conductors and the amount of copper needed have to increase. Though the larger conductor diameter also reduces the voltage stresses around it, thus reduces the insulation requirement.

A steady-state study of the cable connection, presented at the PEDG 2012 conference [5], showed that at it is possible to transmit 5 MW using the thickest commercially available three-core cable with a conductor cross sectional area of 1000 mm^2. It is not possible to connect the WTs at 690 V for cable distribution, at the same

AC voltage level typical for a converter and generator before the voltage stepped up by a transformer. With the 1000 mm^2 copper conductor, it is possible to operate the AC cable from 3.5 kV and above without transformers. However, it is very expensive to use such thick a conductor that is normally used for 45 kV three-core AC cables, and for transmitting up to 110 MW. When this is used for a single connection for a 5 MW WT, only 4.5% of the total potential capability of the conductor is being used.

The transformer is typically located in the nacelle of a powerful WT, and the voltage is step up for connection to the collection network. The cable between the tower and the nacelle is therefore thinner and more flexible to allow the WT to yaw and twist by a number of rotations. Without the transformer, thicker cables for a low-medium voltage connection may restrict the yaw range of the WT, and the cable has to be divided into several thinner flexible cables.

The fundamental problem with operating at higher currents and lower voltage levels, is the significant I^2X reactive power consumption and the IX voltage drop across the cable, assuming the nominal frequency is 50 Hz. The current capacity in the cables and converters are taken up by the reactive currents, leaving little room to export real power. It is suggested that the frequency of the network should be lower. Operating at a lower frequency in a low voltage star network can minimise the voltage drop and reactive power consumed by the inductance in the cable, because the reactance reduces with frequency ($X = \omega L$). However, slower circuit breaking and arc extinction must be taken into account as the frequency of zero-crossings is also reduced. Deep temperatures cycles at low frequencies may also contribute to fatigue in converter switching devices [105]. The capacitance of the cable has very little effect on the production of reactive power at lower voltage levels, according to equation (2.1).

The strength of the AC connection depends on voltage as well as the impedance according to Section 2.1.2 in page 12. Changing cross sectional area of the conductor reduces the resistance but has little effect on reducing the inductance, but the proximity distance between the phases does. Reducing the voltage can also limit the power the cable transmit according to the power angle equation (3.1), which as-

sumes that the AC system impedance is purely inductive with X reactance between the voltage points V and E [17]:

$$P = \frac{V.E}{X}\sin(\delta) \tag{3.1}$$

The power stability limit is reached when $\delta = 90°$ or $\sin(\delta) = 1$, though in practise the limit is slightly lower than the theoretical limit due to noise and small power fluctuations near the point of roll-off at $\delta = 90°$. The maximum power limit is then defined as:

$$P_{\text{lim}} = \frac{V.E}{X} \tag{3.2}$$

Reducing the distribution network voltage level to suit the device voltage level is expensive because of the additional cables required to support higher currents. Likewise increasing the voltage level of devices to suit that of the network is also expensive because it demands higher insulation requirements and device voltage blocking capability. Further work is required to find an optimum voltage level for the system that is ideal for both the network and device in terms of cost and cable thickness. It would become more challenging as the WTs are more more powerful as discussed in Section 2.2.3.

It is common for WT generators to have a nominal rating of 690 V in the low voltage level, because of the cost and voltage rating limitation of frequency converters. As the voltage ratings of a generator increases towards the MV level, the physical size, insulation requirement and complexity also increases. The long-term performance is also uncertain due to the higher electrical stresses. More spacing and insulation between the windings for isolation from the laminated core and structure of the machine is needed due to the higher safety requirements. Though, this decreases the current and the thickness of the windings decrease, and the number of windings has to increase, which lengthens the manufacturing process and adds to the cost of the total system [9].

As WTs are becoming more powerful, the windings in the generator simply increase in thickness to handle higher current. At the moment ratings up to 7.0 MW can be achieved for WT generators operating at the 690 V voltage level, for example with the wind turbine model SWT-7.0-154 by Siemens [106]. Eventually a current

limit will be reached at this voltage level, where it will be too high to handle. The cost of increase the voltage rating of the generator and converter has to be justified by a higher wind power capacity. As discussed in Section 2.1.4, the low voltage level of 690 V for wind power generator has also remained popular because the two-level power converter at this AC voltage rating is one of the most cost effective.

The voltage peak and the frequency are the major factors that contribute to accelerated ageing of insulation in machines and transformers [107]. This may go against increasing the frequency and voltage using wide-bandgap SiC devices that operate at higher voltage and frequency as described in Section 2.1.5. However, the higher PWM switching frequency harmonics require smaller filters to eliminate them, although the filter will have to endure the high frequency voltage stresses and losses. After most of the high frequency harmonics are attenuated, the ageing of insulation material will depend on the peak voltage at the fundamental frequency.

3.1.5 Transformer-less Connection

Normally transformers are located at the top of the wind turbine in the nacelle, where access for installation, maintenance, or repair is complicated, and downtime per failure can be relatively high. They are large and heavy, so weight and space can be saved if they are eliminated, along with their losses and maintenance requirements. The design of the wind turbine nacelle will be lighter and more compact without transformers [108, 109].

As shown in Figure 3.3, the power converter represents 5% of the total cost of the WT and the transformer represents 4% [110]. Islam et al. proposes to eliminate the cost of the transformer and justifies using medium voltage converters rated up to 33 kV [111]. However, the problem of distributed converter access for converter repair and maintenance still remains in this case. Furthermore the reliability of new multilevel converter technology not exactly unknown and its increased complexity may contribute to higher probability of failure.

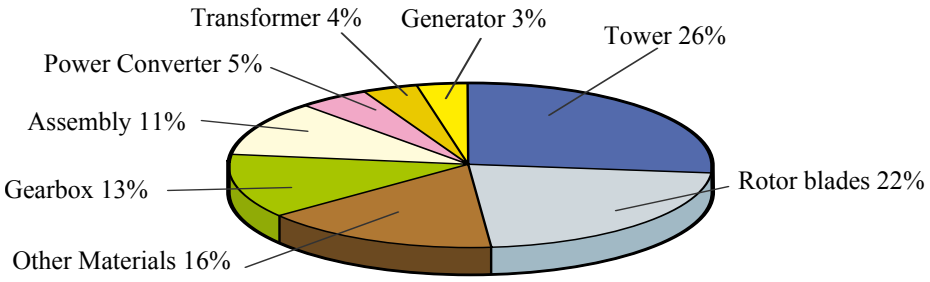

Figure 3.3: Wind turbine component cost percentage of total [110].

3.1.6 Drawbacks of Eliminating Transformers

Eliminating the transformer is not as trivial as simply removing it from the electrical system, because this may lead to other problems in term of performance, cost and reliability in other areas of the system. When there is no transformer to step the AC voltage between the WT electrical devices and the offshore local network, everything must operate at the same voltage level. Higher voltage ratings for converters and generators are much more expensive, whether the converters have multi-level topology or use SiC devices. But when the voltage level is lowered in favour of cheaper device, it is then too low for the cables, which then requires more copper to cope with the higher currents and losses.

The transformer can be very reliable and robust, like the gear-box, it is generally regarded as a mature technology and with years of industrial experience. A failure in the transformer is generally caused by over-heating from excess loads, fault-currents and/or failure of an auxiliary cooling devices if not cooled passively. Although active cooling devices requires more maintenance than passive ones, they tend to be favoured because the overall transformer size is more compact. Again, transformers for the offshore environment should be designed to be resistant against corrosion and fire. A transformer failure tends to be a rare event, but if a fire breaks out, it can cause significant damage to the rest of the WT, and not a lot can be done except to let it burn, due to the remoteness being high up in the nacelle and far away from shore, making it difficult to fight.

Another main function of a transformer is to provide reactance and to transform the AC voltage level and current, and provide isolation between converters operating in parallel. The transformer inherently has a leakage inductance, which can useful

for fault current limiting and filtering of converter harmonics [28].

Zero Sequence Isolation

It would be difficult to completely eliminate the transformers, since they are necessary for zero-sequence isolation between the AC and DC side of the converter. A three phase two-level converter naturally has zero-sequence harmonics because of the nature of switching where only two phase legs conduct at a time. As a result, the phase voltages do not add to zero, thus a zero-sequence component or a common-mode voltage exists at the AC neutral point against ground [112]. It is also present in multi-level converters but it is less severe as the order of levels increase. A common ground points in both the AC and the DC side of a converter cannot exist, because it will lead to circulating common-mode currents that will cause EMC problems and noise in transducer measurements for control feedback [113].

Normally, a point at the DC-side is grounded, typically at the centre terminal, and the AC-side of the converter does not have a grounded neutral. As also found in [114], a delta-wye transformer configuration is typically used for isolating the inherent zero-sequence components in the voltage from converter switching and phase unbalance. The AC-side of the converter is connect to the delta windings of the transformer, where there is no grounded neutral.

The wye-side of the transformer is connected to the network where the grounding of the neutral point is needed so that ground-fault current will be large enough to be detected for circuit breaking. Failure to protect the cable from a phase-to-ground fault early will result in further deterioration of the insulation and conductor material resulting in a more expensive repairs. Therefore neutral point grounding at the wind farms collector network is recommended [115]. However, on the contrary, it is also better to have the ground point at the DC-side instead of the AC-side of the converter, because this minimises the dv/dt at the collector pin of the IGBT devices and therefore minimises the minimises the leakage currents through the stray capacitance between the collector plate and the grounded heat-sink [20]. Therefore, the transformer is needed if ground points are desired on both the AC-side and DC-side.

3.2 Wind Turbine Interconnection

The most traditional connection is an AC collection network that allows WT interconnection as shown in Figure 3.4. The chain-like connection can be radially lined up in a string, or in a ring in case an interconnection is lost [103]. The fundamental drawback of a DC collection network was that DC fault protection is too difficult, slow and expensive. Breaking an AC circuit is simple, quick and cost effective owing to zero crossings of the alternating current waveform. All AC devices can be easily interconnected in the network and be protected from AC faults. Even if one of the phases were lost, the system can continue transmitting power at a reduced capacity. Three-phase AC systems are mature, reliable, robust and simpler to control [116].

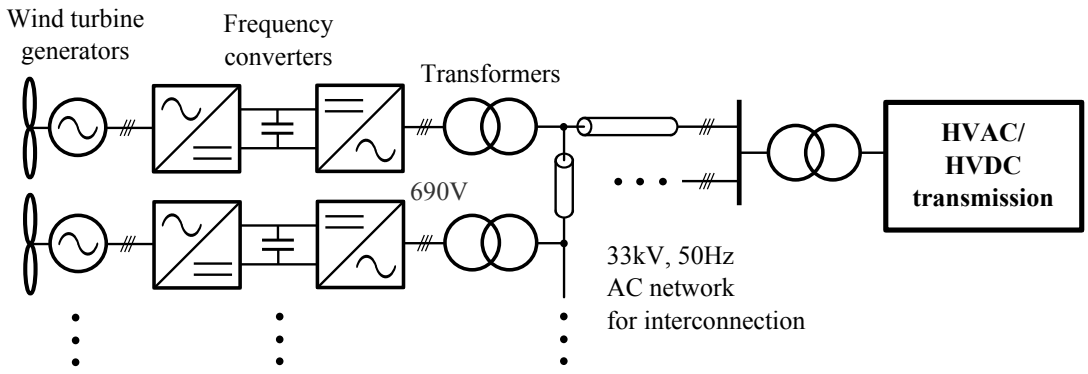

Figure 3.4: A typical offshore AC network connection with Type D wind turbines and fully rated frequency converters that can be interconnected in the network.

3.2.1 AC Interconnection Voltage Level

For a conventional interconnection scheme at the medium voltage level, for WT connection via transformers, the maximum power is limited by the current rating of the cable. For 11kV transmission over a 5 km three core cable (1000mm^2), power is limited to 15.7 MW as presented in [5]. This means a maximum of three 5 MW wind turbine can be connected to the same cable at this voltage level. In this case, the associated steady-state voltage drop was 0.98% and cable efficiency was 99.8%. For 33 kV transmission over the same distance and using the same conductor cross sectional area, the current limit is reached when power is 47.14 MW. Increasing the

voltage three folds can increase power transmission capability by three times. In this case, nine 5 MW wind turbine can be interconnected on to the same cable. The voltage drop is lower at 0.38% for this case and the efficiency is slightly lower at 99.6%. The next standard voltage level from 33 kV is 66 kV, and a doubled power capacity will be expected for the same current capacity. However, as the voltage increase, the cost of insulation, cable joints and terminals increases due to higher electrical stresses, and the Ferranti effect with the cable capacitance at no load becomes more pronounced.

3.2.2 DC Network for Interconnection

If multi-terminal and medium voltage direct current (MVDC) grids were possible, wind turbines can be interconnected as shown in Figure 3.5. In comparison with the DC star network as described in Section 3.1.3, the total cable length can be reduced with interconnection.

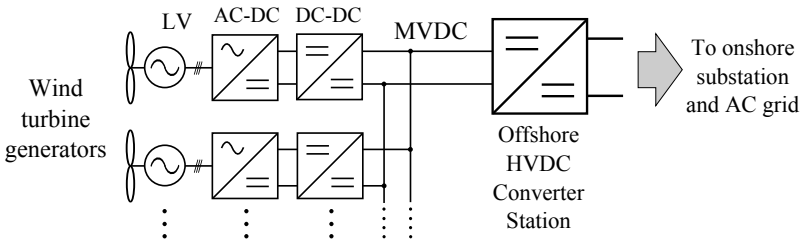

Figure 3.5: MVDC network with parallel interconnections between WTs.

A DC-DC chopper or a buck converter is simple, efficient and cheap in design but has a limited DC voltage gain between conversion. DC-DC converters with higher voltage gains for serving a large wind farm can be very large in size. The space required in offshore platforms adds to further structural costs. The MVDC network voltage needs to be converted to AC for transformer stepping and HV isolation and then converted again to HVDC for onward transmission to shore. Compared with an HVDC connected AC collection topology, there is another converter stage in the line of the power flow contributing to loss and overall cost of the system [117]. The AC transformer at the intermediate stage of the DC-DC converter is used to step up the voltage and can operate at the medium frequency range around 500 Hz.

The peak flux is lower at higher frequencies, therefore the core can be considerably smaller and lighter than traditional 50/60 Hz AC transformer solutions [118].

Although the DC cables are more efficient and cheaper than AC cables for distribution and transmission, the main challenges associated with DC networks are the loss and cost of converters, and limited DC fault protection. As discussed in Section 2.1.8), DC circuit breakers (CB) are currently very expensive and do no react quick enough [119]. The high costs of DC CB devices makes it difficult to justify their practical use. One of the most cost effective method to isolate the fault in the DC network is to de-energise the entire DC system first and then re-energise it once the fault is cleared, but this can be very disruptive for the power flow. If the power from the WT has nowhere to go, energy storage or a resistor load bank would be necessary to store or dump the surplus energy offshore. A sudden disconnection of a large source of wind generation will disrupt the grid system unnecessarily. Fast onshore spinning reserves and ancillary services are expensive, and if they are required to keep the grid stable, it will inadvertently increase the overall cost of energy.

Using Diode Rectifiers

Elliot in [120] has studied a simplified DC network approach that requires minimum power electronics. Power from permanent magnet synchronous generators (PMSG) can be converted to DC using robust passive diode rectification instead of a VSC at the WT. The speed of all the PMSGs in a multi-terminal cluster network is regulated by the DC side voltage. Due to the nature of diode rectifiers, the 6th order harmonic component is present in the machine torque and in the DC side current. As the rotor speed of adjacent WTs vary, this creates a 'beat' on the aggregated currents. The study was based on the standard three-phase PMSG and rectifier bridge. This topology does not have to keep with the three-phase standards because the generators are decoupled from the main power system. A multi-phase PMSG, for example with at least six phases up to 60° apart, should exhibit higher frequency harmonics in the machine torque and current, which is easier to filter and should have less impact on the mechanics of the machine and the DC network voltage. PMSGs are the only generators suitable for this type of rectifier topology

because a supply for the magnetising currents is not required. Although the overall system is simple and reliable, the permanent magnets are expensive due to restricted global supply (as discussed in Section 2.2.5).

DC Series Interconnection

If the DC side of each converter is connected in series, as shown in Figure 3.6, the sum of the voltages can be enough for direct HVDC transmission without an expensive offshore platform. This topology has potential cost benefits as the cable layout is simple and the large offshore HVDC converter substation and platform structure are not necessary [102]. The onshore side HVDC converter station can be either VSC-based or even thyristor-based LCC, which is more cost effective, efficient and feasible because the onshore AC grid is strong. The larger filter, converter, and switch yard required on the onshore side not a problem because the onshore space is not as expensive compared to the offshore. More than one set of series WT can exist in parallel, sharing the same long distance HVDC cable.

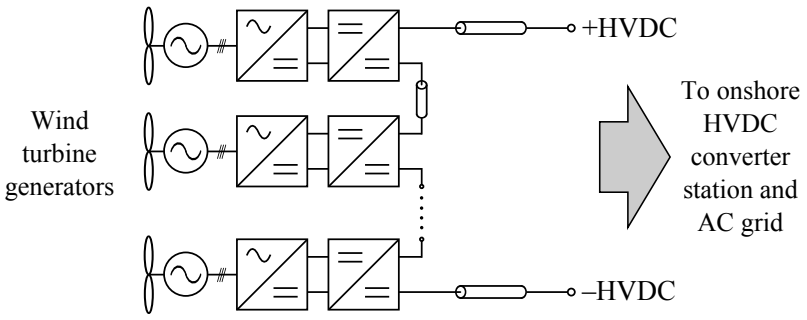

Figure 3.6: WT interconnected at the DC side in series, which then builds up to the HVDC voltage.

Major practical challenges for the series DC connection topology include ensuring there is even voltage sharing between the terminals of each WT when they are generating uneven power, and requiring expensive high voltage insulation and clearance with respect to ground. A transformer with XLPE insulated windings between the AC-DC converter and the WT generator isolates the HVDC potential from the generator. The insulation requirement is reduced for WTs closer to the ground point. If a WT device is out of service, a by-pass switch shorting its DC

terminals ensures continuity of power flow for the rest of the system [121]. The one-quadrant DC-DC buck converter ensures the continuity of current in the HVDC during operation [122].

A ring interconnection is not possible with a DC series topology as with AC or DC parallel ring interconnection, which can cover a fault in one of the interconnections and still keep all the WTs connected. If one cable interconnection in the DC series connection fails, the entire string of WTs in that series is lost because the circuit is cut. The cable fault has the longest downtime in the offshore system, therefore a cable failure can be very disruptive if no redundancy is in place. Adding effective redundancy in the DC series case significantly increases the cost because all the connection has to be at least doubled up. Little is also known about DC fault current protection in practise for the topology.

3.2.3 Variable Frequency AC Network

A group of wind turbines can share a common converter as shown in Figure 3.7. This concept network topology benefits from centralising the converters as discussed in Section 3.1 and improving cable interconnection for reduced cable length and cost as discussed in the beginning of Section 3.2. This topology eliminates the need of a frequency converter directly at the WT. A generator will be connected directly to the network via a transformer and switch gear as a Type A or Type B configuration WT would. The total number of converter stages that the power has to go through in the line of power flow before reaching the onshore grid is reduced, which contributes to reduced converter losses as well as saving cost, weight and space [123].

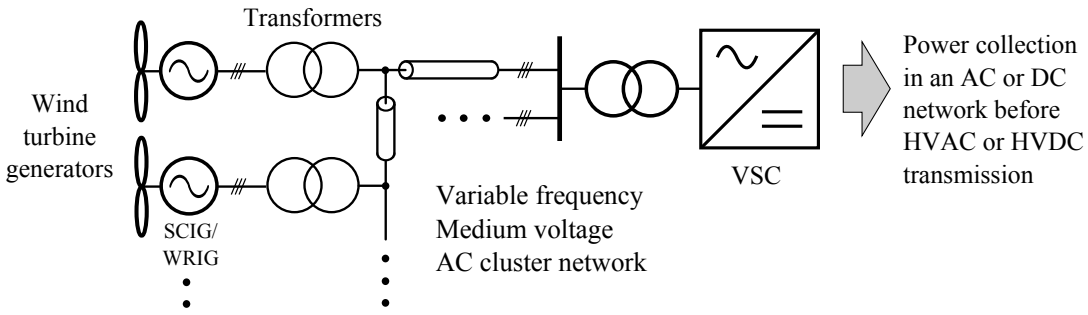

Figure 3.7: A variable frequency network topology.

The variable frequency concept topology has been investigated in literature. Jovcic presented a system where the VSC-HVDC offshore converter is divided into 25 modules connecting to the same HVDC link as the multi-terminal configuration. Each module is connected to an independent cluster network consisting of 4 WTs [124]. The operation of this network topology is similar to a WT with a fully rated frequency converter, except that multiple WTs are sharing a single VSC. The AC frequency of a network cluster is controlled using MPPT, which is determined for the average wind speed in that group. For generators connected directly to the network like the Type A configuration, the rotor speeds of the WTs are assumed to be synchronised and proportional to the network frequency. The SCIG would be the simplest and least expensive for this application. The WT rotor frequency of the generator can be varied by varying the frequency of the cluster network. However, the actual wind speed varies between WTs due to the wake effect caused by neighbouring WTs as mentioned in Section 2.2.9. The tip speed ratio λ would not be optimal and there will be a loss in the coefficient of performance C_p compared to individual MPPT control in Type C and Type D wind turbines where the maximum power could be extract from wind [125]. This loss increases with the number of WT per cluster, but the percentage loss begins saturating at about 16% after having more than 6 WTs per cluster [126].

Improving the Overall MPPT

In the variable frequency network topology, it is more advantageous to use an asynchronous induction generator with a wide slip speed range than a synchronous generator. WTs that experience a higher than average wind speed will produce more power and increase the induction generator slip speed with torque. As a result, more power can be further extracted as the tip speed ratio λ is improved towards the maximum power point. When there is high variability in the wind speed across the WTs in the cluster, the constant rotor resistance in the induction generator could be tuned to optimise the slip speed and the tip speed ratio λ for a better overall power extraction. Furthermore, a wide slip speed variation with torque helps to reduce the rotor shaft stress as the asynchronous speed of the rotor N_a increases.

Variable slip control in Type B configuration WTs can be used to vary the rotor speed in the individual WTs, which is achieved by varying the rotor resistance and therefore the slip speed as described in Section 2.2.5 and as shown in the torque-slip characteristic curve for a variable rotor resistance in Figure 2.13. The individual rotor speed control with Type B WTs further optimises the tip speed ratio λ of the turbines to improve the overall MPPT in the variable frequency network to minimise the C_p losses and extract the maximum power [127]. A Type B configurations can be achieved without slip ring and brush connections, by using an OptiSlip® type technology, as mentioned in Section 2.2.5. This can more robust compared with frequency converters in Type C and D systems where a potential high failure rate in the power electronics can render the WT system to be unstable or useless during operation. A failure in the variable resistor mechanism only affects the MPPT and does not have to affect the operability of the WT to generate power, assuming the failure mode is a short circuit or a constant stuck resistance state. The variable rotor speed range of the induction generator N_a can only be above the synchronous speed of the stator field N_s and the network frequency. Therefore, the set variable network frequency will be skewed for WTs experiencing the lower spectrum of the wind speeds instead of the average wind speed in the cluster, while the rotor speed of Type B WTs can be adjusted to cater for higher wind speeds.

When combining the variable frequency network and Type B limited variable speed WT, the variable speed range of the turbines is maximised on a per WT basis, which are then able to individually fine tune the tip speed ratio for maximum power extraction. The WF does not need to be split into smaller clusters and controlled in groups to minimise the MPPT loss as Jovcic and Strachan did without flexible rotor speeds [126]. The variable frequency can be applied for entire WF, which offers simplicity and greater degree of freedom to connect in any WF layout and cable path, without being restricted into small clusters.

The variable frequency AC network topology already uses the frequency as a guide for the synchronous speed of the WT generators. Therefore it cannot use the frequency droop communication method to communicate a signal to the wind turbines to indicate how much power it should generate in the same way as described

in Section 2.4.6. Alternatively, it would be possible to manipulate the frequency away from the maximum power point to stall the WTs to curtail and control the power output of the wind farm.

Concern of Low Frequencies in Transformers

A concern for a variable frequency network is transformer saturation at low frequencies. When the frequency is reduced while voltage level remains constant, the flux density B in transformer core increases, which may exceeding the saturation level. When the transformer core saturates, the magnetising inductance becomes a hundred to a thousand times smaller, and the magnetising current becomes larger as a result, until it effectively becomes like shorting the transformer windings. Increasing the core cross-sectional area to accommodate more flux (or volt-seconds) at lower frequencies is not practical as it will be larger, heavier and more costly. Transformers are an essential and cost effective method for isolation and voltage stepping for more efficient network transmission and thinner copper in the cables.

According to the transformer EMF equation (3.3), the flux density B in the transformer is proportional to the ratio of the EMF voltage and the frequency (E/f), assuming the turns ratio N and the transformer core cross-sectional area A are constant.

$$E = 4.44fNAB \tag{3.3}$$

The EMF voltage level should be reduced linearly with frequency in order to keep the flux in the transformer constant and prevent transformer saturation. As the voltage and frequency is reduced, the current rating of the transformer is also reduced linearly [128]. The WT power has a cubic characteristic with respect to frequency as described in Section 2.2.7, assuming constant C_p with MPPT and that the WT rotor speed and frequency are proportional to the wind speed. When the WT is operating below the rated wind speed, the power output level is significantly reduced at lower frequencies and is well below the dynamic rating of the transformer. Therefore, there will be no danger of current overloading at the transformer [126]. Low frequency AC is also more efficient due to lower reactive losses, eddy currents and hysteresis losses in both cables and transformers.

The network voltage is controlled by the VSC-HVDC and the start up current is minimised by starting from low voltage and low frequency. Therefore, the soft-starter device shown in Figure 2.12 for Type A and B configurations would not be necessary.

Low frequency AC circuit breaking would usually take longer to extinguish because the current is cutting through the zero crossing less often. However, the system only operates at lower frequencies when the wind speed is low. Therefore the lower maximum power point, together with a lower voltage level at low frequencies should aid quicker circuit breaking.

The transformer design needed must take into account of the increased magnetising currents at lower frequencies. This is due to the magnetising reactance decreasing as the frequency is reduced ($X = \omega L$). Therefore more turns per unit voltage are needed.

Constant Current

The network voltage characteristic against frequency may follow a constant current regime instead of a linear characteristic for constant transformer flux. Although the overall I^2R conduction losses will be higher when operating at constant current when operating below rated wind speed, the loss will be constant and therefore the device temperature will be constant. This would help reduce the frequency of deep thermal cycling in transformers, and therefore reduce fatigue failure and increase the reliability performance. It may then not be required to overrate the devices or even use heating elements to minimise the thermal cycling. However, the thermal cycling in the individual junction of the switching devices in the VSC will be worse with low frequency and high peak currents [105]. Furthermore, it will be difficult to implement constant current control in an interconnected system with many WTs because the margin for variability in the load sharing is low and the odd WT may overload.

3.2.4 Total Network Cable Length Comparison

As discussed in Section 2.2.9, wide spacing between the wind turbines reduces the impact of the wake effects but imposes a challenge for the length of cabling required. A wind farm layout scenario with 100 wind turbines uniformly spaced 1km apart in a 10 by 10 grid is assumed. The actual network may not be arranged linearly in this way, and the positions should be optimised for minimum the wake effect interactions. The simplified arrangement is only for the purpose of estimating the total cable length for the different cable connection layouts. Max Parker et al. has performed a further cost and annual loss comparison with different offshore wind farm collection networks including the star networks, interconnected string networks and cluster networks that were described above [129].

A WF connection layout with strings of radially interconnected WTs is shown in Figure 3.8a, where up to nine WTs can be supported by the cable as suggested in Section 3.2.1 for the 33 kV voltage level. The cable length of this network is 111.2 km, which is almost the same as the distance from shore to one of the Round 3 wind farm sites. In comparison, a wind farm connected using a star network layout as shown in Figure 3.8b has a total cable length of 391.2 km, which is more than three times longer than the interconnected network topology. Although the star network connection is relatively more robust, the cable infrastructure is very expensive and the cost of laying the cable will be more expensive than the cable itself, depending on the site and depth [130]. If the network is equally divided into four smaller star network clusters as shown in Figure 3.8c, the total cable length is reduce to 197.4 km. However, extra offshore platform structures and foundations are needed for the collector stations, which will significantly contribute to the total cost and technical complexity of the offshore electrical system [131]. Therefore number of collector station platforms should ideally be reduced or eliminated where possible.

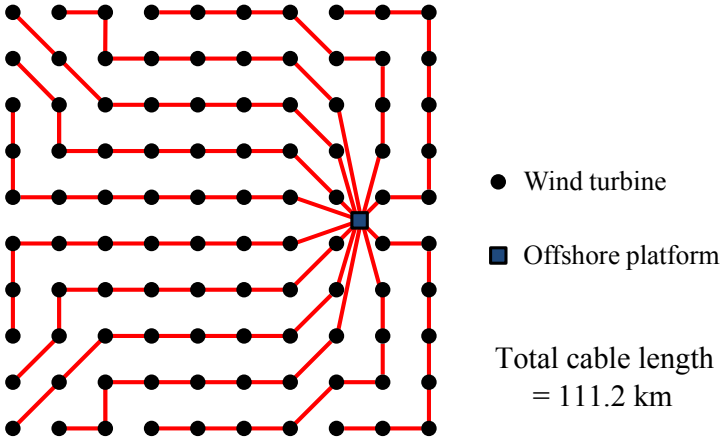

(a) Radial interconnected string network, with maximum of 9 WTs per string.

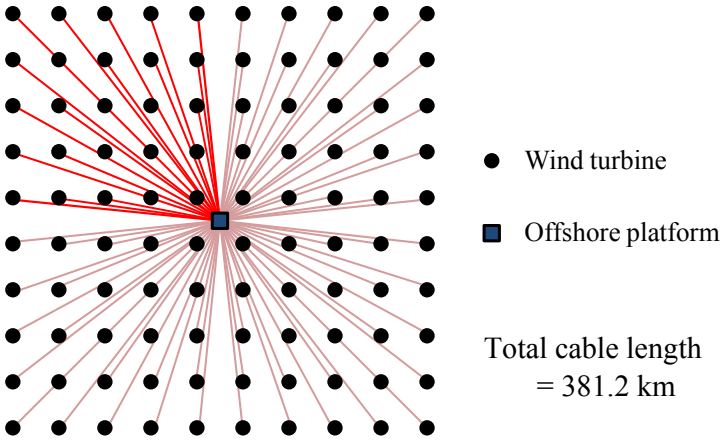

(b) A star network, where all WTs are connected to a single substation

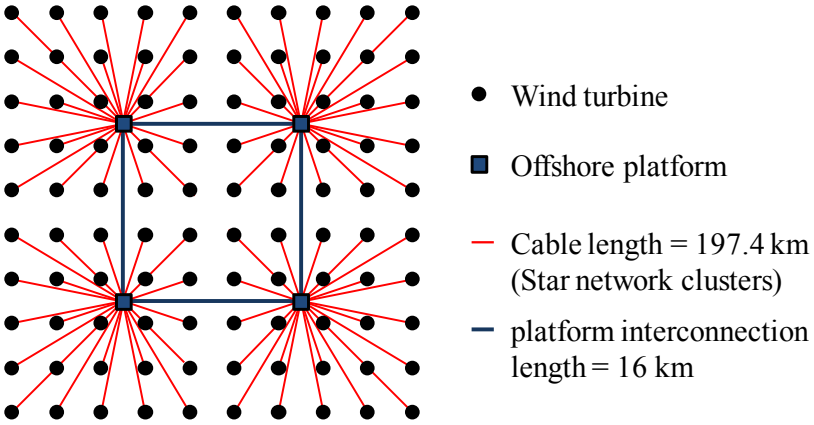

(c) Four clusters of star networks

Figure 3.8: Network cable arrangements for a wind farm with 100 wind turbines uniformly spaced 1 km apart in a 10 by 10 grid.

3.3 Modularisation with Parallel Configuration and Redundancy

A failure of a component in a series configuration will disrupt the power delivery in an electrical system [132]. The concept of modularisation can be applied to any system or component, which is then divided into n number of modules to increase the level of parallel connection, as shown in Figure 3.9. The fault tolerance of the system is improved, because if one module fails, the rest of the system can still operate but with partial rated capability [133]. Unless each module has a higher design rating to allow the output to increase and not compromise the overall capability [134].

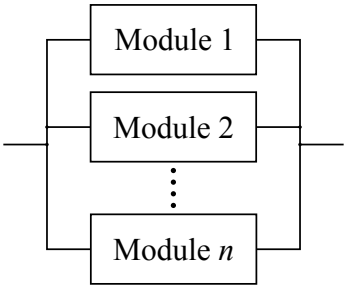

Figure 3.9: A simple representation of a parallel modularisation concept.

Including extra redundancies in a parallel modular systems is straight-forward because the same design repeated, although the assembly process can be more labour intensive and costly. If a fault would occur, the redundancy will help maintain an operational system at the full power rating until a safe window of opportunity is opened for offshore access to fix the problem. This will also minimise the urgency to carry out the work immediately. It is then possible to delay this until a planned shut-down period, when wind speed is low and conditions are ideal for access and low impact on wind power production. Although adding redundancies is expensive for semiconductor devices, system efficiency is improved and less resistive as the area of conduction is increased with more parallel paths for current flow.

Caution should be taken when increasing the number of parallel elements. If there is a module component failure mode that causes the overall system to fail, this may decrease the overall reliability [135]. For example, this issue can be found within the challenges in DC network protection as discussed in Section 2.1.8, where

without proper protection, the entire system shuts down. Each module must require its own protection devices so that it is able to fully isolate itself from the system when there is a fault within itself. However, it is difficult and expensive to do so at the moment with DC networks with today's circuit breaker technology.

Considering that the power electronic components tend to have higher failure rates (See Section 2.3), it may not be ideal to focus all the collected power through a single centralised VSC. If this VSC fails, then all the WTs connected to that VSC will become unavailable. It would be beneficial to divide the centralised VSC into a numbers of parallel operating modules with extra redundancy, which provides a level of fault tolerance and the power flow is only partially disrupted when a VSC module fails. The system has to rely on timely fault detection to quickly disconnect a faulty module and isolate it from the rest of the health system to resume operation and power export.

3.3.1 Wind Energy Availability while a Module is Lost

The power capability of a modularised system will be partially rated when a module fails and disconnects from the system. They system can remain in this state over a long time without repair. As discussed in Section 2.3, the downtime period for an offshore failure can be considerable due to difficult access. The energy produced when the power capped in a system that is is partially rated, is compared to energy produced the when the system is fully rated and operational. This section will also see how the wind distribution can affect the total percentage energy throughput in this case.

The total MWh annual energy produced from each WT is calculated by multiplying the Weibull probability $W(v)$ with the WT power P_{WT} for each discrete wind speed between the cut-in and cut-out wind speed, as shown in equation (3.4). Then 8765 hours in a year is factored in, and then summed together for the total estimate annual energy generation, assuming all other components in the system have 100% availability. The WT power curve and the Weibull probability distribution used are

from Figure 2.14.

$$E_{\text{annual}} = \sum_{v=3.0}^{25.0} W(v) P_{\text{WT}}(v) \times 8765 \tag{3.4}$$

In a modularised VSC system, n is the number of modules required for the system to be fully rated at 100% and no redundancies will be considered at this moment. When a system with n modules loses one module due to a fault, this event will be expressed as an $n-1$ fault scenario. The annual wind energy production is calculated using the same equation 3.4 for the $n-1$ scenario. The power curve characteristic (P_{WT}) is assumed to be capped to the partial power rating when a module is lost ($1-\frac{1}{n}$), as shown in Figure 3.10. For example if there are four modules (n=4) and one module fails, then the overall capability of this modularised system is dropped to 75% of the original rating, which is $(1-\frac{1}{4})$. The wind power curve characteristic $P_{\text{WT}}(v)$ is then changed as the power output is capped to the reduced capability level.

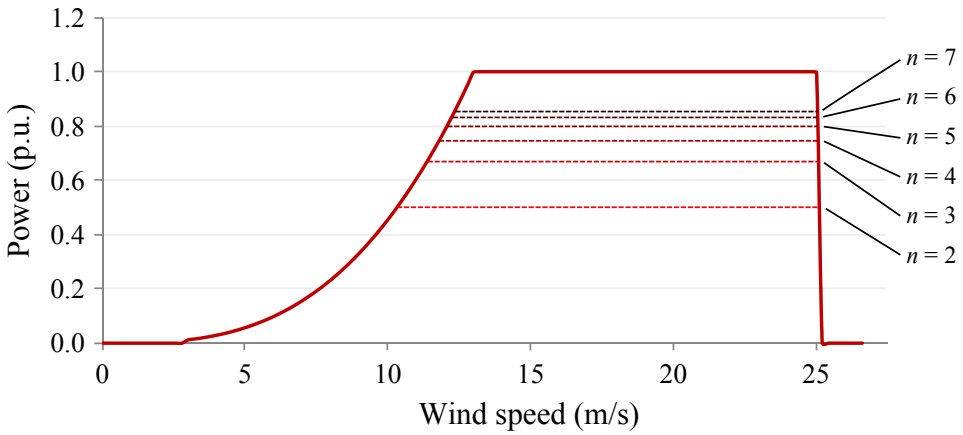

Figure 3.10: The wind power curves with caps for reduced electrical system capability for a failure of one module ($n-1$) for systems with n number of parallel modules between 2 and 7.

The 'energy availability ratio' will be used to describe the ratio of the annual energy generation from wind for a specific fault case (e.g. $n-1$) to the annual wind energy generation availability for a system that is 100% rated with no faults. Figure 3.11 shows the n−1 case energy availability over a range of n number of smaller parallel modules, for the two wind speed distribution cases in Section 2.2.8, which serve as a 'best' and a 'worst' case scenario. If there is $n+1$ redundancy in the sys-

tem, the $n-1$ availability results may be treated as the availability ratio for an $n-2$ case. For a system with a single module ($n = 1$), the availability is assumed to be zero if this module fails. The probability of failure was ignored, and the downtime of such failure is assumed to last for one year when it occurs.

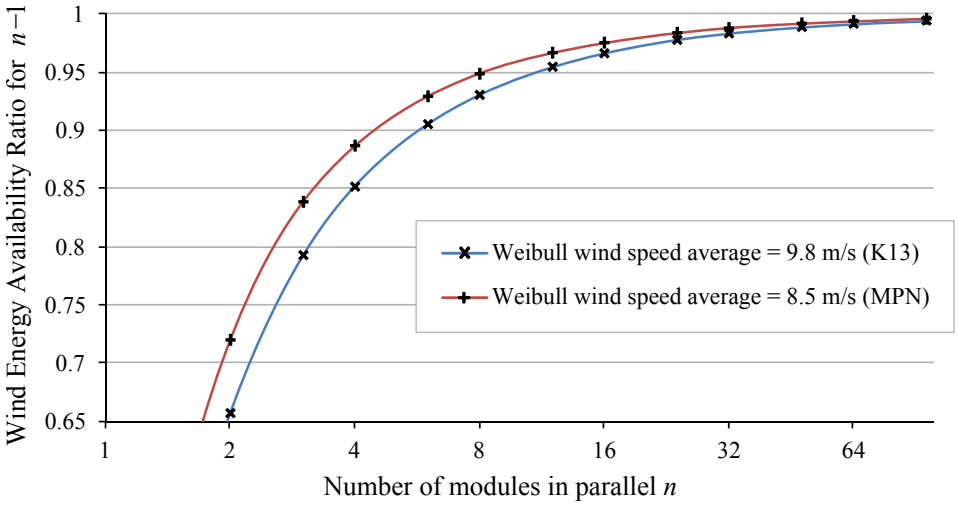

Figure 3.11: The wind energy availability for an $n-1$ fault in a modularised system with n parallel modules for two different Weibull wind speed distributions.

The energy availability ratio is higher for a distribution curve with a lower average wind speed, because there is a higher probability that the WT will be operating below the rated wind speed. Therefore it is affected less by a cap in the maximum rated power compared to the distribution curve with higher average wind speed. The higher number of module divisions n, the higher the availability ratio for an $n-1$ fault, because capability of the system will be reduced by a smaller fraction of $1/n$ for each module failure.

3.3.2 Cluster Scenario with 10 WTs

Given a cluster of 10 WTs and n=10 VSC units, in topologies where each WT is pair with a fully rated VSC, the entire availability of a WT generator is lost if the VSC fails. Therefore the power capacity available in this cluster for an $n-1$ case is 90%. However, if the 10 VSCs were centralised, connected in parallel to serve as a single modularised VSC system and shared between all the turbines in the cluster, then the energy availability ratio for $n-1$ VSC module failure is between 94.5% and

96.0% for the two wind distribution. The difference of at least 4.5% for this cluster is a significant improvement. The total number remains unchanged (n=10) when they are centralised, because the WT fully rated VSCs are simply relocated to the offshore platform. The centralised VSC topology can be divided in to n=6 modules instead, where the estimated energy availability ratio will be 90.5% at worst, which is not too far off from the availability if a VSC failed in the original VSC-per-WT case with 10 WTs.

Fully rated VSCs inside the WTs, are already locally modularised to improve their availability in case of a module fault. Such as the model SWT-3.6-120 by Siemens, which have six 600kW VSC modules for their 3.6 MW WTs. Considering six parallel VSC modules (n=6), when an $n-1$ module fault occurs, the maximum rating of the system will be reduced to 83.3% of the original rating. When factoring the wind speed distributions and the wind power curve, the worst and best case energy availability ratio will be 90.5% and 92.9%.

Consider a cluster group of 10 WTs, where each WT will have n=6 VSC modules in parallel. The overall energy availability for one module failure out of the 10×6 VSC modules in the cluster, is $(9 \times 100\% + 90.5\%)/10 = 99.05\%$, and 99.28% for the best case scenario. If all the VSCs were centralised and grouped together so that there are n=60 modules in one system, the $n-1$ availability will be between 99.11% and 99.35%. This is a slight improvement compared to the original case for n=6 modularisation of local VSCs at the WT. The number of modules cannot be reduced to any less than n=56 to closely match the original $n-1$ availability.

The difference in the availabilities translates to about 108 to 123 MWh of estimated annual energy per cluster of ten 5 MW WTs, which is not very significant. The probability of failure of the VSC was assumed to be the same in both topologies and the $n-1$ downtime that lasts for one year. This is not very significant. Although the slight availability improvement for centralising a modular VSC system is not every significant, being centralised provides easier access to the VSCs for faster maintenance and repair, allows for lighter, smaller and compact WT nacelle design. When carrying out a series maintenance and other repetitive tasks on the centralised components, the travel time between components is shortened compared

to if they were in distributed locations.

3.3.3 Including Redundancy

If an n+1 redundancy was included in a modularised system, and a fault occurred in one module, the system rating would remain at 100%. If the maximum system rating can be maintained and the odd fault is covered by redundancy, the repair of this fault can be delayed to a more convenient time and operation can continue as normal. This assumes the fault can be cut-off and isolated.

Every VSC should include at least one redundancy for the whole system to cover an $n-1$ fault and then benefit from full rating availability. The total number and cost of adding redundancies is higher if n+1 redundancy is needed for every distributed fully rate WT converter. However, only at least one redundant module is needed for cover a fault for a centralised VSC system that is shared by a cluster of WTs.

The alternative notion to n+1 redundancy is increasing the rating of each module and a scale factor of $n/(n-1)$ for maintaining the maximum wind power throughput in case of a module failure. If one module is lost $(n-1)$, the power is distributed across the remainder modules and the increased power throughput per module is supported by the higher module rating. For example, the modules need to be over-rated by 20% higher for an n=5 case, which is the same overall rating for an n=5 case with n+1 redundancy.

3.4 Chapter Summary

- Power electronics tend to have higher failure rates than traditional electrical components in the electrical system. Centralising the power electronics components in a station for each network cluster can provide a central and direct access for faster group maintenance and repair. Elimination of the converter from the WT improve the compactness of the WT nacelle.

- Centralising and modularising a VSC system can significantly improve its availability in case a VSC module fails. Although the difference in the avail-

ability is not very significant between modularising the distributed VSCs in the WTs and a centralised VSC in the substation platform, the latter topology benefits from easier and faster access to the VSCs for maintenance and repair. A centralised converter scheme would also need fewer redundancies to maintain full availability in case of module failure, than including redundancies for each VSC if they were distributed inside individual WTs.

- A star network topology is robust and can provide higher availability with a centralised converter network topology. The WT will have its own cable connection to the substation platform, there is capacity to operate at the low-medium voltage level. Such topology at such voltage levels also presents opportunity to eliminate the transformer for further WT weight reduction. However, technical challenges need to be addressed for such topology. The relatively higher current needed per connection will increase the losses, the cost of the conductors, the reactive power consumption and voltage drop across the cable. Although low voltage cable terminals and insulation is low cost and robust due to lower electrical stresses, the total cable length requirement for the star network is too high.

- The cost of installing a cable in the harsh offshore environment is more expensive than the cable itself, therefore an interconnected WT topology with a shorter total cable length is more ideal. As converter systems become more reliable, the need will reduced for a such a star network topology with centralised converters.

- Transformers add inductance to the system, and potentially contribute to very high downtimes and cost of repair if a failure occurred offshore, because they are heavy and bulky. However, it is a relatively mature technology that is robust and reliable. The transformer is also necessary for isolation from high voltage and electrical zero sequence components. The large voltage step gains also enable the WT to employ cheaper LV devices and still be connected to an efficient MV collector network. A transformer-less connection would require more expensive MV devices or a reduction in the voltage level of the

distribution cable connection to the substation, which is also expensive in terms of copper requirements.

- The variable frequency AC network topology in Section 3.2.3 can have both centralised frequency converter and network cable interconnection. The maximum power point tracking is not optimal but could be improved if combined with Type B limited variable speed WTs to individually fine-tune the tip speed ratio for maximum wind power extraction. When operating below the rated wind speed and power, the voltage must reduce with frequency to ensure that the transformer does not saturate at low frequencies. The frequency and the voltage output of the VSC can be highly controllable for this application. Further investigation is needed to study the dynamics characteristics of this control.

Chapter 4

AC Voltage Controller for the Offshore Wind Farm Network Connected by VSC-HVDC

This chapter discusses an AC voltage control of the offshore AC network topology connected by VSC-HVDC. The offshore wind farm connection scheme used in this study assumes a traditional AC collection network connected by VSC-HVDC, as shown in Figure 4.1. Although the graphical representation only shows two wind turbines, there would be hundreds interconnected in a radial, ring or star network cable arrangement [103]. Each could represent a group of turbines without the centralized converter arrangement. The entire offshore network will be islanded and fully decoupled from the onshore grid frequency. The AC voltage and frequency for the network are established by the VSC-HVDC converter station.

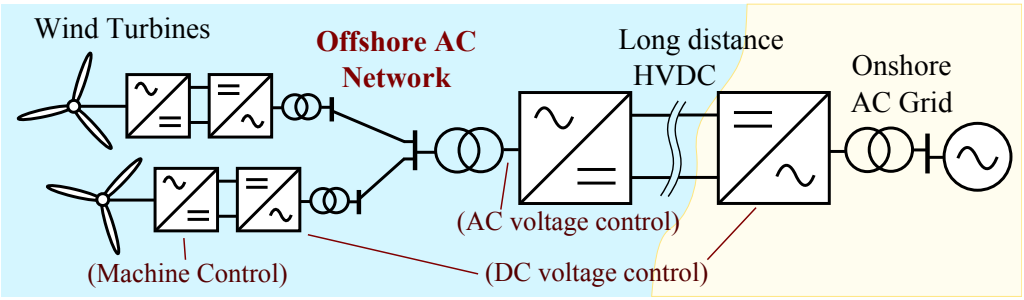

Figure 4.1: A basic representation of a typical concept of a large scale offshore wind farm electrical system connected by VSC-HVDC.

The traditional AC collection network topology is chosen for this study, because AC technology is mature and readily available. Although conceptual DC collection networks have cost saving benefits of having efficient transmission transformers-less connection with reduced and number of converter stages, AC systems on the other hand are maturer, simpler, and more reliable. Circuit breaking protection is simpler and faster, due to the fact that the AC waveform has inherent zero crossing once every half cycle [5]. AC grid connection voltage and frequency is standardised in industry, and therefore an AC network topology will not discriminate against any WT manufacturers that are already using AC.

4.1 Direct-Quadrature Coordination System

Three-phase *abc* electrical magnitudes can be transformed into two-component vectors relative to a stationary alpha-beta ($\alpha\beta$) frame or a direct-quadrature (dq) dynamic reference frame that is rotating at ω rad.s^{-1} relative to the stationary $\alpha\beta$ frame, as shown in Figure 4.2.

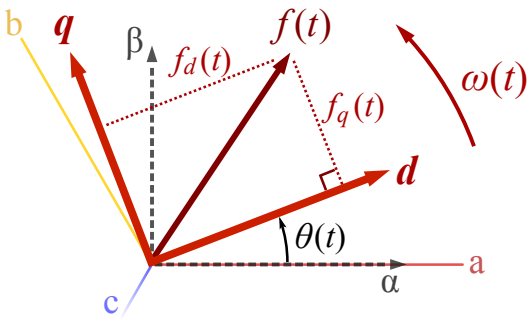

Figure 4.2: The dq reference system relative to the *abc* and $\alpha\beta$ stationary reference frame.

The d-axis is typically synchronised with the angle position θ of the AC grid voltage or the synchronous generator rotation speed, depending on the application. Components of any AC electrical magnitude $f(t)$ will be sinusoidal functions, in the steady-state, when referred to the $\alpha\beta$ reference frame. However, they will appear as DC magnitudes when referred to a dq reference frame if its angular speed ω is equal to the grid frequency [136].

Therefore control with these DC components in the dq frame is simpler and the control gains can be smaller. In comparison, a control system in the $\alpha\beta$ reference frame needs higher control gains in order to keep up to speed with the AC fundamental frequency [137].

4.1.1 Derivation of the *dq* Transformation from the $\alpha\beta$ Transformation

The three-phase abc to two-phase $\alpha\beta$ transformation (without zero sequence), also known as the Clarke transformation, is shown in equation (4.1). The abc three-phase values are projected to the α and β axes, a two-axis Cartesian frame. The result is a space vector $f(t)$ rotating at an angular speed that depends on the power system frequency.

$$\begin{bmatrix} f_\alpha(t) \\ f_\beta(t) \end{bmatrix} = \frac{2}{3} \begin{bmatrix} 1 & -\frac{1}{2} & -\frac{1}{2} \\ 0 & \frac{\sqrt{3}}{2} & -\frac{\sqrt{3}}{2} \end{bmatrix} \begin{bmatrix} f_a(t) \\ f_b(t) \\ f_c(t) \end{bmatrix} \tag{4.1}$$

Transformation to the dq reference frame, also known as Park's transformation, can be built on the $\alpha\beta$ transformation. The $\alpha\beta$ components are projected to the d and q axes, where the direction of the d-axis is specified by a rotating angle reference $\theta(t)$. The projection of $\alpha\beta$ to dq uses basic trigonometry as shown in equation (4.2). Merged together with equation (4.1), this completes the abc-to-dq transformation.

$$\begin{bmatrix} f_d(t) \\ f_q(t) \end{bmatrix} = \begin{bmatrix} \cos[\theta(t)] & \sin[\theta(t)] \\ -\sin[\theta(t)] & \cos[\theta(t)] \end{bmatrix} \begin{bmatrix} f_\alpha(t) \\ f_\beta(t) \end{bmatrix} \tag{4.2}$$

4.1.2 The *abc* to *dq*0 Transformation

A direct $dq0$ transformation is shown in equation (4.3) can be derived from equations (4.1) and (4.2). The zero-sequence part, also known as the homopolar component, is included here as well. This zero component can be neglected because the abc current components sum to zero in a three-wire VSC system without a neutral connection. The zero component dynamics are independent from the dq ones and

can be considered in a separate study if required.

$$\begin{bmatrix} f_d(t) \\ f_q(t) \\ f_0(t) \end{bmatrix} = k_1 \begin{bmatrix} \cos[\theta(t)] & \cos[\theta(t) - \frac{2\pi}{3}] & \cos[\theta(t) + \frac{2\pi}{3}] \\ -\sin[\theta(t)] & -\sin[\theta(t) - \frac{2\pi}{3}] & -\sin[\theta(t) + \frac{2\pi}{3}] \\ k_2 & k_2 & k_2 \end{bmatrix} \begin{bmatrix} f_a(t) \\ f_b(t) \\ f_c(t) \end{bmatrix} \tag{4.3}$$

The coefficients k_1 and k_2 in equations (4.1) and (4.3) depend on the transformation type as listed in Table 4.1. The k_2 coefficient are only important for homopolar components, but they are not used in this thesis because they are zero for a balanced system. There is no standard convention for the *dq* transformation, and the variables and coefficients appear to be chosen to uniquely suite a the particular application [138]. A "peak-value invariant" transformation will produce space vectors in the *dq* frame with moduli equal to the peak values of the corresponding three-phase magnitudes. For the "RMS-value invariant" transformation, the moduli of the space vectors will be equal to the RMS values of the three-phase magnitudes. For a "power invariant" transformation, the instantaneous power of the variables in the *dq* frame is the same as the instantaneous power calculated from the *abc* magnitudes as shown in Section 4.1.4.

4.1.3 The Inverse Transformation

After computing the required control effort in the *dq* domain, the inverse transformation equation (4.4) is needed to convert back to the *abc* domain for three-phase implementation. The coefficients k_3 and k_4 for the inverse transformation depend on the type of transformation used as listed in Table 4.1.

$$\begin{bmatrix} f_a(t) \\ f_b(t) \\ f_c(t) \end{bmatrix} = k_3 \begin{bmatrix} \cos[\theta(t)] & -\sin[\theta(t)] & k_4 \\ \cos[\theta(t) - \frac{2\pi}{3}] & -\sin[\theta(t) - \frac{2\pi}{3}] & k_4 \\ \cos[\theta(t) + \frac{2\pi}{3}] & -\sin[\theta(t) + \frac{2\pi}{3}] & k_4 \end{bmatrix} \begin{bmatrix} f_d(t) \\ f_q(t) \\ f_0(t) \end{bmatrix} \tag{4.4}$$

The choice of transformation type should not greatly affect the control performance and dynamics as the coefficients are simply gains and therefore the gain difference can be compensated within the *dq* controller. This thesis will use the "RMS-value invariant" *dq* transformation method for simpler direct interpretation

Table 4.1: Coefficients for three types of $dq0$ transformations.

Transformation	*abc* to *dq0*		*dq0* to *abc*		
type	k_1	k_2	k_3	k_4	k_5
Peak-value invariant	$\frac{2}{3}$	$\frac{1}{2}$	1	1	$\frac{3}{2}$
RMS-value invariant	$\frac{\sqrt{2}}{3}$	$\frac{\sqrt{2}}{2}$	$\sqrt{2}$	$\frac{\sqrt{2}}{2}$	3
Power invariant	$\sqrt{\frac{2}{3}}$	$\frac{\sqrt{2}}{2}$	$\sqrt{\frac{2}{3}}$	$\frac{\sqrt{2}}{2}$	1

of results in the dq domain, which will reflect very close to the RMS values. Assuming the q-axis component is zero, then the d-axis component value directly relates to the RMS value. The transformation equations have been implemented in PSCAD® using FORTRAN. Further details on this can be found in Appendix A.1.

4.1.4 Instantaneous Real and Reactive Power Equations

The calculation for the instantaneous real power $P(t)$ and reactive power $Q(t)$ using the *abc* instantaneous voltages and current variables are respectively shown in equations 4.5 and 4.6 [137, 139]:

$$P(t) = V_a(t).i_a(t) + V_b(t).i_b(t) + V_c(t).i_c(t) \tag{4.5}$$

$$Q(t) = \frac{1}{\sqrt{3}}\Big[\Big(V_b(t) - V_c(t)\Big).i_a(t) + \Big(V_c(t) - V_a(t)\Big).i_b(t) + \Big(V_a(t) - V_b(t)\Big).i_c(t)\Big] \tag{4.6}$$

The same $P(t)$ and $Q(t)$ can be calculated using the dq voltage and current variables as shown in equations (4.7) and (4.8), where k_5 depends on the transformation type used from Table 4.1. For the chosen RMS-value invariant transformation, $k_5 = 3$. Note that k_5 is not required if the transformation is "power invariant".

$$P(t) = k_5\left[V_d(t).i_d(t) + V_q(t).i_q(t)\right] \tag{4.7}$$

$$Q(t) = k_5\left[V_q(t).i_d(t) - V_d(t).i_q(t)\right] \tag{4.8}$$

4.2 The Offshore AC Frequency

A traditional power system normally has a large inertia depending on the number of generators connected to the grid. The power generation and the load demand must match and be balanced in order to maintain a constant frequency that is equal to the speed of the synchronous generators. The generators in the power system have no control over the load dynamics that can freely change and causes the frequency to deviate from the nominal frequency if generation does not respond accordingly. A generation system would typically adjust the power using speed governors, in order to speed up or slow down the frequency back to the desired reference [140].

In a WF case, where the wind power generation cannot be controlled, then the HVDC export power can be controlled in order to balance the flow and maintain the offshore frequency [141]. However, an AC offshore wind farm network connected by HVDC is islanded and fully decoupled from the onshore grid frequency. The inertia in the network will be very small, and frequency can be subjected to relatively large variations, making it difficult to control without a strong voltage source or fast power response.

As discussed in Section 2.2.5, WTs with Type D configuration are increasingly used for offshore wind farms. Their fully rated frequency converters will fully decouple the generators from the network frequency. Type D WTs have mechanical inertia but the control of the converters tend to cancel its effect and inertial impact on the network, hence methods are proposed so they can provide "synthetic inertia" for supporting traditional power system [142]. However, if all the WTs are of Type D and used in a WF that is only connected by VSC-HVDC, the entire offshore network will have no mechanical inertia and no AC grid frequency coupling with synchronous generators. Therefore, in this case, a voltage source should establish a set frequency and voltage on the offshore AC network, which must absorb abrupt power disturbances in the AC network.

4.2.1 Setting the Master Frequency

The voltage and frequency in the offshore network should be established by the strongest voltage source converter in the network. In this case, it would be the offshore HVDC converter station. The frequency in the master VSC is set in an "open loop" manner by first defining a rotating angle reference frame for the θ input of the dq transformations in equations (4.3) and (4.4). As shown in equation (4.9), the angle reference output θ in radians is derived from the integral of the desired reference frequency f in hertz, which can be easily modified in real-time. To prevent continuous ramping to infinity, the integral output is "wrapped" so the angle signal is reset at every 2π, which will then appear like a sawtooth waveform in the time domain.

$$\frac{\theta(s)}{f(s)} = \frac{2\pi}{s} \tag{4.9}$$

Assuming that wind turbines will operate in the usual power (or current) control mode, they will need to track a master AC frequency in order to inject their currents with the appropriate phase shift with respect to the voltage at the point of connection to the AC network. If the converter of the VSC-HVDC system is the only one imposing the frequency to the offshore network, undesirable small signal power oscillations can easily be avoided while all other converters can be synchronised using phase locked loops (PLL).

In the future, multiple HVDC terminals may co-exist in the same offshore network, but one terminal could still be chosen to act as the master VSC to fix voltage and frequency while all the others operate in power control mode. A fixed voltage and frequency set at the master VSC station will act like a slack bus voltage source and will therefore inherently be capable of absorbing power changes in the network. The master role taken by a VSC in this situation, cannot be used when the VSC is connected to a strong grid with a very large inertia and a strong voltage. This is because the limited control effort of the VSC cannot drive the grid voltage to a desired voltage reference.

4.2.2 Variable Frequency Option

If the offshore network is inertia-less, then the variation of the frequency can be very flexible and able to speed up and slow down very quickly to any desirable set reference without much power change. Some studies in literature suggest that the offshore AC network frequency should be artificially coupled with the onshore grid frequency instead of using a fixed frequency at the offshore network [101]. As discussed in Section 2.4.6 (page 54), this would allow the wind turbines to contribute to the grid frequency support. The frequency can then be used as a reference to signal the offshore WTs whether to transmit more or less power. It assumes that the WTs would provide more (or less) power if the frequency decreases (or increase), very much like a conventional power stations. This control mode could be made more flexible with the aid of distributed offshore energy storage and generation capacity reserves. (Please also refer to Section 3.2.3 about the variable frequency networks in Chapter 3).

4.2.3 Phase Locked Loop

The phase locked loop (PLL) allows the converters and distributed power generators to be synchronised to the AC frequency of the network. The PLL is a feedback control system that is able to track the frequency and the space-vector angle or phase of network voltage. The derivative of this angle with respect to time is equal to the AC angular frequency ω. The d-axis of the dq reference frame would conventionally be aligned with this angle of the network voltage vector, and then the q-axis voltage component becomes zero. As a result, the d and q components of the steady-state currents are directly related to the active and reactive power respectively, which is an advantage if they can be controlled independently.

In an ideal simulation model, the exact angle of the voltage space vector with respect to the α-axis can be calculated using the inverse tangent of the ratio of the $\alpha\beta$ components from equation (4.1). However, harmonics in a non-ideal model can propagate into the angle for the dq transformation, which leads to noisy signals and unstable control. The filtering effect of the closed-loop nature of the PLL, as shown

in Figure 4.3 can eliminate undesired harmonics in the tracking of the angle of the network voltage. The loop filter is typically a proportional-integral (PI) controller. The frequency ($\omega/2\pi$) can also be extracted from the PLL.

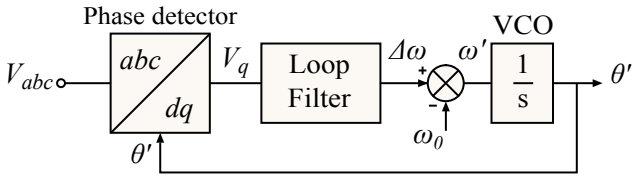

Figure 4.3: A block diagram of a generic PLL

A distortion in the grid voltage will lead to an error in the phase angle tracking and contribute to degraded performance of the converter if the PLL is not robust [143]. Gao et al. have presented and compared five different PLL methods in [144], each have their differences in terms of dynamic characteristic response, robustness to distortion and ability to recover from unbalanced faults. This thesis will use the PLL already provided in the PSCAD library for simulation (see Appendix A.2). For small signal analysis, the model of the PLL can be simplified to the transfer function of a simple first order fixed time delay for linearisation.

4.3 Closed-Loop Offshore AC Voltage Control

The location of the point of common coupling (PCC) is defined at the terminal of the LC filter, where the voltage v is measured as shown in Figure 4.4. Here, the converter is represented by an ideal voltage source, e.

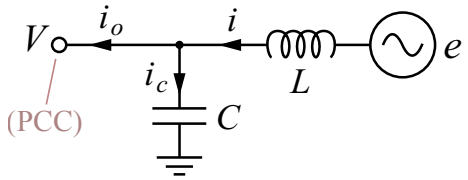

Figure 4.4: The schematic of the LC filter.

The voltage closed loop approach with proportional-integral (PI) control minimises the steady state error at the PCC. This is useful for removing voltage drop across the filter inductor, which can be significant as it varies greatly with load and

if its impedance is relatively large. The voltage drop across the inductor L, between e and V, can vary depending on its impedance and the current. The PCC is essentially turned into a constant "voltage source" instead of the immediate output terminals of the converter at e.

The voltage controller proposed, shown in Figure 4.5, has a cascaded control structure with an inner current loop and a voltage outer control loop with full state feedback. The outer loop determines the current needed to control the voltage at the PCC. The inner loop then uses this as a reference to control the current through the filter inductor L by determining the necessary converter output voltage, e. The cross-coupling terms decouple the inherent interactions between the d and q coordinates, reduce oscillations and deteriorated transient response, and enable faster response with lower control gains [137]. The same decoupled control structure, particularly for the inner loop, can also be found in previous literature [101, 145–147].

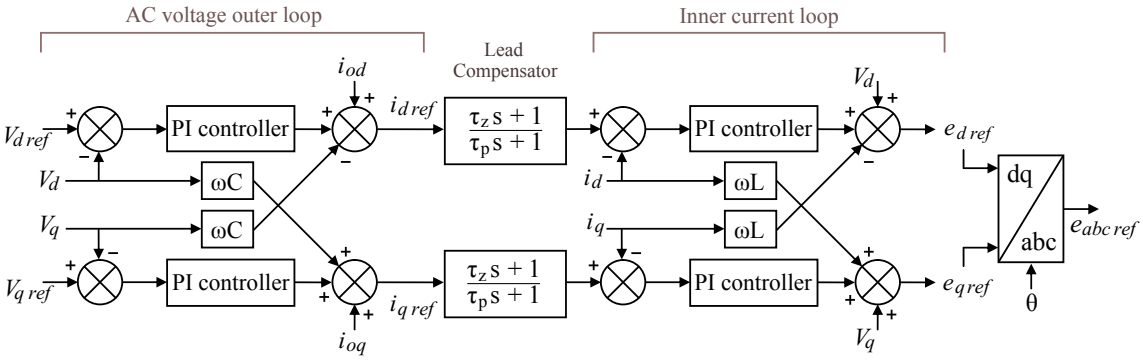

Figure 4.5: Decoupled dq voltage outer controller and inner current control loop with compensator for offshore AC network control.

The same decoupled inner loop current controller part can be found and used for different outer loop control applications, such as in DC voltage control, power control, machine torque control, etc. This study will focus on AC network side master voltage control that appeared only recently in offshore wind farm applications. The angular frequency term ω in the cross-coupling for the master voltage controller depends on a desired frequency reference set, but for slave devices following its frequency, the angular frequency ω can be taken from the PLL frequency output.

4.3.1 Decoupled Inner Current Loop Control

The current control loop controls the I_d and I_q current components independently. The error between the reference and the measured current goes through a proportional-integral (PI) controller that will drive the voltage output of the converter e in order to achieve the set-point current, $i_{dq\,ref}$. The decoupling strategy chosen here is based on the ideas of feedback linearisation used in vector control of AC drives [136, 148]; similar strategies are also found in [141]. Once decoupled, controller gains for the d and q axes can be designed using pole placement with a state-space approach with integral action.

Equations (4.10) and (4.11) are the differential equations for the d and q current dynamics through an inductor. The substitution terms γ_d and γ_q controls the inductor currents i_d and i_q respectively. The v_d and v_q terms come from the measured abc voltages of the filter capacitor for the LC filter as shown in Figure 4.4. The converter terminal voltages e_d and e_q are the inputs that can be manipulated to control the i_{dq} currents. There is inherent coupling between the d and the q axes because there is a q-axis term in γ_d and a d-axis term in γ_q. These interactions between the two axes are decoupled using cross-coupling feed-forward terms, which are the ωL terms in equations (4.12) and (4.13) and as shown in Figure 4.5.

$$\frac{di_d}{dt} = -\frac{R}{L}i_d + \overbrace{\frac{1}{L}e_d + \omega i_q - \frac{1}{L}v_d}^{\gamma_d} \tag{4.10}$$

$$\frac{di_q}{dt} = -\frac{R}{L}i_q + \overbrace{\frac{1}{L}e_q - \omega i_d - \frac{1}{L}v_q}^{\gamma_q} \tag{4.11}$$

The required converter output is calculated in two steps:

1. The d-axis and q-axis controllers calculate γ_d and γ_q respectively.

2. The actual converter voltages e_d and e_q are derived from γ_d and γ_q, using the system state variables to compensate the d and q coupling. The converter output d-axis and q-axis reference voltages are:

$$e_{d\,ref} = L\gamma_d + v_d - \omega L i_q \tag{4.12}$$

$$e_{q\,ref} = L\gamma_q + v_q + \omega L i_d \tag{4.13}$$

4.3.2 Decoupled Outer Voltage Loop Control

The differential equations (4.14) and (4.15) are for the capacitor dynamics. The d-axis output voltage is controlled by η_d and the q-axis output voltage is controlled by η_q. Again there are inherent coupling and interactions between the d and the q axes, which needs to be decoupled. The feed-forward terms i_{od} and i_{od} are the output currents from the LC filter. Section 4.3.1 showed that the currents i_d and i_q can be controlled, therefore it can now be used to control the capacitor voltage v_d and v_q at the PCC.

$$\frac{dv_d}{dt} = \overbrace{\frac{1}{C}i_d - \frac{1}{C}i_{od} + \omega v_q}^{\eta_d} \tag{4.14}$$

$$\frac{dv_q}{dt} = \overbrace{\frac{1}{C}i_q - \frac{1}{C}i_{oq} - \omega v_d}^{\eta_q} \tag{4.15}$$

Once the system is augmented with the voltage integrals for PI control, the actual reference currents for the inner loop is calculated in two steps:

1. The d-axis and q-axis voltage PI controllers calculate η_d and η_q.

2. The reference currents, derived from η_d and η_q, are:

$$i_{d\,ref} = C\eta_d + i_{od} - \omega C v_q \tag{4.16}$$

$$i_{q\,ref} = C\eta_q + i_{oq} + \omega C v_d \tag{4.17}$$

4.3.3 Decoupling the DC-side Voltage Dynamics

The dynamics in the DC-side voltage will distort the voltage output on the AC-side if a constant modulation index is used without a decoupling technique. A decoupling method chosen uses DC-side voltage feed-forwarding in the sine wave comparator-based PWM generator model as shown in Figure 4.6. Alternatively, a constant carrier-wave can be used and the DC feed-forward signal can be inversely applied on the voltage reference waveform before comparing it with the carrier wave. The effect of keeping the AC voltage output with the voltage reference $e_{abc\,ref}$ is very similar, and is important for correct current control. This kind of decoupling is ideally recommend in both open-loop and closed-loop method of establishing the network

voltage to decouple DC-side voltage dynamics. This will prevent harmonics and disturbances from the DC side propagating into the AC side.

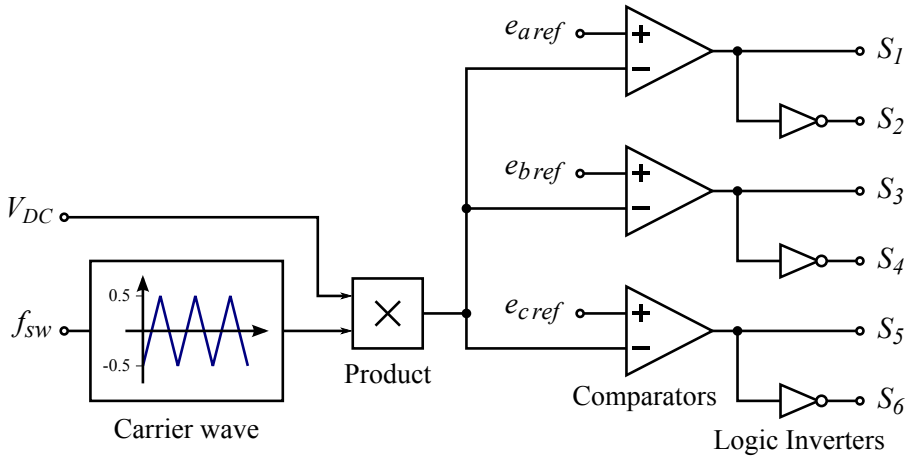

Figure 4.6: Carrier-based PWM generator for a two-level three-phase converter, using comparators with DC voltage feed-forward.

Assuming there is no delay in the signal, sudden changes in the DC-side voltage will not affect the average AC voltage output. The nominal DC voltage level should be sufficient enough so that there is some margin in case it drops, so that the maximum duty ratio remains less than one. Ripple frequencies in the DC side that are higher than the switching frequency cannot be decoupled, but they can be attenuated by the AC filter and prevented from further propagating to the AC network. The magnitude of dynamics depend on the size of the DC link capacitor, which is responsible for limiting the time constant of the change in the DC voltage.

4.3.4 Calculation for Controller Gain Parameters

The PI control gains can be calculated using closed-loop pole placement design with state feedback in MATLAB® [149]. The `place` command used require the state matrix, input matrix and the desired closed loop pole (CLP) positions to calculate the gains. The state matrix depends on the LC filter parameters.

The MATLAB® script and matrix parameters for the gains calculations for are given in Appendix B.2. The closed loop voltage controller has a pair of current-control loops and a pair of voltage-control loops. Control gains are assumed to be the same for both the d and q axes in each pair [150].

For each control loop, the closed-loop pole (CLP) positions are chosen for the desired damping ratio ζ and natural frequency ω_n of the closed-loop transfer function. The gain calculation for the voltage outer loop assumes the inner loop current control response speed is instantaneous. Therefore, the lead compensator in between the control loops needs to be designed to compensate for the lag in the inner loop current control response [6].

4.3.5 Choosing the Closed-Loop Poles

The location of the CLPs can be represented on the complex plane as shown in Figure 4.7. The second order pole is usually paired with its conjugate in the negative imaginary side of the axis, mirrored along the $\Re$eal-axis.

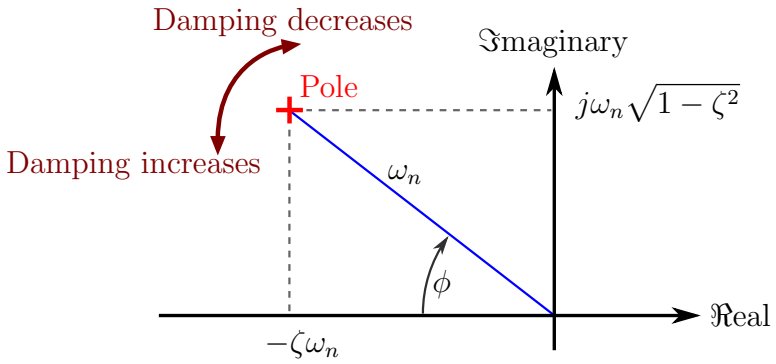

Figure 4.7: A plot demonstrating how the pole location in the complex plane is related to the natural frequency and damping.

The dynamics of the poles of a second-order system can be characterised by just the two variables; the natural frequency and the damping factor (ω_n and ζ). The natural frequency is the magnitude of the pole and gives an indication of the speed of the response. The damping factor is equal to the cosine of the angle ϕ in Figure4.7 as shown in the following equation:

$$\zeta = \cos\phi \tag{4.18}$$

As a general rule of thumb, the CLPs should not be too far away from the open loop poles, otherwise it will demand high control effort. CLPs that are too negative, with very large ω_n magnitudes, i.e. small time constants, are very fast

acting. They require very large gains and lead to large bandwidth in the frequency domain, meaning that the noise will be amplified. The response should also be well damped to minimise oscillatory response, but not too damped that the response will be slowed. A typical damping factor is often chosen between 0.6 and 0.8 [151].

4.4 Simplified Offshore Network Model

The simplified system model considers only two converters, as shown in Figure 4.8. The case study is mainly interested in the converter dynamics and voltage control. Only devices connected to the offshore network are considered, all other devices including the onshore grid side converter and offshore machine side converter are ignored. The offshore HVDC substation converter, labelled VSC1, is filtered by a simple L_1C_1 filter. The closed loop voltage controller, as outlined in Section 4.3, will control the voltage V_1 across the capacitor C_1, which is also at the defined point of common coupling (PCC).

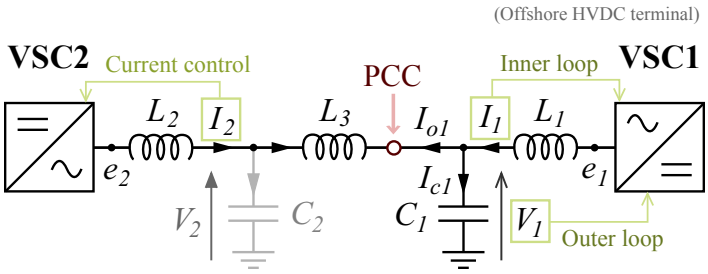

Figure 4.8: Single line representation of the simplified case study model of the three phase offshore electrical AC network and converters.

The converters are simplified to the Thévenin equivalent voltage e_1 and e_2 with series resistance (that is not shown in Figure 4.8) for converter losses. The voltage source of the converters is initially assumed to be an ideal sine wave for small-signal analysis and is then later modelled as two-level converter with IGBT switches for time domain simulation. The cable inductance and the electrical transformers are simplified to a single inductor, L_3.

4.4.1 Parameters

The parameters chosen are based on an existing converter system in [137], see Table 4.2. Although the scale of size and rating does not reflect an actual HVDC system, it serves as a base reference for comparison and laboratory experimentation. Although not shown in the schematic diagram, the resistance R_1 is a very small value in series with the inductance L_1.

Table 4.2: Passive component parameters

L_1, L_2	$0.1\,\mathrm{mH}$
L_3	$0.15 \times L_1$
C_1	$2500\,\mu\mathrm{F}$
C_2	$1\,\mathrm{pF}$
R_1	$0.0021\,\Omega$

It is assumed that variables and parameters can be converted to the per unit system and then scaled accordingly for the voltage and power rating HVDC connection system. The original base values for the small scale system are shown in Table 4.3. From the apparent power S_{base}, line to line voltage $V_{\mathrm{line\,base}}$ and frequency f_{base}, all the other base values can be calculated: the base impedance Z_{base}, inductance L_{base} and capacitance C_{base}. The per unit values are calculated according to equation (4.19). The actual values were used in the models, calculations and simulations, but the results are scale to the per unit values for simpler comparison and interpretation. The calculation in MATLAB® is also shown in Appendix B.1.

$$\text{Per unit value} = \text{Actual value/Base value} \tag{4.19}$$

4.4.2 Structure of the PI Controller

In a state-feedback controller, the input of the proportional controller is the feedback signal as shown in Figure 4.9a. This is used instead of the reference-feedback error, which is normally used for a traditional PI controller, as shown in Figure 4.9b.

Table 4.3: Per unit base values

S_{base}	700 kW
$V_{\text{line base}}$	400 V
f_{base}	50 Hz
Z_{base}	$V^2_{\text{line base}}/S_{\text{base}}$
L_{base}	$Z_{\text{base}}/(2\pi f_{\text{base}})$
C_{base}	$2\pi f_{\text{base}}/Z_{\text{base}}$

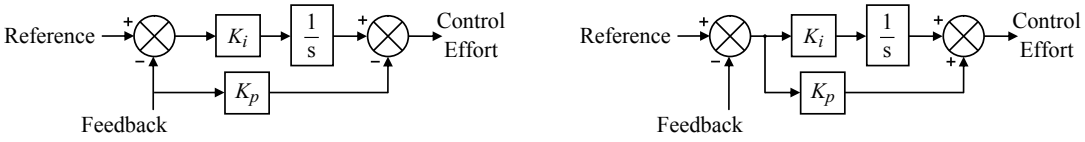

(a) State-feedback into the proportional controller input.

(b) Reference-feedback error for the proportional controller input.

Figure 4.9: Proportional-integral control structures.

The voltage step input was simulated while the VSC1 converter is only connected to a resistive load bank. Figure 4.10a shows that the response is smoother and desirable when state-feedback is used for all the proportional controllers. In Figure 4.10b, when the reference-feedback error is used for all the proportional controllers, the initial response speed is slightly quicker, but less damp and distortion is present the voltage control response.

4.4.3 Aggregated Fully Rated WT Converter

VSC2 is the single aggregated converter model representing all the wind turbine converters, which should be in constant power or current control mode through L_2. Finally, C_2 is a small dummy capacitor used to ease small-signal analysis and simulation, preventing the connection of two inductances in series. The leakage inductance of the transformer, which is also related L_2, may also be used for filtering.

The amount of power VSC2 can export depends on power in the WT prime mover and the wind speed. An actual fully rated frequency converter in a WT is composed of two converters in a back-to-back configuration. The machine side

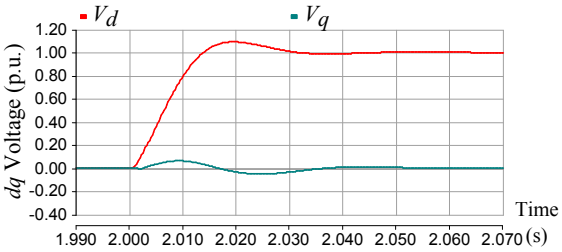

(a) When state-feedback for proportional control is used.

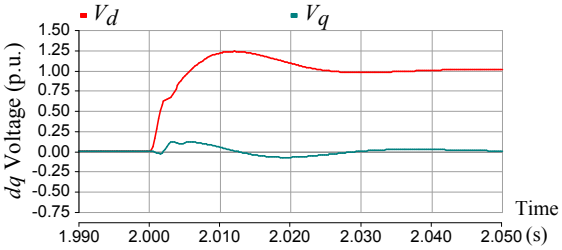

(b) When reference-feedback error for proportional control is used.

Figure 4.10: Voltage control response to a step input in the voltage controller reference.

converter is normally in charge of MPPT and power control. The grid side converter would have to maintain a constant DC-link voltage and will have to absorb all the power coming from the machine side, assuming converter losses are negligible.

In this chapter, VSC2 will not control DC side voltage as on an actual system. Instead, the DC side of the converter will used a fixed ideal DC source, and then the current or power of VSC2 can be controlled directly. The scope of this chapter is only interested in the control and interactions within the offshore AC network.

In terms of AC voltage control, this thesis is only focused on the control of V_1. Assuming V_1 is constant, if the cable parameter (L_3) is large, the voltage at V_2 would vary with power. The WT (VSC2) may control the supply of reactive power in order to control voltage at this point of connection. A strong PI controller may not be recommended for this type of voltage control in case control "fighting" interactions take place between V_1 and V_2, in case L_3 is small. A simple proportional controller or droop control for voltage control at VSC2 may be suitable instead, which would be usually used.

4.4.4 WT Converter Current Control Mode

The structure of the current controller for the VSC2 aggregate WT is the same as the inner current loop part of the controller with *dq* decoupling as described in Section 4.3.1 and as shown in Figure 4.5, ignoring the outer loop and the lead compensator part.

4.4.5 WT Converter Power Control Mode

A constant current control reference for the WT converter model had to assume the network voltage is constant. When the current is constant, the voltage is coupled with power, therefore if the voltage fluctuates this will also cause the powers to fluctuate and would not be representative of the behaviour of the WTs. Furthermore, allowing the power to fluctuate will also cause ripple in the DC link voltage of the WT frequency converter. In order, to maintain a constant voltage in this DC link, the power flow in the grid-side converter in the WT must be equal to the power through the machine side converter, assuming no losses. Therefore, VSC2 should be modelled as a controllable constant power source, and in order to achieve this, dynamics in the AC side voltage of the network should be compensated.

Constant power control is achieved by dividing the references for the active power P_{ref} and reactive power Q_{ref} by the magnitude of the AC voltage, which is fed forward as shown in Figure 4.11. The result will be used for the *dq* current references in the current controller as described in Section 4.4.4. This method would require the current control response to be very fast in VSC2 in order to properly compensate the AC-side voltage dynamics. How fast the current control loop needs to be in VSC2 depends on how fast is the AC side voltage fluctuation. Depending on the *dq* transformation coefficient type used, the appropriate gain may need to be applied in order to correct the power level to match the power reference. There is no power feedback loop in this method.

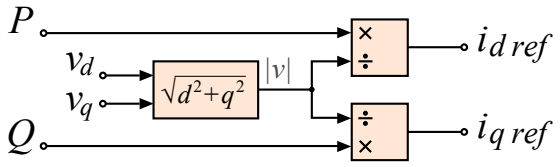

Figure 4.11: Block diagram for constant power control mode, an extension of the *dq* current controller.

4.5 Design and Analysis of the AC Voltage Control Dynamics

The AC voltage controller, as shown in Figure 4.5, is applied to a simplified offshore network model. The aim is to design a fast controller with sufficient damping. The dynamic response characteristics of different control gain design parameters are analysed. Interactions with an aggregate WT power controller were also studied.

4.5.1 Small Signal Analysis Method

For simplicity, small signal analysis is performed in a common reference frame. All components in the electrical system are modelled in the same *dq* reference frame as the controller. The output of the controller is already the converter voltage e_{dq}. The inductors and capacitor components are modelled according their *dq* differential equations as outlined in equations (4.10) to (4.15). Each component has been built in modules in Simulink, and then their inputs and outputs can be connected according to the schematic the simplified case study system in Figure 4.8. A valid operating point is found for 1.0 p.u. of active power and 0.2 p.u. of reactive power supplied by VSC2, which is under power control mode. The operating points must be reachable, as small signal analysis with invalid operating points have no meaning. No operating point can be found if the system does not satisfy the power limit equation (3.2). The model can then be linearised in MATLAB using the `linearize` command. The small signal analysis can be used to observe the eigenvalues in the complex form for all the state variables, from which the damping factor ζ can be calculated in a similar way using equation (4.18) and Figure 4.7 for reference. The results are then processed to find the minimum damping ratio in the system for each test case. If

damping is negative, an unstable system is predicted and the eigenvalues have no meaning.

4.5.2 Speed Limit of the Inner Current Loop Control

The control speed, or the bandwidth, of the inner current loop controller is limited by the PWM frequency [145]. The duty ratio can only change once every switching cycle. This discretisation effect introduces a small delay in the converter voltage output e.

In this case study, the input inner control loop dynamics of VSC1 will be constant and designed to have a CLP value of -1000 in the real axis. The damping ratio ζ will be constant at 0.7, therefore its natural frequency magnitude ω_{ni1} is 1428.6 rad/s. The rise time response of the inner loop in this case should be approximately 2.2 ms using equation (4.20) [151].

$$T_r \approx \frac{2.2}{\zeta \omega_n} \tag{4.20}$$

Typically, the PWM switching frequency is usually needs to be faster than the chosen current control natural frequency, about eight times. Therefore the delay in the converter voltage output e will be assumed to be negligible and therefore ignored. Assuming this is true, the closed-loop dynamics expected with the designed pole placement, will match the actual system response.

4.5.3 Tuning the Outer Loop Controller and Lead Compensator

The current control performance in the inner loop is not perfect and will produce a phase lag, which should be appropriately compensated. A first order lead compensation has been added between the inner and outer loops as shown in Figure 4.5. It is simply a zero-pole pair transfer function in the s-domain, see equation (4.21). This introduces a phase lead before the input of the current reference to improve the dynamics by compensating the phase lag in the current inner loop response. The zero is placed near the dominant CLP of the inner control loop, and the lagging pole that is placed to its left is needed to suppress the high frequency noise amplification

by the zero.

$$\frac{\tau_z s + 1}{\tau_p s + 1} \tag{4.21}$$

The lead compensator behaves like the derivative part of a proportional-integral-derivative (PID) controller, which accelerates the control effort at the begining of the step input. Here, the lead compensator is considered separately so that the PI control parameters can be calculated independently using the method already described. Later, all the control parameters can be merged together into a traditional PID control structure, and the PID gains can be found by deriving from the PI control and lead compensator parameters and making sure the open loop and closed loop poles and zeros are the same.

Small signal analysis have been performed for a range of different inner to outer control loop speed ratios, $\omega_{ni1}/\omega_{no1}$. The natural frequency ω_n and damping ratio ζ are design parameters for the method described in Section 4.3.4 and therefore do not reflect the actual response. The inner loop speed of VSC1 has been made constant due to the speed limit as described in Section 4.5.2. The desired outer loop CLP positions for the gain calculation will depend on the control loop speed ratio, $\omega_{ni1}/\omega_{no1}$. The i in subscript here denotes the inner current loop, the o denotes the outer voltage loop, and the number denotes the VSC number in the case study.

The process of gain calculations and small signal analysis for the range of control loop speed ratios has then been repeated for a range of zero leading time constants τ_z, where the zero positions are near CLPs of the inner control loop. The purpose of this method is to facilitate seeking an optimum control parameter. The time constant of the lagging pole τ_p is assumed to be always 10 times smaller than of the zero, so $\tau_p = 0.1\tau_z$. The result is a set of minimum system eigenvalue damping as shown Figure 4.12, which was also published in the ICRERA 2013 conference [6].

4.5.4 Choosing the Control Parameters

As a general rule of thumb, according to Wade (Chapter 9 in [152]), the speed of the outer loop should be three times slower than the inner loop. Therefore, a tight current-controlled loop is essential in the voltage source converters in order to leave sufficient room for a sufficiently fast outer loop controller. If the outer loop speed

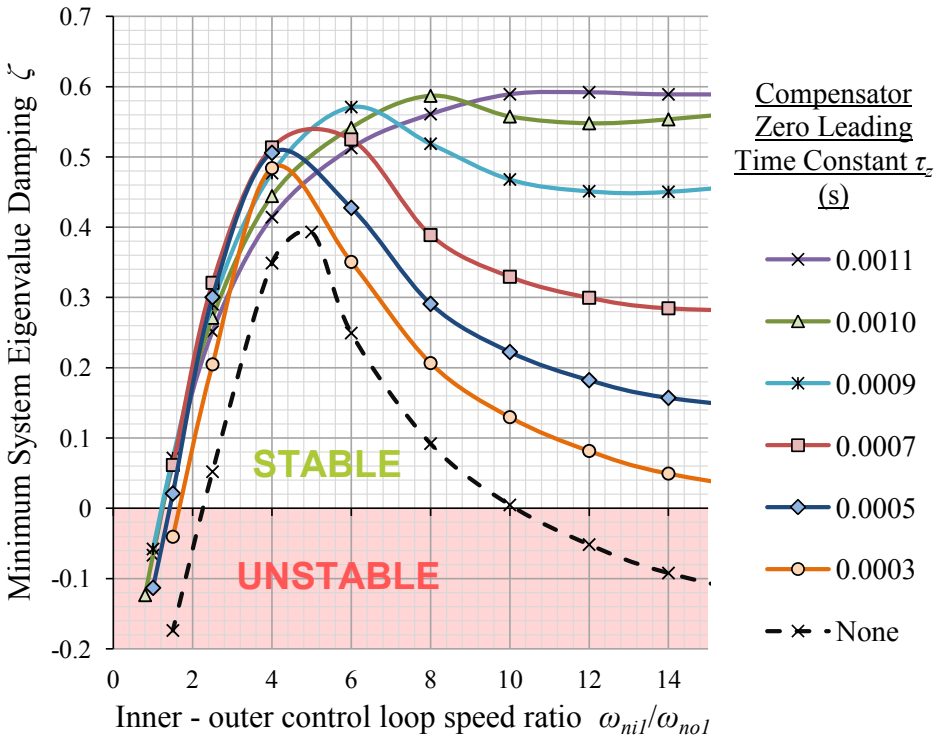

Figure 4.12: The minimum damping in the system against the VSC1 inner to outer loop speed ratio $\omega_{ni1}/\omega_{no1}$ for a range of lead compensation parameters. The current controller in VSC2 is half the speed of outer loop of VSC1, $\omega_{ni2}/\omega_{no1} = 0.5$.

is too close to the inner loop speed, adverse interactions or "fighting" will occur between the controllers. The outer loop usually can be damped by reducing the controller gain and lengthening the integration time, which slows down and reduces the bandwidth of the outer loop control. The results in Figure 4.12 may first suggest that this might not always be the case, where the damping is not always increased as the outer loop control speed is reduced. This is likely due to the interactions with VSC2, which is further discussed in Section 4.5.7.

Figure 4.12 also demonstrates the importance of having the compensator. Without the compensator, the system has significantly less damping and is only theoretically stable between 2.3 and 10 for $\omega_{ni1}/\omega_{no1}$. Outside this range, the damping is negative and the system is unstable. At first, this was surprising for the slower outer loop control case, where a previous hypothesis suggested the slower the outer loop for the voltage control is better and more stable. However, there are interactions with the wind turbine converters to take into account. The ideal control parameters

should have the lowest $\omega_{ni1}/\omega_{no1}$ speed ratio for fast AC voltage control, and the highest system minimum damping for maximum stability margin. This would be the uppermost point at the left side of the plot. Based on the results so far, the compensator parameter τ_z should be between between 0.0007 s and 0.0009 s.

Generally, there should be enough margin for error when choosing the control parameter. It is desirable to have a fast voltage outer loop controller, but it is also important that is robust and not too close to a position where it can become insufficiently damped. A control speed ratio of $\omega_{ni1}/\omega_{no1} = 5$ would be ideal because it is where the minimum damping is high for a wide range of compensation parameters. The proportional K_p and the integral K_i gains for this case are shown in Table 4.4. The reference values, denoted by the subscript 'ref', for ω_n and ζ are mainly for the purpose for the control gain calculation method and the control parameter design process as outlined in Section 4.3.4 and Appendix B.2, and therefore do not exactly reflect the actual dynamic characteristics. The inner current loop speed has already been decided in Section 4.5.2.

Table 4.4: VSC1 control parameters for $\omega_{ni1}/\omega_{no1} = 5$.

VSC1 control loops	$\omega_{n\,\mathrm{ref}}$	ζ_{ref}	K_p	K_i
Inner current loop (d and q axes)	1428.6 rad/s	0.7	0.198	204.08
Outer voltage loop (d and q axes)	285.7 rad/s	0.7	1.00	204.08

4.5.5 Root Locus and Closed Loop Pole Analyses

The purpose of this section is to better understand the pole interactions between the inner current control loop and the outer voltage control loop. So far, the inner loop dynamics was approximated as a simple first order delay TF as in [137]. A second order TF will be used here instead, which will reflect the second order CLP position of the inner current loop controller. The transfer function approximations of difference components in the voltage control loop are shown in Figure 4.13. This simplified block diagram is representative for both d and q axes if the interactions between them are assumed to be fully decoupled.

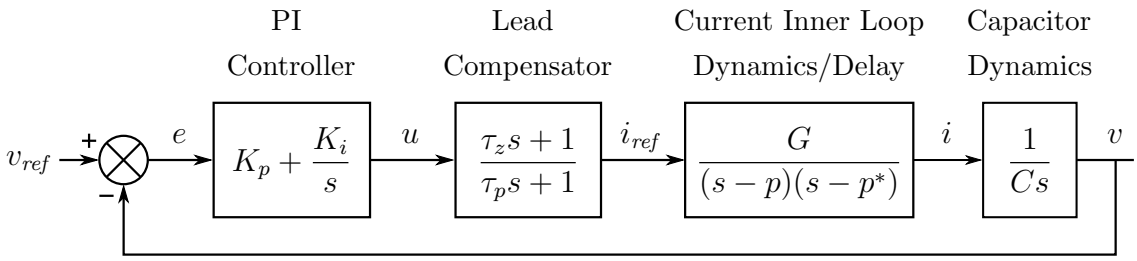

Figure 4.13: Simplified control block diagram of the *dq* voltage controller with transfer functions.

Figure 4.14 shows the root locus plots and closed loop pole (CLP) positions for three difference cases, represented by different colours. The root locus is the trajectory of the CLPs as the gains in voltage control feedback loop is varied. The plot is found using the root locus (`rlocus`) command in MATLAB® with the relevant transfer functions put together as the system. The CLPs are found using the `feedback` command to generate the closed loop TF and then the `pzmap` command is used to map out the pole locations, which are represented by the square symbols. The same PI control gains that were calculated using the `place` method as described in Section 4.3.4 were included to find the CLP for each case. The inner-outer loop speed ratio used here is $\omega_{ni1}/\omega_{no1} = 2.5$, and the damping factor and inner current loop base speed remains the same as previously discussed.

The original gain calculation method used assumed that the current inner loop control response is instantaneous. If the assumption was true, the expected root locus and CLP is represented in blue as the 'ideal case', shown in Figure 4.14.

The root locus and CLPs for the 'no compensation case' are shown in black, which is where the closed loop response poles of the inner loop (current control CLP) are taken into account in the transfer function model. In comparison with the 'ideal case', it shows how the root locus of the voltage control loop for the 'no compensation case' is distorted and the CLP position is displaced further away than intended. The 'no compensation case CLP2' is on the root locus leading from the second-order inner loop poles denoted as 'current control CLP'. It is the 'no compensation case CLP2' that repels the 'voltage control CLP' towards right hand side towards the unstable region, where the damping is reduced. The chosen control gains for this case seems to be higher than it should be and the margin before it

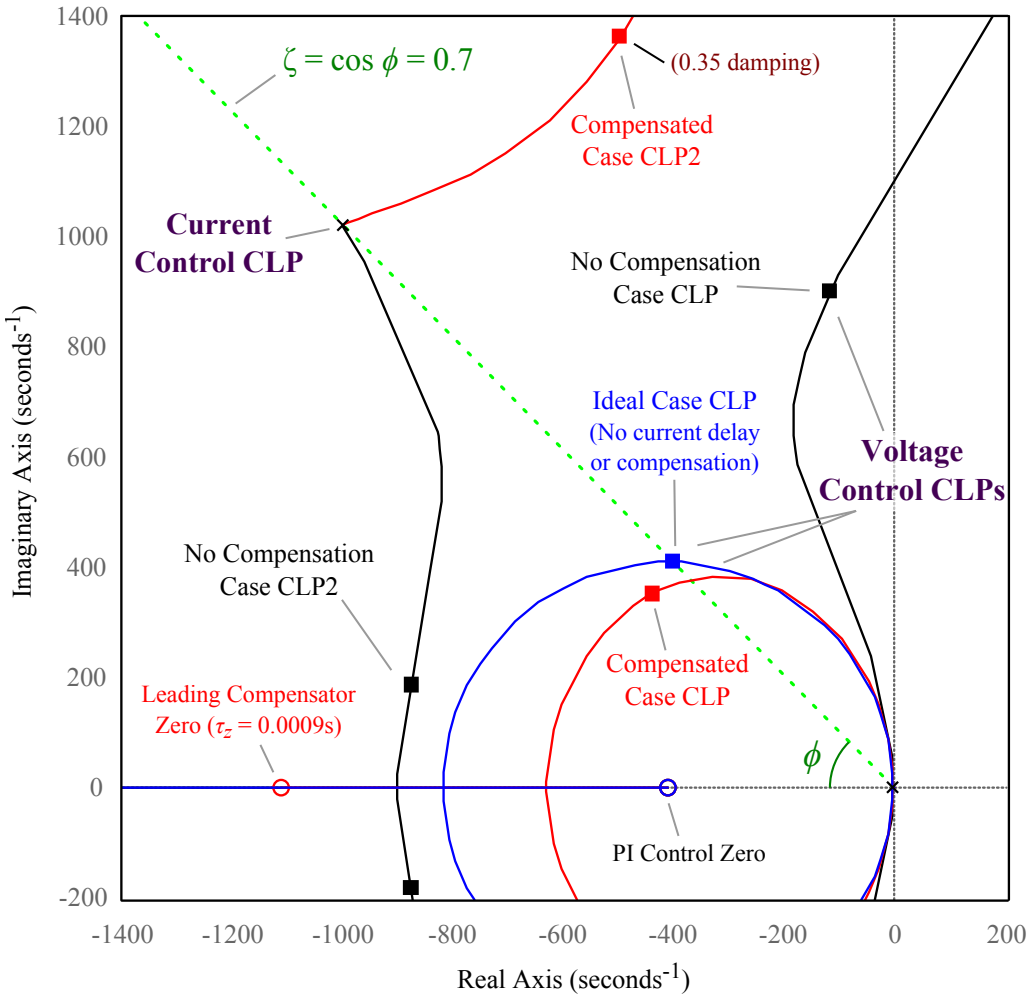

Figure 4.14: Root locus plots and closed loop pole positions of a voltage controller design ($\omega_{ni1}/\omega_{no1} = 2.5$) for a case with a leading compensator, a case without one and an ideal case.

reaches the unstable region is smaller. However, even if the gains are further lowered and the voltage control CLP is moved further down along the root locus, the voltage control action will slow down and the damping will not significantly increase. This is because vector angle of the CLP will still remain quite high, based on the root locus trajectory.

The root locus and CLPs shown in red are for the 'compensated case', where a leading zero with a time constant of $\tau_z = 0.0009$ second is included, which partially compensates the phase lag of the inner loop current control response. The lagging pole that is usually paired with this zero is ten times further away and therefore has little impact on the area of interest. There should be four CLPs in this'compensated

case', but only two are shown as Figure 4.14 is cropped, and only showing mostly the top half of the plot. This is mirrored along the the $\Re$eal-axis, at $\Im \mathrm{m} = 0$, for the conjugates at the bottom half. The 'voltage control CLP' of interest for the 'compensated case' seem to be reasonably close to the CLP positions for the 'ideal case CLP'.

The angle of the compensated voltage control CLP is slightly lower than the designed target damping angle $\phi = \cos^{-1} 0.7$, therefore this particular CLP is slightly more damped. However, the angle of the 'compensated case CLP2', on the root locus trailing from the 'current control CLP' position, is greater than the reference angle for $\zeta = 0.7$. The root locus from here is projected towards the top right hand side, which is why the minimum damping will always be less than the designed damping of the inner loop current controller. The magnitude does not significantly change, so its natural frequency response speed is maintained. The damping factor of 0.35 for the 'compensated case CLP2' matches quite closely with minimum system eigenvalue damping in Figure 4.12 (approximately 0.37 at $\omega_{ni1}/\omega_{no1} = 2.5$). By increasing the damping of the 'current control CLP', it may be possible shift the root locus starting position for the 'compensated case CLP2' to a lower position with increased damping as well.

4.5.6 Minimum Damping Lower than Expected

The calculation method for outer loop control gains assumed the current inner loop response is instantaneous. Therefore, the expected results will only be fully applicable if the delay in the inner loop is appropriately compensated. However, the minimum damping in closed loop response in the end does not meet the original 0.7 damping design reference requirement. As shown in Figures 4.12 and 4.16, this value is in between 0.55 to 0.6.

Figure 4.15 shows how the ideal case and compensated case CLP locations move, for a variable inner-to-outer control loop speed ratios between 1.5 and 15.0 at intervals of 0.5 (`for` $\omega_{ni1}/\omega_{no1}$ `= 1.5 : 0.5 : 15.0`). The CLP plots for each case are all superimposed on to the same figure. As the outer loop voltage control speed increase towards the inner loop speed, the group of CLPs in the upper part of the figure are

repelled towards the right hand side which then produces decreased damping. It shows how the minimum eigenvalue damping factor reference requirement of 0.7 or greater could not be achieved for any given inner-to-outer loop speed ratios with the parameters tested so far.

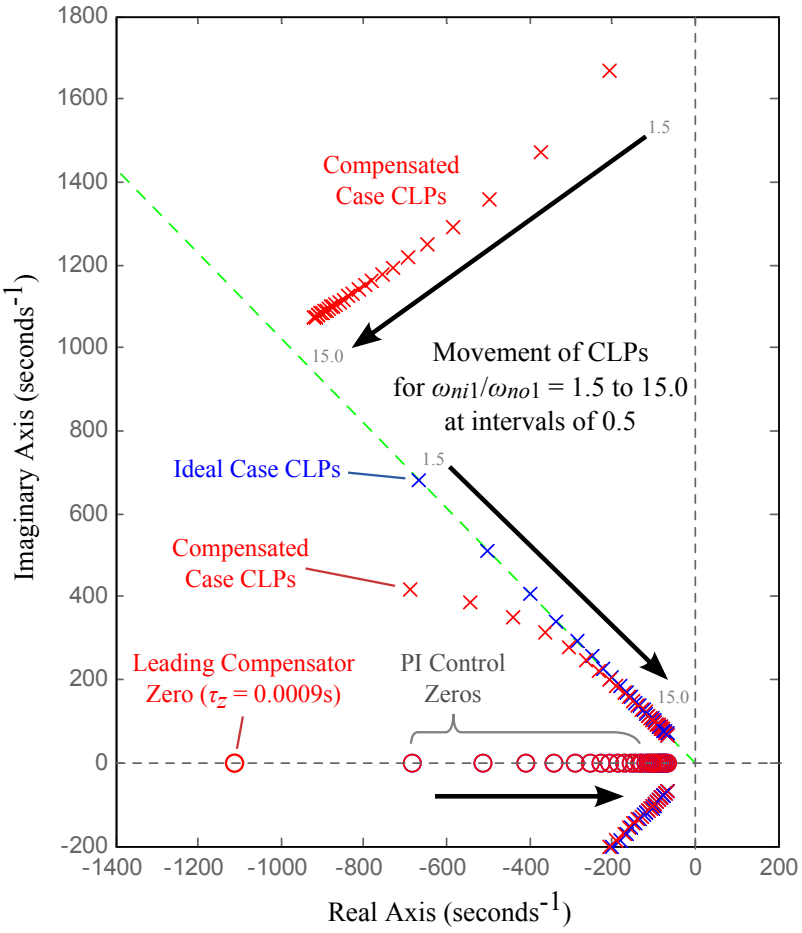

Figure 4.15: Pole-zero plot of the closed loop pole positions of the voltage controller design for a range of inner-outer loop speed ratios ($\omega_{ni1}/\omega_{no1}$ `= 1.5 : 0.5 : 15.0`) for compensated case in red and ideal case in blue.

4.5.7 Interaction with the Aggregated WF Dynamics

VSC2 represents the aggregated WF, and its dynamics results were kept proportional and always half of the design reference of the outer loop control speed of VSC1 for the results in Figure 4.12. Therefore the absolute control speed of the VSC2 is not constant. Small signal analysis was repeat for an absolute VSC2 control speed that is constant instead. The current control dynamics of VSC2 was chosen to be equal

to the inner control loop speed of VSC1, therefore $\omega_{ni2} = \omega_{ni1}$. The results are shown in Figure 4.16.

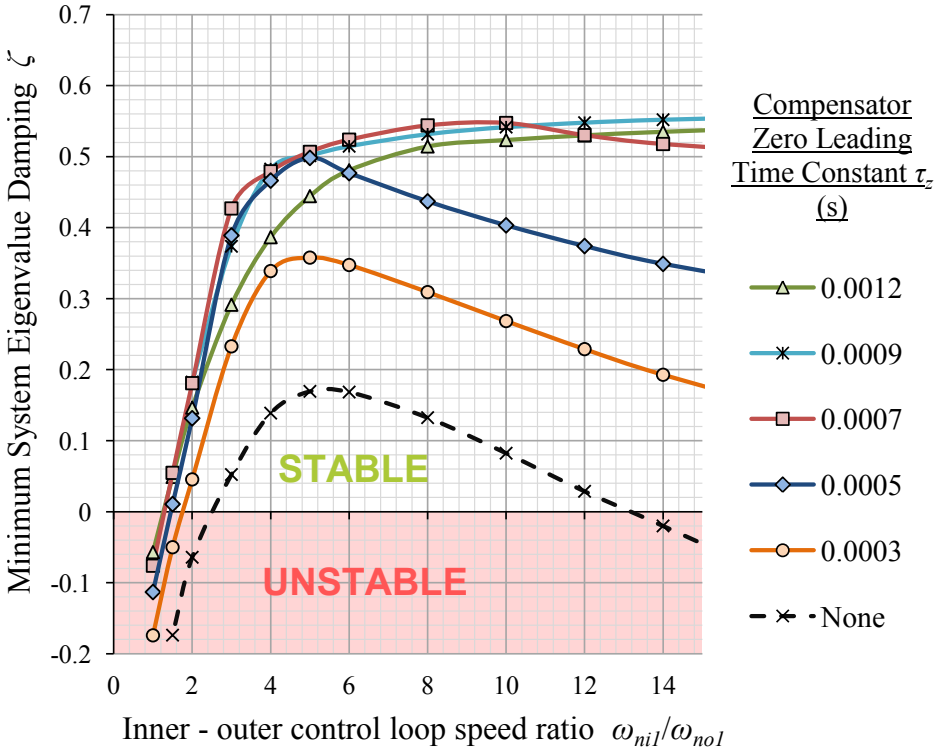

Figure 4.16: The minimum damping against VSC1 $\omega_{ni1}/\omega_{no1}$ speed ratio. VSC2 current control speed is constant and equal to inner loop speed of VSC1.

There are some notable differences between Figure 4.12 and Figure 4.16, especially that the overall eigenvalue damping for having no compensator is now significantly lower. This suggests that ω_{ni2}, the control speed dynamics of the aggregated wind turbine converter VSC2, has an influence on the response and relative stability of the system.

Small-signal analysis was carried out again for a range of $\omega_{ni2}/\omega_{no1}$ speed ratios. The minimum system damping was investigated when the current control speed in VSC2 is varied for a fixed outer voltage loop control speed in VSC1. The results for this are shown in Figure 4.17. The voltage controller in VSC1 used a ratio of $\omega_{ni1}/\omega_{no1} = 5$ for its control speed. Figure 4.17 also shows that, if no compensator is used in VSC1 and the current controller in VSC2 is faster than the voltage controller of VSC1, then the minimum damping is reduced as expected, and vice versa, the damping is higher if VSC2 is slower.

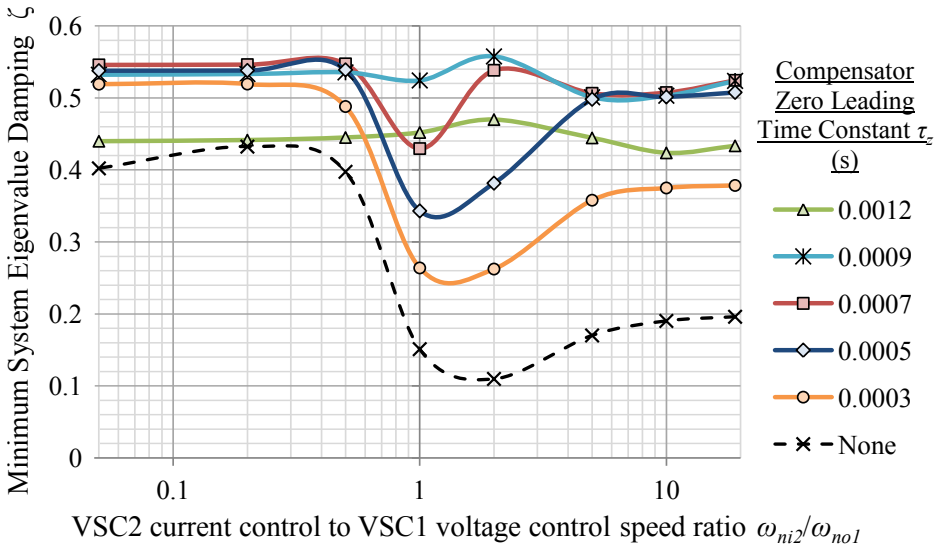

Figure 4.17: The minimum system eigenvalue damping against $\omega_{ni2}/\omega_{no1}$ VSC2 current control to VSC1 voltage control speed ratio, for $\omega_{ni1}/\omega_{no1}$=5, and for a range of lead compensation parameters

When the zero leading time constant parameter of the compensator is 0.0009 s, the plot is relatively constant with high minimum damping compared to the other curves. Unexpectedly, this is true for relatively high speed ratios, when the dynamics of VSC2 are faster than VSC1. This characteristic is desirable because this suggests that the speed of the current controller in the network side converters of the wind turbines does not depend on the voltage control speed of the HVDC converter substation. Therefore, $\tau_z = 0.0009$ s seems like a suitable value for the zero leading compensator in this case study.

This was verified using PSCAD® simulation, again assuming an ideal voltage source without PWM switching. The control gain parameters used were for $\omega_{ni1}/\omega_{no1}$ = 5 and $\omega_{ni2}/\omega_{no1} = 1$. The response to a step change in the reference input of VSC2 for the case without compensator in the VSC1 voltage controller is shown in Figure 4.18a. Under-damped oscillation in V_q and distortion in the power output P were then found. Although, the magnitude of these distortions in the power output seem small in the PSCAD simulation response, the V_d voltage spike that is 40% above the nominal voltage is very significant. When using the chosen compensator in the VSC1 voltage controller, the response is smoother and much better damped in comparison, as shown in Figure 4.18b, which is expected according to the small

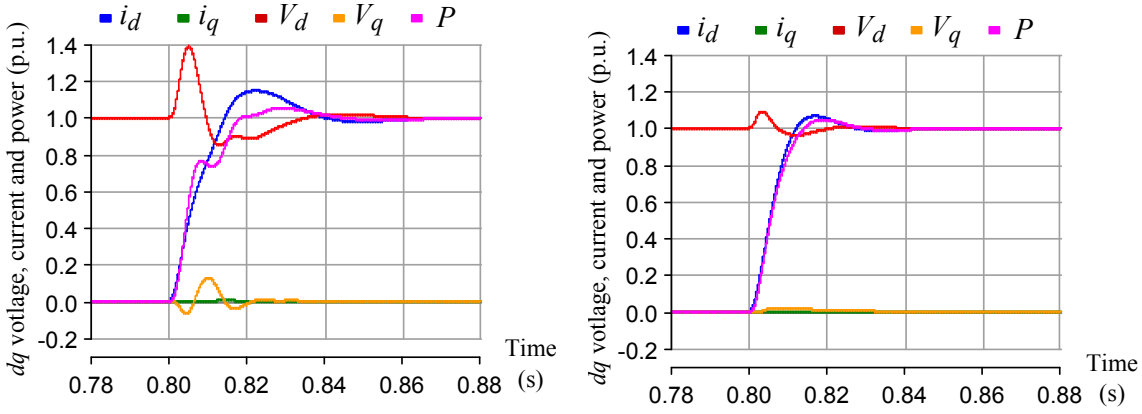

(a) Without leading compensator. **(b)** With compensator, $\tau_z = 0.0009\,\text{s}$.

Figure 4.18: VSC2 dq current, dq voltage and power response to a step input at VSC2, from PSCAD simulation for $\omega_{ni2}/\omega_{no1} = 1$, with and without the compensator.

signal analysis results in Figure 4.17.

Furthermore, Figure 4.17 shows that the minimum damping is higher when $\omega_{ni2}/\omega_{no1}$ is higher above one, which is when the current control loop in VSC2 is much faster than the voltage outer loop control speed in VSC1. VSC2 was under power control mode for the small signal analysis. As mentioned in Section 4.4.5, the current loop controller needs to be very fast in order to compensate the AC voltage dynamics. On the other hand, when the $\omega_{ni2}/\omega_{no1}$ ratio is less than one, the power dynamics from VSC2 is very slow and it does not have an impact on the voltage fluctuation.

In Figures 4.12 and 4.16, the minimum damping was not expected to decrease as the speed ratio $\omega_{ni1}/\omega_{no1}$ increases as discussed in Section 4.5.4. The inner loop and outer loop poles are very far away from each other an have very little impact on each other to displace any poles towards low damping and instability in VSC1 alone. Results so far suggests that there are further interactions between the VSC1 and VSC2 controller. It is possible that if the VSC1 voltage control regulation is slow, the voltage fluctuation will become larger, underdamped and faster, to the point where VSC2 current loop will not be fast enough to compensate the AC voltage dynamics while under constant power control.

4.5.8 Voltage Control Speed Comparison in PSCAD® Simulation

Small-signal analysis is not entirely conclusive, because the model was ideal and simplified. The system is assumed to be linear, and does not take into account the effect of PWM harmonics, noise, delays, phase-locked loops in VSC2, and so on.

The PSCAD/EMTDC® model for VSC1 is a two-level 3 phase IGBT converter model with a carrier based PWM. VSC2 in this case will be also be under current control mode now instead of power. It is assumed the output of VSC2 is filtered and therefore is modelled as non-switching ideal voltage source. This also keeps dynamics of the current disturbance consistent for testing the converter of interest, VSC1. The compensator uses a zero leading time constant of 0.0009 s and $\omega_{ni1}/\omega_{no1} = 5$ for the voltage controller, as chosen in the Section 4.5.4. The current controller response speed of VSC2 remains equals to that of the inner loop in VSC1. A very large current step input of 1 p.u. in the d-axis current reference was applied to the controller in VSC2 at time $t = 0$. The controller in VSC1 is able to to regulate the dq voltage at the PCC against this large disturbance, as shown in Figure 4.19. These results were also presented in the ICRERA conference paper [6]. For a switching frequency of 2000 Hz, the filter was sufficient as the switching harmonics are not present in PCC voltage, which is an ideal voltage characteristic for smooth PLL operation at the WTs.

Higher and lower $\omega_{ni1}/\omega_{no1}$ speed ratios are simulated for comparison. For a speed ratio of 2.0 and 5.0 in Figure 4.19, there is little difference between the settling times. This is because when the speed ratio is 2.0, it is less damped and the oscillations continue for longer. The dynamics of the voltage response for all three speed ratio cases agree with the corresponding minimum system eigenvalue damping points in Figure 4.16. Small-signal analysis can be a useful design tool to understand the interactions among power electronic devices and help deciding the controller parameters.

Furthermore, it is noted that the faster the voltage controller, the better the voltage regulation and the smaller the voltage deviation from the nominal reference.

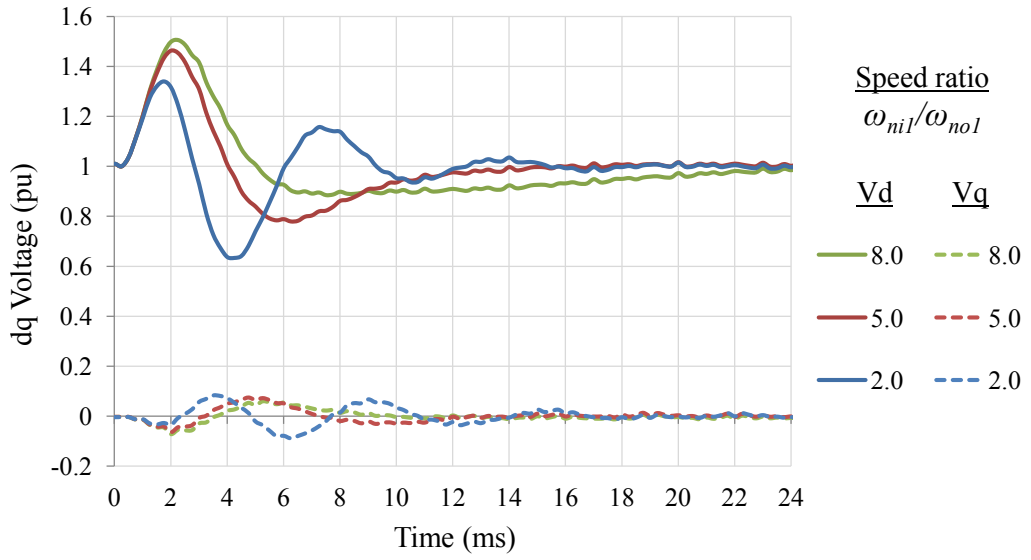

Figure 4.19: PSCAD time domain simulation *dq* voltage response to large current step input in VSC2, for three different outer loop control speeds

This is true until the speed of the outer voltage loop controller is too close to the speed of the inner loop, and the poles start to interact with each other and damping deteriorates as explained in Section 4.5.6.

The amount of voltage deviation from the nominal reference level also depends on the magnitude of the current disturbance. In a real wind farm, the machines will have a larger time constant, and each turbine would respond independently. The magnitude and the change in current with respect to time of the wind farm system is not likely to be as large as in this scenario, which can be regarded as an unusual and very adverse case. Then under normal conditions, the voltage regulation should be relatively stiff and the voltage fluctuation at the PCC should be minimal.

In Figure 4.19, there is an over-voltage up to 1.5 p.u., which is undesirable. However, this can only happen if there is a large current step input into VSC1. It could mean a fast sudden generation from the WF, which is an unlikely to happen as a sharp step, even if there was a fast sudden gust. A step current drop from a sudden disconnection is more likely to occur. The PCC voltage response in that case will first drop instead and then rebounds as the control effort aims to recover it back to the nominal level, like a mirror of Figure 4.19 along the nominal level. The damping will be important for minimising the over-shoot as the voltage rebounds

and therefore over-voltage. When the speed ratio of 2.0 was used and the damping factor was smaller, even though the initial peak was smaller, the rebound voltage would deviate by more than 0.35 p.u. from the nominal, which is too much.

The current response plot from VSC1 and VSC2 is shown in Figure 4.20. The direction toward onshore (VSC2 to VSC1) is the convention for positive current in this plot. There is a difference for the I_q plots because reactive power is consumed or generated in the cable, transformer and filter. Ideal non-switching voltage source models were used for both converters for these results, so current dynamics can be easily compared without superimposed switching harmonics. VSC2 current dynamics strongly agree with the designed natural frequency and damping specification. On the other hand, VSC1 current response is initially delayed, then the overshoot amount is approximately 2 times higher than that of VSC2, and appears to have a reduced damping. This is expected because the voltage error through the outer loop controller is the reference for the inner current control loop. The points of intersection of the VSC1 and VSC2 currents in Figure 4.20 are also the points of zero gradient on the voltage plot in Figure 4.19.

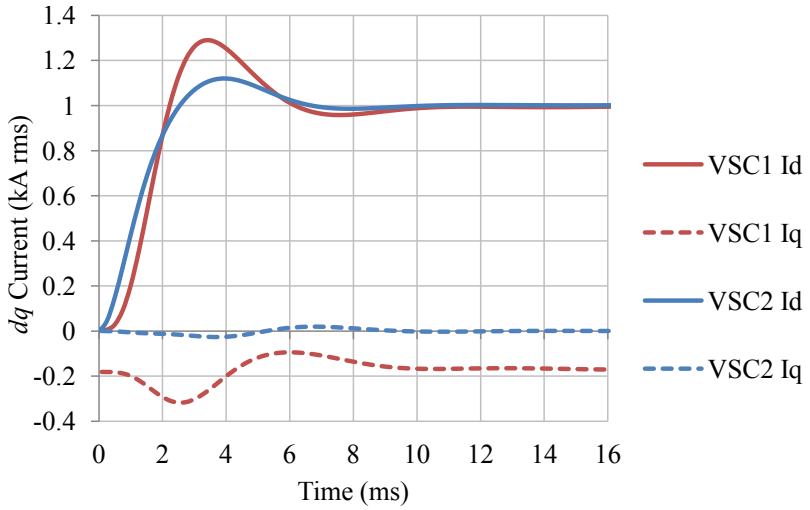

Figure 4.20: PSCAD time domain simulation dq current response in VSC1 and VSC2 for $\omega_{ni1}/\omega_{no1}$=5, and non-switching ideal voltage source used for both converter.

4.6 Chapter Summary

- Voltage control in offshore VSC-HVDC station has been considered and a cascade configuration has been proposed and analysed in detail. The control is also in the dq coordinate system, and the d- and q-axis components are fully decoupled, which gives it a fast and damped control action. The inner loop controls the current through the inductor of the LC filter. By being able to control this current that feeds into the filter capacitor, its voltage can be controlled.

- The calculation of the control gain parameters uses the `place` command in MATLAB®, which is a simple and fast pole placement method. The method was found to be sufficient and accurate for current control gains assuming there are no PWM delays. However, the gain calculations for outer loop voltage controller assumed the inner loop response was instantaneous. The actual current control response has a significant phase lag, which must be appropriately compensated in order to implement a fast outer loop control.

- Small signal analysis was used to gauge the eigenvalue damping in the system. The tool was used to tune the voltage control parameters for a fast control and sufficient minimum damping. The speed of the outer voltage control loop should be five times slower than the inner current control loop, which is the point where the minimum system damping is the highest. A first order leading compensator was enough to compensate the second order delay in the current control loop.

- When the control speed of the outer loop is too close to that of the inner loop, the system minimum eigenvalue damping is reduced. The analysis of the root locus and movement of the closed loop poles helped to better understand the "fighting" interactions between the control loops. The closed loop poles were shown to repelled right, towards the imaginary axis of the pole-zero plot, reduced damping and reduced stability margin.

- A fast AC voltage controller in the dq frame that is fully decoupled is necessary

to minimise the voltage fluctuation caused by a current or power disturbance in the offshore wind farm network. The voltage at the filter capacitor can then be controlled as a constant voltage source. If the control can be fast enough, this can help eliminate low order harmonics and resonance.

- Interactions between the AC voltage controller at the substation and the power controller in the aggregated WT converter were studied. The control loop speed for constant power control has to be fast in order to compensate for the dynamic changes in PCC voltage, and the minimum system damping was shown to be better when this was case.

- The AC inductor filters of the aggregated WT and the HVDC station are controlled as current sources using the inner control loops. These current sources are only allowed to be connected if there is a voltage source in between. In this case a fast controlled constant voltage source at capacitor in the PCC is used. The inner current loop of the voltage voltage controller may later be exploited for current saturation control.

Chapter 5

Evaluation of the AC Voltage Controller and its Performance

The benefits of using the AC voltage controller and the chosen control parameters, for the simplified case study offshore network, which was introduced in Chapter 4, are evaluated in this chapter and compared with open loop voltage method of establishing the network voltage, without closed loop control. The comparison will find that the control action was able to keep a constant capacitor voltage and minimise resonant oscillations. The current can be limited between the outer loop and inner loop of the voltage control structure and can be advantageous for VSC device protection. The performance of a current saturation technique is studied and further interactions were found with the WT power controller during saturation. Current saturation during balanced and unbalanced fault scenarios were also considered in the study. The problem of having a large number of sensors required for feedback and feed-forward with the proposed voltage controller is addressed. The complexity of such a system may have an impact on its reliability and operability in case of a failure.

5.1 The Voltage Controller for Suppressing Filter Resonance

As discussed in Section 2.3.5, the Borwin1 HVDC connected offshore wind farm was having problems with over-voltage in the filter capacitors, which will cause them to either fail or trip. The voltage at the PCC, as shown in the case study model in Figure 4.8, is also the same voltage point for the capacitor of the LC filter. If this voltage can be controlled to a fixed reference voltage and frequency, this can limit over-voltage in this capacitor and therefore restrict the resonance in the filter.

The LC filter inherently has a second order dynamics resonant characteristic. If this is not properly damped, the voltages and currents in the LC filter will amplify to unstable levels at the resonant frequency, which is defined as:

$$\omega_0 = \frac{1}{\sqrt{LC}} \tag{5.1}$$

In this section, the closed loop voltage control method of establishing the network voltage will be compared to an "open loop" case. Resonance in LC filter will be observed and the effectiveness in reducing this using the controller will be studied.

5.1.1 "Open-Loop" AC Voltage Approach

The open loop approach simply sets the reference voltage at the converter terminals e_1 in Figure 4.8, which then becomes the AC voltage source point. The reference waveform v_{abc} is generated using the inverse dq transformation, except with a constant input voltage E_{dref} for a desired variable frequency. This is usually compared with a triangular carrier waveform to generate the PWM switching sequences for the IGBT gates. An alternative method is to use a space vector pulse width modulation (SVPWM) algorithm to calculate the timing sequence for the switching.

Control feedback is not required for this method, so the number of sensors required is dramatically reduced. If a sensor fails and outputs erroneous measurement, this would lead to complication and instability in a full state feedback control system. Therefore a simplified system would be better for robustness and reliability. However, the control benefits of the closed-loop method is lost, such as current satu-

ration at the input of the inner current loop control for limiting fault currents. The DC voltage feed-forward signal, as described in Section 4.3.3, may still be necessary to decouple the dynamics in the DC voltage so they do not propagate into the AC side.

5.1.2 Resonance in the AC Filter Using the "Open Loop" Approach

The PSCAD simulation for the open loop case in Section 5.1.1, found resonance when a step change is applied to the current (I_{1dq}) input to the AC system, as shown in Figure 5.1 and 5.2a. The resonance occurs for either rising or falling step change in both d and q axes. It is also found that the resonance distorts the PCC voltage V_{1dq}) and the output frequency (f) of the PLL. The frequency signal here is obtained from the PLL block in the PSCAD software package, using the default gains. The frequency is intended as a reference indicator for the power demand, if the resonance in the signal is fed back into the system, it can lead to further unnecessary oscillations in the power output. In this case, a filter or a slower power control speed is needed to eliminate these oscillations.

The size of the current step change used in the aggregated WT converter model may not directly represent the actual magnitude and response of the individual WT current outputs, however fast large step changes can still occur where there are network faults and system interrupts. The used step size of 0.5 pu current is half of the rating of the system and this may, for example, represent a fault tripping of a feeder connection to half of the turbines in the system. Such a disturbance can propagate to the rest of the system that is still connected [153].

The controller in VSC2 may not always be fast enough to compensate fast AC voltage dynamics, so when the voltage oscillates while the current control is constant, the power output will also oscillate. These oscillations can propagate into the wind turbine such as in the DC link voltage or as torque ripple which is undesirable for the health of the components. Coordinated design of the machine controller and mechanical shaft is also necessary to avoid electromechanical interactions and resonances [154].

Performing a fast Fourier transform on one of the three-phase voltage variables in Figure 5.1a, reveals a peak corresponding to the LC resonant frequency as shown in Figure 5.1b. The theoretical resonant frequency of the LC filter is 318 Hz or 2000.0 rad/s, as calculated using equation (5.1). Resonance involving other passive elements in the network, such as in wind turbine filters, transformers and feeder cables, were not fully considered in the case study.

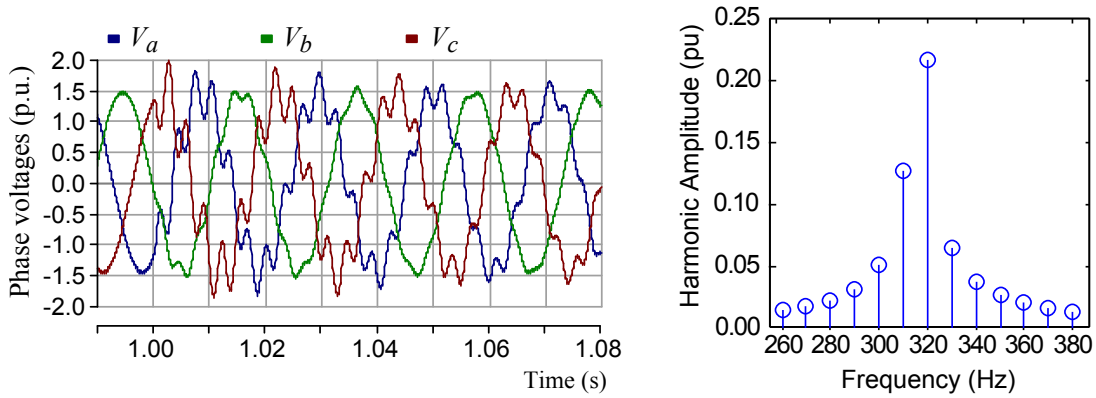

(a) *abc* phase voltage response at the PCC **(b)** FFT of phase A

Figure 5.1: (a) The PCC phase voltage in the stationary *abc* frame, open loop resonance response from Simulation, (b) Fast Fourier transform (FFT) of the resonance in the phase A voltage

In the case study model in Figure 4.8, the presence of L_3, which was 0.15 times the size of L_1 should shift the resonant frequency higher to 5537.7 rad/s, according to the LCL resonant frequency equation (5.2) . However, this equation does not apply in the case study. The size of the C_2 dummy capacitor was very insignificant, that the current in $L3$ is equal to the current in L_2, which is controlled by VSC2. Therefore, L_3 is technically a controlled current source and does not play a passive part in exhibiting LCL resonance.

$$\omega_0 = \sqrt{\frac{L_1 + L_3}{L_1 L_3 C}} \tag{5.2}$$

5.1.3 Comparison with Closed Loop Voltage Control Approach

Figure 5.2b shows the response for the same step input current used in Section 5.1.2 but with the closed loop control system that controls the voltage at the PCC. Closed loop control is able to suppress the resonance in the AC-side LC filter and minimise the power oscillations in the system. Controlled active damping is effectively provided without the need of lossy resistors, however its effectiveness depends on the control loop speed which should be fast [155]. As before, resonances in the rest of the network were unaccounted for in the model. The voltage is controlled at the PCC, which has effectively become the new fixed voltage source point.

5.1.4 Eliminating Passive Resistive Damping

There are several different circuit topologies for passive damping with resistance in the LC filter circuit [114]. Power loss generally increases with increased passive attenuation at the resonant frequency. If the resonance problem can be addressed without passive damping resistors, this will minimise the losses and maximise the efficiency of the filter and converter system. In the previous section, where resonances were found and then later suppressed using the voltage controller, very little to no resistance was used for passive damping in the filter model for VSC1.

If a 5 MW WT passive filter damping system is scaled up by a hundred times for a 500 MW HVDC system, and assuming the percentage loss is constant for scaling, then the absolute heat loss will be very large and more difficult to manage. For example, if the 0.032% loss from one of the passive filter design in [114] is assumed, then the absolute heat loss will be 150 kW. Such passive filter designs already need additional passive components arranged in ways to reduce losses. In comparison, the filter model used in this thesis is simpler. On a per WT basis, in comparison, the absolute heat in the filter will be 100 times smaller for the same percentage loss, and therefore more manageable to keep cool as the losses are distributed. It is usual for WTs to have LCL filters with resistive passive damping, therefore their output is assumed to be filtered and sufficiently damped, hence a simplified model

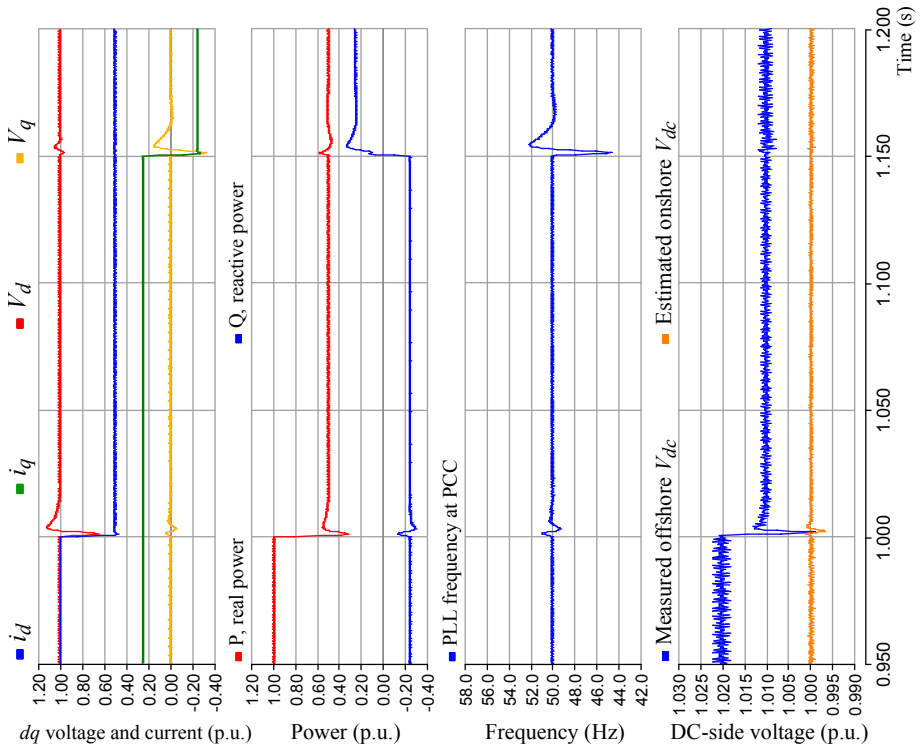

(b) Closed loop voltage control at the PCC.

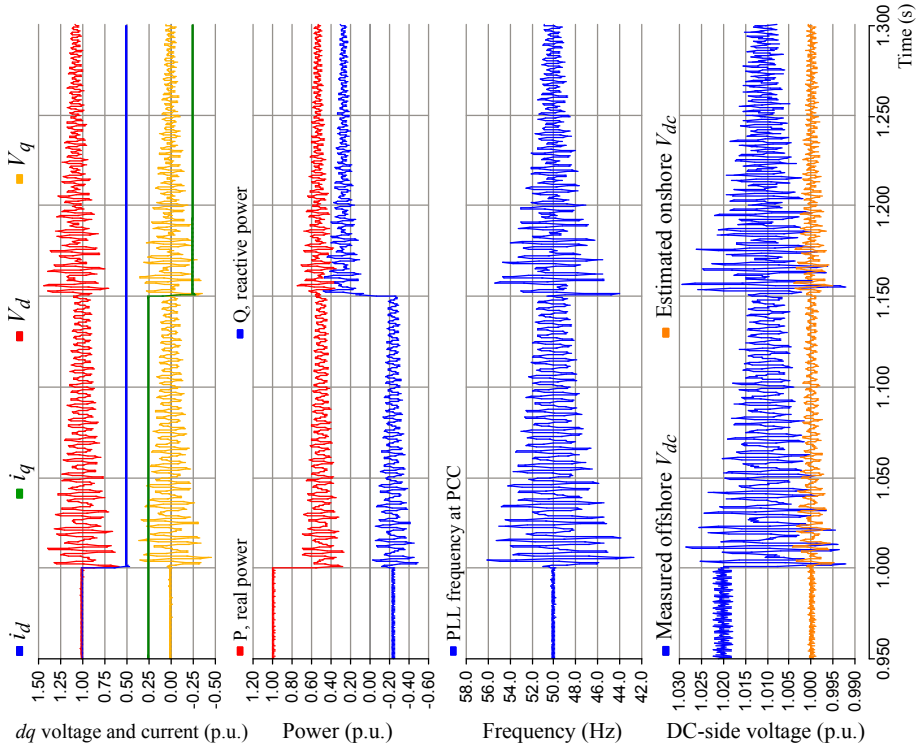

(a) Open loop voltage method.

Figure 5.2: VSC1 *dq* PCC voltage and current response and VSC2 PLL frequency response to a step current input for the voltage set using the (a) open loop method and (b) the closed loop method.

with an ideal source was used to represent the WF. Often additional losses in the transformers, inductors and converters will contribute to additional damping [156].

In order to minimise the thermal management requirement, devices in the offshore HVDC station are designed to be very efficient. The natural losses in the system will make a very little contribution to passive damping of the filter resonance. Therefore, the closed loop voltage controller should be used to suppress the resonance while maximising the system efficiency. Eliminating passive damping resistors and minimising the cooling requirements also save space in the offshore HVDC substation.

5.1.5 Implications of Resonance in the System

Resonance can cause undesirable over-currents and over-voltages in the system. Power electronic converters are sensitive devices because they have a very small heat capacity and limited blocking voltages. An over-voltage event can be damaging for shunt capacitors in the AC filters and reactive power compensation. Over-rating the power electronics and/or capacitor voltage ratings would increase the size and cost of the system.

Keeping the resonance under control and preventing over-voltage would also prevent the filter capacitor from tripping to protecting itself from such events. VSC1 represents the offshore HVDC converter substation and its filter capacitor will be the largest in the wind farm system. If this capacitor has to trip, this may lead to other problems and affect system operation and stability.

5.1.6 Resonance with Power Control Mode

For an open loop voltage set at VSC1, the impact of the control gains in VSC2 on the resonance in the filter of VSC1 is further investigated in this section. The resulting dynamics for a step change in the reference input when VSC2 is under power control mode are different to the dynamics when VSC2 is under current control mode.

As observed in Figure 5.2a, it is understood that resonance is triggered when a current disturbance is injected into the filter system. VSC2 was in current control

mode in this case, and the current control speed ω_{ni2} was faster than the resonant frequency ω_0. In Figure 5.3a, current control speed is equal to the resonant frequency, and the damping is just slightly reduced in comparison with the previous case because of the low pass filter effect of slowing down the control speed, which slightly attenuates the magnitude of current at the resonant frequency. The resonance will have the maximum settling time if a true unfiltered step input is used, i.e. very fast ideal current control response speed. The power oscillation is a problem, which occurs when the voltage resonates while the current is controlled to be constant according to the input reference.

As described in Section 4.4.5, power control mode for VSC2 aims to compensate the dynamics in the AC network voltage so it can maintain constant power control according to the reference input. Therefore current control needs to be faster than the AC-side dq voltage dynamics in order to decouple this effectively. If the current control loop is made seven times faster than the resonant frequency, the response in Figure 5.3b showed that the real power P output was able to follow the 0.5 per unit step input reference without significant oscillations. When power control is used, the current control reference is reduced when the voltage is high and the current is increased when the voltage is low, therefore it does not exacerbate the resonance. Although the real power was well controlled, the oscillations in the reactive power Q were found because the control and decoupling was not perfect, and ideal PLL tracking and zero voltage in V_q were original assumed when the controller was designed. However, the resonance in the voltage is more damped in comparison to Figure 5.3a where current control mode was used for VSC2.

The results suggest that if proper power control and AC side voltage decoupling is used, the impact on the resonance can be minimised. However, it is not very practical to achieve very fast current control speed that is much faster than the resonance frequency for VSC2 (the WT converters). As mentioned in Section 4.5.2, the switching frequency and delays are factors that limit the current loop control speed. Furthermore, the resonant frequency is not ideally fixed. It is likely that over the course of the lifetime and ageing of the filter capacitor, the capacitance will slightly decreases, shifting the resonant frequency higher, the controller may

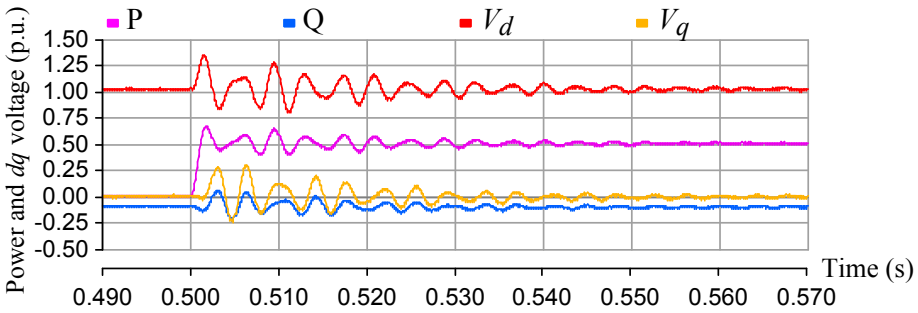

(a) VSC2 is in current control mode and the current loop control bandwidth is equal to the resonant frequency $\omega_{ni2} = \omega_0$.

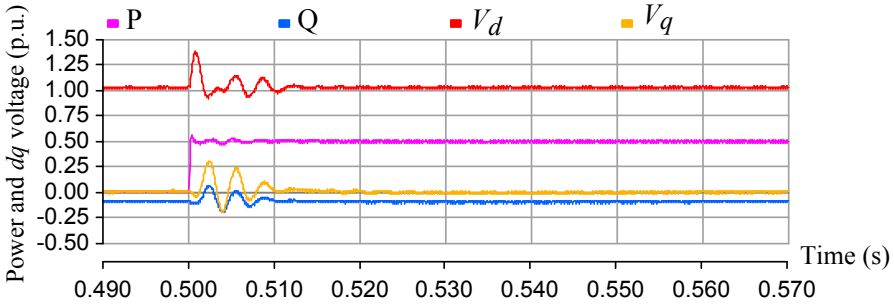

(b) VSC2 is in power control mode and $\omega_{ni2}/\omega_0 = 7$.

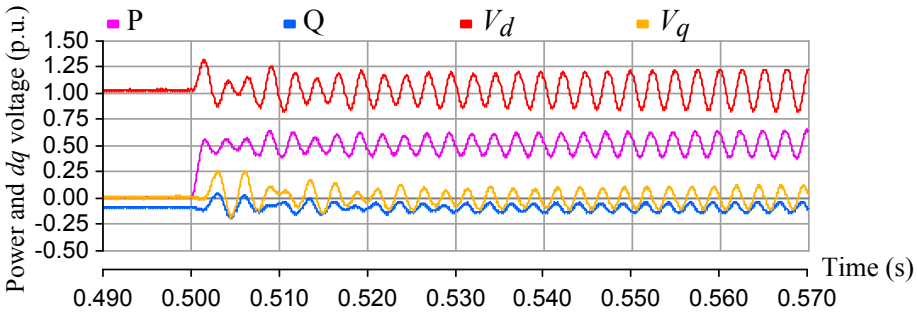

(c) VSC2 is in power control mode and $\omega_{ni2} = \omega_0$.

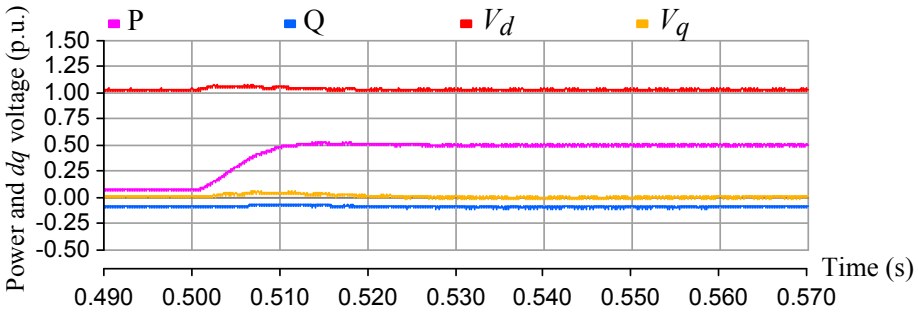

(d) VSC2 is in power control mode and $\omega_{ni2}/\omega_0 = \frac{1}{7}$.

Figure 5.3: VSC2 power and dq voltage response to a 0.5 p.u. step change in VSC2 reference input for current control or power control mode with a specified control bandwidths relative to the filter resonant frequency (ω_{ni2}/ω_0), while the voltage is set at VSC1 using the open loop method.

also need to take this into account in order to be able to compensate the faster dynamics.

When the speed of the current control loop ω_{ni2} for power control mode is equal to the resonant frequency ($\omega_{ni2} = \omega_0$), the current is not able to respond in time and properly compensate the AC-side voltage dynamics while its resonant oscillations in the signal are being fed forward. Therefore, the response becomes very underdamped, and keeps oscillating as shown in Figure 5.3c.

For a case when current control speed ω_{ni2} is seven times slower than the resonant frequency ω_0, the response is very well damped as show in Figure 5.3d. The control is very slow and it did not trigger significant resonance. However, the grid-side converter in a WT is responsible for regulating its DC link voltage. Therefore, limiting the power control speed will limit the capability of the WT converter to keep a stiff DC link voltage. How fast the control speed is required depends on how fast the DC voltage can change and, therefore, on the size of the DC link capacitance. If the power control can be faster and smoother, the size of the DC link capacitor in fully rated WT converters can be smaller and, therefore, less expensive [157]. Even though VSC2 did not trigger resonance in this cases, if the resonance in the AC network voltage was triggered by a third converter or a current disturbance event in that network, the controller would not be able to compensate these dynamics if the control speed is too slow.

5.1.7 Compensating the Voltage Drop across the HVDC Transmission Cable

As discussed in Section 2.4.6, the onshore station can detect the state of the onshore grid frequency and then vary the HVDC voltage to communicate whether the offshore wind farm should be producing more or less power using a DC voltage droop characteristic. The HVDC voltage change is detected by the offshore station, which is then used to decide the offshore frequency based on an HVDC voltage-frequency droop characteristic. When the system is set up this way, the frequency of the offshore network and onshore grid are coupled, and the WTs and any offshore energy storage device will respond to frequency changes and support the grid when neces-

sary. However, studies on the dynamics and decoupling of the voltage drop across the resistance of the HVDC transmission cable are not common.

The voltage drop across the transmission cable varies and will depend on the current through it. Therefore, the HVDC voltage measured at the offshore and onshore terminals will be different. If the offshore power and current ripples, for example in the case of resonance, the offshore DC-side voltage will also ripple, as shown in the 4th frame of Figure 5.2a. This is because the cable voltage drop also varies according to the current. Although this ripple in the signal can be filtered using signal processing there is still a voltage difference between the two terminals in steady-state. The offshore station is able to estimate the actual HVDC voltage at the onshore station by taking into account the voltage drop of the cable resistance.

The system to be studied is depicted in Figure 5.4. The model assumes that the onshore converter is a ideal DC voltage source, hence delays in the DC voltage controller were not considered in this study. The resistance of the cable is also assumed to be constant.

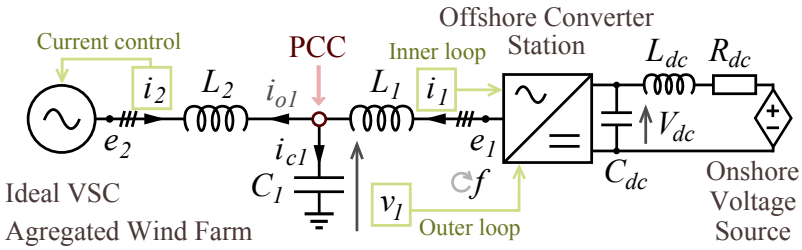

Figure 5.4: The schematic diagram of the system model including the DC-side impedances for the HVDC link.

The DC current in the cable can be directly measured, but here it is determined from the AC side power and divided by the known DC voltage (the VSC losses are ignored). The voltage drop across R_{dc} is calculated as the product of the estimated DC current and the cable resistance (R_{dc}). This is then subtracted from the offshore-side DC voltage measurement to estimate the onshore DC voltage. The DC base voltage for the DC system was made 700 V and the chosen resistance is 0.021 p.u. A small first order filter with a time constant of 1 ms was also used to eliminate noise in the signal afterwards.

Figure 5.5 shows the response to a 4% stepwise decrement in the onshore DC

voltage from the nominal level and back up again, while the wind farm power output is 0.5 pu. The offshore station was able to accurately estimate the onshore HVDC terminal voltage, but with a time delay of approximately 2 ms. The effect of the DC-side inductance and capacitor of the cable were not taken into account in the compensation of the cable voltage drop.

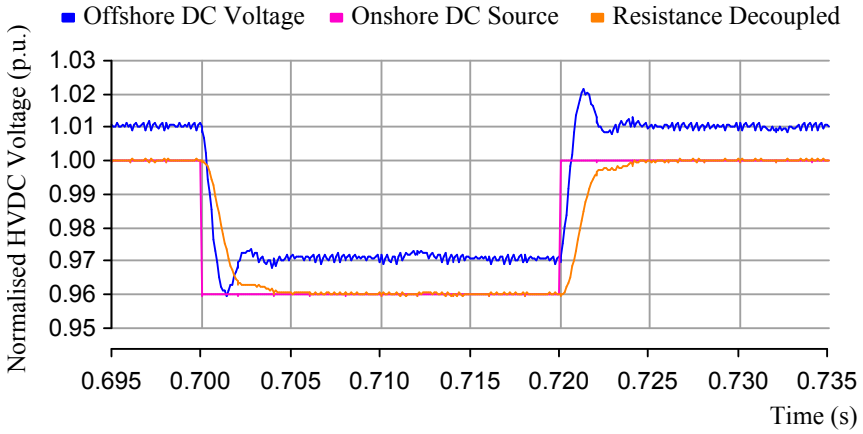

Figure 5.5: Response to DC voltage step on the onshore side, voltages are normalised to the DC base voltage.

If DC variations are slower the switching frequency, they can be compensated by the DC feed-forward voltage, as explained in Section 4.3.3, provided there are no delays in the PWM output and the DC measurement. The DC feed-forwarding used in the simulation was ideal and instantaneous, therefore the DC-side oscillations did not feed back into the AC side.

5.1.8 Variable Frequency Dynamics

The offshore network frequency should be able to vary for onshore grid support and power demand communication by coupling the offshore and onshore grid frequencies as discussed in Section 2.4.6. The frequency variation required will be as small as the frequency range in the power system, which is only about ± 1 Hz from the nominal frequency. The impact on inductive and capacitive components in the system is expected to be minimal. The method for setting and varying frequency is outlined in Section 4.2.1.

When an HVDC voltage drop is detected, the offshore wind farm network can

respond with a frequency drop to communicate the onshore grid energy demand to the wind turbines with integrated energy storage (see Section 2.4). Resonant oscillations in the AC offshore network also appear when there is a small step change in the frequency applied by the HVDC converter station. A frequency step change from 50 Hz to 49 Hz at time 0.8 s has an impact on the voltage and frequency at the PCC without closed-loop voltage control (open-loop) as shown in Figure 5.6a. Once again, in comparison with the closed loop case as shown in Figure 5.6b, the controller is able to damp the oscillations at the PCC as the voltage and frequency are controlled at this point. At times 0.7 and 0.75 seconds, the frequency step changes were filtered by a first order TF system with a 4 ms time constant. This did not trigger significant resonant oscillations in the system because the cut-off frequency of the filter is less than the resonant frequency.

Application for a Variable Frequency Network

The network topology described in Section 3.2.3 uses variable frequency and variable voltage. The same voltage controller described in Section 4.3 may be used to control the voltage in the cluster network. The variable frequency range in this type of system is larger compared to the application in Section 5.1.8. The variable speed WT can have a rotor speed and frequency range from 33% to 100% of the maximum [121]. The voltage must also vary with frequency in order to maintain the flux level in the transformer and prevent core saturation.

Figure 4.10a is an example of a set of time domain results showing the response to step change in the reference of the voltage controller from zero to the maximum voltage level. The small signal analysis eigenvalue results may only be valid for the original nominal voltage level and frequency and rated power. Therefore, the analyses may need to be repeated for the different operating points at the reduce frequency and voltage levels.

Jovcic et al. [126] also used a type of two-stage cascaded controller to control of the voltage of this cluster type of network topology, but it did not detail the use of a filter or dq decoupling strategy. However, in this case, the network in this case is no longer inertia-less and the interactions with the WT generators may be different.

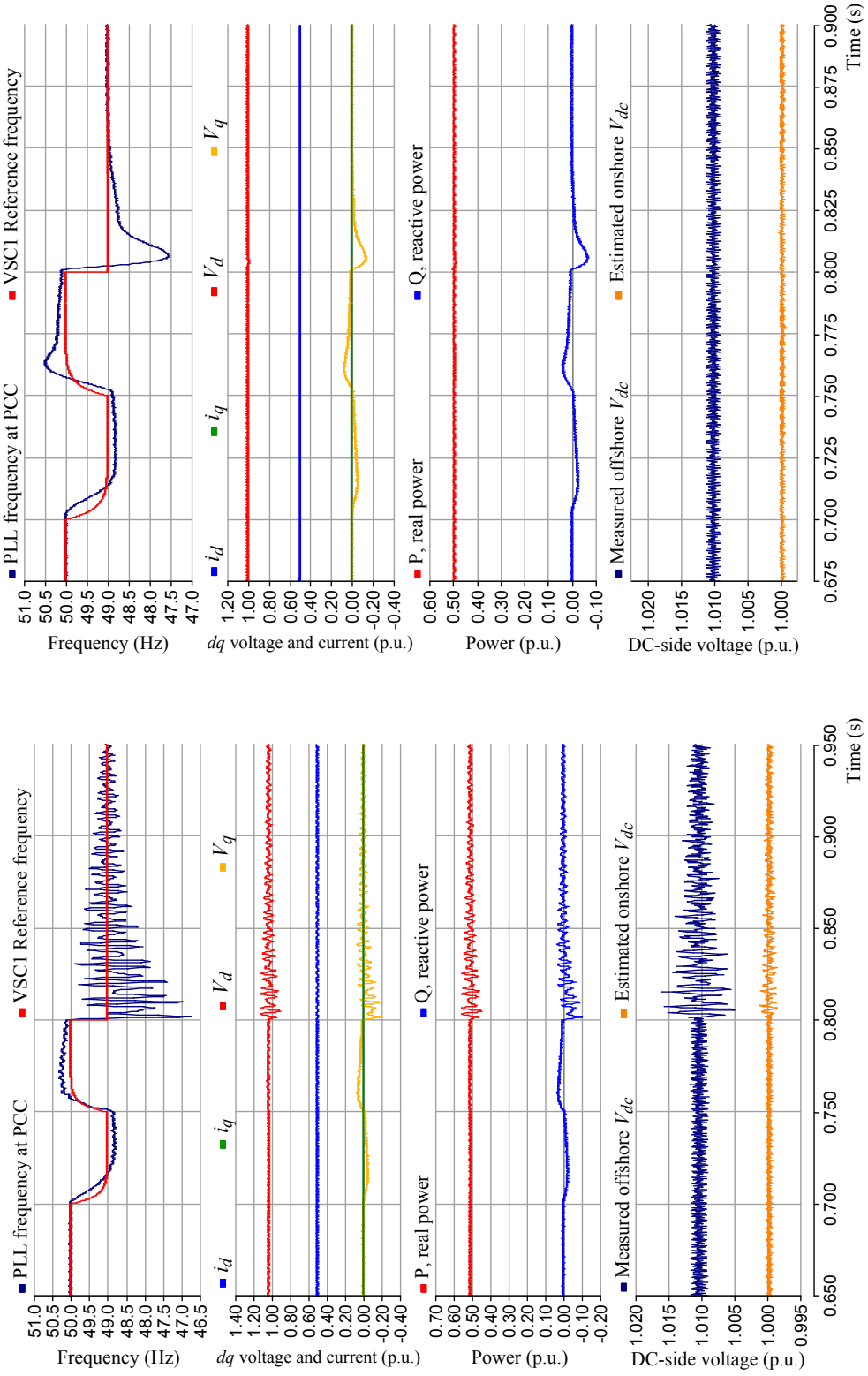

(a) Open loop method response

(b) Closed loop method response

Figure 5.6: VSC1 response to frequency change in the offshore AC network for (a) an open loop and (b) a closed loop method.

If the frequency and voltage changes too fast, the generators in the network may be able to react to it due to their inertia. Further work is also required to study this and whether it is possible to achieve individual torque and rotor speed control of the generator using SCIG rotor resistance control and OptiSlip® technology (see Section 2.2.5).

5.1.9 Benefits of Capacitor Protection with Voltage Control

The filter capacitor for the offshore VSC-HVDC converter (VSC1), is the largest capacitor in the system. The capacitor ageing increases with voltage and temperature and further deterioration may lead to a short circuit failure [158]. The voltage controller regulates the voltage of the filter capacitor at the PCC to be constant. Over-voltage caused by resonance in the filter can be minimised and the life of the capacitor can be prolonged, thus reducing the frequency and cost of maintenance and repair, and the number of capacitor tripping events can be minimised. If the filter capacitor trips, the filter properties change and unfiltered harmonics will have an impact on the WT system.

There are other capacitive and inductive components in the system that are unaccounted for in this study. A lengthy cable network has significant capacitance and this, in combination with the inductance in the filter reactors and transformers, will produce additional resonant frequencies. When setting the voltage from the open loop to the closed loop case, the constant voltage source point is just shifted from the converter terminal (e) to the filter capacitor at the PCC.

When there is another set of LC resonance elsewhere in the same network, this resonance can still draw oscillating currents from the VSC1 converter, even if the PCC voltage is controlled to follow a constant reference. Further work is needed to address this issue. Already, power control and AC voltage dynamic decoupling was able to alleviate the resonance as discussed in Section 5.1.6.

When using the controller, the PCC is the only point under constant voltage control, therefore only the capacitors connected in shunt at the PCC are protected from resonance. Capacitors in the filter for the WT frequency converter were assumed to be already damped [114], hence an ideal model was used to represent the

WT in simulation studies.

Saturating the current at VSC1 while the WF is still trying to export power, leads to over-voltage at the filter capacitor, and will be further explained in Section 5.2.2. The excess power, which is not sent to shore from VSC1, charges the filter capacitor. During current saturation the integral controller in the voltage outer loop is lost and the voltage is allowed to rise. Communication with the WTs is needed to reduce their power output and therefore reduce this voltage rise. It is challenging to have over-voltage and over-current protection at the same time and the power must be limited.

5.2 Current Saturation

One of the benefits of using the cascaded control structure for voltage control described in Section 4.3, is that the current magnitude from the converter output can be saturated between the inner and outer loop controller. This method intends to provide protection from over-currents to prevent fatal device failures in the converter and overloading at the filter inductors can cables. VSC devices are usually very sensitive to current overloads because of fast thermal runaway. A current saturation technique is presented in this section. Its capability and impact on the offshore network are identified and evaluated.

Sections 3.3 discussed about modularisation of subsystems, such as the HVDC converters, so it can be more fault tolerant. If a module fails, it is isolated and the capability of the system is reduced. When this occurs, the level for the current limit of this converter should ideally be lowered accordingly. Other sources of over-currents also include excess wind power generation from sudden gusts and network faults.

5.2.1 The Current Limiter in the Control Loop

Figure 5.7 shows a hard-limiter for the current level, which will be implemented between the outer and inner loop controllers. The magnitude of the dq current reference can be saturated to a defined limit that depends on the converter capability

and device temperatures. The ratio of the original d-axis or q-axis current to the magnitude of the current is then the gain for scaling the saturated current magnitude back the corresponding dq components.

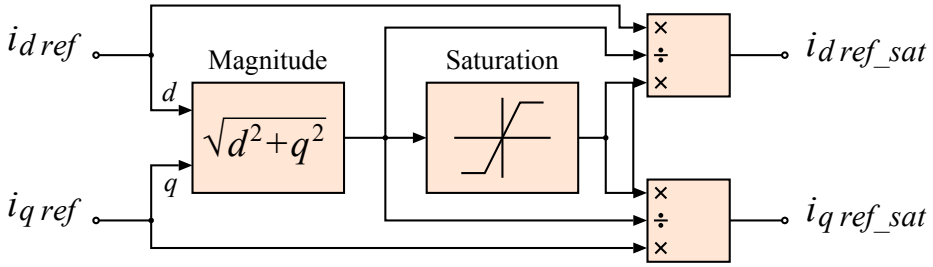

Figure 5.7: A limiter for saturating the magnitude of the current for implementation between the outer voltage and inner current control loop.

The outer loop integrators must be disabled when the current is saturated. This will prevent their output from continually rising when the inner loop is unable to drive the current control effort required to eliminate the steady-state error. The detection of saturation was implemented by detecting a difference between the input and output of the saturation block. If saturation is detected, a signal is sent to switch the input of the outer loop integrators to zero. Therefore, the outer loop controller will not be able to maintain the required voltage and an steady-state error will be present during saturation mode.

5.2.2 Voltage Rise During Saturation

The current limiter from Section 5.2.1 was implemented in PSCAD/EMTDC to study the effects of current saturation on the voltage controller. Figure 5.8 explains how the voltage rises when the current saturates at the converter.

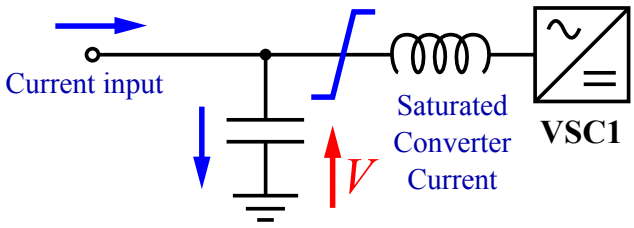

Figure 5.8: The current is diverted to charge the capacitor during current saturation in the converter.

During current saturation at the converter, the excess current has no where else to go except to charge the filter capacitor. If VSC2 was a constant-current source feeding the input of the filter during saturation, the voltage will rise towards instability. However, a constant-power source is a more appropriate model for the WT. If the voltage rises when using the power control model as described in Section 4.4.5, the current required for maintaining a constant power will be reduced.

The effects of saturations for constant power input to VSC1 was simulated on PSCAD®. The power is ramped from 0 to 1 p.u. for a short period then ramped back down. Figure 5.9a shows that when the converter current is saturated to 0.9 p.u., the outer loop control integrator is disconnected and the dq voltage rises very quickly. But as the voltage rises the current output from VSC2 is reduced to a level that brings VSC1 out of saturation mode. The integrator is activated and voltage control is resumed and the d-axis voltage is quickly brought back down to 1 p.u. However, VSC2 continues to maintain power at 1 p.u. and will therefore raise the current back up and the cycle repeats.

The PCC voltage rises to a level that can be very damaging. The case in Figure 5.9b has lower saturation current level at 0.7 pu. and uses the same power reference in VSC2 as the Figure 5.9a case. The voltage rise and oscillations is much more significant. For both cases in Figures 5.9a and 5.9b, the converter voltage output e was assumed to be an ideal voltage source with no DC side voltage limit.

The voltage rise is undesirable because it overloads the filter capacitor. The VCS1 converter can no longer control the voltage at the PCC to the desired reference, because the integrators in voltage outer loop control is lost during saturation. In order to bring down the voltage, the current level must be brought down below the saturation level.

This voltage rise from current saturation can be prevented by communicating to the WTs to reduce their power output. Alternatively, the power can be diverted to another HVDC terminal station or an offshore energy storage unit if present in the same network. However, the voltage oscillations during saturation cause the frequency output from the PLL in VSC2 to also oscillate as shown in Figure 5.10. The oscillations must be minimised in order to effectively use the frequency droop

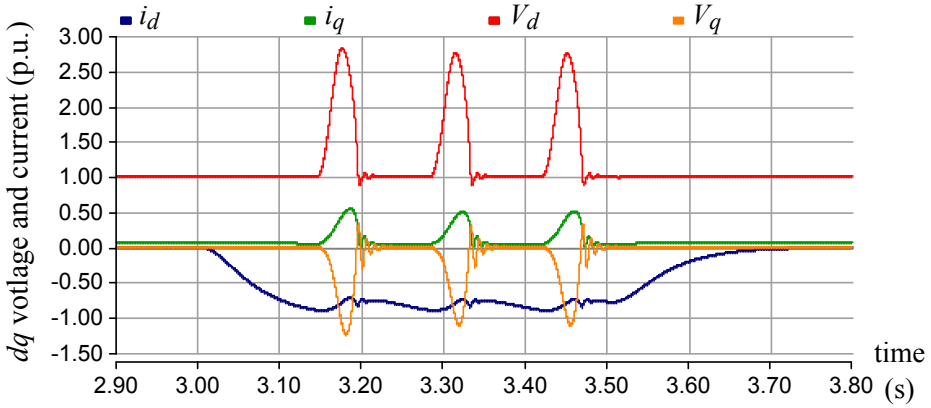

(a) VSC1 current saturation level is at 0.9 p.u.

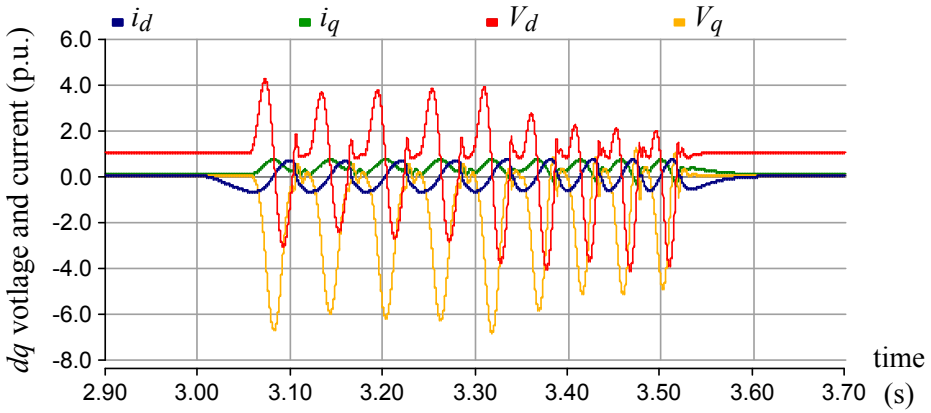

(b) VSC1 current saturation level is at 0.7 p.u.

Figure 5.9: The VSC1 *dq* voltage and current response to a 1 p.u. power rise and fall in VSC2 between 3.0 s and 3.5 s, for a defined current saturation level at VSC1

communication method as described in Section 2.4.6, for the WTs to control the wind power based on the offshore network frequency.

The oscillations are present in Figures 5.9 and 5.10 because the controller went in and out of saturation mode and the VSC1 outer voltage loop switch between proportional only control and PI control. The AC voltage dynamics were not properly compensated and the current from VSC2 was found to be oscillating around the saturation level. For the cases shown in Figure 5.9, the control speed used for VSC2 in power control mode has a current loop response time constant of about 0.15 s, which is much slower than the VSC1 outer loop. The reason it was that slow, was because a slower power control speed in VSC2 with full voltage control at VSC1, as shown in Figure 5.3d, originally meant the system response was more damped

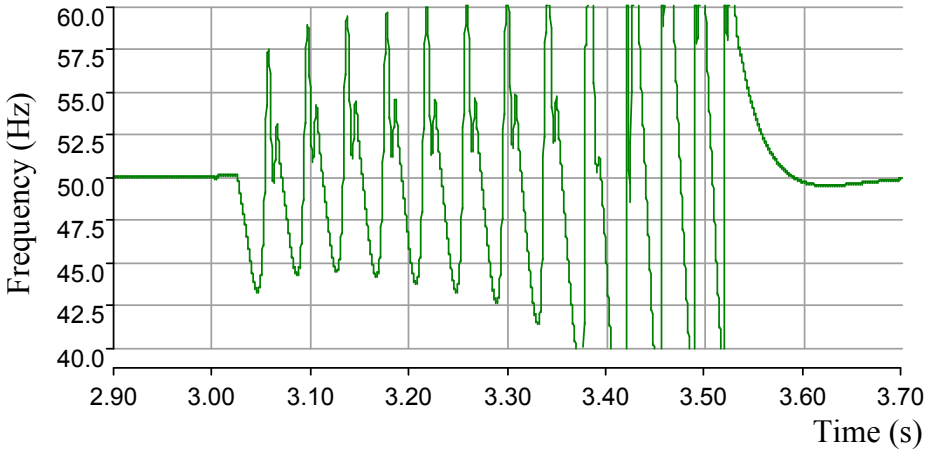

Figure 5.10: Frequency output from VSC2 PLL when power rise to 1 p.u. while the saturation level for the converter current is at 0.7 p.u.

and did not trigger resonance and the voltage deviation was smaller as the power change would be more gradual. However, this would only be the case if the integral in VSC1 outer loop control remained active.

The saturation test is repeated but this time VSC2, under power control mode, is ten times faster than the inner loop control speed of VSC1, and the compensation of the AC voltage dynamic is more effective. The power reference input is also smoothed by a first order delay with a time constant of 2 ms. VSC1 is now not ideal and it is a two-level converter instead with the DC-side voltage being 24% higher than the peak of nominal line-to-line voltage. In Figure 5.11a, the power rises to 1.0 p.u. and falls to zero from time 1.0 s to 1.2 s in VSC2 while the current saturation level in VSC1 is 0.9 p.u. VSC2 is able to maintain power control at 1.0 p.u. of power at a steady-state voltage higher than the nominal voltage without significant oscillations. Without the integral part of the voltage controller during saturation, VSC1 cannot precisely control the voltage to follow the nominal reference and a steady-state error is present. When comparing Figure 5.11a with Figure 5.9a, it is clear that a different parameter in the VSC2 power control has an influence on the PCC voltage dynamics during current saturation at VSC1. The oscillations were minimised because VSC2 was able to maintain constant power and properly compensate the voltage dynamics. In Figure 5.11a, the fast sudden large power change causes a small voltage spike at time = 1.0 s. Minimising this spike is suggested

by further increasing the time constant of the first order delay to smooth the power output response. Furthermore, a fast power change is not very likely in practise. Although the PLL frequency output signal jumps at the transient of step input, the response was not oscillatory.

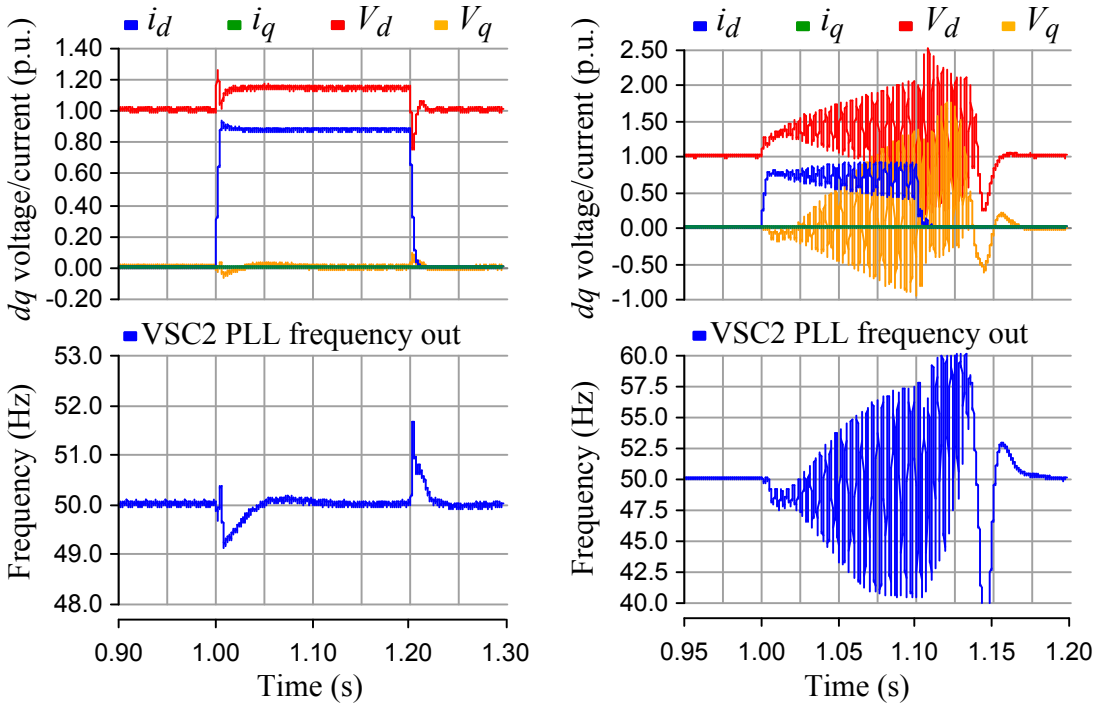

(a) Current saturation level at 0.9 p.u. **(b)** Current saturation level at 0.7 p.u.

Figure 5.11: The VSC2 *dq* voltage and current response and PLL frequency output for a 1.0 p.u. power rise and fall, while the current in VSC1 is saturated to a defined level.

In Figure 5.11b, the power rises to 1.0 p.u. and falls to zero from time 1.0 s to 1.1 s in VSC2 while the current saturation level in VSC1 is lowered to 0.7 p.u. instead. Oscillations are found with a frequency six times the fundamental because the peak of the AC-side voltage has risen and surpassed the DC-side voltage level. The free-wheeling diodes then conduct and distort the AC waveform as it caps the VSC1 AC voltage output. When the power drops back to zero at 1.1 s, operation of the voltage controller was restored quickly within 50 ms. This presents an opportunity to prevented the oscillations by sending a signal to the WTs to reduce the power output when the voltage rise is detected.

The offshore AC network is inertia-less, therefore the frequency is simply set and

fixed by the strongest VSC at the offshore HVDC station. The frequency is not really affected by imbalance of the power flow in the case study network, but the network voltage is liable to fluctuate instead. A fast effective power controller was shown to have the potential to compensate short transient voltage rises and oscillations. The current is reduced when the voltage rises in order to maintain constant power. However, if the voltage rises too excessively, the WT power generation must be quickly reduced, which can be assumed achievable with temporary free-wheeling and over-speed with torque reduction, and then stall control, pitch control, power diversion to an energy storage device or a load bank to be dumped as heat at the WT.

If the HVDC power transmission is limited by the current saturation, then the offshore substation cannot emulate inertia by withdrawing the excess energy from the offshore AC network. Increasing the HVDC converter rating may solve this problem, but this route is very expensive and difficult to justify for an already expensive offshore wind farm system as a whole. Until power electronics become significantly cheaper, it is recommended to limit the power output of the WTs to prevent the voltage rise problem during current saturation of the HVDC converter.

It may be possible for the WT to detect an excessive voltage rise straight from the network reduce the power output to prevent further voltage rise in the network. However, if the WT current rises in response to the voltage decrease, this may lead it back to saturation and voltage rising back up again. Further work is needed to implement and study a power limit control technique that does not introduce oscillations in the steady-state. The frequency droop communication method would be more advantageous to solve the voltage rise problem over the steady state and while the HVDC converter is derated over the long term. To help prevent the WT power exceeding the saturation level the first place, the frequency level can be an indicator to represent the maximum cap on the WT power output rather than scaling the power for grid support as previously described in Section 2.4.6.

Limiting the power rating of the HVDC converter reduces the strength of the AC network, according to equation (2.2) in Section 2.1.2. In the case of current or power saturation in VSC1, fine voltage control is lost, which then lets the voltage

level fluctuate or drift from the reference point.

5.2.3 Saturation with Passive Loads

As discussed in Section 5.2.2, the voltage can rise to unsustainable levels when the converter current is saturated while power is flowing into the converter. Figure 5.12 shows the current and voltage response when the current is saturated while the power is flowing the opposite direction, out of the converter. In this saturation case, the voltage level is dropped instead. Here, hard switching is used to connect and disconnected a high passive load, consisting of an arbitrary low value resistor and inductor in series, connected in shunt at the PCC to ground. The magnitude of the current is saturated at 1.0 p.u.

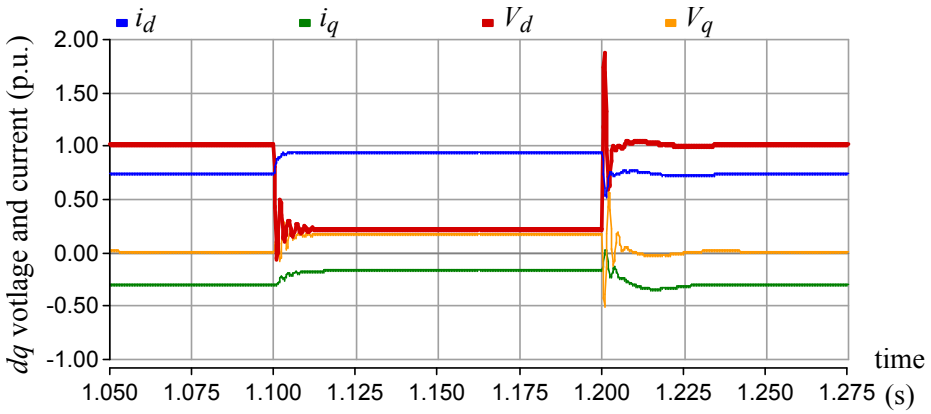

Figure 5.12: VSC1 *dq* voltage and current response to a sudden load rise in a passive load scenario. The saturation level for the converter current magnitude is 1.0 p.u, VSC2 is ignored in this case.

While AC side fault currents can be easily limited, DC side faults cannot be blocked using saturation in the control. VSC converters traditionally have anti-parallel free-wheeling diodes, so when the DC side voltage is dropped below the peak of the AC voltage, it will behave as a passive rectifier and therefore continue conducting. On the other hand, a modular multilevel converters (MMC) with full bridge modules, that was presented in Figure 2.6 (page 18), are capable of fault blocking, but the costs and power losses are higher. MMC with half-bride modules use less switching devices and the losses are lower, but cannot block fault currents at it also has free-wheeling diodes [159].

The saturation technique is very capable of saturating the current without adverse stability problems when the power is flowing out of the converter for a passive load as opposed to constant power flowing into the converter. Therefore it is more suited for applications, such as uninterruptible power supply (UPS) systems and HVDC connection to islanded networks with load rather than for an offshore network with generation.

5.2.4 Saturation with an Unbalanced Fault

The current level would be high as fault currents without current saturation used in the previous section. Therefore it will be assumed that VSC1 will able to saturate balanced fault currents across all three phases. However, AC faults are typically a single phase line-to-ground fault or line-to-line fault, and rarely balanced. The aim here is to see how the controller with current saturation can cope in these unbalanced fault scenario with passive load. Referring to the original case model in Figure 4.8, the fault will occur between VSC1 and VSC2, in the middle of the L_3 as shown in Figure 5.13. Here, $L_3 = 0.055$ p.u. is used. The fault is simulated by switching to a short circuit resistance of 0.0438 p.u. for 50 ms and then switching it off. It assumes redundant connections exist for each phase in the AC network to continue with power transmission after the fault is isolated.

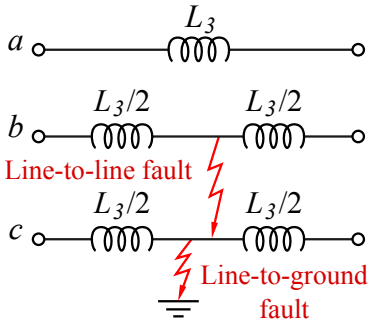

Figure 5.13: Three-phase representation of the line-to-line fault and single phase line-to-ground fault configuration.

When the fault occurs without current saturation implemented in the controller, current level will rise beyond the rated level. As shown in Figure 5.14a, the control system becomes unstable and is unable to recover after the fault is disconnected at

time = 1.55 s. When compared to the case when the current is saturated at VSC1 shown in Figure 5.14b, it demonstrates the importance of saturation to maintain the system running when a fault occurs in the network, and preventing the current reaching a level that will cause the system to go beyond to the point of no return.

In Figure 5.14c, the response to a line-to-line fault case in VSC1 is similar to the response to the line-to-ground fault case. Although, there are negative sequence oscillations for both of these cases, which would cause ripples in the DC-side voltage, VSC1 is protected from over-currents and is able to ride through the fault. After disconnecting the fault at time = 1.55 s, the control system is able to quickly recover back to the normal operating state in about 30 ms after the fault is cleared. Further work is needed to implement negative sequence control to maintain a smooth power output during unbalanced faults using a similar technique as described by Ng et al. [160]. Besides, further work is needed to study the current limitation in power electronic devices on a per-phase basis as explained in [161, 162], because limiting the space-vector modulus might not be enough.

The VSC2 model assumed constant power control mode, therefore its current would increase to compensate for the voltage drop in the phases with the fault in order to maintain the power. When the negative sequences are also controlled and the over-currents are limited, the power that VSC2 will be able to export during the fault will be limited. This will cause the DC-link voltage to rise in an actual system if the WT continues with constant power generation through the machine side converter, although the DC-link is not modelled in this study. To prevent this, the aerodynamic power from the turbines must be reduced, but the time constant for the pitch blades to react is slow, taking several seconds. In the meantime, the torque can be reduced, and the rotor is allowed to momentarily speed up, provided the rotor inertia is large enough so it does not over-speed too quickly. This will reduce the power going into the electrical system until the pitch control fully responds. Further excess energy needs to be diverted and be dumped through a DC resistive load bank or an energy storage device, especially when the network is disconnected.

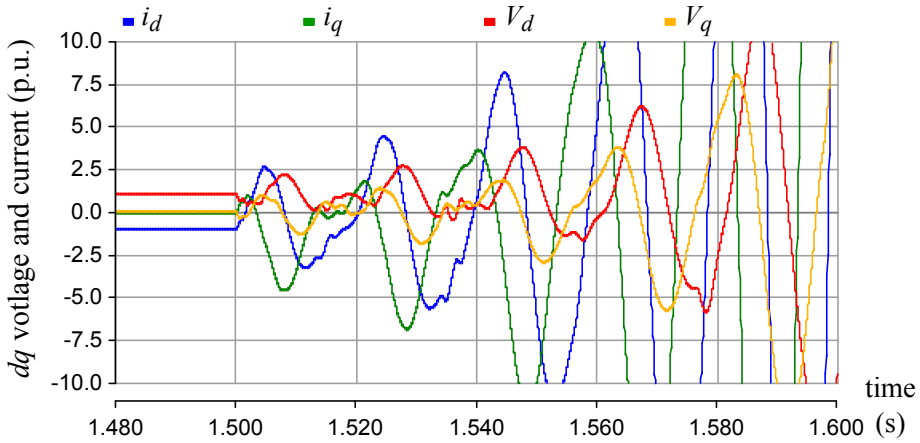

(a) Without current saturation, line-to-ground fault

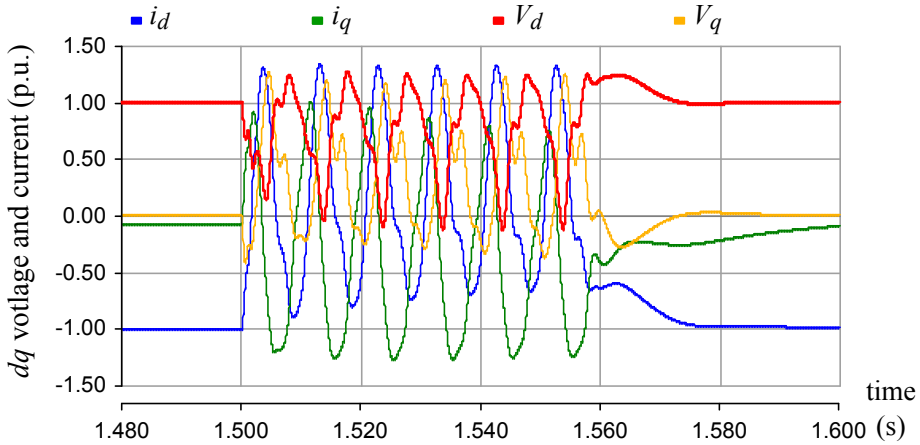

(b) With current saturation at 1.1 p.u., line-to-ground fault

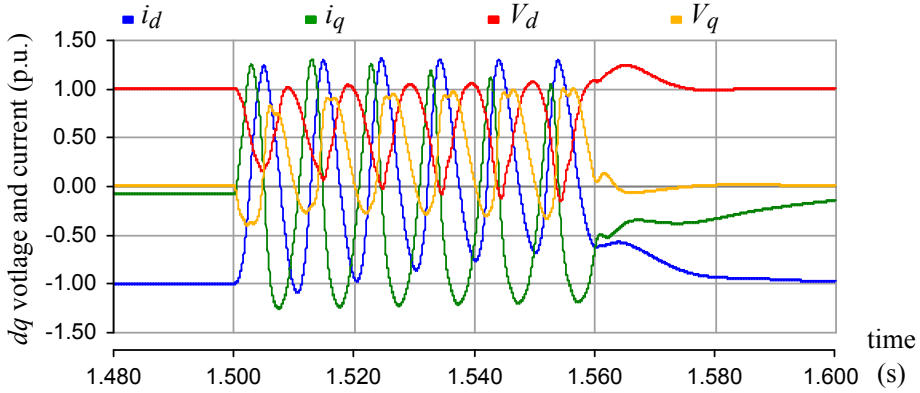

(c) With current saturation at 1.1 p.u., line-to-line fault

Figure 5.14: VSC1 *dq* voltage and current response to a fault at time = 1.50 s to 1.55 s, with and without current saturation, while VSC2 is under constant power control mode.

5.3 Controller Sensor Reliability

The voltage and current levels in an electrical system are too high and unsafe and they must be isolated from the control system when they are measured. A transducer device converts high currents and voltages into a small manageable, measurable and safe analogue electronic signal. An analogue to digital converter (ADC) will convert this signal to a digital form, where it can be processed for a real-time digital controller.

A current transducer (CT) would typically use a closed loop compensated Hall effect device. The magnetic field around the wire is detected and converted to a tiny voltage signal, which is proportional to the current in that wire. An amplifier will then scale this so that the voltage signal can be measured by the ADC. There is no direct contact with the wire, therefore it is isolated and safe. For a voltage transducer (VT), the differential measurement probes are connected to a constant large known value resistor with a very low temperature coefficient. The voltage is then proportional to the current through the resistor, which is measured and scaled using a device similar to a CT but more sensitive. High voltage divider probes available commercially are used for much high voltage levels up to 100 kV.

A number of current and voltage transducers are required for full state feedback voltage controller in Figure 4.5 (page 95). A failure of a single sensor can compromise the stability and operation of the system. Sensors increase complexity of the system and reduce reliability. The impact of the downtime due to any failure is very significant for the offshore wind farm due to the difficult access and high cost, therefore offshore reliability is extremely important [73]. This section will consider sensor reduction without altering voltage controller and its performance. Some simple sensor topologies and designs are also considered for improving its fault-tolerance using the same modularisation concept discussed in Section 3.3. The control sensitivity to and error in the gain of the controller's many sensors and signal inputs is also studied.

5.3.1 Sensor Reduction

As discussed in Section 2.3.4, sensors also have a high failure rates. The intention of reducing the number of measurements for the voltage controller in Figure 4.5 is to simplify and improve the reliability of the control system.

The measurement for the output current i_o from the PCC is a feed-forward term in the outer loop controller. This can be estimated using Kirchhoff's law as shown equation 5.3 and using Figure 4.4 as reference for the variable names and the direction of the current measurements. The i and i_c currents branch off from the same PCC node, where v is measured. The inductor current i is known because the measurement required for the inner loop current control. The capacitor current i_c is estimated from the known capacitance and derivative of the measured PCC voltage v with respect to time as shown in equation 5.4. The voltage v measurement is already required for the outer voltage loop control.

$$i_{o1} = i - i_c \tag{5.3}$$

$$i_c = C\frac{dv}{dt} \tag{5.4}$$

Not all three phases for the current and voltages need to be measured. In a three wire system with no zero sequence, only two of the phase need to be measured, as the third phase can be estimated using equation (5.5). Where f denotes a function that can represent the current or voltage, not frequency here.

$$f_c(t) = -f_a(t) - f_b(t) \tag{5.5}$$

When there is no neutral point to use as a reference to measure the phase voltage, the line-line voltage measurements can be taken and then converted to the v_a and v_b phase voltages using equations (5.6) and (5.6), assuming there are no zero sequence present or zero sequence is removed from the measured voltage. The voltage at phase c can be calculated using equation 5.5. In this case, only two voltage measurements are required instead of three: the line-line voltages, v_{ab} and v_{bc}. Conversion to the phase voltages is useful for the abc to dq transformation equations already defined

in Section 4.1.2.

$$v_a = (2v_{ab} + v_{bc})/3 \tag{5.6}$$

$$v_b = (v_{bc} - v_{ab})/3 \tag{5.7}$$

Comparing between using full measurements and reduced sensors with estimated variables in simulation, found that the control response was exactly the same. This is because all the signals and variables between the two methods are numerically the same for an ideal simulation model. Equation 5.4 assumes the capacitance C is constant, linear and no other impedances that can distort the actual current exist.

5.3.2 Sensitivity to Error in the Sensor Measurements

There are different modes of errors associated with the sensors. In the analogue to digital converters (ADC) and sampling, non-linearity, clipping, and aliasing distortions may be found. These are treated as noise and disturbances and ignored here. The *abc* phase measurements is assumed to be balanced because the model for the small signal analysis is in the *dq* co-ordinate system as explained in Section 4.5.1. An error in one of the phases leads to negative components to be present in the *dq* signals. These erroneous components in the signal can be injected into the controller as a separate study.

The type of error focused on here is the precision and/or accuracy of the linear scaling of the measurement output. Measurements are not always fully accurate or properly calibrated. Partial failures in sensors are not so easily detected and may continue operating with erroneous output readings. As the capacitor degrades over times, its capacitance also changes. A change or a degradation in some resistor components and reference voltages inside the sensor may also affect its accuracy and gain.

Figure 5.15 are small signal analysis results showing how the eigenvalue with minimum damping in the system changes as the scaling error in nine different sensor measurements and control parameters. The results are also a good indicator for the gain margin for the difference parameters in the control system. Generally the damping degraded as the error increases in either positive or negative direction.

The error is modelled as a gain block in line of the signal of interest, which can be varied independently for each test case. The error from -100% to zero and then to +100% means the gains are respectively 0 to 1 and then to 2. For the filter inductor inner loop control parameter, the error was also simultaneously applied for the inductances L in the cross-coupling and its control output, and is labelled in as "all inductor parameters" in Figure 5.15. The same is repeated for the filter capacitor parameters C. Studying the effects of the error in the cross-coupling gains only, also studies the effects of the error in the angular frequency ω parameter here. For the result labelled as "all combined", the same error is applied to all parameters and simultaneously scaled together. Although different combinations of $+/-$ directions have not been tested, this is sufficient to show that errors within $\pm 5\%$ are tolerated and the minimum system damping remains at an acceptable level. Most CTs and VTs are well within this accuracy when they are in a healthy state.

When observing a single error in an individual parameter or signal while there are no errors in anything else, the individual error can be around $\pm 15\%$ before the dynamics of the system significantly deteriorates. This tolerance for error is a useful characteristic that will be enough for current output i_o sensor-less state variable, which will be estimated in real-time as described in the previous section.

A small error inside the control loop is usually corrected by the controller. However, a significant error in the gain affects the closed loop control dynamics. For the gain error in the C parameter at the outer voltage control loop, the closed loop poles (CLP) are expected to follow the same trajectory as the root locus plot for variable control gains in the "compensated case" voltage control as shown in Figure 4.14. When the gain is reduced, the CLPs move back along the root locus towards the open loop pole locations, which are marked by $\times$ crosses. This explain why the minimum damping is slightly higher when the error is -5% in Figure 5.15.

For the error in the L gain parameter at the current inner loop output, minimum damping is 0.63, which is 18.4% higher than the original case and can be considered as a significant improvement. This is because damping of the inner loop CLP has increased. Although the actual root locus is for the current inner loop is not presented, its root locus trajectory is the same as the "ideal case" voltage outer loop

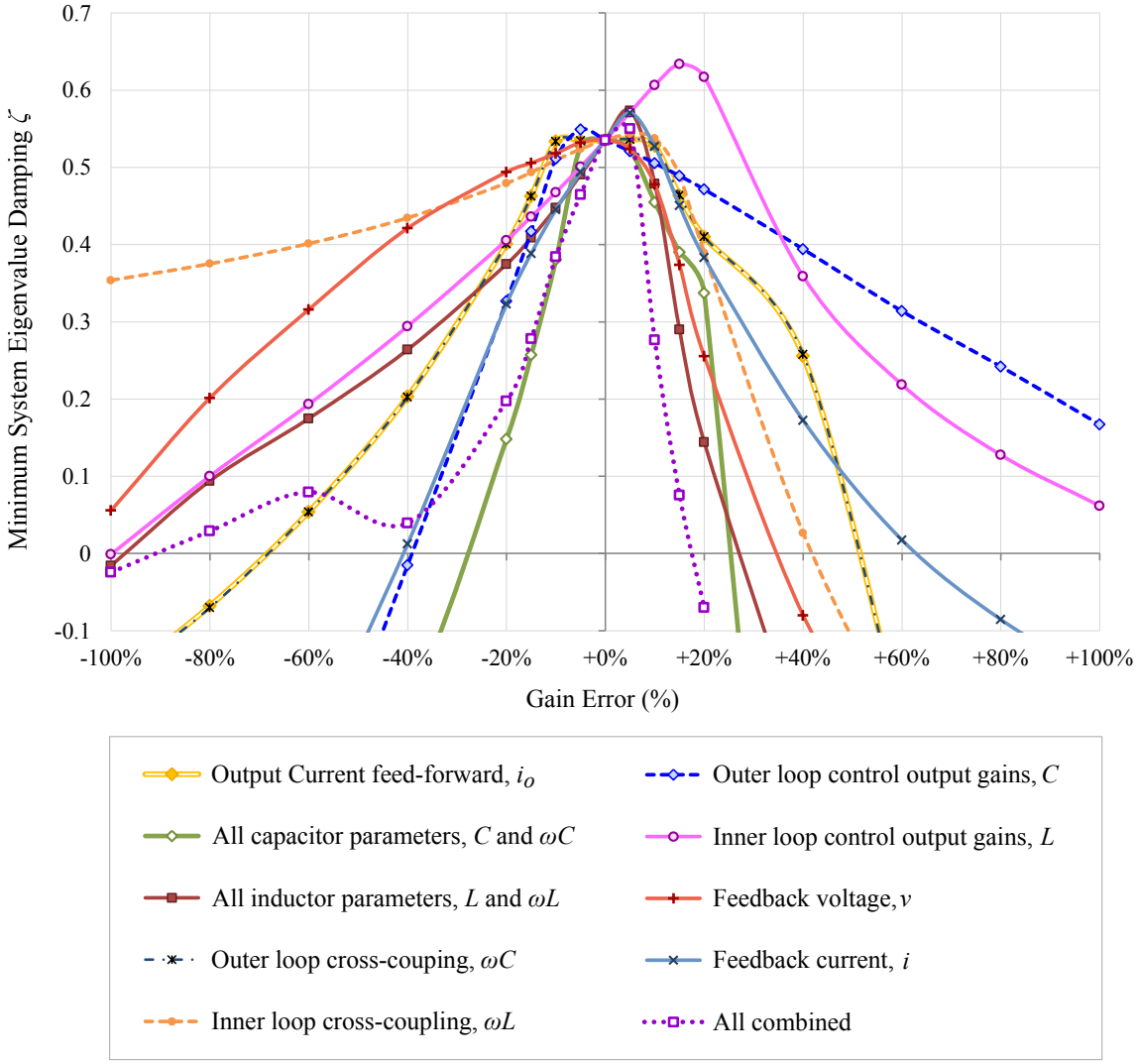

Figure 5.15: The minimum system eigenvalue damping for a range of linear errors in individual parameters or sensor measurements in the voltage controller.

root locus in Figure 4.14. Using this trajectory as a reference, the original inner loop CLP position starts at at the turning point where the imaginary component is at the maximum. As the gain increase, the CLP follows that root locus from that point towards the left-hand side, which increases the damping in the inner loop and the minimum eigenvalue damping in the overall voltage control system. When the gain is further increased, the response of the inner control loop becomes over-damped and too slow to respond to the control effort requirements of the outer loop controller, and then the minimum system damping is reduced as a result.

5.3.3 Fault Tolerant Sensors

When the gain error is -100% in Figure 5.15, the signal in the model is zero and will represents a failed signal with a constant zero output failure mode. This failure mode can occur due to a loss of power supply in the individual sensors, a failure in the ADC or a loose connection. This also shows how important the feed-forwards signals are for the stability of this controller, because the minimum damping is around zero and unstable when the feed-forward error is -100%. They cannot be simply eliminated to reduced the number of sensors in this type of system.

The primary failure modes and root causes of a sensor in the electrical system are not clear. Sensors are made up of a number of small components: the hall effect device, amplifiers, passive components, voltage power supply, the connectors and the ADC. These can all be grouped together as a sensor module. Applying the modularisation concept as described in Section 3.3, multiple modules can then be used for the same measurement. Each set of measurements will have multiple signals which can be processed. If they are averaged to a mean signal, the accuracy is improved. When there is at least three sensor modules for each measurement, an algorithm can be designed to detect if a signal is very far away from the mean signal over a number of samples. This can then be rejected as a failed sensor and the system continues with the remainder sensors until the next inspection for maintenance.

Although redundancy is more expensive, this is a smaller price to pay relative to the cost of the rest of the system. Sensor reliability is very important, since a total failure will cause the system to be unstable as discussed in Section 5.3.2 and shown in Figure 5.15. Reliability is more important for the voltage controller at VSC1, which is the largest and the most important VSC in the system as the HVDC terminal station where all the generated power is channelled through. A single failure here would disrupt the bulk of the power flow from wind energy being transmitted back to shore. Normally, root cause analysis is carried out so the reliability can be improved by directly targeting the root cause. However, if the root cause is unknown and there are multiple factors involved, the modularisation solution would make the sensor system more fault tolerant and reliable. It would not matter how the module has failed or where inside it, as long as the signal from the failed sensor module can

be ignored and does not affect the control system. Further work is needed to test this.

5.3.4 Further Work for Controller Reliability

The controller software and hardware is assumed to be more reliable. The signals all come to this single point in the system. If this fails, it may cause the whole system to fail or become unstable. It is challenging to modularise the voltage controller and to add levels of parallelism. There can be only one voltage controller in the system with many current/power sources. Two strong voltage sources cannot be easily connected together without stability issues and "fighting".

Assuming there is more than one outer loop controller on separate circuit boards and only the output of one of them is connected. An error detection algorithm is needed to detect the failure in order to switch. Failure to do so may result in an unstable system. Care must also be taken not to over complicate the system, which may make the system less reliable. It is also assumed that the error detection and control switching system will be more reliable. This part requires further work to understand the robustness of this kind of system.

5.4 Chapter Summary

- When comparing between the open loop and closed loop voltage control cases, the designed voltage controller was able to suppress the resonance in the LC filter that was triggered by current disturbance as found in the open loop case. In the case study, the LC filter resonant frequency was 2000 $\mathrm{rad.s^{-1}}$, the frequency bandwidth of the VSC1 inner loop control (ω_{ni1}) was 1428.6 $\mathrm{rad.s^{-1}}$ and the outer loop voltage controller was five times slower than the inner loop. Overall the speed of the outer loop voltage controller was seven times slower than the LC filter resonant frequency and yet it was able to suppress the filter resonance by controlling the filter capacitor to be a constant voltage source. Therefore, the voltage control bandwidth does not have to be faster than the resonant frequency of the LC filter. Constant voltage controlled helps to

minimise over-voltage in the offshore HVDC filter capacitor, therefore it may help to minimise filter capacitor tripping events as experienced by Borwin1.

- One key advantage of using a closed-loop voltage control with a cascade configuration is being able to limit the current reference in between the inner and outer loop of the controller. This is useful for protecting the converter from overloading. Simulation found that current saturation works for both balanced and unbalanced fault cases, and the control system is able to ride through the fault with low voltage and quickly recover back to the original state after the fault has cleared.

- The current carrying capability of the offshore HVDC converter station may be reduced due to a loss of a module and current saturation can be used to prevent overload in this scenario. If the current is saturated while power is still flowing into the offshore station from the WF, this will cause the AC-side to over-voltage at the filter capacitor. In order, to overcome this issue, the system must signal the WT turbines to reduce their power output.

- System dynamics depend on how the offshore WT power control interact with the network and VSC-HVDC station. For the open-loop method of setting the converter terminal voltage, it is not recommended to have WT control speed too close to the resonant frequency of the station's LC filter. Further work is also needed to refine power control and compensation of the dynamics in the AC voltage. The power control method used is not perfect but it was enough to study the impact of a change in the power input on the HVDC substation converter (VSC1). If the resonance in the AC side voltage can be compensated, and true power control is implemented, the damping in the system can be improved compared to the case when current control was used in the WF.

- Some feed-forward signals for the controller can be estimated and therefore the sensors for this may be eliminated. However, the voltage controller is complicated and still require a number of sensors for feed-forward and two layers of feedback control, and is not very ideal for control system reliability.

A failure in one sensor signal can undermine the performance of the controller. Modularisation with redundancy for each sensor was suggested to improve sensor reliability. Small signal analyses were carried out to observe the system eigenvalue damping when errors occur in these signals.

Chapter 6

Practical Experimentation

An attempt was made to practically implement and validate the model of the controllers for the VSC-HVDC converter station and the aggregated WT converter as described in Chapter 4. This chapter will discuss about the limitations of the available laboratory hardware used and what can be done to solve these issues. Time and funding were limited to continue the work, therefore considerations for further practical experimentation work on the AC voltage controller has also been made.

6.1 The Experimental Rig

The experimental test rig, as shown in Figure 6.1, is a large safety cabinet enclosure to house the converters and all electrically exposed devices, such as the current and voltage transducer boards, protection circuits, and filter circuits. It was designed to operate with a DC voltage source power supply rated up to 600 Vdc and 24 A. Interlocks are in place to isolate everything inside the enclosure to reduce risk of electrical hazard in case of unauthorised access. Cooling fans are also installed to keep everything inside the enclosure as cool as possible. The shelves inside test enclosure are reconfigurable and the total size is big enough to house two converters together.

The three-phase high power resistor load bank shown in Figure 6.2 has switches to discretely vary the resistance per phase. This will be used for initial testing of the converter and control system before connecting with other converters and devices,

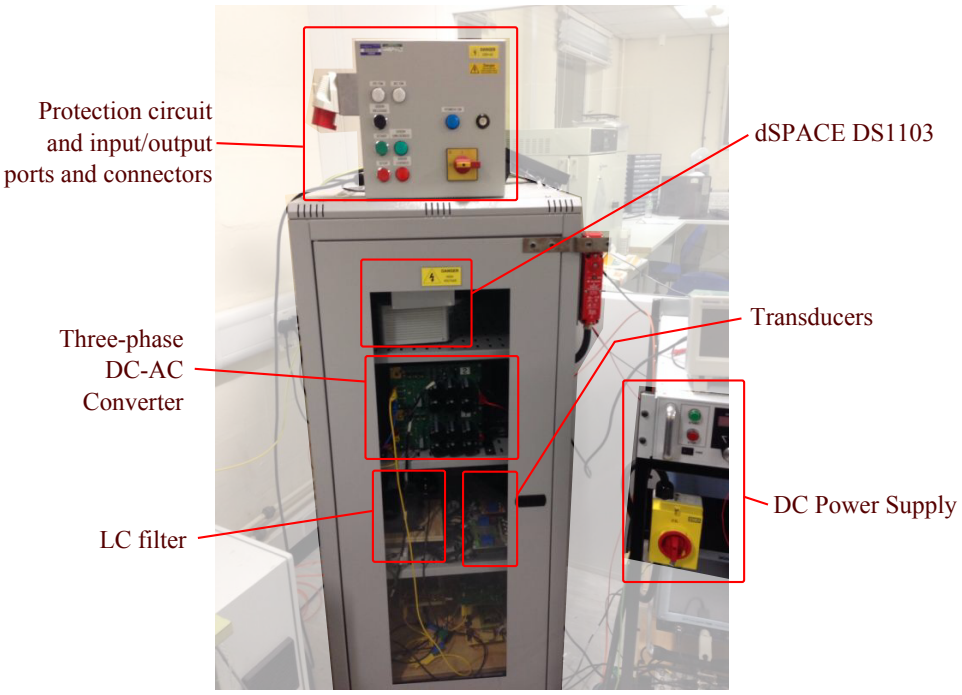

Figure 6.1: The experimental test rig safety cabinet set-up.

such as a grid simulator.

6.1.1 Three-phase Inverter Board

The three phase inverter board shown in Figure 6.3 is adapted from previous laboratory projects by M. Parker and D. Xiang. The DC capacitors, gate driver circuit, and opto-isolators for the gate signals are all included on board.

The original board did not have any protection from the signal feeding to both top and bottom part of the inverter legs being both high, causing device failure due to short circuiting between the DC link. This used to happen frequently because the default signals from dSPACE were all high when on standby and require strict operational procedures to prevent this failure. A digital NAND gate chip was included in the printed circuit board (PCB) so that a signal could be sent to the 'shut down' pin of gate drivers to prevent the fault from happening. Details on other improvements and modifications to the board are included in Appendix C.1.

The switching devices used is a PCB mounted IGBT module manufactured by Semikron (SK35GD126ET) as shown in Figure 6.4. It fits on the underside of the

Figure 6.2: The high power load bank used for initial controller testing with the converter.

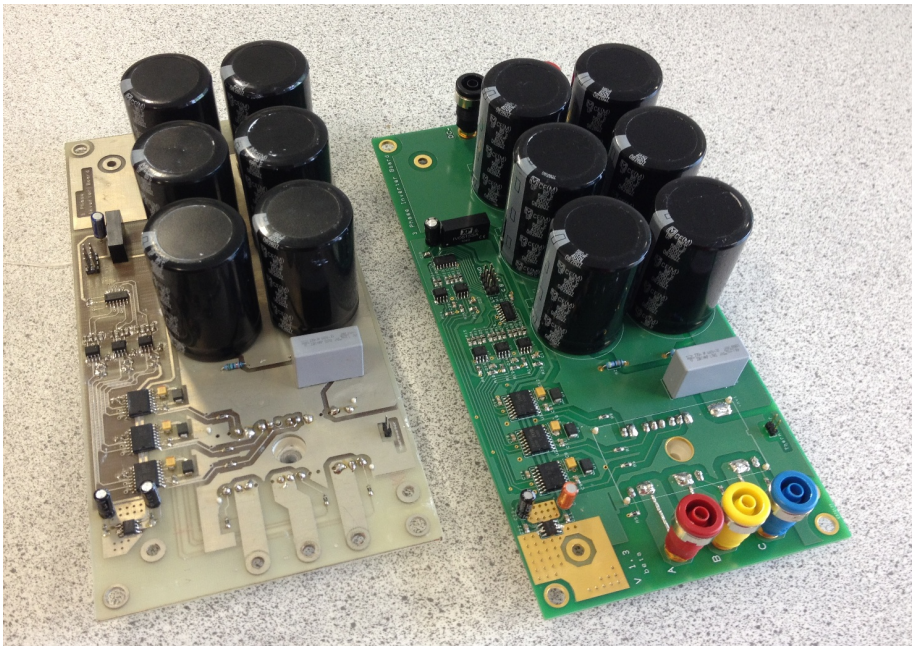

Figure 6.3: A photo of the old three phase inverter board on the left side by side with the new redesigned board on the right.

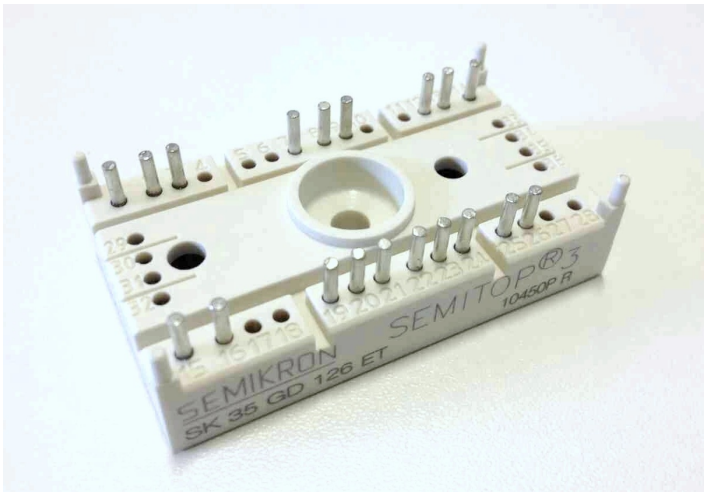

Figure 6.4: A photo of the three phase Semikron IGBT module.

PCB and is attached to a heat-sink by a screw through the middle of the device.

6.1.2 Scaling the Parameters

Only one converter and one LC filter set are tested at this step. The original base power and voltage used in Section 4.4.1 for the original simulation is beyond the rating of the available DC power supply. The system must scaled down below the rating of the test rig, while maintaining constant per unit values in the original system. The chosen base parameters for this experiment is 5.36 kW 350 V_{line}, meaning that base impedances should be scaled by 100. The resulting parameters are shown in Table 6.1. Three off-the-shelf 10 mH 20 A inductors (Hammond 195J20) and 25 μF 450V capacitors (EPCOS B32332I6256J080) were used.

Table 6.1: Experimental parameters.

S_{base}	5.36 kW
$V_{\text{line base}}$	350 V
L	10 mH
C	25 μF

Initially, a lower base level for the apparent power S_{base} and line voltage ($V_{\text{line base}}$) was used, such as 530 W and 110 V_{line}, while the base impedance Z_{base} is constant so that the same LC filter parameters can be used for the similar control dynamics.

This would be necessary for the first test and controller tuning stage, in case of control instability, thus minimising the probability that the voltage or current goes beyond the rating of test rig.

In terms of the DC voltage, it should just be simply sufficient enough so that output phase voltage is not clipped. An average modulation index around 0.7 to 0.9 would be sufficient. As first discussed in Section 4.3.3, a DC feed-forward method is used to decouple the changes in the DC-side voltage. The RMS-value invariant dq transformation was used, therefore a dq vector would directly correspond to the RMS value.

6.1.3 The dSPACE controller

The DS1103 PPC controller board and interface by dSPACE GmbH was available in the laboratory to be used for converter control. It also has enough analogue to digital converter (ADC) input ports for all the necessary feedback and feed-forward signals. The controller can be graphically designed using block diagrams in Simulink, which allows a simple transfer of the same control structure from the original simulation model. The model will then be compiled and downloaded onto the hardware for converter control experiments. Data can be recorded onto a .MAT file and for export to MATLAB for analysis and plotting.

dSPACE has a timer board with a built-in three-phase PWM function, which only requires the duty ratio input for each phase, with values ranging from 0.0 to 1.0. Therefore the e_{abc} voltage output references must be biased and scaled depending on the DC link voltage.

6.1.4 Delay in the Timer-based PWM Output

The three-phase PWM signal generator in dSPACE is based on a separate timer hardware module on the slave DSP board. Therefore it has fast clock frequency and built-in dead-band for inverter switching and its is able to produce PWM signals with high resolution duty ratios. Although this is computationally efficient, there is an inherent delay between the duty ratio reference input and the actual PWM

output. When there is a change in the duty ratio reference input, it can only be updated at the next duty cycle. In essence, the faster the switching frequency, the shorter the delay times. The converter uses silicon IGBT switching devices, where losses increase further with frequency.

Another problem with the timer based PWM was that the delay was not consistent. Over time, this delay gradually increases or decreases between a maximum and a minimum delay as shown in the Figure 6.5 example, where the CH3 purple trace is the digital output, signalling when the duty ratio steps from 0.0 to 0.7 and the CH1 yellow trace is the PWM output signal. A snapshot on the oscilloscope was taken when the delay was at its maximum and minimum. In this case, the delay is between 0.69 and 1.64 times the switching period the PWM frequency. The choice of the sample frequency and switching frequency can affect the rate and direction of the change in the delay to be increasing or decreasing. When the delay has reached the maximum/minimum, the delay will then reset and jump back to the minimum/maximum. This could be a synchronisation problem between the master PPC board and the slave DSP board, and further work is needed to address this issue and keep the delay constant. When the sample frequency was made equal to the switching frequency parameters in the configuration settings, the delay was still not constant over-time. It was also challenging to use the interrupts to synchronise the two boards, and the PWM frequency could only synchronise with the ADC measurements. Although this helped to reduce the noise in the measurements by making sure that it is not sampling during the switching transients.

6.2 Closed Loop Testing

PSCAD® was used to simulate the effects of the delays in the PWM output of dSPACE as found in Section 6.1.4. The performance was found to be deteriorated, and therefore the controller needed to be retuned to factor in the delay. The redesigned control gains were also tested in the practical test rig in Section 6.1 and then compared with the simulation results.

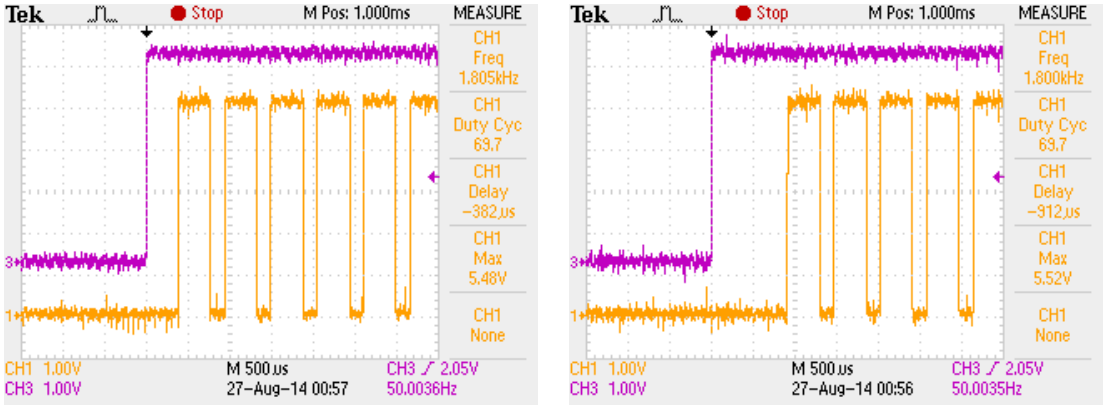

(a) Minimum PWM delay **(b)** Maximum PWM delay

Figure 6.5: Delays in the timer-based PWM output of dSPACE, measured on a digital oscilloscope for a switching frequency of 1800 Hz. CH1 is the PWM out, CH3 is the digital out signalling when the duty ratio is changed from 0.0 to 0.7.

6.2.1 Limitation in the Control Performance with the Delay

The effect of the delay in the PWM output is simulated in PSCAD®, the same voltage controller and gains chosen in Chapters 4 and 5 remain unchanged for now. A tranfer delay of 0.6 ms at the PWM output is placed between the reference and actual converter voltage output voltage. The resulting regulation performance, while the circuit is open (i.e, no VSC2 or no load), is shown in Figure 6.6. There is a noticeable phase difference between the reference $E_{a\,ref}$ and the measured V_a phase voltages, where normally during no load, there is no difference in the steady-state.

Generally, the originally designed voltage controller cannot tolerate delays greater than 5.5 ms, where the controller is will not be able to regulate a constant voltage and significant oscillations are observable. The largest delay that was found in PWM output of dSPACE for 1800 Hz switching frequency was 0.91 ms.

The PWM delay introduces a voltage lag in the actual converter voltage output compared to the output voltage reference e_{ref}, which then has an impact on the current control performance. The entire controller needs to be retuned to factor in the delay, starting with retuning the decoupled inner current control loop.

The non-constant PWM delay is difficult to quantify and compensate for. The original control gain calculations did not factor in this delay and therefore those

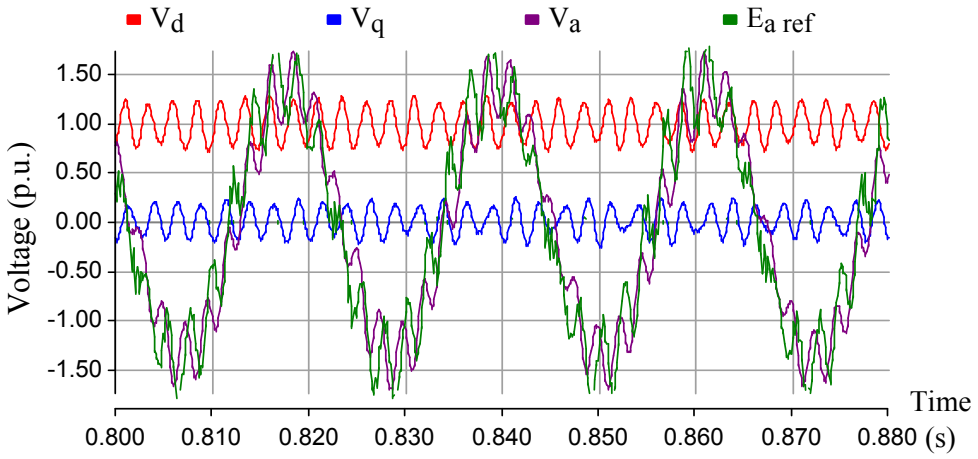

Figure 6.6: Simulation results for a constant voltage control with a 0.6 ms transfer delay at the PWM converter voltage output.

parameters are no longer valid for this practical experiment. Retuning the current controller must, at least, factor in the worst case delay.

6.2.2 Retuning the Current Controller

The delay is factored in as a first order approximation in the output of the current controller, as a pole with a time constant τ. Its transfer function is shown in equation (6.1).

$$\frac{1}{1+\tau s} \tag{6.1}$$

Assuming the interactions between the d and q axes are decoupled, the single-input single-output transfer function for the dynamics of the filter inductor is shown in equation (6.2) [137]:

$$\frac{I(s)}{V(s)} = \frac{1}{Ls+R} \tag{6.2}$$

Equations (6.1) and (6.2) can then be put together to become the open loop system $G(s)$, which will be put in the `sisotool` function in MATLAB®. As a starting point in the `sisotool` environment, the PI controller was set up using control gains from the gains using the original calculation method (Appendix B.2) for LC parameters of the experimental rig. The delay pole repelled the root locus and CLPs of interest towards to the right hand side of the pole-zero map and reduced their damping factor as a result. Trail and error was used to optimise the speed and

ensure that the CLPs are well damped enough, i.e. a CLP that is 0.7 or greater and does not fall in the non-yellow constraint region in Figure 6.7. The control parameters from this analysis are then extracted and implemented on the current controller on dSPACE.

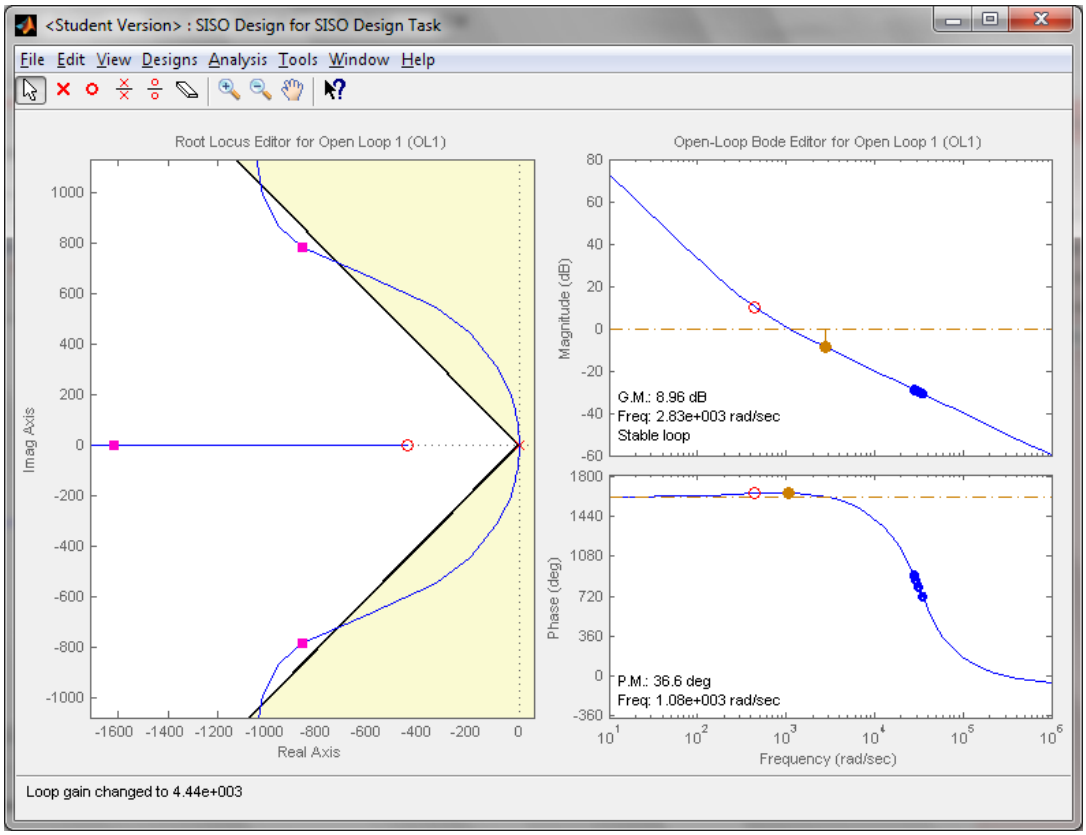

Figure 6.7: The `sisotool` environment used to tune the current controller with at least 0.7 damping ratio.

The initial current control response that could be achieved with sufficient damping on the converter test rig is shown in Figure 6.8. Here the AC-side of the converter was connected to a high power resistor load bank (see Figure 6.2), and the reference current in the d-axis (i_d) is stepped from 1A to 7A. The rise time in the response in this case is approximately 15 ms, which is about seven times slower than the original current control rise time response defined in Section 4.5.2.

The control speed is then further fine tuned using trial and error on dSPACE by varying the control gains. The fastest control response found with reasonable overshoot or damping has improved, as shown in Figure 6.9, which has a rise time of approximately 6 ms, but it is still slower than the original desired speed by about

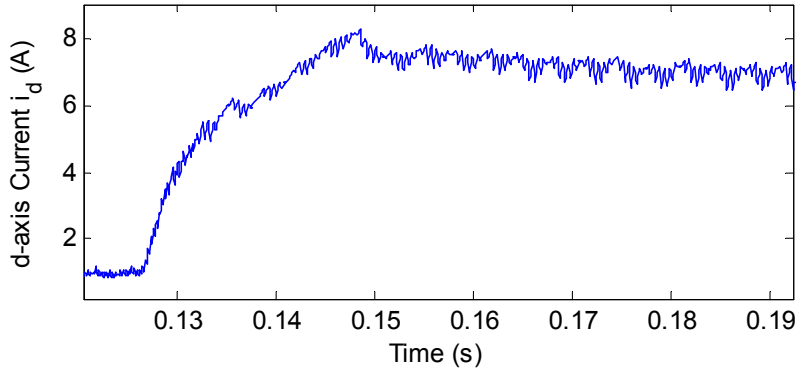

Figure 6.8: The d-axis current response to a step input from 1A to 7A, using the converter and under current control with dSPACE.

2.7 times. The PI control gains used in this case are 14.0 and 5000 for K_p and K_i respectively in the current control loop. Note that the absolute value of these gains appears to be higher for slower control compared to the gains in Section 4.5.4 for faster control. This is because the gain depends on the factor of the actual inductance L for the current control loop, which is high in this case for the experimental test rig (see Appendix B.2).

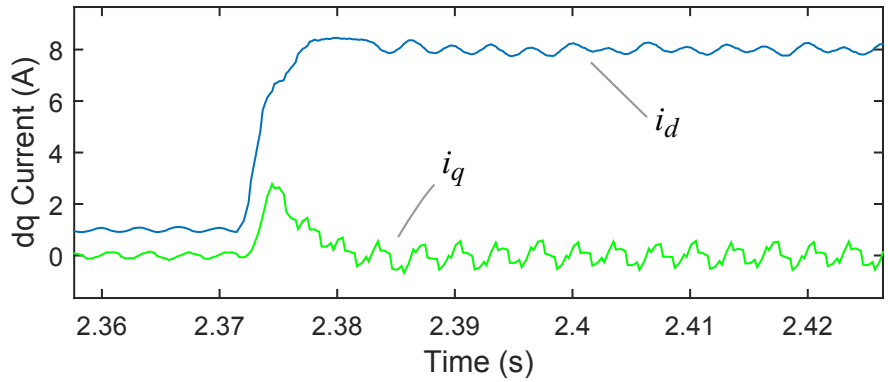

Figure 6.9: Faster d-axis current response to a step input from 1A to 8A, using the converter and under current control with dSPACE.

6.2.3 Outer Voltage Control Loop Test

The current control parameters found in Section 6.2.2 will then be used for the inner control loop of the AC voltage controller. The slower inner control loop was approximated as a second order TF, based on the estimated damping and natural frequency

of the current response. The outer loop control is designed using `sisotool`, based on the analyses and criteria in Section 4.5.5 as shown in Figure 6.10. The outer voltage loop control gains found are 0.002 and 0.100 for K_p and K_i respectively and the leading compensator time constant is 0.0023 s.

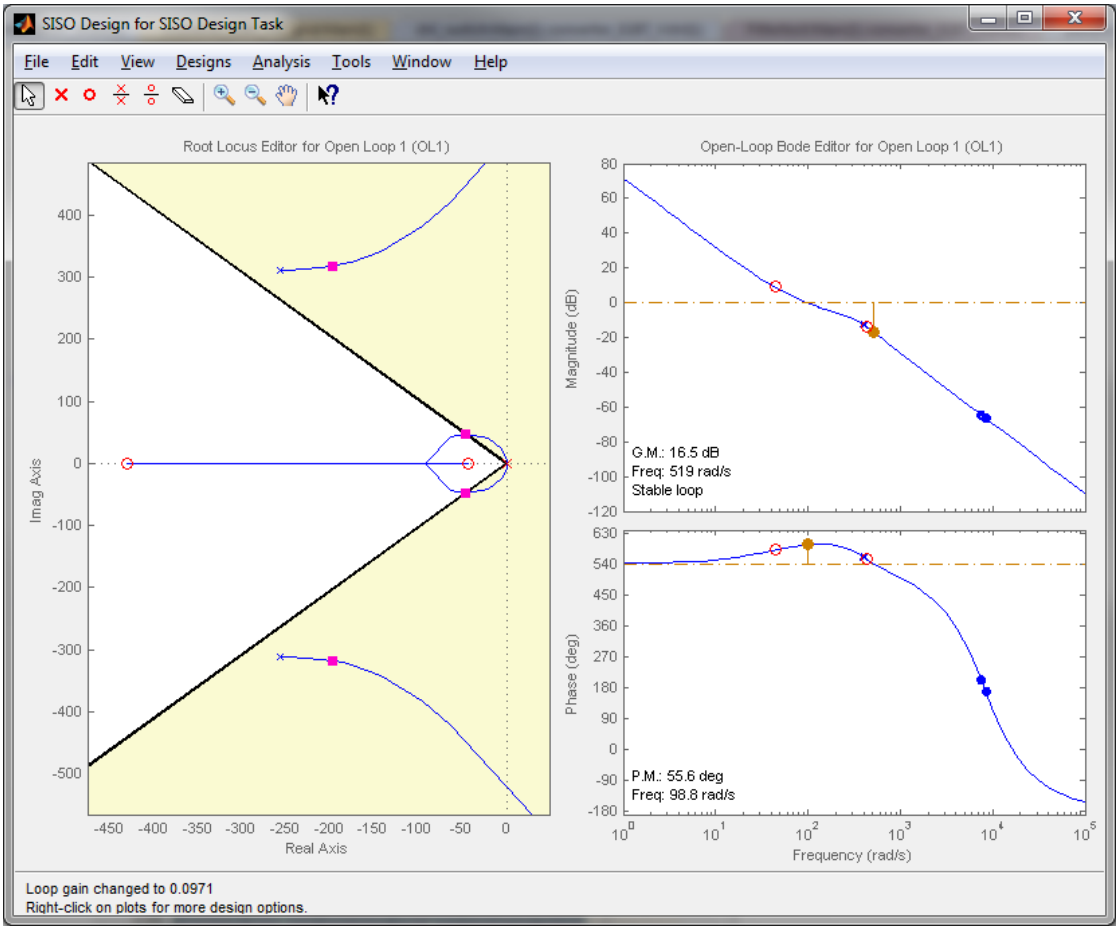

Figure 6.10: Re-tuning of the voltage controller using `sisotool` with new current control loop dynamics.

However, when the control gains are used in dSPACE with the experimental test rig, while controlling the voltage at 60 V, significant oscillations were present in the steady-state as shown in Figure 6.11. The voltage regulation is comparable to the oscillations in the current and voltage in the initial simulation results in Figure 6.6.

The second order approximation of the current dynamics may not exactly fit the actual current response, where an initial delay is present before the current starts rising. Furthermore, higher order characteristics were ignored. A better approximation of there inner loop control dynamics is needed if `sisotool` is to be

used for tuning the outer voltage control loop.

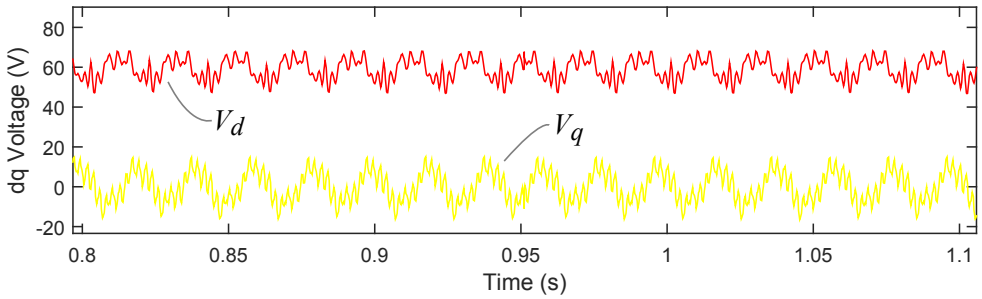

Figure 6.11: Experimental results for AC voltage control using with the outer loop gains found with `sisotool`.

6.2.4 Comparison with PSCAD® Simulation

A PSCAD® model of the experimental test rig and a transfer delay of 0.9 ms were used at the PWM converter voltage output, and the current control gains were adjusted to replicate the current response in Section 6.2.2. Using the outer control loop gains found in the previously, the steady-state voltage regulation found in the simulation is as shown in Figure 6.12. There is no second converter or load for any other control interaction to take place, here in this case, for both experimental and simulation.

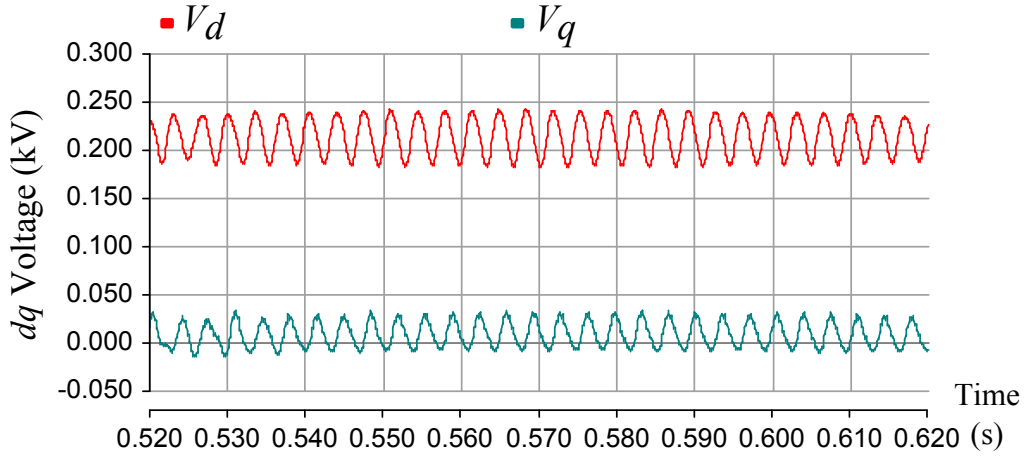

Figure 6.12: PSCAD® simulation of AC voltage control with outer loop gains found with `sisotool` and a transfer delay of 0.9 ms.

In Section 6.2.3, the controller was retuned to factor in the delay. The delays

lead to increased oscillations in the steady steady voltage regulation, because when the transfer delay is reduced from 0.9 ms to 0.8 ms, the steady-state voltage is stable and contains no significant oscillation. The retuned controller is able to tolerate a larger delay in comparison to the initial simulation of the voltage controller with 0.6 ms transfer delay Figure 6.6. However, the control performance is still not good enough with the PWM delay, as shown in the simulation results in Figure 6.13.

This time a second converter (VSC2) that is under current control was included and a step current of 5 A was applied at time = 1.00 s. Although the voltage step input was good before 1.00 s, the response to a step current is under-damped. The dynamics are more oscillatory and do not match what was designed using `sisotool` where a first order approximation was used for the delay.

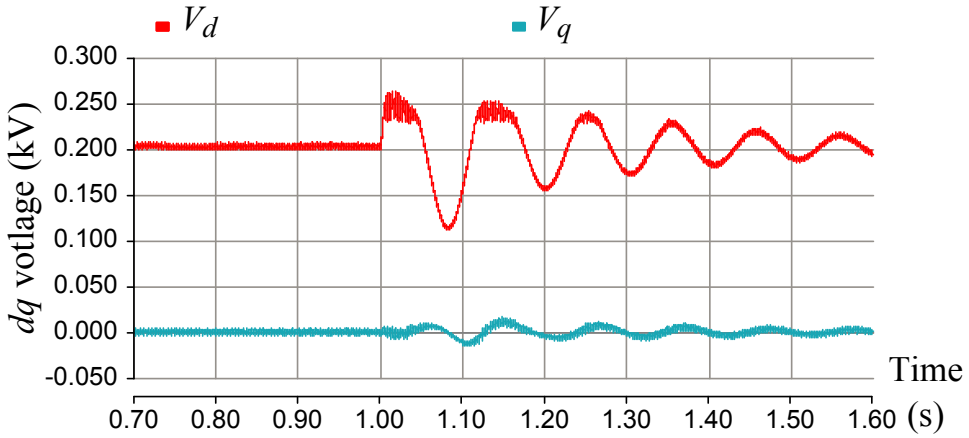

Figure 6.13: PSCAD® simulation of AC voltage control and a transfer delay of 0.8 ms, a 5 A current step input is applied from VSC2 at time = 1.00 s.

6.3 Discussion and Further Work

On closer inspection, steady-state oscillations are also found in the current response as shown in Figures 6.8 and 6.9. It was initially thought that this was just noise and not very significant. The oscillations in the current response may have then contributed to the steady-state oscillation found in the voltage control. The maximum delay of 0.91 ms in the PWM output of dSPACE for 1800 Hz switching frequency is too significant and therefore must be eliminated where possible. As a result, the

voltage controller will not be fast or stable enough to be used for AC voltage control at the offshore HVDC station if there are these significant delays in the PWM output.

6.3.1 Proposed Carrier-based PWM Hardware

A fully stable and well-damped voltage controller could not be implemented experimentally yet. The delay in the timer-based PWM function in dSPACE limits the control speed or bandwidth of the inner loop that can be achieved with sufficient damping. This limitation would ultimately have an impact on the outer voltage control speed, where the outer loop has to be five times slower than the inner loop speed, as discussed in Chapter 4. Therefore, a fast inner current control loop is important for fast outer voltage control loop and ideally the delay must be eliminated.

There were no significant delays in the simulation results when the triangular carrier wave and comparator based PWM method was used in the original PSCAD® models. Implementing this digitally in real-time is, however, computationally intensive and requires very high sample frequencies. In is not possible on the master PPC dSPACE controller board because the its processing speed is limited, and the maximum sample frequency that could be used before the system crashes is about 10kHz, which is not fast enough to achieve a sufficient resolution for the duty ratio. Programming a dead-band time using a sample period in this case would further severely distort the converter voltage output.

A high precision triangle carrier wave and comparator is necessary to accurately modulate the reference voltage. This would require a very fast dedicated DSP add-on hardware board, which is expensive but easy to implement. An analogue circuit would be cheaper for the same job for generating the carrier wave and using an electronic comparator against the reference waveform from the digital to analogue converter output of dSPACE. However, the analogue method may be vulnerable to electromagnetic interference from the converter. In the end, the carrier-based PWM could not be implemented due to the lack of time and resources.

6.3.2 Dynamic Characteristic of the LC Filter

The response of the filter to a step voltage or current was more damped than expected and resonance could not be replicated using a step in the current, voltage or frequency. This could be due to the eddy current and hysteresis losses associated with high frequency.

The inductor used was originally designed and manufactured to be used as a choke or a reactor rated for the fundamental AC frequency, and not specifically for filtering high frequency switching harmonics in the current. The 195J20 was the only commercially available off-the-shelf inductor with desired inductance value and current rating. Most of the losses would most likely have dissipated in the laminated ferrous metal core. The inductance and the series resistance against frequency were measured using an LCR meter, and the results are shown in Figure 6.14. As the frequency increases, the effective inductance also decreases. This could mean that the actual resonant frequency is shifted higher, where there is more damping because the effective resistance is higher at the increased frequency.

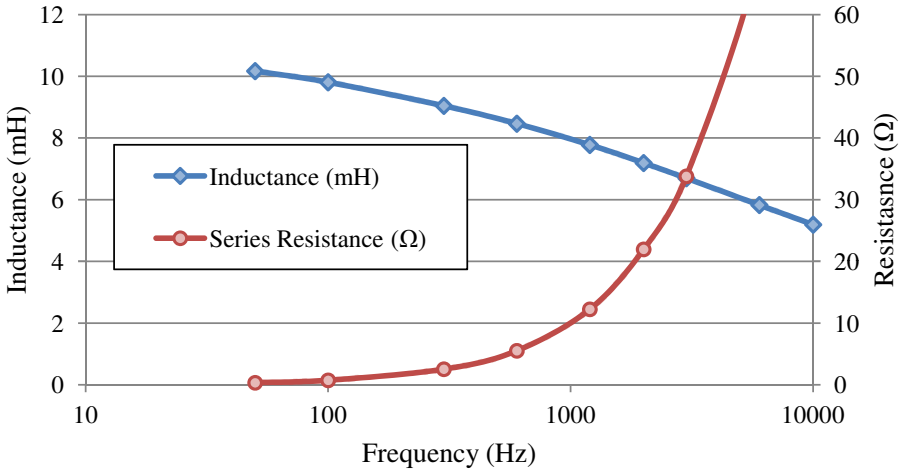

Figure 6.14: The inductance and series resistance against frequency for the 195J20 inductor, measured using an LCR meter.

The resonance that was as found in Section 5.1 must be replicated in order to practically test the voltage controller for suppressing them. Manufacturing new air-core inductors is recommended instead of using the ones with the laminated cores. The only main concern for losses in this case would be the proximity and skin effect

in the windings, which would be considerably less in total.

When designing a new inductor, a higher base power, and therefore smaller base impedance value, should be considered so that the inductor size can be reduced for the experiment. The inductance of 10 mH is too large and for an air-core inductor the proximity effect losses increases with the number of windings. Although the size of the capacitor would have to increase to maintain a constant filter cut-off frequency, it should be affordable for this experiment because the inductor was originally more expensive than the capacitor. A break-even cost between the inductor and capacitor can be found. The per unit values are maintained constant to keep the same equivalent dynamic characteristics.

6.3.3 Loss in the System

The AC side of the converter and filter system is connected to a high power resistor load bank. The converter will operate in open loop with a set DC voltage, a constant modulation index of 0.8 and a switching frequency of 2500 Hz. This was arbitrarily chosen to first get an idea of the loss in the system. The current and voltage was measured to calculate the power from the DC supply, which was 200.2 V $\times$ 7.37 A = 1,475.5 W. At the same time, the real power on the AC side, after LC filtering, is found by recording the three phase currents and voltage waveforms for a few seconds. The instantaneous power is calculated using equation (4.5) at each time frame, and average over the recorded period was found to be 1,368.9 W.

Approximately 7.2% of the power is lost in the converter and filter system. Most of it is likely lost in the inductor as the losses in the converter should not be very significant because the IGBT module was operating below its rating of 1200 V and 35 A for each inversion stage. The losses in the filter should be reduced so that it reflected the per unit losses of an efficient and high power HVDC terminal.

6.4 Chapter Conclusion

A timer-based PWM method in the dSPACE hardware used for the experiment may be cost effective and computationally efficient, but the PWM output has significant

delays and the current control speed is limited as a result. Although a slow current control may be acceptable for a number of other applications, it is not fast enough to be used for the original outer loop voltage control speed desired in this thesis. In order to overcome the PWM delay issue, a carrier based PWM should be implemented instead of the default timer-based PWM in dSPACE. The practical experiment was not able to go forward as the time and the resources were limited, therefore this will be recommended for further work.

Control performance is limited by the PWM delay and there is sufficient damping by the losses in the filter. For the experimental components used, the voltage controller is not suitable. Instead, a simple open loop method (Section 5.1.1) to establish the voltage at terminal of the converter would be have no issue with any delay.

High frequency losses in filter contribute to damping in the LC filter. Therefore resonance could not be replicated to test the voltage controller to suppress it. If the losses in the system provide enough damping in the experiment, then an active damping strategy is difficult to investigate. The losses were too high in the inductor with the laminated core, and therefore this thesis recommends using a more efficient inductor for the purpose of continuing the investigation. Air-core inductors are efficient and cost effective, but a higher number of turns is needed to achieve the same inductance without a magnetic core. No core loss will exist, but the small skin effect and conduction losses will dominate instead. Alternatively the inductor may use more efficient composite power laminated cores if inductance still needs to be high or it is required to be fully shielded, although this option will be much more expensive. If a lower inductance value is used, then a larger capacitor is required to maintain a constant filter cut-off frequency of the LC filter.

Chapter 7

Conclusions and Recommendations

HVDC connection would be necessary for efficient high power transmission for large offshore wind farms that are very remote from the shore. The offshore AC network connected by HVDC is weak and inertia-less and islanded from the onshore grid. Without proper control, the offshore voltage and frequency can deviate from the nominal level. The experience from Borwin1, the first HVDC connected offshore wind farm, found that the system was vulnerable to over-voltage at the filter capacitor, causing it to trip as a result. Due to the confidential nature of the private companies that design, install and operate Borwin1, there is little useful public information to draw a conclusion about the exact detail of the mechanism of the failure, the configuration of the capacitors and what caused it to over-voltage. Although the models used in this thesis may not exactly reflect the actual system, the approximation was enough to understand some of the mechanisms of over-voltage and how to control and limit these events. This thesis has identified two major sources of voltage overload, filter resonance and current saturation at the offshore converter station.

Two level converter VSC-HVDC topologies, akin to the ABB HVDC Light® systems, are a cheaper but still require a relatively large filter and therefore require voltage control of the filter capacitor. A simple inductor-capacitor LC filter without resistive damping was assumed for the study and assumed that the inductor

insulation at the terminal of the converter output can tolerate the large dv/dt. The resonance in the LC filter is triggered by a disturbance in the current input or sudden frequency change, which then leads to over-voltage in the capacitor at the point of common coupling (PCC). The proposed voltage controller aims to control the capacitor voltage at the PCC to behave like a constant voltage source, and therefore limits resonant oscillations and over-voltage. This method will be more efficient than using passive damping resistors. The harmonics in the voltage output of a MMC multilevel converter is much lower and the filter capacitor size requirement is reduced. The voltage controller will then not be required in this case. However, an MMC system is still more expensive due to the complexity and number of devices and components required.

Voltage control is important in the offshore network, especially if the connection to the onshore grid is weak and offshore electrical system is vulnerable to over-voltages. The full state feedback controller has a cascaded structure with a inner current control loop and an outer voltage control loop. As general rule of thumb, the outer voltage control loop speed should be five times slower than the inner current control loop speed. The phase lag in the inner current loop must also be appropriately compensated by using a first order leading compensator between the inner and outer loop, or using the derivative part of a PID controller for the voltage outer loop. Both will effectively place a zero near the closed loop poles of the current inner loop control.

As discussed in Section 4.5.7, dynamic interactions were found between the VSC-HVDC converter station and the aggregated WT converter over a range of control speed ratios. Not only is a fast PCC voltage control needed by HVDC converter station, but generally a sufficiently fast power controller that can fully compensate the voltage dynamics would be beneficial for the stability and damping of the system. The chosen voltage control bandwidth was slower than the resonant frequency of the LC filter, and results suggest that it was fast enough to keep the voltage level at the filter capacitor constant and prevent resonating oscillations caused by current disturbances.

The thesis has only considered the resonant frequency in the HVDC station

LC filter and has not considered resonance elsewhere in the offshore wind farm network. Filters for WT generators were assumed to be already well damped and therefore they were modelled as ideal sources. Resonance due to the capacitance and inductance in the entire AC cable network was ignored and assumed to be outside the operating frequencies of interest. Further study will be required to consider the cable resonance and how it is affected by changes in the network configuration and total cable length.

The weakness off the offshore wind farm AC network connected by HVDC is attributed to the limited power rating of the HVDC converter. The current can be saturated at the input of the inner current control loop to protect the converter from over-currents. Power electronics devices are very sensitive to over-currents because the temperatures can rise very quickly due to the low thermal capacity. The odd circumstances that a the current will need be saturated at the offshore HVDC substation, will be during excessive generation from sudden gusts and derating of the substation due to failed modules. While the current is saturated, the integral part of the outer voltage loop controller has to be disabled, and the excess current coming from the WTs then charges the filter capacitor and increases its voltage. In order to prevent over-voltage in this case, the WTs must reduce their power output, which is achieved by curtailment with stall or pitch control, diverting the excess energy to an energy storage device, or dumping it through a load bank. This can be communicated from the offshore substation using an offshore network frequency droop method (or voltage rise detection at the WT point of connection). It was also suggested to use the AC frequency level as an indicator for representing the maximum cap on the WT power output to help prevent the WT power exceeding the saturation point the first place. Further work is needed to implement and test this. It is difficult to control both current and voltage at the same time without power control as well. Although the thesis recognises the benefits of energy storage on the offshore network voltage during HVDC current saturation, the storage devices may be too expensive. Cost benefit analysis needs to be carried out to fully realise the cost effectiveness of such a system, however, it is beyond the scope of this thesis.

If the network voltage drops too low, for instance due to a fault ride through

scenario, the power export capability of the wind turbine is limited. The excess power that is not exported will lead to over-speed in the WT rotor or over-voltage in the DC link of the fully rated frequency converter if not controlled. If the network voltage rises too high and exceeds the rating of a device, this will lead to tripping or failure. Saturation during unbalanced fault scenarios is possible with the voltage control structure and current saturation method used, but further work is needed to further smooth the power flow during unbalanced faults with negative sequence and/or individual phase control.

Although this thesis has mainly focused on VSC systems, the voltage controller has not yet been implemented and experimented with the option to hybridise with the LCC system for the HVDC station, following up from Section 2.1.6. It is possible that the voltage controller tested in this thesis may be able to provide active filter and eliminate voltage harmonics that come from passive diode rectification and thyristor-based LCC converters. This is based on the fact that the voltage controller with the VSC-HVDC was capable of eliminating the AC-side filter resonant frequency when it is maintaining a constant r.m.s voltage at the filter capacitor. LCC is a more robust and cheaper technology for bulk power conversion and the reduced filter requirement after active filtering may help reduce the size and weight of the large filters that are normally required for LCCs. Most importantly the VSC converter should provide a strong voltage source and prevent commutation failure in the LCC converter. Further work is needed to test voltage controller with such a system and see if it can also eliminate harmonics.

This thesis has primarily focused on the voltage control for a single VSC-HVDC in-feed in the offshore network. In an offshore network system where there are at least two HVDC terminals in-feeds, further work is also needed to consider a failure of the master HVDC station responsible for AC voltage control. Another HVDC station will then have to switch from slave power control mode to master voltage control mode without any phase jumps to maintain the voltage control in the network.

The voltage controller has also been considered for practical experimentation. The delay in the output of the PWM was found to affect the control performance,

and made the regulation more oscillatory. Ideally the delay must be eliminated in order to continue the practical experiments for further work. A change in experimental set-up is also recommended, where an efficient air-core inductor should be used instead so that the resonance can be replicated to test if the voltage controller is able to suppress it.

References

[1] P. Tavner, *Offshore Wind Turbines: Reliability, Availability and Maintenance*. IET Renewable Energy Series 13, The Institute of Engineering and Technology, 2012.

[2] J. Arrillaga, *High Voltage Direct Current Transmission*. IEE power and energy series 29, London: IEE, 2nd edition ed., 1998.

[3] OffshoreWIND.biz, "TenneT working to power up BorWin1." www.offshorewind.biz/2014/06/26/tennet-working-to-power-up-borwin-1/, June 2014. Accessed: 10/04/2015.

[4] 4C Offshore Ltd, "BorWin1 converter." www.4coffshore.com/windfarms/hvdc-converter-borwin-alpha-(nor-6-1-in-o-nep)-cid1.html. Accessed: 25/03/2015.

[5] T. C. Y. Ho and L. Ran, "A study on the electrical system arrangement for offshore wind turbines and factors influencing the voltage level choice," in *3rd IEEE International Symposium on Power Electronics for Distributed Generation Systems (PEDG) 2012 (PEDG'12)*, (Aalborg, Denmark), pp. 442–449, June 2012.

[6] T. C. Y. Ho, L. Ran, A. García-Cerrada, J. L. Zamora-Macho, and P. Brogan, "Voltage source converter AC voltage controller design and dynamic response for a large offshore wind farm network," in *2nd International Conference on Renewable Energy Research and Applications (ICRERA)*, (Madrid, Spain), pp. 1–6, Oct. 2013.

[7] Department of Energy & Climate Change, "UK renewable energy roadmap." www.decc.gov.uk, July 2011. Last accessed: 3/05/2015.

[8] RenewableUK, "Offshore wind project timelines May 2013." Development Rounds, Offshore Wind, www.renewableuk.com, May 2013. PDF, Last accessed: 24/01/15.

[9] T. Ackermann, *Wind Power in Power Systems*. John Wiley & Sons Ltd, 2005.

[10] The Crown Estate, "Popular maps." Offshore wind energy, Energy & Infrastructure, www.thecrownestate.co.uk. Last accessed: 23/04/2015.

[11] RenewableUK, "Wind energy in the UK: State of the industry report 2014." Reports, Publications, www.renewableuk.com, Oct. 2014. PDF, Last accessed: 18/04/15.

[12] R. Sullivan, J. Cothren, S. Winters, C. Cooper, and D. Ball, "An assessment of offshore wind turbine visibility in the united kingdom," in *Oceans 2012*, pp. 1–9, Oct. 2012.

[13] T. J. E. Miller, *Reactive Power Control in Electric Systems*. Wiley-Interscience, 1982.

[14] P. Bresesti, W. Kling, R. Hendriks, and R. Vailati, "HVDC connection of offshore wind farms to the transmission system," *IEEE Transactions on Energy Conversion*, vol. 22, pp. 37–43, Mar. 2007.

[15] E. Spahić and G. Balzer, "Impact of the VSC HVDC connection of large offshore wind farms on power system stability and control," in *Power Tech, 2007 IEEE Lausanne*, pp. 207–212, July 2007.

[16] J. Arrillaga, Y. Liu, and N. R. Watson, *Flexible Power Transmission: The HVDC Options*. John Wiley & Sons Ltd, 2007.

[17] J. Z. Zhou and A. M. Gole, "VSC transmission limitations imposed by AC system strength and AC impedance characteristics," in *10th IET International Conference on AC and DC Power Transmission (ACDC 2012)*, (Birmingham), pp. 1–6, Dec. 2012.

[18] L. Zhang, L. Harnefors, and H.-P. Nee, "Interconnection of two very weak AC systems by VSC-HVDC links using power-synchronization control," *IEEE Transactions on Power Systems*, vol. 26, pp. 344–355, Feb. 2011.

[19] P. Kundur, *Power System Stability and Control*. The EPRI Power System Engineering Series, McGraw-Hill, 1994.

[20] N. Mohan, T. M. Undeland, and W. P. Robbins, *Power Electronics: Converters, Applications, and Design*. John Wiley & Sons, 3rd Edition, Nov. 2002.

[21] S. Krohn, P. Morthorst, and S. Awerbuch, "The economics of wind energy," The European Wind Energy Association, EWEA, Mar. 2009.

[22] D. Xiang, L. Ran, J. Bumby, P. Tavner, and S. Yang, "Coordinated control of an HVDC link and doubly fed induction generators in a large offshore wind farm," *IEEE Transactions on Power Delivery*, vol. 21, pp. 463–471, Jan. 2006.

[23] N. Flourentzou, V. Agelidis, and G. Demetriades, "VSC-based HVDC power transmission systems: An overview," *IEEE Transactions on Power Electronics*, vol. 24, no. 3, pp. 592–602, 2009.

[24] M. Islam, Y. Guo, and J. G. Zhu, "Performance and cost comparison of npc, fc and schb multilevel converter topologies for high-voltage applications," in *International Conference on Electrical Machines and Systems (ICEMS) 2011*, pp. 1–6, Aug. 2011.

[25] F. Auerbach, J. Bauer, M. Glantschnig, J. Gottert, M. Hierholzer, A. Porst, D. Reznik, H.-J. Schulze, T. Schutze, and R. Spanke, "6.5 kv IGBT-modules," in *34th IAS Annual Meeting. Conference Record of the 1999 IEEE Industry Applications Conference*, vol. 3, pp. 1770–1774, 1999.

[26] P. Palmer and A. Githiari, "The series connection of IGBTs with active voltage sharing," *IEEE Transactions on Power Electronics*, vol. 12, pp. 637–644, Jul. 1997.

[27] B. W. Williams, *Power Electronics: Devices, Drivers, Applications, and Passive Components*. Mcgraw-Hill, 1992.

[28] F. Schettler, H. Huang, and N. Christl, "HVDC transmission systems using voltage sourced converters design and applications," in *IEEE Power Engineering Society Summer Meeting*, vol. 2, pp. 715–720, July 2000.

[29] M. Otsuki, H. Kanemaru, Y. Ikeda, K. Ueno, M. Kirisawa, Y. Onozawa, and Y. Seki, "Advanced thin wafer IGBTs with new thermal management solution," in *2003 IEEE 15th International Symposium on Power Semiconductor Devices and ICs Proceedings (ISPSD '03)*, pp. 144–147, April 2003.

[30] S. Jahdi, O. Alatise, and P. Mawby, "On the performance of voltage source converters based on silicon carbide technology," in *Proceedings of 2013 35th International Telecommunications Energy Conference 'Smart Power and Efficiency' (INTELEC)*, (Hamburg, Germany), pp. 1–6, Oct. 2013.

[31] S. Jahdi, O. Alatise, P. Alexakis, L. Ran, and P. Mawby, "The impact of temperature and switching rate on the dynamic characteristics of silicon carbide schottky barrier diodes and MOSFETs," *IEEE Transactions on Industrial Electronics*, vol. 62, pp. 163–171, Jan. 2015.

[32] H. Zhang and L. Tolbert, "Efficiency impact of silicon carbide power electronics for modern wind turbine full scale frequency converter," *IEEE Transactions on Industrial Electronics*, vol. 58, pp. 21–28, Jan. 2011.

[33] M. S. Chinthavali, "Silicon carbide GTO thyristor loss model for HVDC application," Master's thesis, University of Tennessee, Knoxville, Dec. 2003.

[34] G. Bower, P. Rogan, J. Kozlowski, and M. Zugger, "SiC power electronics packaging prognostics," in *IEEE Aerospace Conference*, pp. 1–12, Mar. 2008.

[35] W. Brokaw, J. Elmes, B. Grummel, Z. Shen, and T. Wu, "Silicon carbide high-temperature packaging module fabrication," in *2013 IEEE Workshop on Wide Bandgap Power Devices and Applications (WiPDA)*, pp. 178–181, Oct. 2013.

[36] J. Lutz, "Packaging and reliability of power modules," in *8th International Conference on Integrated Power Systems (CIPS 2014)*, (Nuremberg, Germany), pp. 1–8, Feb. 2014.

[37] P. Alexakis, O. Alatise, L. Ran, and P. Mawby, "Modeling power converters using hard switched silicon carbide MOSFETs and Schottky barrier diodes," in *15th European Conference on Power Electronics and Applications (EPE 2013)*, pp. 1–9, Sept. 2013.

[38] K. Hatua, S. Dutta, A. Tripathi, S. Baek, G. Karimi, and S. Bhattacharya, "Transformer less intelligent power substation design with 15kV SiC IGBT for grid interconnection," in *2011 IEEE Energy Conversion Congress and Exposition (ECCE)*, pp. 4225–4232, Sept. 2011.

[39] Y. Lee, S. Cui, S. Kim, and S.-K. Sul, "Control of hybrid HVDC transmission system with LCC and FB-MMC," in *IEEE Energy Conversion Congress and Exposition (ECCE)*, pp. 475–482, Sept 2014.

[40] F. Fein and B. Orlik, "Dual HVDC system with line- and self-commutated converters for grid connection of offshore wind farms," in *International Conference on Renewable Energy Research and Applications (ICRERA)*, pp. 280–285, Oct 2013.

[41] C. Guo, Y. Zhang, A. Gole, and C. Zhao, "Analysis of dual-infeed HVDC with LCC-HVDC and VSC-HVDC," *IEEE Transactions on Power Delivery*, vol. 27, pp. 1529–1537, July 2012.

[42] C. Guo, C. Zhao, and X. Chen, "Analysis of dual-infeed HVDC with LCC inverter and VSC rectifier," in *IEEE PES General Meeting, Conference Exposition*, pp. 1–4, July 2014.

[43] G. O. Kalcon, G. P. Adam, O. Anaya-Lara, S. Lo, and K. Uhlen, "Small-signal stability analysis of multi-terminal VSC-based DC transmission systems," *IEEE Transactions on Power Systems*, vol. 27, pp. 1818–1830, Nov. 2012.

[44] C. Franck, "HVDC circuit breakers: A review identifying future research needs," *IEEE Transactions on Power Delivery*, vol. 26, pp. 998–1007, April 2011.

[45] A. Sannino, G. Postiglione, and M. Bollen, "Feasibility of a DC network for commercial facilities," *IEEE Transactions on Industry Applications*, vol. 39, pp. 1499–1507, Sept. - Oct. 2003.

[46] D. Jovcic, D. van Hertem, K. Linden, J.-P. Taisne, and W. Grieshaber, "Feasibility of DC transmission networks," in *2nd IEEE PES International Conference and Exhibition on Innovative Smart Grid Technologies (ISGT Europe)*, pp. 1–8, Dec. 2011.

[47] Ieda and Nawata, "DC treeing breakdown associated with space charge formation in polyethylene," *IEEE Transactions on Electrical Insulation*, vol. EI-12, pp. 19–25, Feb 1977.

[48] T. Ve, F. Mauseth, and E. Ildstad, "Effect of water content on the conductivity of XLPE insulation," in *Annual Report Conference on Electrical Insulation and Dielectric Phenomena (CEIDP 2012)*, pp. 649–653, Oct. 2012.

[49] A. Bulinski and R. Densley, "The voltage breakdown characteristics of miniature XLPE cables containing water trees," *IEEE Transactions on Electrical Insulation*, vol. EI-16, pp. 319–326, Aug. 1981.

[50] O. E. Gouda and A. A. Farag, "Factors affecting the sheath losses in singlecore underground power cables with two-points bonding method," *International Journal of Electrical and Computer Engineering (IJECE)*, vol. 2, pp. 7–16, Feb. 2012.

[51] ABB, "XLPE submarine cable systems." Online PDF Brochure from ABB.com, April 2010. Filename: XLPE Submarine Cable Systems 2GM5007 rev 5.pdf.

[52] A. Betz, *Introduction to the Theory of Flow Machines*. Oxford: Pergamon Press, 1966.

[53] E. Muljadi and C. Butterfield, "Pitch-controlled variable-speed wind turbine generation," *IEEE Transactions on Industry Applications*, vol. 37, pp. 240–246, Jan. 2001.

[54] H. Polinder, "Overview of and trends in wind turbine generator systems," in *IEEE Power and Energy Society General Meeting*, pp. 1–8, July 2011.

[55] F. Spinato, P. Tavner, G. van Bussel, and E. Koutoulakos, "Reliability of wind turbine subassemblies," *IET Renewable Power Generation*, vol. 3, pp. 387–401, Dec. 2009.

[56] A. D. Hansen and L. H. Hansen, "Wind turbine concept market penetration over 10 years (1995–2004)," *Wind Energy*, vol. 10, no. 1, pp. 81–97, 2007.

[57] M. Khadraoui and M. Elleuch, "Comparison between OptiSlip and fixed speed wind energy conversion systems," in *5th International Multi-Conference on Systems, Signals and Devices (IEEE SSD 2008)*, pp. 1–6, July 2008.

[58] D. Burnham, S. Santoso, and E. Muljadi, "Variable rotor-resistance control of wind turbine generators," in *IEEE Power Energy Society General Meeting (PES 2009)*, pp. 1–6, July 2009.

[59] H. Li and Z. Chen, "Overview of different wind generator systems and their comparisons," in *IET Renewable Power Generation* [56], pp. 123–138.

[60] C. Mi, M. Filippa, J. Shen, and N. Natarajan, "Modeling and control of a variable-speed constant-frequency synchronous generator with brushless exciter," *IEEE Transactions on Industry Applications*, vol. 40, pp. 565–573, Mar. 2004.

[61] E. Abdi, M. Tatlow, R. McMahon, and P. Tavner, "Design and performance analysis of a 6 MW medium-speed brushless DFIG," in *2nd IET Renewable Power Generation Conference (RPG 2013)*, pp. 1–4, Sept. 2013.

[62] Y. Xia, J. Fletcher, S. Finney, K. Ahmed, and B. Williams, "Torque ripple analysis and reduction for wind energy conversion systems using uncontrolled

rectifier and boost converter," *IET Renewable Power Generation*, vol. 5, pp. 377–386, September 2011.

[63] European Wind Energy Association, "Powering europe: wind energy and the electricity grid." report booklet, November 2010.

[64] A. D. Hansen and L. H. Hansen, "Market penetration of wind turbine concepts over the years," in *European Wind Energy Conference EWEC*, (Milan), 2007.

[65] J. Coelingh, A. van Wijk, and A. Holtslag, "Analysis of wind speed observations over the north sea," *Journal of Wind Engineering and Industrial Aerodynamics*, vol. 61, no. 1, pp. 51–69, 1996.

[66] F. Castro Sayas and R. Allan, "Generation availability assessment of wind farms," *IEE Proceedings - Generation, Transmission and Distribution*, vol. 143, pp. 507–518, Sep. 1996.

[67] N. Jenkins, "Engineering wind farms," *Power Engineering Journal*, vol. 7, pp. 53–60, April 1993.

[68] N. Kirby, L. Xu, M. Luckett, and W. Siepmann, "HVDC transmission for large offshore wind farms," *Power Engineering Journal*, vol. 16, pp. 135–141, June 2002.

[69] M. Wilkinson, B. Hendriks, F. Spinato, E. Gomez, H. Bulacio, J. Roca, P. Tavner, Y. Feng, and H. Long, "Methodology and results of the reliawind reliability field study," in *Scientific Track, European Wind Energy Conference EWEC*, (Warsaw), 2010.

[70] C. J. Crabtree, "Operational and reliability analysis of offshore wind farms," in *EWEA 2012 Scientific Track*, (Copenhagen, Denmark), Apr. 2012.

[71] Ø. Rui, C. Öhlén, J. Solvik, J. Thon, K. Karijord, and T. Gjengedal, "Design, operation and availability analysis of a multi-terminal hvdc grid - a case study of a possible offshore grid in the norwegian sea," in *IEEE Trondheim PowerTech 2011*, pp. 1–7, June 2011.

[72] H. Arabian-Hoseynabadi, H. Oraee, and P. Tavner, "Failure modes and effects analysis (FMEA) for wind turbines," *International Journal of Electrical Power & Energy Systems*, vol. 32, no. 7, pp. 817–824, 2010.

[73] S. Faulstich, B. Hahn, and P. J. Tavner, "Wind turbine downtime and its importance for offshore deployment," *Wind Energy*, vol. 14, no. 3, pp. 327–337, 2011.

[74] S. Faulstich, P. Lyding, and P. J. Tavner, "Effects of wind speed on wind turbine availability," in *EWEA 2011 Scientific Proceedings*, (Brussels, Belgium), pp. 85–88, March 2011.

[75] A. Sannino, H. Breder, and E. Nielsen, "Reliability of collection grids for large offshore wind parks," in *International Conference on Probabilistic Methods Applied to Power Systems PMAPS 2006.*, pp. 1–6, June 2006.

[76] "Operations report 2009 - noordzeewind," pp. 1–32, Internet: www.noordzeewind.nl, Nov. 2010.

[77] Y. Qiu, Y. Feng, P. Tavner, P. Richardson, G. Erdos, and B. Chen, "Wind turbine SCADA alarm analysis for improving reliability," *Wind Energy*, pp. 1–16, 2011.

[78] J. Ribrant and L. Bertling, "Survey of failures in wind power systems with focus on swedish wind power plants during 1997–2005," *IEEE Transactions on Energy Conversion*, vol. 22, pp. 167–173, Mar. 2007.

[79] W. Qiao, X. Yang, and X. Gong, "Wind speed and rotor position sensorless control for direct-drive pmg wind turbines," *IEEE Transactions on Industry Applications*, vol. 48, pp. 3–11, Jan. - Feb. 2012.

[80] ABB, "One of the most remote offshore wind farm clusters in the world is connected to the German grid by a 400 MW ±150 kV HVDC Light transmission system from ABB." http://new.abb.com/systems/hvdc/references/borwin1. Last accessed: 25/03/2015.

[81] Renews, "'Dirty electricity' probe at BorWin1." http://renews.biz/68145/, June 2014. Last accessed: 25/03/2015.

[82] A. Beddard and M. Barnes, "Availability analysis of VSC-HVDC schemes for offshore windfarms," in *6th IET International Conference on Power Electronics, Machines and Drives (PEMD 2012)*, pp. 1–6, Mar. 2012.

[83] V. Sankaran, C. Chen, C. Avant, and X. Xu, "Power cycling reliability of IGBT power modules," in *IAS '97, Conference Record of the 1997 IEEE Industry Applications Conference, 32nd IAS Annual Meeting*, vol. 2, pp. 1222–1227, Oct. 1997.

[84] X. Liu, T. Zhang, Y. Bai, X. Ding, and Y. Wang, "Effects of accelerated repetitive impulse voltage aging on performance of model stator insulation of wind turbine generator," *IEEE Transactions on Dielectrics and Electrical Insulation*, vol. 21, pp. 1506–1515, Aug. 2014.

[85] D. J. Bang, H. Polinder, J. Ferreira, and R. Van Rooij, "New active speed stall control compared to pitch control for a direct-drive wind turbine," in *EWEC 2007 Conference Proceedings*, (Milan, Spain), May 2007.

[86] G. Lalor, A. Mullane, and M. O'Malley, "Frequency control and wind turbine technologies," *IEEE Transactions on Power Systems*, vol. 20, pp. 1905–1913, Nov. 2005.

[87] R. Goic, D. Jakus, and J. Krstulovic, "Wind power plant as ancillary service provider," in *8th International Conference on the European Energy Market (EEM)*, pp. 562–567, May 2011.

[88] P. van den Bosch, A. Jokic, R. Hermans, J. Frunt, W. Kling, F. Nobel, P. Boonekamp, and W. de Boer, "Reduced risks and improved economic operation of ancillary services," in *7th International Conference on the European Energy Market (EEM)*, pp. 1–6, June 2010.

[89] D. Xiang, L. Ran, P. Tavner, and S. Yang, "Control of a doubly fed induction generator in a wind turbine during grid fault ride-through," *IEEE Transactions on Energy Conversion*, vol. 21, pp. 652–662, Sept. 2006.

[90] E. Muljadi, M. Singh, and V. Gevorgian, "Fixed-speed and variable-slip wind turbines providing spinning reserves to the grid," in *IEEE Power and Energy Society General Meeting (PES)*, pp. 1–5, July 2013.

[91] E. Ela, B. Kirby, N. Navid, and J. Smith, "Effective ancillary services market designs on high wind power penetration systems," in *IEEE Power and Energy Society General Meeting*, pp. 1–8, July 2012.

[92] J. Morales, A. Conejo, K. Liu, and J. Zhong, "Pricing electricity in pools with wind producers," *IEEE Transactions on Power Systems*, vol. 27, pp. 1366–1376, Aug. 2012.

[93] E. Naswali, C. Alexander, H.-Y. Han, D. Naviaux, A. Bistrika, A. von Jouanne, A. Yokochi, and T. Brekken, "Supercapacitor energy storage for wind energy integration," in *2011 IEEE Energy Conversion Congress and Exposition (ECCE)*, pp. 298–305, Sept. 2011.

[94] B. Grainger, G. Reed, A. Sparacino, and P. Lewis, "Power electronics for grid-scale energy storage," *Proceedings of the IEEE*, vol. 102, pp. 1000–1013, June 2014.

[95] J. Zhu, C. D. Booth, G. P. Adam, A. J. Roscoe, and C. G. Bright, "Inertia emulation control strategy for vsc-hvdc transmission systems," *IEEE Transactions on Power Systems*, vol. PP, no. 99, 2012.

[96] U. Dayaratne, S. Tennakoon, N. Shammas, and J. Knight, "Investigation of variable DC link voltage operation of a PMSG based wind turbine with fully rated converters at steady state," in *Proceedings of the 2011-14th European Conference on Power Electronics and Applications (EPE 2011)*, pp. 1–10, Aug. 2011.

[97] B. Kazemtabrizi and S. Hogg, "A new simulation and control model for a variable speed variable pitch direct drive large offshore wind turbine generator with integrated energy storage," in *ASME Turbo Expo 2014: Turbine Technical Conference and Exposition*, vol. 3B, (Dusseldorf, Germany), pp. 1–10, June 2014.

[98] A. Stock and W. Leithead, "Providing grid frequency support using variable speed wind trubines with augmented control," in *Proceedings of European Wind Energy Association (EWEA) Conference*, (Copenhagen, Denmark), pp. 1–8, 2012.

[99] C. Baone and C. DeMarco, "Distributed control design to regulate grid frequency and reduce drivetrain stress in wind systems using battery storage," in *2012 American Control Conference (ACC)*, pp. 1368–1375, June 2012.

[100] L. Ran, J. Bumby, and P. Tavner, "Use of turbine inertia for power smoothing of wind turbines with a dfig," in *11th International Conference on Harmonics and Quality of Power 2004*, pp. 106–111, Sept. 2004.

[101] T. Haileselassie, R. Torres-Olguin, T. Vrana, K. Uhlen, and T. Undeland, "Main grid frequency support strategy for VSC-HVDC connected wind farms with variable speed wind turbines," in *PowerTech, 2011 IEEE Trondheim*, pp. 1–6, June 2011.

[102] M. Popat, B. Wu, and N. Zargari, "A novel decoupled interconnecting method for current source converter based offshore wind farms," in *Electric Machines Drives Conference (IEMDC), 2011 IEEE International*, pp. 711 –716, may 2011.

[103] G. Quinonez-Varela, G. Ault, O. Anaya-Lara, and J. McDonald, "Electrical collector system options for large offshore wind farms," *IET Renewable Power Generation*, vol. 1, pp. 107–114, June 2007.

[104] B. Falahati, A. Kargarian, and Y. Fu, "Impacts of information and communication failures on optimal power system operation," in *2013 IEEE PES Innovative Smart Grid Technologies (ISGT)*, pp. 1–6, Feb. 2013.

[105] P. B. Wyllie, *Electrothermal Modelling for Doubly Fed Induction Generator Converter Reliability in Wind Power*. PhD thesis, Durham University, 2014.

[106] Siemens, "Wind turbine swt-7.0-154 - techical specifications." http://www.energy.siemens.com/hq/en/renewable-energy/wind-power/. Accessed: 16/01/2015.

[107] T. Lebey, P. Castelan, G. Montanari, and I. Ghinello, "Influence of PWM-type voltage waveforms on reliability of machine insulation system," in *8th International Conference On Harmonics and Quality of Power Proceedings*, vol. 2, pp. 994–998 vol.2, Oct 1998.

[108] L. Tolbert and F. Peng, "Multilevel converters as a utility interface for renewable energy systems," in *2000 IEEE Power Engineering Society Summer Meeting*, vol. 2, pp. 1271–1274, 2000.

[109] C. Ng, M. Parker, L. Ran, P. Tavner, J. Bumby, and E. Spooner, "A multilevel modular converter for a large, light weight wind turbine generator," *IEEE Transactions on Power Electronics*, vol. 23, pp. 1062–1074, May 2008.

[110] ABB, "Techical application papers no. 13 - wind power plants." Online: www.abb.com, filename: 1SDC007112G0201.pdf, 2011. Last accessed: 18/04/15.

[111] M. Islam, Y. Guo, and J. Zhu, "A transformer-less compact and light wind turbine generating system for offshore wind farms," in *IEEE International Conference on Power and Energy (PECon)*, pp. 605–610, Dec. 2012.

[112] J. Das and R. Osman, "Grounding of AC and DC low-voltage and medium-voltage drive systems," *IEEE Transactions on Industry Applications*, vol. 34, pp. 205–216, Jan 1998.

[113] Hammond Power Solutions Inc., "Zero sequence harmonics." www.hammondpowersolutions.com/files/HPS_article_Zero_Sequence_Harmonics.pdf. Last accessed: 03/06/2015.

[114] K. Ahmed, S. Finney, and B. Williams, "Passive filter design for three-phase inverter interfacing in distributed generation," in *Compatibility in Power Electronics, CPE '07*, pp. 1–9, June 2007.

[115] C. Feltes, R. van de Sandt, F. Koch, F. Shewarega, and I. Erlich, "Neutral grounding in wind farm medium voltage collector grids," in *IEEE/PES Power Systems Conference and Exposition (PSCE)*, (Phoenix, AZ), pp. 1–7, March 2011.

[116] A. Madariaga, J. Martn, I. Zamora, I. M. de Alegra, and S. Ceballos, "Technological trends in electric topologies for offshore wind power plants," *Renewable and Sustainable Energy Reviews*, vol. 24, no. 0, pp. 32 – 44, 2013.

[117] D. Nilsson and A. Sannino, "Efficiency analysis of low- and medium- voltage dc distribution systems," in *Power Engineering Society General Meeting, 2004. IEEE*, vol. 2, (Denver), pp. 2315–2321, June 2004.

[118] P. Monjean, J. Delanoe, J. Auguste, C. Saudemont, J. Sprooten, A. Mirzaian, and B. Robyns, "Topologies comparison of multi-cell medium frequency transformer for offshore farms," in *9th IET International Conference on AC and DC Power Transmission, 2010. ACDC*, pp. 1–5, Oct. 2010.

[119] M. Barnes and A. Beddard, "Voltage source converter HVDC links the state of the art and issues going forward," *Energy Procedia Journal*, vol. 24, pp. 108–122, Jan. 2012.

[120] D. W. Elliott, C. E. Jones, and S. J. Finney, "Offshore wind farm cluster based DC collection network - operation and design considerations," in *10th IET International Conference on AC and DC Power Transmission, ACDC 2012*, (Birmingham), pp. 1–6, Dec. 2012.

[121] D. Jovcic, "Offshore wind farm with a series multiterminal CSI HVDC," *Electric Power Systems Research*, vol. 78, no. 4, pp. 747–755, 2008.

[122] E. Veilleux and P. Lehn, "Interconnection of direct-drive wind turbines using a series-connected DC grid," *IEEE Transactions on Sustainable Energy*, vol. 5, pp. 139–147, Jan. 2014.

[123] L. Trilla, O. Gomis-Bellmunt, A. Junyent-Ferré, A. Álvarez, and A. Sudrià-Andreu, "Control of a squirrel cage induction generator wind farm connected to a single power converter," in *45th International Universities Power Engineering Conference (UPEC) 2010*, pp. 1–6, 31st Aug - 3rd Sept 2010.

[124] D. Jovcic, "Interconnecting offshore wind farms using multiterminal VSC-based HVDC," in *2006 IEEE Power Engineering Society General Meeting*, pp. 1–7, 2006.

[125] D. Elliott, S. Finney, and C. Booth, "Single converter interface for a cluster of offshore wind turbines," in *IET Conference on Renewable Power Generation (RPG 2011)*, (Edinburgh), pp. 1–6, Sept 2011.

[126] D. Jovcic and N. Strachan, "Offshore wind farm with centralised power conversion and dc interconnection," *IET Generation, Transmission & Distribution*, vol. 3, pp. 586–595, June 2009.

[127] L. Trilla, O. Gomis-Bellmunt, A. Sudria-Andreu, J. Liang, and T. Jing, "Control of SCIG wind farm using a single VSC," in *Proceedings of the 2011-14th European Conference on Power Electronics and Applications (EPE 2011)*, pp. 1–9, Aug-Sept 2011.

[128] V. Gevorgian, M. Singh, and E. Muljadi, "Variable frequency operation of a HVDC-VSC interconnected type 1 offshore wind power plant," in *2012 IEEE Power and Energy Society General Meeting*, (San Diego, CA), pp. 1–8, July 2012.

[129] M. Parker and O. Anaya-Lara, "Cost and losses associated with offshore wind farm collection networks which centralise the turbine power electronic converters," *IET Renewable Power Generation*, vol. 7, pp. 390–400, July 2013.

[130] S. Wright, A. Rogers, J. Manwell, and A. Ellis, "Transmission options for offshore wind farms in the United States," in *Proceedings of the AWEA annual conference*, (Renewable Energy Research Lab, University of Massachusetts, Department of Mechanical and Industrial Engineering, Amherst, MA 01003 USA), pp. 1–12, 2002.

[131] H. Ahmad, S. Coppens, and B. Uzunoglu, "Connection of an offshore wind park to HVDC converter platform without using offshore AC collector platforms," in *2013 IEEE Green Technologies Conference*, pp. 400–406, April 2013.

[132] R. Billinton and R. N. Allan, *Reliability evaluation of power systems*. Pitman Books, 1984.

[133] T. Zhang and A. Zain, "Modular converter system reliability & performance analysis in design," in *2nd IEEE International Symposium on Power Electronics for Distributed Generation Systems (PEDG 2010)*, (Hefei, China), pp. 252–258, June 2010.

[134] J. Birk and B. Andresen, "Parallel-connected converters for optimizing efficiency, reliability and grid harmonics in a wind turbine," in *European Conference on Power Electronics and Applications*, pp. 1–7, Sept 2007.

[135] R. Billinton and R. N. Allan, *Reliability Evaluation of Engineering Systems: Concepts and Techniques*. Springer, 2nd ed., 1992.

[136] P. Vas, *Vector Control of AC Machines*. Oxford Science Publications, 1990.

[137] A. Yazdani and R. Iravani, *Voltage-Sourced Converters in Power Systems: Modeling, Control, and Applications*. Wiley-IEEE Press, 2010.

[138] P. C. Krause, *Analysis of electric machinery*. McGraw-Hill, 1986.

[139] MathWorks, "Matlab r2014a documentation," 2014.

[140] E. Muljadi, V. Gevorgian, M. Singh, and S. Santoso, "Understanding inertial and frequency response of wind power plants," in *IEEE Power Electronics and Machines in Wind Applications (PEMWA)*, (Denver, CO), pp. 1–8, July 2012.

[141] T. Haileselassie and K. Uhlen, "Primary frequency control of remote grids connected by multi-terminal hvdc," in *2010 IEEE Power and Energy Society General Meeting*, pp. 1–6, July 2010.

[142] M. Seyedi and M. Bollen, "The utilization of synthetic inertia from wind farms and its impact on existing speed governors and system performance," in *Part 2 Report of Vindforsk Project V-369, Elforsk rapport 13:02*, Jan. 2013.

[143] F. Hassan and R. Critchley, "A robust PLL for grid interactive voltage source converters," in *14th International Power Electronics and Motion Control Conference (EPE/PEMC 2010)*, pp. T2–29 – T2–35, Sept. 2010.

[144] S. Gao and M. Barnes, "Phase-locked loop for ac systems: Analyses and comparisons," in *6th IET International Conference on Power Electronics, Machines and Drives (PEMD 2012)*, pp. 1–6, Mar. 2012.

[145] H. Liu and J. Sun, "Voltage stability and control of offshore wind farms with AC collection and HVDC transmission," *IEEE Journal of Emerging and Selected Topics in Power Electronics*, vol. 2, pp. 1181–1189, Dec. 2014.

[146] T. Midtsund, J. Suul, and T. Undeland, "Evaluation of current controller performance and stability for voltage source converters connected to a weak grid," in *2nd IEEE International Symposium on Power Electronics for Distributed Generation Systems (PEDG)*, pp. 382–388, June 2010.

[147] T. Haileselassie, K. Uhlen, J. Tande, and O. Anaya-Lara, "Connection scheme for north sea offshore wind integration to UK and norway: Power balancing and transient stability analysis," in *2011 IEEE Trondheim PowerTech*, pp. 1–5, June 2011.

[148] P. Alberto and A. Sala, *Multivariable Control Systems: An Engineering Approach*. Springer, 2004.

[149] J. Kautsky, N. K. Nichols, and P. Van Dooren, "Robust pole assignment in linear state feedback," *International Journal of Control*, vol. 41, no. 5, pp. 1129–1155, 1985.

[150] R. Roncero-Sánchez, V. Feliu-Batlle, and A. García-Cerrada, "Active- and reactive-power control for a wind generator connected to the grid using a predictive-integral control and a pi control schemes," in *2005 European Conference on Power Electronics and Applications*, (Dresden), pp. 1–10, Sep. 2005.

[151] G. F. Franklin, J. D. Powell, and A. Emami-Naeini, *Feedback Control of Dynamic Systems*. Prentice Hall, 6th ed., 2009.

[152] H. L. Wade, *Basic and Advanced Regulatory Control: System Design and Application*. The instrumentation, Systems, and Automation Society, 2nd ed., June 2004.

[153] R. Lohde and F. Fuchs, "Analysis of high and low voltage grid failure propagation in large wind farms considering transformers, cables and VAR-compensators," in *PESC 2008, IEEE Power Electronics Specialists Conference*, pp. 1164–1168, June 2008.

[154] L. Ran, D. Xiang, and J. Kirtley, "Analysis of electromechanical interactions in a flywheel system with a doubly fed induction machine," *IEEE Transactions on Industry Applications*, vol. 47, pp. 1498–1506, May 2011.

[155] V. Blasko and V. Kaura, "A novel control to actively damp resonance in input LC filter of a three-phase voltage source converter," *IEEE Transactions on Industry Applications*, vol. 33, pp. 542–550, Mar. 1997.

[156] M. Liserre, F. Blaabjerg, and S. Hansen, "Design and control of an LCL-filter-based three-phase active rectifier," *IEEE Transactions on Industry Applications*, vol. 41, pp. 1281–1291, Sept-Oct. 2005.

[157] X. Yuan, F. Wang, D. Boroyevich, Y. Li, and R. Burgos, "DC-link voltage control of a full power converter for wind generator operating in weak-grid systems," *IEEE Transactions on Power Electronics*, vol. 24, pp. 2178–2192, Sept. 2009.

[158] E. N. Power, "Capacitors age and capacitors have an end of life." A White Paper from the Experts in Business-Critical Continuity, 2008. sl-24630.pdf.

[159] E. N. Abildgaard, "Exploring the properties of a modular multilevel converter based hvdc link: With focus on voltage capability, power system relations, and control system," Master's thesis, Norwegian University of Science and Technology, Faculty of Information Technology, Mathematics and Electrical Engineering, Department of Electrical Power Engineering, 2012.

[160] C. Ng, L. Ran, and J. Bumby, "Unbalanced-grid-fault ride-through control for a wind turbine inverter," *IEEE Transactions on Industry Applications*, vol. 44, pp. 845–856, May-June 2008.

[161] A. Milicua, G. Abad, and M. Rodriguez Vidal, "Online reference limitation method of shunt-connected converters to the grid to avoid exceeding voltage and current limits under unbalanced operation – Part I: Theory," *IEEE Transactions on Energy Conversion*, vol. PP, no. 99, pp. 1–12, 2015.

[162] A. Milicua, G. Abad, and M. Rodriguez Vidal, "Online reference limitation method of shunt-connected converters to the grid to avoid exceeding voltage and current limits under unbalanced operation – Part II: Validation," *IEEE Transactions on Energy Conversion*, vol. PP, no. 99, pp. 1–10, 2015.

Appendix A

PSCAD/EMTDC®

Power System Computer Aided Design (PSCAD) is the software graphical interface for power system modelling and time-domain simulation. EMTDC (which stands for Electromagnetic Transients including DC) is the electro-magnetic transients simulation engine behind it.

A.1 FORTRAN script for *dq*0 transformation

Equation A.1.1 is the transformation equation used in the built-in $dq0$ transformation block in PSCAD®. The direction of the q-axis is reversed because the q row (second row) of the matrix is positive. This is a different from the convention used in equation (4.3) on page 89.

$$\begin{bmatrix} f_d(t) \\ f_q(t) \\ f_0(t) \end{bmatrix} = \frac{2}{3} \begin{bmatrix} \cos[\theta(t)] & \cos[\theta(t) - \frac{2\pi}{3}] & \cos[\theta(t) + \frac{2\pi}{3}] \\ \sin[\theta(t)] & \sin[\theta(t) - \frac{2\pi}{3}] & \sin[\theta(t) + \frac{2\pi}{3}] \\ \frac{1}{2} & \frac{1}{2} & \frac{1}{2} \end{bmatrix} \begin{bmatrix} f_a(t) \\ f_b(t) \\ f_c(t) \end{bmatrix} \tag{A.1.1}$$

A new custom PSCAD® module block for the dq transformation was created with the desired convention. This was implemented in FORTRAN as shown in Code A.1, note the minus in the q row. Both forward and inverse transformations have been implemented into a single module. The direction of the transformation is selected using the `dir` variable.

Code A.1: FORTRAN script for *abc* to *dq*0 transformation and the inverse

```
!abc to dq0 transformation
#IF dir == 0
 $d= $K1*($abc(1)*COS($th)+$abc(2)*COS($th-PI2_BY3)+$abc(3)*COS($th+PI2_BY3))/$base
 $q=-$K1*($abc(1)*SIN($th)+$abc(2)*SIN($th-PI2_BY3)+$abc(3)*SIN($th+PI2_BY3))/$base
 $z= $K1*$K2 * ( $abc(1) + $abc(2) + $abc(3) ) / $base
!inverse transformation dq0 to abc
#ELSE
 $abc(1) = $base * $K1 * ( $d*COS($th) - $q*SIN($th) + $z*$K2)
 $abc(2) = $base * $K1 * ( $d*COS($th-PI2_BY3) - $q*SIN($th-PI2_BY3) + $z*$K2)
 $abc(3) = $base * $K1 * ( $d*COS($th+PI2_BY3) - $q*SIN($th+PI2_BY3) + $z*$K2)
#ENDIF
```

The control parameter were originally designed in the per unit system. The base value is included in the equation for as built-in conversion between actual and per unit values.

The transfomation type (power invariant, peak resultant, RMS resultant) is selected using the variable `coeff` as shown in Code A.2. It determines which `K1` and `K2` constants to be use.

Code A.2: Initialisation FORTRAN script for the selection of coefficients for the *dq*0 transformation and its inverse

```
!abc to dq0 transformation
#IF dir == 0
!Power invariant
 #IF coeff == 0
    REAL K1=SQRT(2.0/3.0)
    REAL K2=SQRT(2.0)*0.5
!peak resultant
 #ELSEIF coeff == 1
    REAL K1=2.0/3.0
    REAL K2=0.5
!rms resultant
 #ELSE
    REAL K1=SQRT(2.0)/3.0
    REAL K2=SQRT(2.0)*0.5
 #ENDIF
```

```
!inverse transformation dq0 to abc
#ELSE
!Power invariant
 #IF coeff == 0
    REAL K1=SQRT(2.0/3.0)
    REAL K2=SQRT(2.0)*0.5
!peak resultant
 #ELSEIF coeff == 1
    REAL K1=1
    REAL K2=1
!rms resultant
 #ELSE
    REAL K1=SQRT(2.0)
    REAL K2=SQRT(2.0)*0.5
 #ENDIF
#ENDIF
```

A.2 PLL Block in PSCAD

The angle direction in the PLL block in PSCAD® is design for its own $dq0$ transformation (equation A.1.1). The angle is directly synchronised with the voltage of phase A, so the reference for 0° is at the rising zero crossing.

However, with dq transformation equation 4.3 on page 89, the angle should be synchronised with the direction of the space vector of phase A, where the reference for 0° is at the maximum peak of the phase A voltage. Therefore, a 90° offset should be added to the output if the PSCAD's PLL block when using with transformation equation 4.3.

Appendix B

MATLAB

MATLAB/Simulink® version R2011a was used. This was primarily for control gain calculations and small signal analysis.

B.1 Per Unit Base Value Calculations

Code B.1: MATLAB® script for per unit system base value calculations

```
%initial defined base values
Sb=7e5;  %3phase power W
Vb=400/sqrt(3);     % base voltage, phase to neutral V
fb=50;   % base frequency in Hz
%calculated base values
Zb=3*Vb^2/Sb;  % base impedance
Ib=Vb/Zb;  % base current A
wb=fb*2*pi; % base frequency in rad/s
Lb=Zb/wb;   % base inductance H
Cb=1/Zb/wb; % base capacitor F
```

B.2 Control Gains Calculation

The gains calculated in Code B.2 are valid for the RMS resultant dq transformation coefficients. These calculations also assumes ideal conditions. The voltage outer loop control gain calculations assumes that the current inner loop is instantaneous. Matrices and gain outputs for both d and q axes are symmetrical, therefore only one set is needed.

Code B.2: MATLAB® script for gain calculation for the current inner loop, AC voltage outer loop and DC outer loop controller

```
%% inner PI control loop desired dynamics
realPI=-1000;  %starting with the real part of desired CLP
zetaPI=0.7;   %zeta is the desired damping factor

% Current control state-space matrices
matAdq=[-Rfilter/Lfilter 0; 1 0];
matBdq=[1;0];

% AC voltage state-space control matrices
matAvdq=[0 0; 1 0];
matBvdq=[1;0];
%C and D matices not needed for gain calculations.

%% GAIN CALCULATIONS %%
%% VSC inner current control loop
wnPI=abs(realPI/zetaPI);   %wn is the natural frequency response in rad/s
imagPI=wnPI*sqrt(1-zetaPI^2);  %imaginary part of desired CLP
polesPI=[realPI+imagPI*j realPI-imagPI*j];  %desired CLP position
K_PIdq = place(matAdq,matBdq,polesPI) * Lfilter; %gain matrix

%% wnPI/wnVC
zetaVC=0.7;
coefPIVC=5;   %How many times is VC1 slower than PI

%% AC Voltage outer control loop
wnVC=wnPI/coefPIVC;  %This way maintains consistent wn while zeta can vary
realVC=-abs(wnVC*zetaVC);
imagVC=wnVC*sqrt(1-zetaVC^2);
polesVC=[realVC+j*imagVC; realVC-j*imagVC]; %desired CLP position
K_VCdq = place(matAvdq,matBvdq,polesVC) * Cfilter; %gain matrix
```

Where not stated in the comments of the code, `PI` denotes inner current loop controller, `VC` denotes the voltage outer loop controller, and `DC` denotes the DC outer loop controller. `Rfilter` is the resistance parameter in series with the inductor parameter `Lfilter`, and `Cfilter` is the shunt capacitor at the PCC. If per unit parameters are used, then `wbase=50*2*pi`, but if actual values are used, then setting this to 1 basically removes the factor of the base angular frequency in the calculation. For the DC control part, `C_dc` is the capacitance of the DC link in Farads and `Vll` is the line-line voltage in kV.

Variables that begin with `mat` are state space matrices, `real` and `imag` are the real and imaginary parts of the `wn` magnitude or CLP position, `wn` are the natural frequency response ω_n in rad/s, and `zeta` are the damping factors. `K` are the output gain matrix, which is what we are interested in.

Variables with the `K_` prefix are the calculated gain matrices (1×2), where the first value in the matrix is the proportional gain and the second is the integral gain ($[K_p, K_i]$). The variable `coefPIVC` was varied for tuning for an optimum outer loop speed control with small signal analysis.

In the *dq* decoupling equations in Sections 4.3.1 and 4.3.2, the coefficients (L and C) for the output of the controllers (γ and η), are not shown in the controller block diagram in Figure 4.5. Instead, the coefficient are factored in the PI control gains. Therefore the respective output of the `place` command is multiplied with the filter inductance `Lfilter` for the inner current loop gains `K_PIdq`, and likewise with the capacitance `Cfilter` for the outer voltage loop gains `K_VCdq`.

B.3 Line to Phase Voltage Calculation

For the practical experiment, only the line to line voltage could be measured because there was no neutral point in the AC output of the converter. For the purpose of the *dq* transformation, the line voltage is converted to the phase voltages in real-time.

Code B.3: MATLAB® function for a Simulink block for line voltage conversion to phase voltage

```
function [a,b,c]= fcn(ab,bc)

zr=(ab+bc+ca)/3; %zero sequence component
ab=(ab-zr); %removing zero sequence
bc=(bc-zr);
% This may be not needed if no zero sequence is present in line voltage

a = (2*ab + bc)/3 ;
b = (bc - ab)/3 ;
c=-a-b;
```

Appendix C

Experimental Converter

C.1 Modifications

Author: Terry Chi Young Ho

3 Phase Inverter Board

Version 1.3 – Sep 2013

Introduction

This documentation describes the modifications made to the three phase inverter PCB board, from v1.2 to v1.3. The main new feature of this board is the protection circuit to prevent erroneous high-high signal short circuiting the DC link at the leg of a half bridge. Other minor aspects to the design of the board have also been improved and listed here.

Protection circuit

Previous Issues

While dSPACE is not running, before start or after stop, all gating signals are logic high by default. This is undesirable for both upper and lower gate of the IGBT 3-phase bridge because it will short the DC link. Low DC voltage testing with a current limiting resistor on a working v1.2 board confirmed that the default gating signals from dSPACE do actually short the DC link. Previously, the DC side voltage must only be activated when a dSPACE model is running, and only stop dSPACE when the DC link has fully discharged. If this strict procedure is not followed, the short circuit currents will destroy the IGBT. Therefore, something has to be done in order to prevent this automatically.

Probing into the board and IGBT module revealed that the failure short circuiting between one of the gating pins and DC positive pin. This voltage would then be in contact with the gate driver chips, which would destroy it. The optocouplers would provide isolation and prevent this voltage from damaging the dSPACE interface.

Design of the protection circuit

The IR chip conveniently has SD pin that is unused in the old board, which stands for “shut down”. The function of this pin stops any gating activity when logic high is applied. Therefore, the protection design is very simple. The input of an AND gate will take the respective ‘high’ and ‘low’ signals and outputs a high when both are high. In effect, when both gating signals are high, it will “shut down” and prevent it from shorting the DC link.

Optocouplers are still necessary for isolation between the logic circuit and the gate driver. The output of the AND gate for SD needs to be inverted to cancel out the inversion in the opto-couplers, therefore a NAND gate is used.

Testing on a prototype showed that this circuit worked and was able to protect the inverter from a high-high signal on the IGBT inverter legs.

Other minor changes and fixes

- Pads have been made wider at the IGBT module gating pins so that they are easier to solder. The same done for pads of other components where previously were too small.
- The AC and DC connection pads holes have been made slightly larger so that the socket connectors can fit in with ease.
- Tidied up some of the tracks and made more compact
- Reduced the total number of via connections for signals
- All common grounds tracks and planes are put together.
- The AC output tracks have been made a little wider, and its connection terminals have been made closer to the IGBT module.
- Gate signal tracks have been re-arranged so that the 3-phase AC output track can be added to the bottom layer to double the current carrying capacity.
- DC+ plane has been added at the bottom layer to doubles its current carrying capacity
- Silk layer has been tidied up and solder mask layers has been made in case it is required.
- Other Minor improvements were made in to meet new manufacturer requirements (from University of Warwick).

Recommended future modifications

The current gate drivers used have increased in price. The current price is £7.29 (22/07/2013) and already a quantity of three is required per board, which totals it to £21.87. This is expensive compared to a 3-phase gate driver, capable of driving 6 IGBTs in one single 28 pin chip, such as the IRS23364DSPBF chip, which costs £5.28. It is cheaper and more compact. The IRS23364D has non-inverting inputs, but IRS2336D has inverting inputs, therefore the first inverter stage with the 74AC04 chip would not be required, which can make the PCB more compact. The chip also has other features such as under voltage lockout protection so the power converters are not operating at high conduction losses that can lead to device failure. It also has a shoot-through protection, which prevents both upper and lower side switches of the IGBT inverter from conducting at the same time. This is ideal for dSPACE as described above. With this feature already built in, the NAND gate and optocouplers for the shutdown logic pins are not required in the circuit; therefore it can be more compact and simpler. The chip also has over current protection and over temperature shutdown protection features if required.

These major modifications to the PCB board would take time. If the Semikron IGBT module device specific for this PCB is out of production, alternative devices often have different form factor and pin arrangement, therefore it would be better to build a new PCB board from scratch with all the latest devices. At the moment, there is a few months lead time for supply the Semikron module, and there are a few spares around from last order.

Software notes

The PCB design was made with Number One Systems' Easy-PC. Most other PCB design software applications do not recognise PCB files made with Easy-PC, even though they share the same file extension name.